IAEA-TECDOC-1654

Advanced Fuel Pellet Materials and Fuel Rod Design for Water Cooled Reactors

IAEA
International Atomic Energy Agency

Advanced Fuel Pellet Materials and Fuel Rod Design for Water Cooled Reactors

IAEA-TECDOC-1654

The following States are Members of the International Atomic Energy Agency:

AFGHANISTAN
ALBANIA
ALGERIA
ANGOLA
ARGENTINA
ARMENIA
AUSTRALIA
AUSTRIA
AZERBAIJAN
BAHRAIN
BANGLADESH
BELARUS
BELGIUM
BELIZE
BENIN
BOLIVIA
BOSNIA AND HERZEGOVINA
BOTSWANA
BRAZIL
BULGARIA
BURKINA FASO
BURUNDI
CAMBODIA
CAMEROON
CANADA
CENTRAL AFRICAN REPUBLIC
CHAD
CHILE
CHINA
COLOMBIA
CONGO
COSTA RICA
CÔTE D'IVOIRE
CROATIA
CUBA
CYPRUS
CZECH REPUBLIC
DEMOCRATIC REPUBLIC OF THE CONGO
DENMARK
DOMINICAN REPUBLIC
ECUADOR
EGYPT
EL SALVADOR
ERITREA
ESTONIA
ETHIOPIA
FINLAND
FRANCE
GABON
GEORGIA
GERMANY
GHANA
GREECE
GUATEMALA
HAITI
HOLY SEE
HONDURAS
HUNGARY
ICELAND
INDIA
INDONESIA
IRAN, ISLAMIC REPUBLIC OF
IRAQ
IRELAND
ISRAEL
ITALY
JAMAICA
JAPAN
JORDAN
KAZAKHSTAN
KENYA
KOREA, REPUBLIC OF
KUWAIT
KYRGYZSTAN
LATVIA
LEBANON
LESOTHO
LIBERIA
LIBYAN ARAB JAMAHIRIYA
LIECHTENSTEIN
LITHUANIA
LUXEMBOURG
MADAGASCAR
MALAWI
MALAYSIA
MALI
MALTA
MARSHALL ISLANDS
MAURITANIA
MAURITIUS
MEXICO
MONACO
MONGOLIA
MONTENEGRO
MOROCCO
MOZAMBIQUE
MYANMAR
NAMIBIA
NEPAL
NETHERLANDS
NEW ZEALAND
NICARAGUA
NIGER
NIGERIA
NORWAY
OMAN
PAKISTAN
PALAU
PANAMA
PARAGUAY
PERU
PHILIPPINES
POLAND
PORTUGAL
QATAR
REPUBLIC OF MOLDOVA
ROMANIA
RUSSIAN FEDERATION
SAUDI ARABIA
SENEGAL
SERBIA
SEYCHELLES
SIERRA LEONE
SINGAPORE
SLOVAKIA
SLOVENIA
SOUTH AFRICA
SPAIN
SRI LANKA
SUDAN
SWEDEN
SWITZERLAND
SYRIAN ARAB REPUBLIC
TAJIKISTAN
THAILAND
THE FORMER YUGOSLAV REPUBLIC OF MACEDONIA
TUNISIA
TURKEY
UGANDA
UKRAINE
UNITED ARAB EMIRATES
UNITED KINGDOM OF GREAT BRITAIN AND NORTHERN IRELAND
UNITED REPUBLIC OF TANZANIA
UNITED STATES OF AMERICA
URUGUAY
UZBEKISTAN
VENEZUELA
VIETNAM
YEMEN
ZAMBIA
ZIMBABWE

The Agency's Statute was approved on 23 October 1956 by the Conference on the Statute of the IAEA held at United Nations Headquarters, New York; it entered into force on 29 July 1957. The Headquarters of the Agency are situated in Vienna. Its principal objective is "to accelerate and enlarge the contribution of atomic energy to peace, health and prosperity throughout the world".

ADVANCED FUEL PELLET MATERIALS AND FUEL ROD DESIGN FOR WATER COOLED REACTORS

PROCEEDINGS OF A TECHNICAL COMMITTEE MEETING
HELD IN VILLIGEN, 23–26 NOVEMBER 2009

INTERNATIONAL ATOMIC ENERGY AGENCY
VIENNA, 2010

For further information on this publication, please contact:

Nuclear Fuel Cycle and Materials Section
International Atomic Energy Agency
Vienna International Centre
PO Box 100
1400 Vienna, Austria
email: Official.Mail@iaea.org

ADVANCED FUEL PELLET MATERIALS AND FUEL ROD DESIGN
FUEL ROD DESIGN FOR WATER COOLED REACTORS
IAEA, VIENNA, 2010
IAEA-TECDOC-1654
ISBN 978-92-0-108910-6
ISSN 1011-4289

Printed by the IAEA in Austria
October 2010

FOREWORD

The economics of current nuclear power plants have improved through increased fuel burnup and longer fuel cycles, i.e. increasing the effective time that fuel remains in the reactor core and the amount of energy it generates. Efficient consumption of fissile material in the fuel element before it is discharged from the reactor means that less fuel is required over the reactor's life cycle, which results in lower amounts of fresh fuel, lower spent fuel storage costs, and less waste for ultimate disposal. Better utilization of fissile nuclear materials, as well as more flexible power manoeuvring, place challenging operational demands on materials used in reactor components, and first of all, on fuel and cladding materials. It entails increased attention to measures ensuring desired in-pile fuel performance parameters that require adequate improvements in fuel material properties and fuel rod designs.

These are the main reasons that motivated the IAEA Technical Working Group on Fuel Performance and Technology (TWG-FPT) to recommend the organization of a Technical Committee Meeting on Advanced Fuel Pellet Materials and Fuel Rod Designs for Power Reactors. The proposal was supported by the IAEA TWGs on Advanced Technologies for Light and Heavy Water-Cooled Reactors (TWG-LWR and TWG-HWR), and the meeting was held at the invitation of the Government of Switzerland at the Paul Scherrer Institute in Villigen, from 23 to 26 November 2009. This was the third IAEA meeting on these subjects (the first was held in 1996 in Tokyo, Japan, and the second in 2003 in Brussels, Belgium), which reflects the continuous interest in the above issues among Member States.

The purpose of the meeting was to review the current status in the development of fuel pellet materials and to explore recent improvements in fuel rod designs for light and heavy water cooled power reactors. The meeting was attended by 45 specialists representing fuel vendors, nuclear utilities, research and development institutions and regulatory authorities from 20 Member States. The papers submitted to the meeting were organized into three sessions, covering the areas of fabrication and design, advanced fuels and innovative fuel designs. In addition, there was a special round table discussion that addressed in detail the regulatory aspects of fuel quality assurance. These proceedings contain all the papers presented and discussed during the meeting, and highlight the key findings and recommendations based on the perceptions of the chairmen.

The IAEA wishes to thank the hosts and all the participants for their contributions to the meeting and especially the local coordinator, J. Bertsch, for the organization of the Technical Committee Meeting and the technical visit to the PSI facilities. The IAEA officers responsible for this publication were V. Inozemtsev of the Division of Nuclear Fuel Cycle and Waste Technology and S. Bilbao y León of the Division of Nuclear Power.

EDITORIAL NOTE

The papers in these proceedings are reproduced as submitted by the authors and have not undergone rigorous editorial review by the IAEA.

The views expressed do not necessarily reflect those of the IAEA, the governments of the nominating Member States or the nominating organizations.

The use of particular designations of countries or territories does not imply any judgement by the publisher, the IAEA, as to the legal status of such countries or territories, of their authorities and institutions or of the delimitation of their boundaries.

The mention of names of specific companies or products (whether or not indicated as registered) does not imply any intention to infringe proprietary rights, nor should it be construed as an endorsement or recommendation on the part of the IAEA.

The authors are responsible for having obtained the necessary permission for the IAEA to reproduce, translate or use material from sources already protected by copyrights.

CONTENTS

SUMMARY

Session 1: Fabrication and Design (FD)

Chairman: H. Bairiot

1. Background

It was interesting to observe that while the previous Technical Meeting (held in Brussels, Belgium in October 2003) was dominated by countries operating industrial scale manufacturing plants, the current meeting has mainly attracted countries operating smaller scale facilities.

A possible explanation for this trend may be that all the advancements that were in the pipeline six years ago have now been widely implemented and have become standard fabrication techniques. This is, in particular, the case for the addition of dopants in fuel pellets, which constituted a highlight at the previous Technical Meeting. An additional reason may be the sharing of technology information and best practices amongst related fabrication plants. While, in the past, each fabrication plant was developing its own improvements, the conglomeration of several plants serving the same fuel vendor has led to the progressive adoption of the best technology features by all those plants. Typical examples are the various fabrication plants of AREVA, Westinghouse and GNF. Furthermore, joint ventures between companies promote the exchange of technologies. Recent examples of such collaboration agreements are the shareholder agreement among AREVA-MHI-MMC-MC, the acquisition of NFI shares by Westinghouse and the joint venture between AREVA and KazAtomProm (involving the Ulba Metallurgical Plant).

In such industrial context, presentations and publications from the companies are rather qualitative and mainly geared to commercial promotion. The technical nature of IAEA Technical Meetings like this one is not an adequate environment for contributions from those manufacturers.

The growing interest in building new nuclear power plants, and therefore, is motivating fuel fabricators devoted to serve the national fuel requirements to pursue research and development efforts for improving and/or developing their technology. Such national organizations welcome the opportunity to contribute to an IAEA Technical Meeting, as well as to gather feedback and comments from the other participants in the Technical Meeting.

With regards to the areas of interest, the subjects of fabrication of mixed oxide (MOX), thorium (Th) and reprocessed uranium (RepU) fuel have no longer been covered by the papers in this session. The most obvious reasons may be that the predominant MOX fuel fabrication technology currently operates without problems and has now proven to be transferable to new facilities, that Th fuel fabrication can be based on the U fuel fabrication technology and that design, licensing and fabrication of RepU fuel has been mastered by all concerned industrial facilities.

The various aspects associated with fuel design aspects, which were not covered in the previous Technical Meeting, are mentioned in two papers in this Session and are the main topic of a third paper. This is, of course, a field that would benefit from peer review and universal consensus, particularly taking into account the licensing implications.

2. Summaries and comments

In Argentina, the best utilization of the operating Atucha–1 and the being constructed Atucha–2 PHWRs calls for optimization of the fuel, which is manufactured domestically, namely by switching to slightly enriched uranium. This evolution requires reconsidering several design aspects, such as pellet density, pellet geometry, dish volume, plenum volume, pellet-cladding gap size and initial rod pressurization. They are analyzed in terms of fuel fabrication constrains and thermal-mechanical

performance and safety of the fuel rod. This paper is a good example of analyses and evaluations to be conducted for modifications of fuel rod designs.

In Brazil, the utilization of UO_2-Gd_2O_3 fuel is considered for improving operation of the Angra–2 PWR (longer cycles and optimized fuel utilization). Fabrication trials by dry blending of the powders have revealed difficulties in achieving the required density. The paper outlines the investigation to clarify the cause and provides the results identifying the mechanism involved. Since the phenomenon was observed already over 30 years ago, but little information is available in published literature, it shows the importance of the IAEA Technical Meetings as a vehicle to disseminate knowledge amongst organizations interested in developing their capabilities.

The presentation from China outlines the successful CANDU–6 fuel fabrication technology transfer from ZPI to BNFP, which started manufacturing it in 2002. Considering the particular aspect of the pressure resistance welding process of end plugs, BNFP analyzed the root cause of leakages observed amongst the fuel assemblies manufactured before 2005. It led to precautions implemented in the process and in the quality control. As a result, no leakage has been observed on fuel manufactured thereafter. This paper shows the importance of developing in-house expertise.

The German paper is the only paper in the session devoted exclusively to the licensing approach for fuel rod design evaluation. The traditional approach is based on a deterministic methodology, using a conservative combination of input parameters. Realizing that this conservative approach restrained possibilities to improve fuel utilization, AREVA developed in the 1990s a probabilistic methodology based on the traditional CARO modelling code, a best-estimate code based on a quite extensive Post Irradiation Examination database. Over the years, increased sophistication of the modelling and progressive expansion of the database has resulted in a methodology able to cope with requirements of all licensing scenarios. This paper is a good example of the approaches required to license improved fuel designs and/or more challenging operating conditions (power uprates, higher burnups …).

Two papers from India are devoted to PHWR fuel pellets. The paper from NFC/Hyderabad focuses in the problems encountered in manufacturing the pellets for this type of reactors with the required levels of quality (density, geometric integrity and microstructure). The causes of problems encountered were spotted and remedies were developed and adopted in the production line. It is a good example of improvements that can be achieved even in facilities with a long industrial experience.

The paper from NPCIL/Mumbai outlines studies undertaken to raise the fuel bundle discharge burnup from 7 GW•d/tU average (15 GW•d/tU peak bundle) currently obtained with natural uranium to 30 GW•d/tU which could be achieved with slightly enriched uranium. Within the constraints of PHWR fuel (no plenum and collapsible cladding), modifying pellet shape and pellet parameters had to be considered. Since use of slightly enriched uranium in PHWRs is now recognized as a possibility to improve fuel cycle cost, this presentation is an important contribution to the Technical Meeting.

The paper from Indonesia focuses on the development conducted in the BATAN fabrication laboratory to switch from PHWR fuel, to which the facility was devoted initially, to PWR fuel, since this type of nuclear power plant is now considered for the first units to be built in the country. Pelletizing technology and sintering parameters were adapted accordingly and the revisited fabrication process is now being experimented. This example illustrates the flexibility that early developers can acquire once they have implemented experienced manpower.

3. Problems, challenges and perspectives

Four of the seven papers in the session were devoted to PHWR fuel fabrication aspects. For any fuel type, the continuously increasing proportion of the back-end in the fuel cycle cost pushes optimum discharge burnup to ever higher levels. While this requires research, development and innovation for any type of fuel, it is particularly a challenge for PHWR fuel, where the pellet is a conditioning structural component. It explains why improvements presented in the previous Technical Meeting dealt essentially with LWR fuel and are not presented anymore in this Technical Meeting, having been

applied industrially, while improvements of PHWR fuel are still going on. No doubt that coping with PHWR fuel improvements can also be considered in the same optimist perspective.

Newcomers in commercial fuel fabrication, even while relying on technology received in the frame of a technology transfer, have to acquire their own mastery of the processes. Presentations in the session have illustrated the effort and time required. It has taken place in Europe and Japan since the 1970s and should not pose a problem to spread over the rest of the world.

In fuel design to support licensing, the German presentation illustrates the improvements that can be considered over the traditional deterministic methodologies. The diverse modelling efforts between countries and even within countries aim currently at improving the physical bases of each modelling code, in an attempt to reach perfection. Unless manpower and resources are available to pursue both alternatives, it may be necessary to choose whether to focus research efforts in the above objective or in the development of methodologies aiming at reducing licensing conservatism. .

4. Recommendations for future work

Mastering the fabrication processes and improving quality control efficiency is a continuous effort to be pursued not only in developing facilities but also in well established fabrication plants. The advancements in this field are often small steps, not amenable to presentation in meetings like this Technical Meeting, taking place with six years intervals. Since they are published in conferences and symposia with a broad commercial aspect, the IAEA should devote a report to summarizing them and presenting them in perspective. No IAEA initiative of this kind was taken since Technical Reports Series No. 221, misleadingly entitled Guidebook on Quality Control of Water Reactor Fuel, was published in 1983 and complemented by IAEA-TECDOC-584, Guidebook on Quality Control of Mixed Oxides and Gadolinium Bearing Fuels for Light Water Reactors, published in 1991. Such overviews should be issued at appropriate intervals, i.e. 5 years, to reflect the advancement of the technologies. The periodic publications of IAEA on the status of fuel failures are a good illustration of what should be achieved also for fuel fabrication and quality control.

The periodic organization of Technical Meetings such as this is a necessary complement to the above publications, since they provide a unique opportunity for experts to present their work and receive feedback from peers in a quite informal meeting environment. A six year periodicity seems adequate.

Session 2: Advanced Fuels (ADV)

Chairman: P. Blanpain

1. Background

The four papers of the session were dedicated exclusively to the development and the qualification of advanced fuels and advanced burnable poison absorbers (advanced, in this context, means improvements of existing concepts as opposed to innovative solutions, which will be covered in the third session).

There are a number of trends in the nuclear power industry, which put additional requirements on the operational flexibility and reliability of nuclear fuel, for example power uprates and longer cycles in order to increase production, higher burnup levels in order to reduce the back end cost of the fuel cycle, and lower goals for activity release from power plant operation. These requirements can be addressed by increasing the fuel density, improving the fission gas retention (FGR), improving the pellet-cladding interaction (PCI) resistance and improving the post-failure performance. Three fuel vendors (TVEL, Westinghouse and AREVA) are proposing solutions which are at different stages of development and qualification.

Advanced burnable neutron absorbers (BNA) for the new CANDU reactor generation are being developed by AECL in order to increase efficiency with regard to coolant void reactivity.

2. Summaries and comments

VNIINM/TVEL presented a programme currently underway to optimize the composition and microstructure of fuel pellets as applied to WWER, to meet the requirements placed on the new fuel that ensures the reliable operation under conditions of higher burn-ups (56 MW•d/kg).

The paper describes a general approach to providing the composition and microstructure of fuel via introducing various dopants. The properties of fuel pellets containing additives have been presented. The implemented investigations of the microstructure of the modified fuel evidence that the selected additives increase grain sizes and are uniformly distributed in the fuel pellet volume. The investigations of the thermal physics properties of the modified fuel (linear thermal expansion, thermal conductivity) have demonstrated that the introduced additives do not deteriorate those properties. Tests have shown that the modified fuel pellets containing additives have a higher corrosion resistance when interacting with coolant. The optimal additive was selected (aluminum silicate) on the basis of test irradiation experiments on high burn-up fuels in the MIR reactor. The acquired experimental results allowed the development of a semi-commercial process of modified fuel fabrication, the manufacture of pellet batches to semi-commercially operated in WWER. Since 2005 the semi-commercial operation of the fuel containing additives has been commenced in two WWERs. The burn-up of 56 MW•d/kg was reached.

In order to achieve the new fuel performance requirement, Westinghouse has developed ADOPT (Advanced Doped Pellet Technology) UO_2 fuel containing additions of chromium and aluminium oxides. The additives facilitate pellet densification during sintering, enlarge the pellet grain size, and increase the creep rate. The investigations have identified three areas of improved operational behaviour: Reduced Fission Gas Release (FGR), improved Pellet Cladding Interaction (PCI) performance thanks to increased pellet plasticity and higher resistance against post-failure degradation. The better FGR behaviour of ADOPT has been verified at 55 MW•d/kgU, as well as transient tests in the Studsvik R2 reactor. Creep measurements performed on fresh pellets show that ADOPT has a higher creep rate which is beneficial for the PCI performance. ADOPT has also been part of a high power Halden test (IFA–677); the results of that experiment were difficult to interpret due to the complicated and different power histories experienced by the tested fuel rods. The AREVA paper discussed how the chromia-doped fuel has proved to bring significant margins in the mitigation of PCI risk of clad failure as well as to the reduction of FGR and induced rod internal pressure at the end of life. The optimized Cr_2O_3-doped characteristics also provide additional fuel robustness by a reduced pellet chipping susceptibility and reliability features. This latter concerns fuel washout behaviour in case of defective rods after the occurrence of primary defects occasionally observed under operation.

The oxidation and washout behaviour of unirradiated non-doped, chromia-doped UO_2 and chromia-doped $(U,Gd)O_2$ fuel pellets have been analyzed by thermogravimetry and by autoclave leaching tests simulating LWR conditions. The entire testing program demonstrates that chromia doping enhances significantly the corrosion resistance of the fuel pellets.

Both fuel types are currently under irradiation in commercial nuclear plants to meet future more demanding operating requirements. The AECL paper describes how historically, BNAs have been added to the UO2 fuel meat to control reactivity in fresh fuel but in AECL's Advanced CANDU Reactor®™† fuel design, BNA is used to achieve a reduced coolant void reactivity. For this application it is desirable to have the BNA separate from the uranium. Zirconium oxide was chosen as a candidate inert matrix material to host the BNA due to its irradiation stability, compatibility with the BNA oxides, and material properties.

BNA pellets were successfully fabricated having a homogeneous distribution of BNA. A solid solution with the cubic phase was achieved for various compositions of dysprosia, gadolinia and/or yttria. Based on the results available to date, BNA pellets do not appear to have exhibited any swelling attributable to irradiation damage. Continued irradiation of full-scale CANDU elements containing BNA pellets to about a 1000 days is planned.

3. Problems, challenges and perspectives

More demanding operational conditions and the so-called ‘nuclear renaissance’ context are boosting the development of advanced or optimized fuels. But this endeavor requires time (10 to 20 years) and financial resources for the developent and qualification of new components or designs before deployment in commercial nuclear power plants.

Additional constraints such as the availability of qualified human resources, the cost of experimental irradiation or the availability of host nuclear plants to test prototype fuels further complicate this development. Nowadays, given the expected performance of these new products, the qualification process has become more demanding, including the verification at operational and accidental conditions, back-end, and environment. In addition, there is an increased need for advanced modelling tools that can appropriately simulate these new products.

International collaboration and information exchange should be encourage for fundamental research and development, to share experimental facilities, and to take advantage from experience, lessons learned and various approaches to licensing. At the same time, in the context of vendor’s competition, international collaboration may not be a good platform for the development of new products.

Finally, a more proactive attitude is needed between fuel vendors, utilities and regulators to promote and facilitate experimental irradiation of advanced fuel products in operating nuclear power plants (LTA or LTR).

4. Recommendations for future work

As in the previous session, the periodic organization of Technical Meetings such as this was encouraged. In addition, wider distribution of the meeting announcements was recommended to ensure the participation of all the relevant experts.

Session 3: Innovative Fuel Designs (INN)

Chairman: R. Pomirleanu

1. Background

Previous Technical Meetings on ‘Advanced Fuel Pellet Materials and Designs For Water Cooled Reactors’ sponsored by IAEA have focused mostly on understanding the behavior of current solid fuel pellet technology (on its own or under interaction with Zircaloy cladding) under extended operating or extreme conditions. With this Session of the current Technical Meeting, inherent limitations of the current technology are addressed via innovative fuel pellet material or geometry.

Research in the area of innovative fuel designs at this Technical Meeting was reflected in papers from member states with long-established nuclear industries (Japan, Republic of Korea, Belgium, and USA), with the exception of the interest in thorium-plutonium cycle expressed by Norway which nevertheless builds on a significant body of research.

Without attempting a rigid classification of the concepts presented, three of the papers in this session discuss details of innovative fuel designs that allow a more efficient burn of plutonium and/or minor actinides (inert-matrix fuels, thorium-plutonium oxide, and uranium-zirconium hydride fuel), while three other papers bring into focus ways of improving the economics of current light-water reactors (higher than 5 wt.% ^{235}U fuel, or annular fuel pellets). While the latter category needs no justification, the former is important as it aims to reduce the plutonium inventory and the foot-print of nuclear energy generation, which is often quoted as one of the problems of this energy source.

Although most research presented in this Session is quite revolutionary from the perspective of this series of IAEA Technical Meetings, it has benefited from many years of analytical and empirical investigations and it is therefore mature enough to be presented at this Meeting. It has to be nonetheless recognized that, unlike the subject matter presented in the other sessions, the research presented in this session has years, and most probably decades, before it can be turned into products that can be successfully licensed and commercialized.

2. Summaries and comments

The advantages of inert matrix fuel (IMF) concept for burning of Pu and minor actinides was stated in the presentation by the Paul Scherrer Institute (Switzerland), its practical application being targeted for the last cycle of commercial PWR and geological disposal. The stabilization by yitria of the zirconia is such that the latter's solid solution with minor actinides oxides and Pu is stable under heavy ion irradiation, and the retention of fission products is a priori stronger, relative to UO_2 pellets. Successful irradiation of IMF in research reactors (Halden, HFIR, Pelten) paves the way for commercial irradiation, although the fuel cycle economics and the licensing aspect of a new fuel will have to be addressed.

The paper on Thorium-Plutonium fuel from Thor Energy (Norway) presents an extensive account of research and development activities needed to bring this concept to fruition. In a first phase, LWR application is pursued, aiming to burn plutonium from other fuel cycles or weapon-grade. While significant research on thorium fuel cycle dates back at least three decades, the study from Norway is a fresh start.

The University of California at Berkley (USA) has presented research on a fuel rod design where the fuel consists of uranium metal embedded in a zirconium-hydride matrix. The main advantages of this design relative to the oxide fuel are its higher thermal conductivity, higher retention of fission products, and the flat neutron flux shape inside the pellet due to the moderating effect of the hydrogen. These come at the expense of enrichment needs outside current commercial experience, higher irradiation swelling at temperatures exceeding 700^{o}C, and hydrogen-embrittlement of the Zirconium-based cladding from the inside if pressed against the pellet. The solution proposed here is to limit the fuel pellet temperature below 650^{o}C without limiting the LHR, and to fill the cladding-to-pellet gap with a liquid metal (lead-tin-bismuth) to resists to reduce the thermal resistance across the gap and protect the cladding from hydrating from the inside.

Two papers from Japan were presented on the concept of erbium-loading of UO_2 fuel pellets to allow use of enrichment higher than 5 w/o ^{235}U. This approach allows pellet manufacturing within the same criticality safety bounds as for the current UO_2 technology, from the point of powder blend onward. The first paper presented by Nuclear Fuel Industries, Kyoto University, and Nagoya University details the set-up and the results of criticality experiments for this material formulation. The analysis of the resulting data leads to acceptance design envelope expressing the required amount of erbium to retain sub-criticality for several relevant configurations.

The second paper presented by Kyoto University focuses on reducing neutronics prediction uncertainty for the UO_2-Er pellet, in the absence of critical experiments using this compound. The approach taken is to adjust the neutron absorption cross-section of Erbium, while applying the bias factor method to the neutronics characteristics of the pellet composition without Erbium. This algorithm allowed reduction of prediction uncertainty for k_∞ for H/U values of 0, 1, and for a PWR-specific case.

KAERI presented new research into the manufacturing of annular fuel rods with cooled inner cladding, focused on the pellet inner diameter tolerance. Annular fuel rods have the potential to increase the power extracted from the same mass of uranium as currently used in PWRs by increasing the heat transfer area. The pellet inner diameter tolerance has a significant effect on the ratio of the heat fluxes through the outer and inner cladding, respectively, and it therefore needs to be controlled as

tightly as possible. The paper details several annular pellet manufacturing processes that successfully reduced the tolerance of the pellet inner diameter, such that inner surface grinding was no longer necessary.

3. Problems, challenges and perspectives

Three of the six papers in the session were devoted to efficient ways of burning minor actinides and/or plutonium (re-processed or weapon-grade) in LWR, thereby aiming to reduce the once-through used fuel and the weapons-grade material inventories. All three subjects represent many years of sustained research activity performed by the authors or other parties, but commercialization at a future point is uncertain because the overall positive economic benefits to the entire fuel cycle are not demonstrated. This should not deter future research on this area, but if the goals of this research are deemed worth of pursuing by the IAEA, a stronger driving need has to be formulated.

The higher than 5 wt.% ^{235}U enrichment study from Japan challenges one of the most long-enduring limits on the design and manufacturing of nuclear fuel. This status-quo can be changed through the combined efforts of nuclear fuel vendors, nuclear power operators, and nuclear regulators. Credit for other types of fuel poisoning besides the one presented in this Session (e.g. ^{236}U from reprocessed fuel, etc.) can be pursued as well.

The annular fuel concept is seeing a revival through the research performed by KAERI. While challenges still remain, the Korean work contributes to promote this concept into a product. Additional work will be needed in other areas of the fuel design (e.g. cooling of inner cladding, differential growth between inner and outer cladding, etc.).

4. Recommendations for future work

The commercial benefits of ^{235}U enrichments larger than 5% reside in reducing the number of feed assemblies and facilitation of longer burn-up. However, commercial implementation of ^{235}U enrichment above 5 wt.% is best pursued as a concerted effort between players within the nuclear energy generation, crossing national and international boundaries. Therefore, this research would benefit from the enlarged framework provided by IAEA.

A number of innovative technologies presented into this session can justify their sustained commercial implementation on non-economic grounds alone (e.g. ecological, reduction of weapon material inventory, etc.). Since there are more technologies than presented herein that fit this profile, and since they may be quite diverse in technical details, it may be beneficial for future Technical Meetings to devote a separate session (if feasible through the amount of submitted papers) to innovative ideas to address the back-end of the fuel cycle. Moreover, since many of these technologies struggle to find financial merit on their own, IAEA could seek to establish a framework within member states where this type of research will be able to find funding towards commercialization.

Panel discussion on regulatory aspects of fuel quality assurance

The session examined the role of regulation in making certain that nuclear fuel designers, manufaturers and operators ensure sound design of fuel assemblies and quality of manufacture, while enabling optimisation of fuel utilisation within safety constraints.

The tasks of the regulator were discussed within the broad topic areas of:

- design approval;
- promotion of research and development;
- surveillance of manufacturing quality;
- and responding to operational experience.

The IAEA is in the process of preparing guidances on the development of nuclear power capabilities and it was felt that a discussion on the role of the regulator could provide assistance to some states in formulating a strategy for regulation of fuel issues.

1. Summary of discussions

Mr. Jones of the Nuclear Installations Inspectorate (NII) outlined the United Kingdom regulatory approach to design assessment. The UK regulator issues licences for nuclear plants and expects licensees to develop a safety case which systematically considers alternative strategies and demonstrates that the preferred proposal ensures that the risk to operators and the public, is *as low as reasonably practical.*

In this context, the test applied has two aspects:

- first, that the cost and trouble of additional measures must be demonstrated to be grossly disproportional to the potential benefit in terms of risk avoided;

- second, the proposal should follow good practice and sound engineering principles as set down in UK guidance and potentially IAEA documentation.

Guidance on good practice includes a number of rules. For example, in the criticality, systems which are inherently safe are preferred over those which rely on engineered protection, but this is preferred to administrative control.

A weak case judged against examples of good practice would require a strong case based on quantitative risk assessment. Acceptance of a design proposal is based on a balanced judgement.

Mr Pomirleanu of Westinghouse welcomed the fact that the approach recognises the economic and risk imperatives and was not solely based on a system of conservative requirements.

Mr Tomov from the nuclear power plant of Kozloduy expressed the view that there was a need for regulators to define the acceptable level of safety margins required in a safety assessment. particularly in cases where a probabilistic response surface method is employed.

Mr Pomirleanu echoed this view suggesting that, in the view of emerging requirements, there is a need for regulators to commission proactive research. This would enable safety limits to be defined for new situations outside the validity of existing standards.

Mr Young-Ho of Republic of Korea Nuclear Fuel gave the example of the maximum cladding oxide thickness. It was acknowledged by other delegates that the limiting value of 100 microns; widely used in the industry, was originally identified before Zircaloy 4 was optimised and should possibly be reviewed for modern cladding.

There was also a call for regulators to be proactive in defining the requirements for future research. However, the consensus among regulators was that the responsibility for developing a safety case lies with the licensee and that while discussions take place from time to time, the regulator would be acting outside its powers in defining the fuel development strategy.

Mr Grant of the Canadian Nuclear Safety Commission explained that there are a number of design modifications under consideration in Canada which the regulator has actively encouraged on safety grounds. These are also likely to bring economic benefits by increasing safety margins and allowing justifiable relaxation of constraints.

Mr Gorzel of the Swiss Federal Nuclear Safety Inspectorate explained how the Swiss industry approaches new developments. This is based on a planned and structured programme of pilot loadings

and post-irradiation examination. Their approach has kept Swiss reactors abreast of current developments, which includes achieving high fuel burnup levels and the loading of advanced fuels. A first load of chromium-doped fuel has taken place recently. Swiss legislation requires that utilities employ the best available current technology.

Mr Gorzel confirmed that Swiss inspection data on chromium-doped fuel is consistent with the information presented at the meeting. He thanked the presenters for the information which was valuable confirmation for him.

There was a consensus among Swiss delegates that the Swiss regulator collaborates closely with Paul Scherrer Institute (PSI), the fuel vendors and the utilities.

Mr Terrani of the University of California expressed the view that in the US, neither the utilities nor the fuel vendors are ready to make more than incremental changes due to the cost and regulatory risk.

Mr Pramanik of the Nuclear Fuel Complex of India reported that this problem did not arise in India because the relevant bodies are state owned and can make integrated plans based on national requirements.

Ms Laine from the Radiation and Nuclear Safety Authority, Helsinki, Finland (STUK) explained that in Finland the responsibility for the safety case is solely with the utility, but that the Finnish regulator carries out extensive inspection and sampling of compliance.

A discussion of design criteria including the limit of 5% on fuel enrichment followed these remarks. The consensus was that the limit is set based on criticality concerns, but the margin inherent in this value appears less certain. It was felt that this would be a useful topic for an IAEA specialist meeting.

2. IAEA perspective

In recent years it is felt that the conservative approach to the assessment of fuel safety margins and the need for evidence has led to unnecessarily long lead times in the development of new designs: typically twenty years between an initial detailed design and the first batch of modified fuel.

This was considered too long; particularly for emerging industries who need to solve technical issues in a shorter time interval.

Close collaboration between fuel suppliers, regulators and utilities is considered necessary to allow proactive programmes of product development to meet future needs as they emerge.

3. Recommendations

The origins of some design criteria are evidently not widely understood. The IAEA should facilitate the review of these limits by targeted topical meetings. One key example is the 5% enrichment limit which the IAEA could profitable review.

The IAEA potentially has a role in facilitating technical developments where both utilities and fuel suppliers are reluctant to take on the full regulatory risk of licensing a modification to current practices. This should be actively pursued where practical.

IAEA standards provide an important role in defining good practice. These should be reviewed from time to time to ensure that they meet current needs and include the appropriate level of conservatism.

FABRICATION AND DESIGN

(Session 1)

Chairperson

H. BAIRIOT

Belgium

Innovative Process Techniques to Optimize Quality and Microstructure of UO_2 Fuel for PHWRs in India

D. Pramanik[a], M. Ravindran[b], G.V.S.H. Rao [c], R.N. Jayaraj [d]

Abstract. Nuclear Fuel Complex (NFC) is the sole manufacturer of UO_2 fuel for the pressurized heavy water reactors (PHWRs) in India and currently supplying fuel to PHWRs–220 MW(e) and PHWRs–540 MW(e) operating in the country. High density (96–98%TD) and defect free UO_2 fuel pellets are produced from UO_2 powder, which is derived through ammonium di-uranate (ADU) precipitate route. The PHWRs fuel pellets are fabricated using process steps such as pressure agglomeration of UO_2 powder, admixing of lubricant, die compaction of green pellets followed by high temperature (1700℃) solid state sintering of green pellets. The in-pile performance of the collapsible clad fuel is largely dependent on pellet density, physical integrity and microstructure. The physical and chemical characteristics of UO_2 powder, powder morphology and pellet fabrication technique are mainly responsible for these attributes of the fuel pellets. Higher amounts of impurity anions like sulphate, carbonate, etc. in magnesium-di-uranate (MDU) raw material and larger fraction of coarser particles in mono-modal particle size distribution of UO_2 powder were found to be the prime reasons for low sintered density and in-homogenous microstructure in UO_2 sintered pellets. Nitrogen pick up was found to be predominant in low density sintered pellets having duplex grain structure having larger grains, larger pores in the core of the pellet. End chipping and end cap defect in sintered pellet was encountered for some powder lots. The pellet integrity was improved by doping 3–5% U_3O_8 powder with UO_2 granules. Doping fine grade ammonium-di-uranate (ADU) with UO_2 granules is found to bring encouraging results for solving low density and microstructure related problems. An innovative technique was also developed to retrieve the acceptable density pellets from non-conforming sintering boats having sintered pellets of variable sintered density. The paper highlights the incidences of low density, end defects and heterogeneous microstructure encountered in sintered UO_2 fuel pellets of certain lots and discusses the problem solving processes attempted in pellet production line.

1. Introduction

Nuclear Fuel Complex (NFC) manufactures high density (96–98% TD) fuel for 220 MW(e) and 540 MW(e) PHWRs operating in the country. There are two fuel manufacturing facilities at NFC, Hyderabad for production of natural uranium oxide fuel. The either facility is engaged in converting MDU/U_3O_8 to UO_2 powder, UO_2 powder to UO_2 pellets and fabrication of fuel assemblies. While one facility manufactures safeguarded fuel for the safeguarded PHWRs, the other manufactures fuel for the un-safeguarded PHWRs. The flow sheet for production of UO_2 powder and fabrication of UO_2 pellets from UO_2 powder are identical in these two facilities and the flow sheet is given in Figure 1. ADU is precipitated in 500–1000kg batches through ammonia gas precipitation process. Ammonia gas precipitate route UO_2 powder is characterized with needle shaped crystallite aggregates (Figure 2).

The starting U_3O_8 material used for production of UO_2 powder in the safeguarded facility is of higher purity, where as the starting MDU (yellow cake) material used for producing un-safeguarded UO_2 powder contains comparatively higher anionic impurities like sulphates, carbonates, chlorides, etc. The un-safeguarded powder facility receives starting MDU (yellow cake) from two Indian source plants. The purity of the source–2 MDU is again comparatively poorer compared to the source–1 MDU material. The physical and chemical characteristics of UO_2 virgin powder, granulated powder and green pellet are similar and they are given in Table 1.

[a] Department of Atomic Energy, Nuclear Fuel Complex, Hyderabad, India.
[b] Department of Atomic Energy, Nuclear Fuel Complex, Hyderabad, India.
[c] Department of Atomic Energy, Nuclear Fuel Complex, Hyderabad, India.
[d] Department of Atomic Energy, Nuclear Fuel Complex, Hyderabad, India.

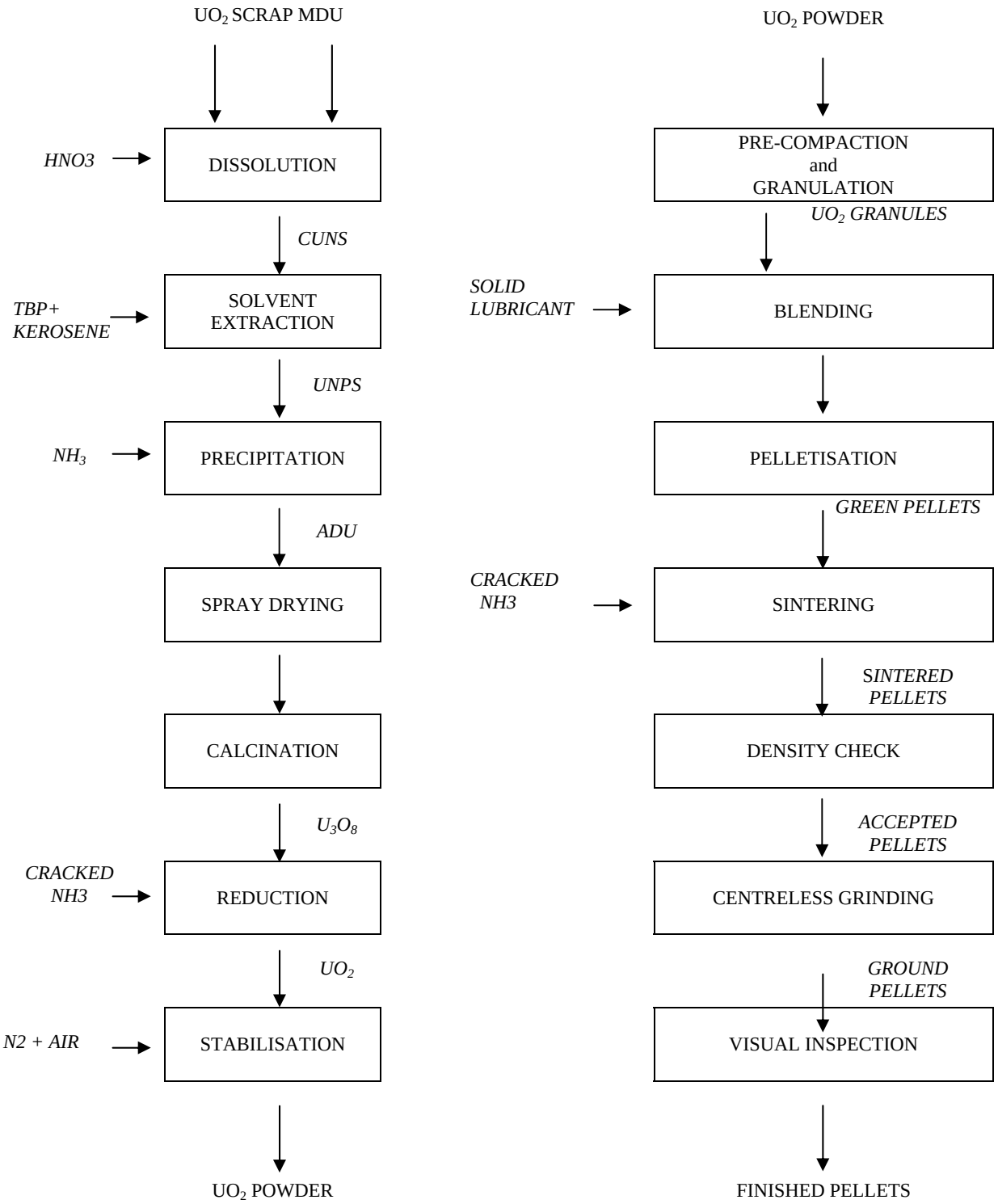

FIG. 1. Process flow sheet from MDU to UO_2 pellet.

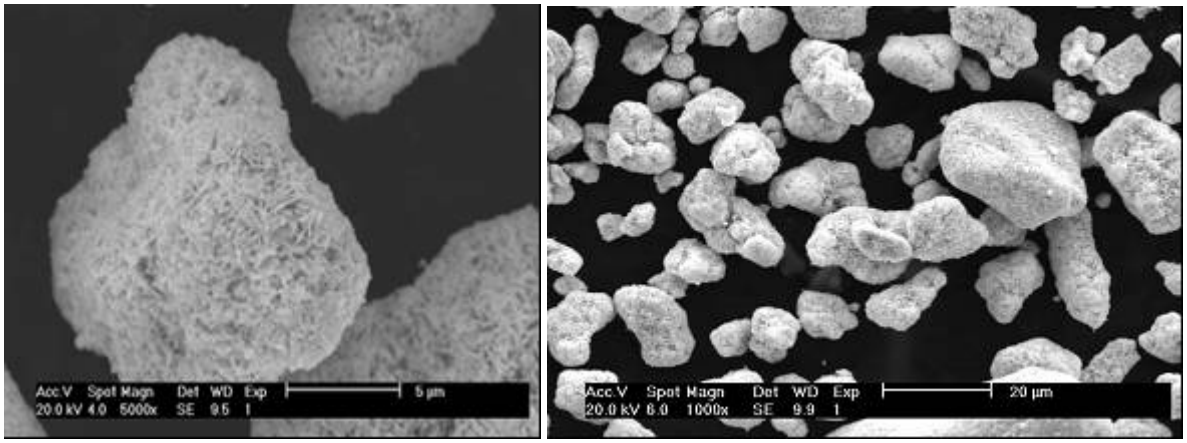

FIG. 2. UO_2 crystallites and particles in ammonia gas precipitate route.

TABLE 1. PHYSICAL AND CHEMICAL CHARACTERISTICS OF UO_2 POWDER AND GREEN PELLET

1.	Specific surface area (BET)	:	2.7–3.2m^2/g
2.	Bulk density	:	2.0–2.1g/cc
3.	Tap density	:	2.8–2.9g/cc
4.	O/U	:	2.10 max.
5.	Purity	:	EBC = 1.1ppm max.
6.	Morphological feature	:	Needle shaped crystallites
7.	Granulated powder bulk density	:	2.8–3.0g/cc
8.	Granulated powder tap density	:	3.8–4.0g/cc
9.	Green density	:	5.70–5.90g/cc

There is no quality issues with respect to sintered density or integrity defects in the fuel pellets produced in the safeguarded plant. But the unsafeguarded fuel facility has been facing now and then low density, density variations, physical integrity defects like end cap and fine cracks in the sintered pellets. As being followed for the last ten years, UO_2 green pellets are sintered in Molybdenum boat with pellets in vertically standing positions. The green pellets as ejected from the press-dies in vertical conditions are transferred over molybdenum spacer sheets by an integrated pick and place mechanism. The pellets are loaded on to the Molybdenum sheet in a close packed manner Ten such loaded sheets are assembled in five vertical layers, two loaded sheets in one layer, by using interlayer spacer pellets over a thick molybdenum base plate. The stack assembly is covered by placing a molybdenum shroud over it (Figure 3). The sintering furnaces are essentially pusher type and when one boat is pushed by one boat length, all the successive boats advance by same distance from their respective position. A green boat is pushed inside the furnace as per a preset pushing interval. At every entry of a green boat, a sintered boat is discharged out of the furnace from the discharge end. The shroud is lifted from the boat to allow unloading of the pellets from the stack (Figure 4). Each and every sintered boat is subjected to density check on sampling basis. Since variation in sintered density is normally observed in the bottom layer of the boat, five sample pellets are randomly selected from this layer for density measurement. In case one or more sample pellets are found to have density less than 10.45g/cc, the boat is rejected and screened out from further operations. The pellets of the reject boat by convention go back to acid dissolution along with other reject material In a density qualified boat, the density variations among the entire population is limited to about 0.15g/cc, the minimum density being greater than 10.45g/cc. The sintering performance of the powder lots produced from reject/scrap source raw material is normally better than that produced from the MDU source–1 and 2. Investigation and analysis are being done to optimize the processes for improving the sintering performances of the UO_2 powder lots being produced using raw material from scrap/reject, MDU source–1 and MDU source–2 in the same facility.

The low density pellets are characterized with coarse grain and coarse pores throughout the matrix (Figure 5) or a duplex grain structure with coarse grain, coarse pore in the inner core of the pellet and small grain, small pore structure in the pellet periphery regions (Figure 6). The as polished and etched microstructure (Figure 7 and Figure 8) of such pellet reveals a typical coarse grain structure having grain size range from 7 micron to 56 micron (average 40 micron) and pore size range from 3 micron to 26 micron (average 20 micron) in the central region. The grain size, pore size in the peripheral region vary from 4 micron to 25 micron (average 14 micron) and 1micron to 3 micron (average 2 micron) respectively.

Nitrogen pick up more than specified limit of 75ppm max was found to be another problem associated with low density pellets having the duplex grain/pore structure. Nitrogen pick up is comparatively less when the low density microstructure is characterized with uniformly distributed larger pores in the fuel matrix. Higher nitrogen in PHWR fuel pellets are not acceptable because the zircaloy clad material is prone to react with higher nitrogen to form brittle nitride phase endangering the in-reactor life of the fuel. A co-relation exists between nitrogen pick up and sintered density (Figure 9). Vacuum degassing of pellets at 400^oC for 4 hours is found to be effective for driving off the nitrogen (Table II). Lower sintered density pellets (>10.30g/cc) are tested for re-densification characteristics and stability of microstructure through re-sintering test at 1700^oC for 24 hours (Table 3). The in-reactor performance of the fuel with concessional density and nitrogen content is under evaluation.

Doping of fine grade ADU with UO_2 granules prior to compaction is found to solve the duplex grain structure and improve sintered density in such material. However, very finer grade ADU is essential to avoid fine cracks in sintered pellets.

The sintered and centre less ground pellets are subjected to 100% visual inspection for sorting out integrity defective pellets. The end cap and crack defects are the ones that mainly contribute to pellet rejection. No liquid binder is used over virgin UO_2 powder or UO_2 granules for controlling integrity defects. Instead, a solid admixed lubricant cum binder is added to the granules to produce defect free UO_2 pellets.

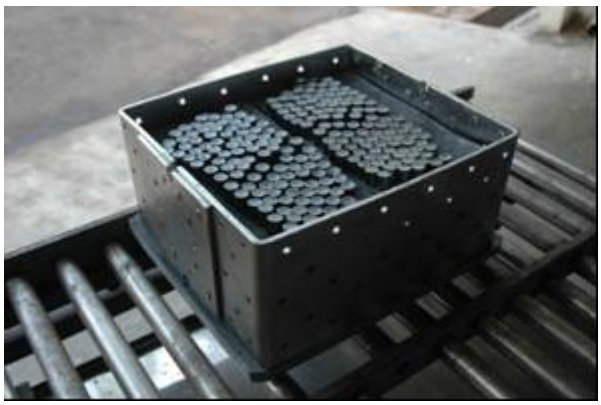

FIG. 3. Typical boat with shroud.

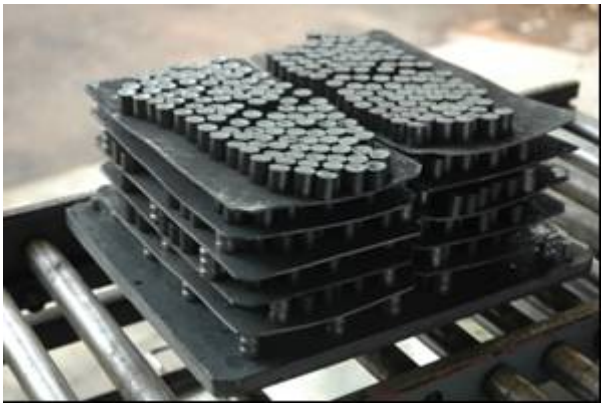

FIG. 4. Typical pellet loading pattern in a boat.

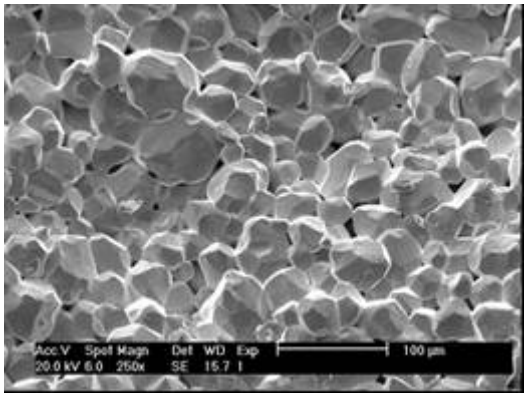

FIG. 5. Large isolated grain with large pores throughout matrix –fracture surface.

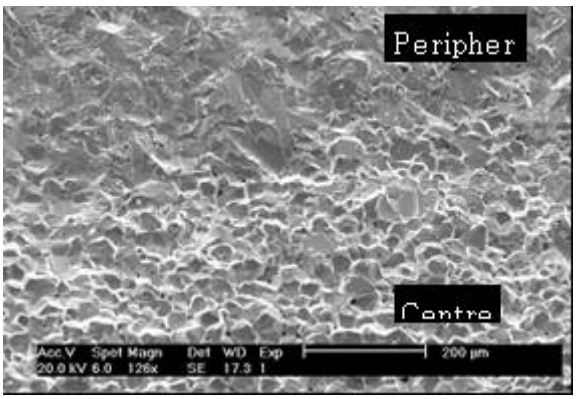

FIG. 6. Coring defect (Large grain in centre and fine grain in periphery)-fracture surface.

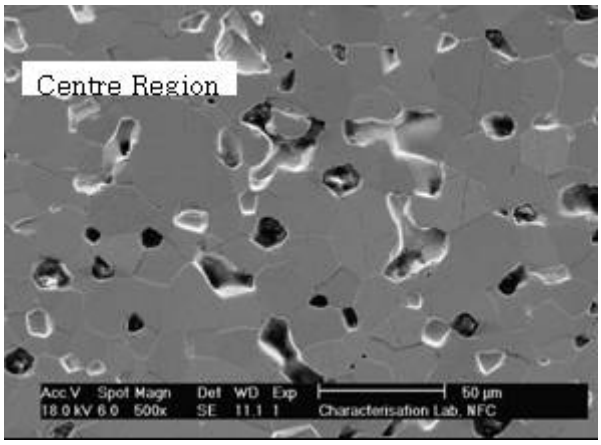

FIG. 7. Microstructure of central region.

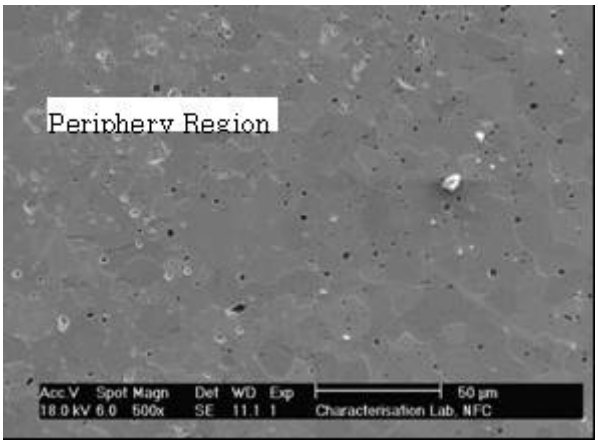

FIG. 8. Microstructure of peripheral region.

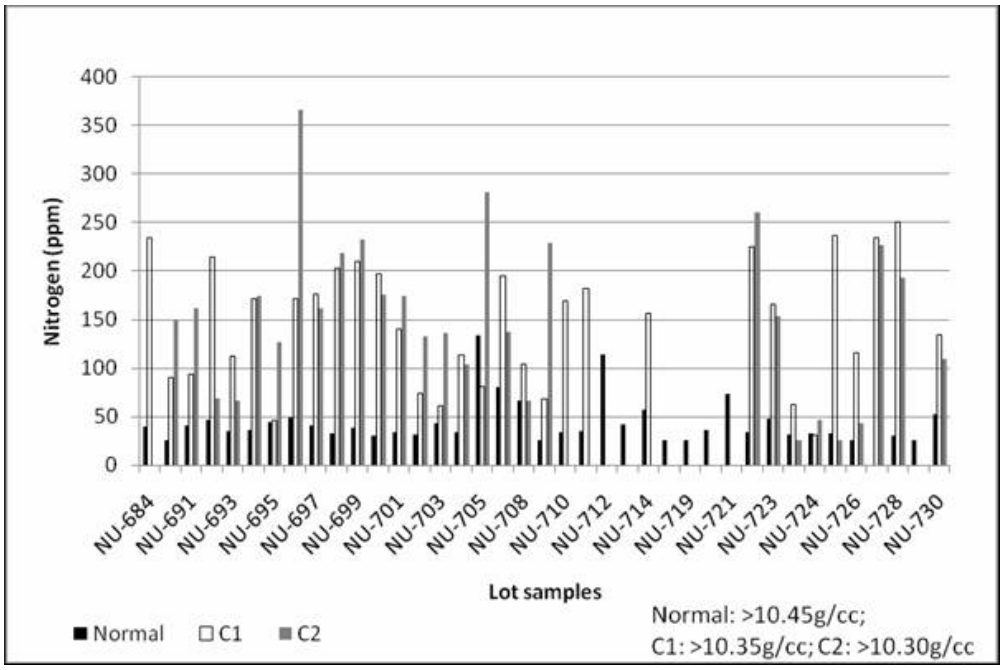

FIG. 9. Nitrogen pick up and sintered.

TABLE 2. TYPICAL VACUUM DEGASSING FOR 4 H AT 10^{-4} MBAR

Sl	Sintered density(g/cc)	Initial Nitrogen (ppm)	Nitrogen After degassing(ppm)
			400°C
1)	10.32	250	60
2)	10.40	167	35
3)	10.33	183	45
4)	10.30	327	70
5)	10.46	168	81
6)	10.31	281	37
7)	10.32	123	71

TABLE 3. RE-SINTERING TEST AT 1700°C FOR 24 h

Sl.No	Before Resintering				Pellet Type	After Resintering				
	Wt.	Ht.	Dia	Density		Wt.	Ht.	Dia	Density	Density Diff in %
1.	16.8	14.26	12.142	10.36	37ele	16.79	14.26	12.139	10.36	0.00
2.	16.69	14.19	12.141	10.35	37ele	16.67	14.17	12.141	10.35	0.00
3.	26.48	16.15	14.318	10.33	19ele	26.48	16.13	14.312	10.35	+0.19
4.	27.4	16.69	14.31	10.35	19ele	27.4	16.68	14.31	10.35	0.00
5.	25.89	15.81	14.31	10.33	19ele	25.89	15.77	14.31	10.36	+0.29
6.	26.35	16.04	14.32	10.35	19ele	26.35	16.04	14.32	10.35	0.00
7.	26.26	15.98	14.317	10.35	19ele	26.25	15.98	14.311	10.36	+0.09
8.	25.88	15.74	14.32	10.36	19ele	25.89	15.74	14.32	10.36	0.00
9.	25.34	15.49	14.28	10.37	19ele	25.33	15.49	14.278	10.37	0.00
10.	26.06	15.93	14.29	10.35	19ele	26.05	15.91	14.29	10.36	+0.09
11.	25.28	15.73	14.3	10.31	19ele	25.66	15.73	14.296	10.31	0.00
12.	26.27	16.09	14.3	10.31	19ele	26.27	16.09	14.289	10.33	+0.19

UO_2 green pellets exhibit spring back effect due to recovery of elastic strain on withdrawal of pressing load. The UO_2 green pellet expands on diameter by about 1.1–1.3% on ejection from the press die. The end cap defect and fine cracks were found to be predominant in the cases where the elastic strain or diameter expansion is on the higher side. In order to counter the elastic stress/strain, addition of 3–5% U_3O_8 (ADU converted) was found to solve the problem. U_3O_8 probably acts as a cementing agent which restrain the spring back stress.

A typical density reject boat is found to have on an average 40–50% pellets having higher than 10.45g/cc. Attempt was made to retrieve the acceptable density pellets from the density reject boat. Density measurement of 100% pellets of the density reject boat is a time consuming laborious process. Instead a salvage process was successfully developed to sort out the low density pellets using a simple technique which relies on the fact that sintered pellets having diameter more than a cut off diameter are low density pellets and pellets having diameter less than cut off diameter are acceptable density pellets. Pre-grinding of pellets to this cut off diameter produces clear appearances based on their initial sintered diameter, which are utilized for sorting.

The following sections of the paper discuss the process techniques attempted and discuss the results obtained:

2. Experiments and analysis of low density phenomenon

2.1 Experiments with reduced charge quantity

Since the coring and associated low density was predominant in the bottom most layer of the boat, sintering experiment was conducted marking the centrally located pellets in the top most and bottom most layer of the boat. Experiments were also conducted to measure the density of pellets in top layer and bottom layer for boats with reduced charge (60% charge, 12 kg instead of 20 kg) keeping the two layers empty from bottom of the boat. Table 4 shows the density results to indicate that density difference between the top layer and bottom layer do exist and difference is minimized for the reduced charge having empty layers in the bottom.

Based on the experimental results, one furnace F3 was operated with reduced charge for many consecutive powder lots and compared with sintering results with other furnaces having full charge boats. It was observed that the sintering recovery of reduced charge boats in furnace F3 was much higher compared to the other furnaces (Figure 10). But for the next succeeding powder lots, the benefit of reduced charge gradually died down (Figure 11). The increase of impurity in the raw material could be the main reason for low density observed even in reduced charge boats.

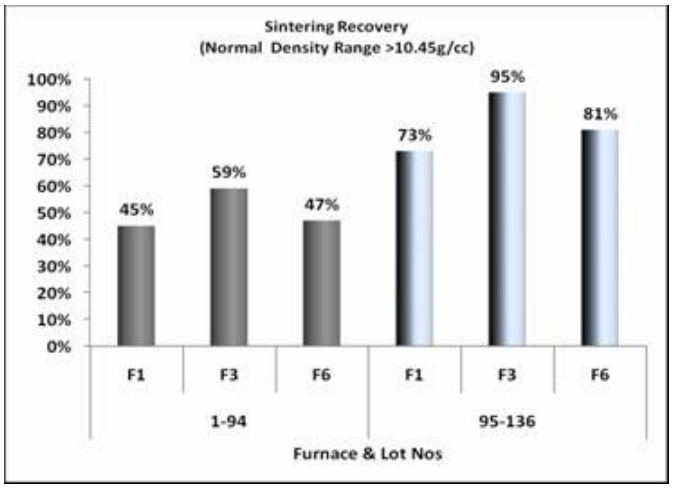

FIG. 10. Higher sintering acceptance for reduced charge in F3.

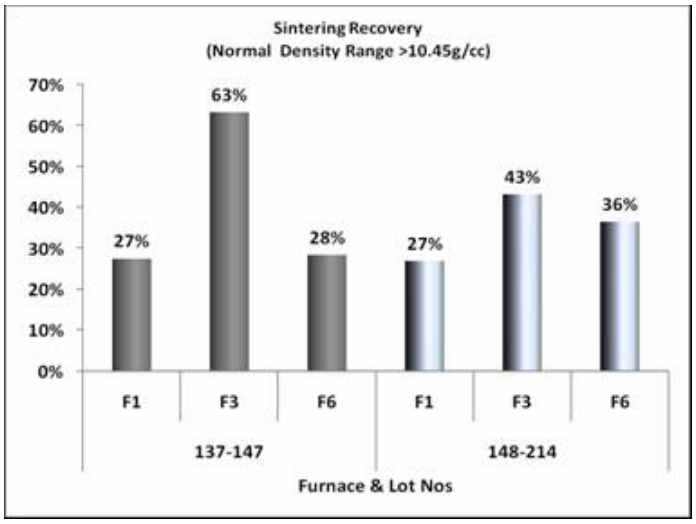

FIG. 11. Gradual decrease in advantage of reduced charge in F3 for succeeding lots.

TABLE 4. LAYER WISE DENSITY EXPERIMENT

Sl. No.	Boat No.	Lot No.	Pellet No.	Position in Boat	Green Density	Sintered density	Remarks
1	F6/702	NU-93	4–6 10–12	Top layer centre	5.53–59	10.63/65/69/64/ 67/70	5 layer horizontal charging
	F6/702	NU-93	1–3 & 7–9	Bottom layer centre	5.54–57	10.51/45/46/48/ 41/44	5 layer horizontal charging
2	F6/703	NU-93	16–18 & 22–24	Top layer centre	5.75–80	10.64/69/64/68/ 68/71	5 layer horizontal charging
	F6/703	NU-93	13–15 & 19–21	Bottom layer centre	5.75–77	10.67/58/39/46/ 48/50	5 layer horizontal charging
3	F6/728	NU-87 RR	7,8,10,12	Top layer		10.64/61/65/67	5 layers vertical charging
		NU-87 RR	1,2,4,5	Bottom layer		10.46/54/54/57	
4	F3/822	NU-55	15–24	Top layer	5.50–53	10.50–58	5 layer vertical charging
		NU-55	3–12	Bottom layer	5.43–53	10.38–58	5 layer vertical charging
5	F6/615	77ADU doped	7–12	Top layer	578–85	10.64–70	5 layer vertical charging
			1–6	Bottom layer	578–85	10.57–68	5 layer vertical charging
			7L–12L	Top layer	5.52–62	10.64–68	5 layer vertical charging
			1L–6L	Bottom layer	5.52–62	10.39–62	vertical charging on Mo Sheet
6	F6/589	NU-72	7–12	Top layer	5.84–89	10.52–76	3 layer vertical charging
			1–6	Bottom layer	5.84–89	10.45–59	
7	F6/590	NU-72	19–24	Top layer	5.84–89	10.55–60	3 layer vertical charging
			13–18	Bottom layer	5.84–89	10.42–52	
8	F6/591	NU-72	31–36	Top layer	5.84–89	10.52–61	3 layer vertical charging
			25–30	Bottom layer	5.84–89	10.45–53	
9	F6/592	NU-72	40–42	Top layer	5.84–89	10.56–62	5 layer horizontal charging
			37–39	Bottom layer	5.84–89	10.39–44	
10	F6/593	NU-72	43–44	Bottom layer	5.84–89	10.42–45	5 layer Horizontal charging
11	F6/594	NU-72	52–54	Top layer	5.84–89	10.55–59	5 layers vertical charging
			49 –51	Bottom layer	5.84–89	10.39–67	

2.2 Sinterability experiments in Nitrogen atmosphere in Dilatometer

The prevalence of low sintered density or coring in the bottom layer pellets give indications that there could be a thermal lag or lack of hydrogen exposure to the bottom layer pellets. During delayed reduction of O/U in UO_{2+x} , pellet can start densifying at a much faster rate like in oxidative sintering. Nitrogen being significantly heavier component than hydrogen and due to gradient of gas flow at the top of the boat and at bottom of the boat, the atmosphere prevailing in the bottom of the hearth could be excessive nitrogen rich atmosphere. In order to examine the sintering results in nitrogen atmosphere, sintering run was taken at 1700 ℃ in nitrogen atmosphere and shrinkage/sintered density was compared with sintering run in N_2 + 4%H_2 atmosphere (Figure 12). The green pellet was heated at a rate of 2 ℃/min and soaked for one hour at 1700 ℃. The% shrinkage of pellet in nitrogen atmosphere was higher even at lower temperature than that in N_2 + H_2 atmosphere at higher temperature. Since the pellet shrinks at a faster rate in nitrogen atmosphere at lower temperature, it is likely to end up with low sintered density due to entrapment of nitrogen gas in the closed pores. Out of the three samples pertaining to three lots, two samples ended up with low density in sintering run in nitrogen atmosphere provided from commercial nitrogen cylinder (about 500ppm Oxygen). The sample that sintered to 10.34 g/cc in nitrogen atmosphere also reveal duplex grain structure, coarser grain in the central region and finer grains in the peripheral region (Figure 13). The polished and etched microstructure reveals the presence of U_4O_{9-y} phase precipitated in the shape of interwoven dendritic structure over the UO_2 grains (widmanstaetten structure). Oxidative sintering gives rise to in-homogenous grain structure [1]. Hence, pellet in the bottom layer of the boat not freely exposed to flowing cracked ammonia but exposed to nitrogen rich atmosphere can produce in-homogenous microstructure leading to low density.

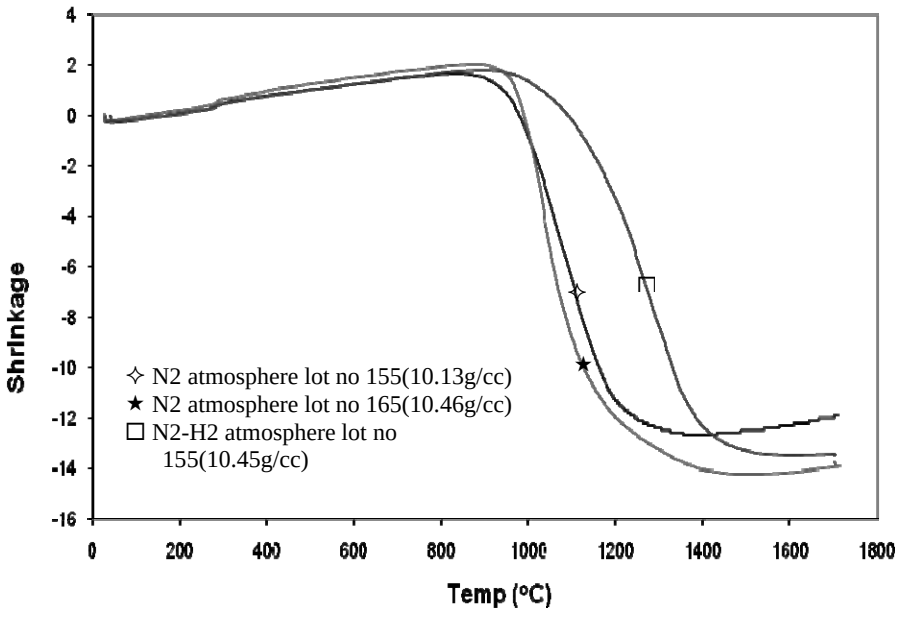

FIG. 12. Comparison of shrinkage in nitrogen and nitrogen-hydrogen atmosphere.

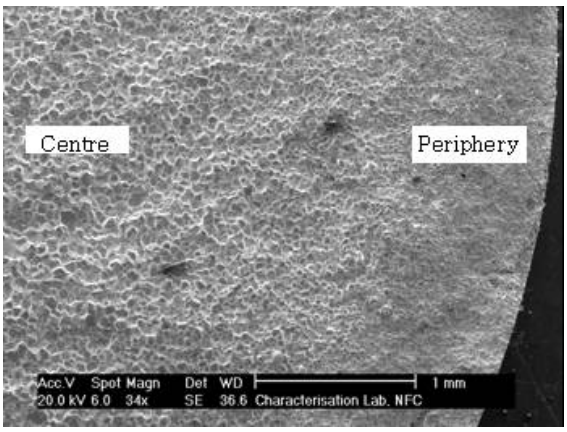

FIG. 13. Duplex grain structure evolved in sintering under nitrogen atmosphere.

3. Doping of fine grade ADU

Filtered ADU cake is made to form slurry and then spray dried at about 120^{o}C using a disc atomizer. LPG fired heat is utilized in the spray drier to dry the droplets under negative pressure. The flu gas containing ultrafine ADU particles passes through a bag filter. During auto cleaning cycle of the bag filter, fine ADU particles get separated from the filter and get collected in a container. This filter retrieved ADU is normally recycled in the acid dissolution step of powder preparation. The sintering rejections are observed to be more prevalent for lots having a skewed distribution of particle sizes and having higher percentage of coarser fraction (Figure 14). Sintering behavior is relatively better for powder lots having normal distribution of particle sizes with much lesser coarser fraction (Figure 15). The bag filter retrieved ADU was used in doping with UO_2 granules for improving the sintered density of the pellet. The typical particle size distribution of the ultra fine ADU is given in Figure 16. The doping was done in batches of 50–60 kg granules. After addition of organic lubricant and fine grade ADU, the cylindrical granule container was tumbled in the same horizontal roller tumbler used for admixing of solid lubricant with granules (Figure 17). The doping of fine grade ADU is found to improve the sinterability of the powder lot. ADU doping showed encouraging sintering results even for powder lots with skewed distribution. Doping of 0.5–1.0% ADU gave rise to best results from density as well as integrity point of view. The sintered density results are depicted in Table 5. The following observations were made :

(i) Change in green density is marginal with ADU doping

(ii) Out of total 39 boat experimented in 8 lots, 36 boats got sintered to normal acceptable density, 2 boats sintered to the density range greater than 10.35g/cc and 1 boat sintered to greater than 10.40g/cc. The density up gradation is lower in 0.5% ADU doping than 1% ADU doping. Sintering acceptance in ADU doped material is much higher (about 92%) as compared to that in un-doped material of same powder lots (30–50%)

(iii) Doping of 0.5% ADU does not produce surface defects, where as doping > 0.5% leaves crazing crack like appearance on surface of pellets, though surface finish of ground pellets are not affected. Still finer grade ADU material is desirable to produce high density sintered pellets devoid of fine cracks.

(iv) Hydrogen and nitrogen values in sintered pellets are not different from normal values.

(v) The sintered pellet microstructure (Figure 18 and Figure 19) in central region and peripheral region are uniform in nature except presence of fine crack predominant in peripheral region.

The fine grade ADU gets directly converted to fine grade UO_2 by self reduction under hydrogen atmosphere [2]. The conversion proceeds through various heat reactions as per the increasing temperature. The conversion proceeds without formation of intermediate U_3O_8. Thus unlike U_3O_8, ADU is not a pore former in UO_2 matrix in direct reduction atmosphere. In stead it enhances the sinterability by enhancing the surface energy of the UO_2 pellet.

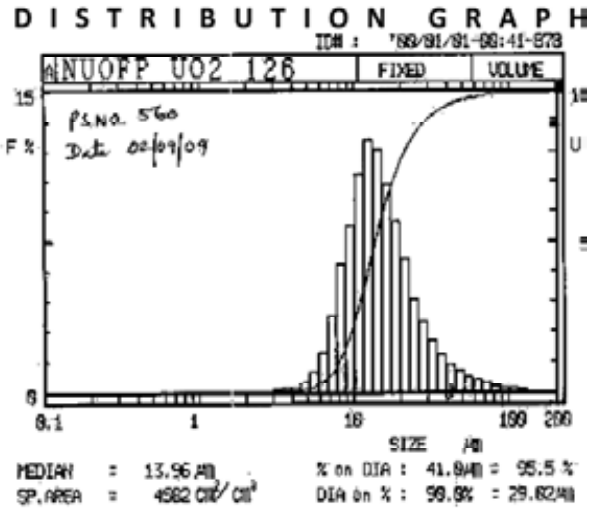

FIG. 14. Typical normal distribution of UO_2 particles.

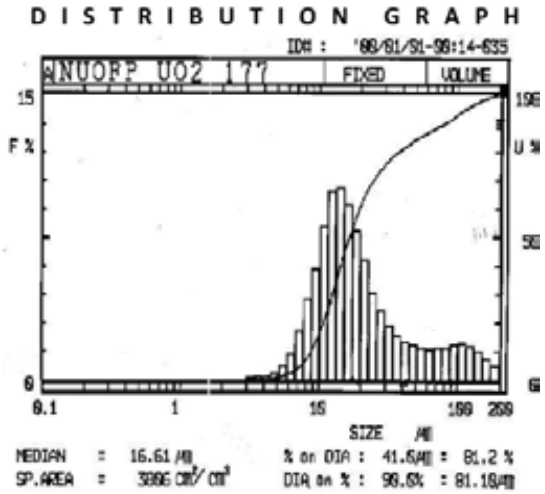

FIG. 15. Typical skewed distribution of UO_2 particles.

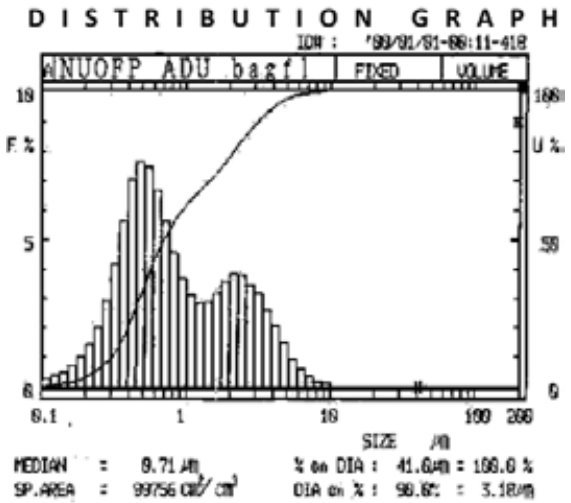

FIG. 16. Typical particle size distribution of fine grade ADU.

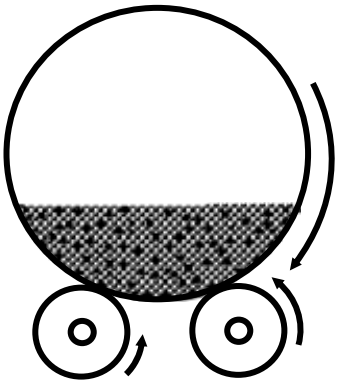

FIG. 17. Cylindrical rollers for in-container blending of granules.

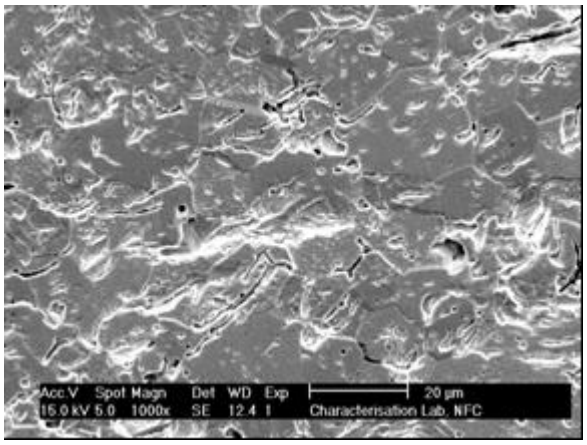

FIG. 18. Micrograph of ADU doped pellet (peripheral region).

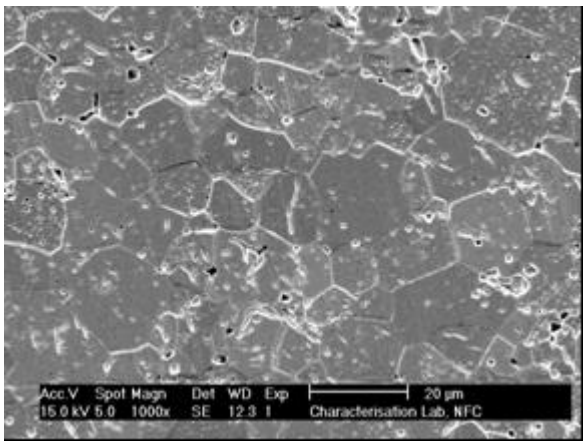

FIG. 19. Micrograph of ADU doped pellet (central region).

TABLE 5. RESULTS OF ADU DOPING

Sl. No.	Boat No. (Furnace/Boat)	Lot No. (Lot recover)	% Doping	Green Density	Sintered density	Remarks
1	F-6	NU-985	2%	5.76 - 5.83	10.54 - 10.66	2cycles green pellets made and sintered. Surface marks seen. N=59 ppm;
2	F-6	NU-997	1%	5.83 - 5.84	10.54 - 10.66	3 cycles, N=42 ppm Surface cracks seen
			2%	5.80 - 5.82	10.55 - 10.67	
			3%	5.70 - 5.74	10.46 - 0.56	
3	F1/367	NU-1000	2%	5.75 - 5.77	10.61 - 10.66	N=131ppm crazing marks as surface. Surface finish OK. 100kg sintering
	F3/482	NU-1000	do	do	10.49 - 10.57	
	F6/107	NU-1000	do	do	10.56 - 10.60	
	F6/108	NU-1000	do	do	10.54 - 10.58	
4	F2/996	NU-14	1%	5.76/88	10.52 / 10.62	N=66ppm
	F2/997	NU-15	1%	do	10.35 / 10.56	N=61ppm; C1
	F2/999	NU-15	1%	do	10.59 / 65	Diluted crazing marks. Surface Finish OK (150kg)
	F3/546	NU-15	1%	do	10.58 / 60	
	F3/565	NU-15	1%	do	10.55 / 62	
	F6/201	NU-14&15	1%	do	10.50 / 58	
5	F1/747	NU-53	0.5%	5.78/5.85l	10.68 / 73	No surface defects, 50kg sintering, N=70ppm
	F2/231	NU-53	0.5%	do	10.45 / 69	
6	F1/801	NU-63	0.5%	5.82/5.88	10.51 / 68	No surface defects, 250kg sintering, N=145ppm
	F1/802	NU-63	0.5%	do	10.54 / 62	
	F6/538	NU-63	0.5%	do	10.51 / 70	
	F6/539	NU-63	0.5%	do	10.51 / 68	
	F6/540	NU-63	0.5%	do	10.54 / 74	
7	F1/867 to 871	NU-73	0.5%	5.72/79	10.50/67	No surface defects, 275kg sintering, N=81ppm
	F6/604 to 609	NU-73	0.5%			
8	F6/615	NU-77	0.5%		10.51/10.66	25kg sintering
9	F1/961 to 965 F2/444 F3/30 F3/31 F6/699 F6/700	NU-92		5.76/82	Out of 10 boats 8boats are 10.47/69 one boat 10.37/62 & one boat 10.42/68	No surface defects, 250kg sintering, N=71ppm

4. Doping of fresh U_3O_8 (converted from ADU)

Unlike metal powder, UO_2 being ceramic in nature undergoes only elastic deformation and rearrangement of particles during application of load in compaction. On withdrawal of load, the pellet expands in all direction (spring back effect) proportional to the elastic deformation of particles due to recovery of elastic strain. The spring back is normally accommodated in a controlled manner by suitable design of ejection taper of the pressing die and a suitable over pressure on pellet during ejection from the die. The elastic deformation and recovery of elastic strain for the same pressing load depends on hardness of particles, hence may vary in powder lots. The excess spring back in certain powder lots in excess of 1.4% tends to increase the end cap and fine cracks in pellets (Figure 20 and

Figure 21). The onset of end chip or end cap was detectable in green pellet by acetone dip test of the pellets. The end discontinuity is identified by evolution of bubbles on dipping the pellet in acetone. In order to control the spring back, fresh U_3O_8 (derived from ADU) was doped (3-5% by wt.) with UO_2 granules. Addition of U_3O_8 was done along with addition of organic lubricant and all other parameters of blending remained unaltered. In all about 4500 kg UO_2 powder consisting of nine lots was processed by doping U_3O_8 powder with UO_2 granules. The visual defects like end cap and cracks were controlled after doping U_3O_8 (Figure 22(a) and (b)). The typical acceptable pellet free from end cap and cracks are shown in Figure 23. There was a remarkable improvement in visual acceptance in the successive lots after doping of U_3O_8 (Figure 24). The following observations were made during process:

i) The green density was attained at normal pressing load and the density difference with or without doping was marginal.

ii) The improvement in physical integrity after addition of U_3O_8 was very clear by comparing the integrity in acetone dip test of the green pellets made with or without doping U_3O_8.

iii) The pressing became smoother and the green pellets were shiner than that produced from un-doped material.

iv) The sintered density apparently dipped marginally with addition of 5% U_3O_8.

v) The sintered pellet microstructure (Figure 25 and Figure 26) show uniform grain and pore size in the central and peripheral region of the acceptable density pellet. Low density pellets did not show any coring defect in microstructure.

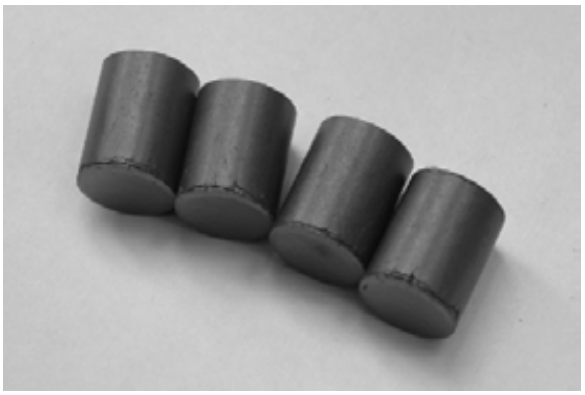

FIG. 20. Typical end caps on sintered pellets.

FIG. 21. Typical visual cracks on sintered pellets.

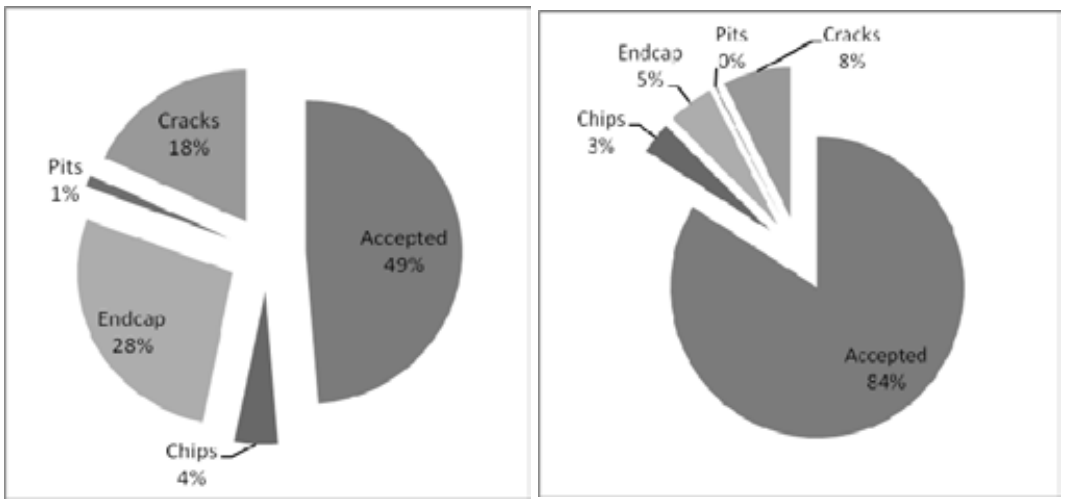

(a) Defects before doping. *(b) Defects after doping.*

FIG. 22. Visual acceptance before and after doping U_3O_8.

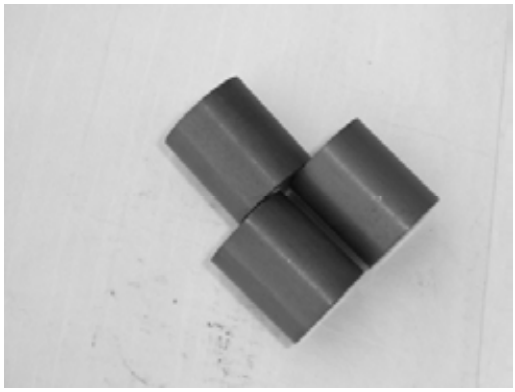

FIG. 23. Typical defect free pellets after U_3O_8 doping.

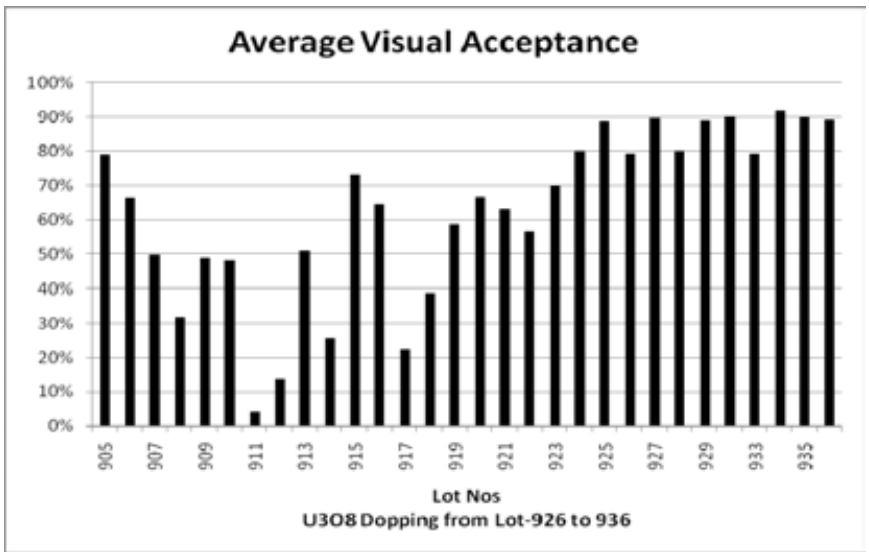

FIG. 24. Improvement in visual acceptance after U_3O_8 doping from lot 926.

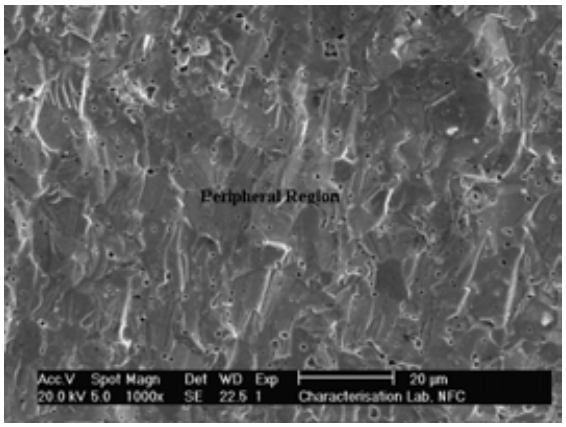

FIG. 25. Micrograph of U_3O_8 doped pellet (peripheral region).

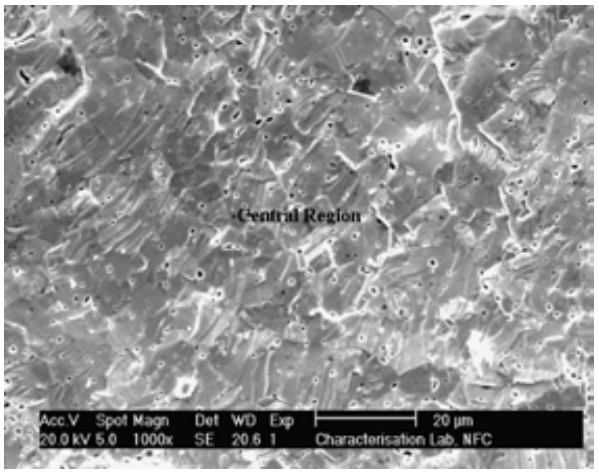

FIG. 26. Micrograph of U_3O_8 doped pellet (central region).

5. Technique to retrieve acceptable density pellets from density reject boats

The typical density distribution in a density reject boat is shown in Figure 27. Since the sintering densification is associated with shrinkage on diameter, the sintered density and diameter of sintered pellets are inter related. Higher the diameter, lower is the sintered density and vice versa. This relation hold good in a system where green diameter is approximately constant and green density is maintained in a close range. Such control was done by process control on green compaction and use of wear resistant tungsten carbide dies in the compaction press. The technique involves pre-grinding of all the pellets of the density reject boat in a centreless grinding machine to a cut off diameter which corresponds to a sintered density of 10.50 g/cc as per theoretical calculation. The pellet having low density below 10.50 g/cc will get fully ground giving a particular appearance different from acceptable density pellets that will either remain unground or be partly ground at ends leaving an un-ground appearance at the centre. The relation between the sintered density and the sintered diameter is worked out as below:

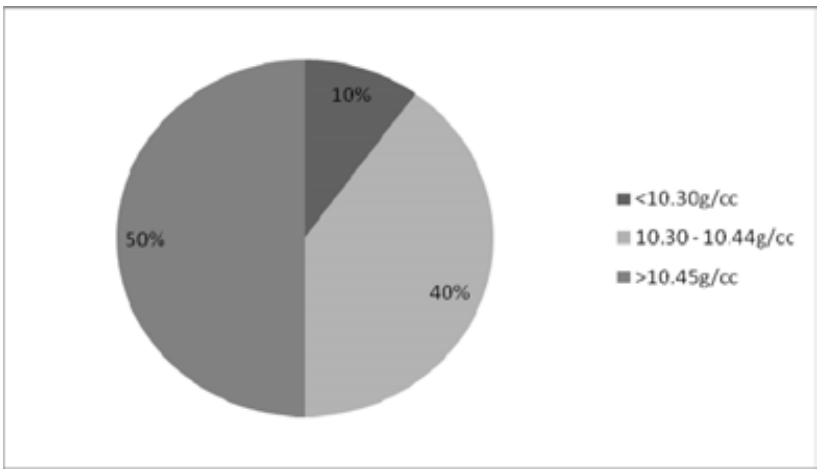

FIG. 27. Typical distribution of sintered density in a boat.

Considering negligible change of mass of pellet after sintering, following relation holds good:

$$\rho_g (\pi/4) d_g^2 l_g = \rho_s (\pi/4) d_s^2 l_s$$

Where ρ_g — Green density of pellet
d_g — Diameter of green pellet
l_g — Length of green pellet
ρ_s — Sintered density of pellet
d_s — Diameter of sintered pellet
l_s — Length of sintered pellet

$$\therefore d_s = \left[\frac{\rho_g d_g^2 l_g}{\rho_s l_s} \right]^{1/2}$$

The length to diameter ratio remains approx. constant before and sintering. Hence the above relation can be written as,

$$\therefore d_s = \left[\frac{\rho_g}{\rho_s} \right]^{1/3} d_g$$

The diameter of the green pellet being approximately constant i.e. 17.95mm for PHWR 220 MW(e), a relation curve (Figure 28) is evolved as per the relation between green density versus sintered diameter. If the sintered pellets having appearance as (Figure 29) of a density reject boat are ground as per the relational diameter, the pellets will have any one of the appearances as in Figure 29 (a) to (d). Low-density pellets are sorted out after initial grinding as per the specific appearances in Figure 29 (a) and (c); whereas targeted acceptable density pellets (Figure 29 (b) and (d)) are subjected to sample density check. Four times higher sampling size (16 pellets) are randomly selected to measure the densities for quality clearance. Normally about 90% pellet trays get accepted and join the main production stream. 10% pellet trays might bring deviation due to human error in sorting which is again subjected to sorting and clearance.

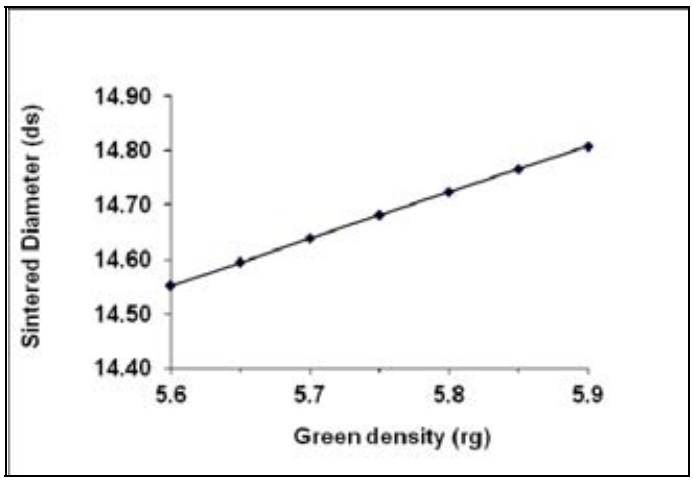

FIG. 28. Green density vs. sintered diameter.

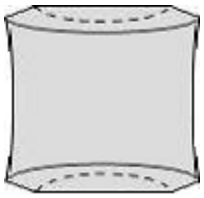

FIG. 29. Sintered pellet before grinding.

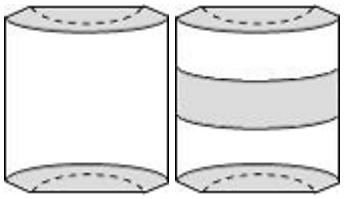

Figure 30 (a) Fully ground surface. Figure 30 (b) Un-ground patch at centre.
(Low Density Pellet) (Acceptable Density Pellet)

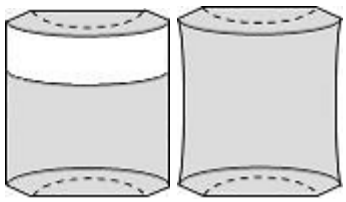

Figure 30 (c) Un-ground patch at off-centre. Figure 30 (d) Fully un-ground surface.
(Low Density Pellet) (Acceptable Density Pellet)

FIG. 30. (a) to (d). Appearances of acceptable density and low density pellets after pre-grinding.

6. Discussion

UO_2 powder is being produced at NFC following the ammonia gas precipitated ADU route. Previously aqueous ammonium hydroxide was used for precipitation of ADU. The process change was to derive productivity related advantages in the powder production processes. Recently the un-safeguarded facility is given to use low grade yellow cake (MDU) from a new raw material source plant in India. The period of onset of low density problem in sintered pellets coincides with the start of consumption of low grade MDU in the plant. The problem is not the uniform low sintered density in the pellets but the occurrences of density variations and in-homogenous microstructure in the pellets.

The physical and chemical in-homogeneity of the starting UO_2 powder produced through a particular route greatly influences the sintered density and microstructure of UO_2 fuel [3]. But though the starting MDU bears higher impurities like sulphate, carbonate, chlorides, etc. in excess of specifications, the impurities are yet to be detected in pure uranyl nitrate solution or in UO_2 powder. Among the physical characteristics, the particle size distribution is found to change at times i.e. from normal distribution to skewed distribution characterized with presence of higher fraction of coarser size particles. The coarser size particles are likely to pack with larger voids in green pellet which may not close during sintering. Hence powder lots having such skewed distribution exhibits variation in sintered density. On the contrary, an uniform normal distribution of particle sizes are likely to produce uniform smaller pores in green pellets that are likely to sinter with higher sintered density. The duplex grain structure with coring defect in sintered pellet associated with nitrogen pick up might be originating from the following process conditions:

i) The excess sulphate, carbonate impurities present in yellow cake and some organic carry over from wet process to dry UO_2 powder might be contributing sulpher and carbon pick up in UO_2 powder. The presence of sulpher is known to cause exaggerated grain growth during sintering [3]. Presence of carbon can aggravate nitrogen pick up in the form of uranium mono nitride as per the reaction: $UO_2 + C + N_2 + H_2 \rightarrow UN + CO + CH_4$ [4]. Under sintering condition, the sulpher and carbon are expected to react with hydrogen to go out of the pellet. However the pellets located interior to the boat might not be exposed to hydrogen as effectively as pellets located at top layers or located near external periphery of the boat. Hence in case of restricted exposure to hydrogen, sulphur and carbon may go out from the surface by reacting with hydrogen but may get trapped in the core of the pellet resulting in coring and nitrogen pick up. In case of excessive sulphur impurity, exaggerated grain growth is expected throughout the pellet.

ii) Another mechanism of in-homogenous microstructure and coring is based on early shrinkage and faster rate of shrinkage at lower temperature under higher partial pressure of oxygen in the pellet. Enhanced rate of shrinkage takes place due to enhanced mobility of U atom under increased U vacancy in the UO_2 lattice and the diffusion co-efficient of U increases at a rate proportional to x^2 [5]. This is expected during delayed reduction of O/U in UO_{2+x} from the total pellet or from the core of the pellet depending on the extent of accessibility of hydrogen to the pellet [6]. There is a possibility of gas entrapment in the pellet core during faster shrinkage situation. Gas entrapment might not allow pores to shrink. In order to reduce the free energy of the system, the grain coarsening and pore coarsening will be favored leading to larger grain, larger pore in the core of the pellet. The occurrence of coring defect is prevalent in pellets located in bottom layer of the pellets. The sintering boat uses a molybdenum box or shroud that covers the pellet stack from all sides. The green pellets standing near the walls of the box might impede the flow of hydrogen inside the boat. Hydrogen being a lighter gas may not reach the bottom layers as effectively as it reaches the top layers of the boat. This could be the reason that the density of pellets located in bottom interior locations is always lesser than the top layer pellets.

Doping of ADU is found to enhance sintering and enable pellets even in bottom layer to sinter without duplex grain structure or coring. ADU doping might not help in case the abnormal grain coarsening is due to presence of sulpher and other impurities. Fine grade ADU incorporates finer UO_2 particles uniformly in the pellet. This could be one reason for density improvement. ADU while converting to UO_2 produces ammonia which can enhance the reduction of UO_{2+x} to UO_2, thus not allowing core to densify at a faster rate with respect to pellet surface. This could be the other reason of density

improvement through doping ADU. The finer the ADU particles used for doping, the better is the integrity of the sintered pellet.

Addition of limited quantity U_3O_8 with UO_2 increases the mechanical strength and integrity of the green pellet [7]. U_3O_8 might be acting as cementing agent between the UO_2 particles. The cementing action of U_3O_8 might be controlling the elastic recovery stress on UO_2 particles. However, addition of U_3O_8 is to be limited to about 5% because a higher percentage is likely to reduce the sintered density since it acts as a pore former in the UO_2 system. The method of retrieval of acceptable density pellet discussed in the paper is based on the very basic principle of densification and shrinkage of diameter. The method is accurate and result oriented provided the green density and green diameter are controlled during continuous production.

7. Conclusion

High sintered density (96–98% TD) defect free pellets are the requirement for PHWR fuel. The variations in sintered density from acceptable density range to low density range occur due to in-homogenous microstructure originated from abnormal grain growth during sintering. The large grains and large pores may prevail throughout the fuel matrix or may be limited to the central region of the fuel pellet called coring defect. Densification of UO_2 fuel pellets is primarily dependent on physical and chemical characteristics of UO_2 powder especially the purity, O/U and particle size distribution. Presence of some impurity elements like sulphur can cause abnormal grain growth during intermediate stage of sintering leading to the duplex grain structure. Coring can be evolved from the situation of restricted exposure of hydrogen to the pellet. The pellet core may start sintering at a differential faster speed than the pellet surface because of higher oxygen partial pressure inside the pellet core i.e. due to lack of reduction of O/U from the core. The closed packed layer wise charging of pellets in the boat surrounded by shroud made of perforated molybdenum sheet might impede the flow of hydrogen gas to the interior pellets. Presence of carbon and nitrogen entrapment in UO_2 pellet might be the reason of nitrogen pick up in sintered pellets.

Doping of fine grade ADU was helpful in avoiding coring defect. Finer grade ADU is desirable to avoid fine cracks in the doped fuel. Doping of about 5% U_3O_8 significantly reduced the integrity defects like end chip, end cap and cracks in UO_2 fuel pellets. U_3O_8 acts as a cementing agent for restraining the spring back stress. The technique for retrieval of acceptable density from density reject boats relied on the basic relation between shrinkage on diameter and densification. Sorting of low density pellets based on pre-grinding surface appearance was an innovative concept. The technique was developed successfully in production scale and is effective because of control of the green diameter and green density.

REFERENCES

[1] ASSMANN, H., et al., Control of UO_2 microstructure by oxidative sintering, Journal of Nuclear materials **140,** (1986), p.1–6.

[2] WOLFREY, J.L., Surface area changes during the calcinations of ammonium urinate, Australian Atomic Energy Commission, AAEC/E329.

[3] GLODEANU, F., et al., Correlation between UO_2 powder and pellet quality in PHWR fuel manufacturing, Journal of Nuclear Material **153,** (1988), p.156–159.

[4] MUROMURA, T., et al., Formation of uranium mono nitride by the reaction of uranium dioxide with carbon in ammonia and a mixture of hydrogen and nitrogen, Journal of Nucl. Material, **71**, (1977), p.65.

[5] KUTTY, T.R.G., et al., Densification behavriour of UO_2 in six different atmospheres, Journal of Nuclear Materials **305,** (2002), p.159–168.

[6] ZAWIDZKI, T.W., et al., Effect of sulfur on grain growth in UO_2 pellets, Journal of the American Ceramic Society", 31st Pacific coast regional meeting, (1978), Paper No. 38–N–78p.

[7] KUN WOO SONG, et al., Grain size control of UO_2 pellets by adding heat-treated U_3O_8 particles to UO_2 powder, Journal of Nuclear Materials **317**, Issues 2–3, (2003), p.204–211.

Studies on the Sintering Behaviour of UO_2-Gd_2O_3 Fuel Pellets

M. Durazzo[a], H.G. Riella[b]

Abstract. The incorporation of gadolinium directly into nuclear power reactor fuel is important from the point of reactivity compensation and adjustment of power distribution enabling thus longer fuel cycles and optimized fuel utilization. The UO_2-Gd_2O_3 poisoned fuel is being proposed to be implanted in Brazil according to the future requirements established for Angra II nuclear power plant. The incorporation of Gd_2O_3 powder directly into the UO_2 powder by dry mechanical blending is the most attractive process because of its simplicity. Nevertheless, processing by this method leads to difficulties while obtaining sintered pellets with the minimum required density. This is due to blockages during the sintering process. There is little information in published literature about the possible mechanism for this blockage and this is restricted to the hypothesis based on formation of a low diffusivity Gd rich $(U,Gd)O_2$ phase. The objective of this investigation has been to study the blockage mechanism in this system during the sintering process, contributing thus, to clarify the cause for the blockage. Experimentally it has been shown that the blocking mechanism is based on pore formation because of the Kirkendall effect, instead the formation of low diffusivity phases. The formation of a solid solution during the intermediate stage of sintering leads to the formation of large pores, which are difficult to remove in the final stage of sintering. The phenomenon is better characterized as a concurrence between formation and elimination of pores during sintering than as a sintering blockage.

1. Introduction

The need to improve reactor performance through longer cycle lengths or improved fuel utilization has been apparent since the beginning of commercial nuclear power generation. Among several modifications introduced as a consequence, the initial fuel enrichment has been increased, which means that the additional amount of fissile material (^{235}U) in the reactor core has to be compensated by the introduction of additional neutron absorber material in the reactor core. The use of a burnable poison in nuclear reactors provides the necessary negative moderator reactivity coefficient at the beginning of core life and help shape core power distributions [1]. From a nuclear viewpoint, gadolinia is an excellent burnable poison, having a high neutron absorption cross section coupled to a burn up rate that, if properly designed, can match approximately the ^{235}U depletion, minimizing the reactivity penalty at end-of-cycle (EOC) [2,3]. The UO_2-Gd_2O_3 poisoned fuel is being proposed to be implanted in Brazil according to the future requirements established for Angra II nuclear power plant.

From the different methods for the conversion of UF_6 to ceramic grade UO_2 in industrial scale [4], the AUC (Ammonium Uranyl Carbonate) process [5] is the most attractive due to the smallest number of process steps involved. In the AUC process the Gd_2O_3 powder is incorporated to the UO_2 powder by the dry mechanical blending method. Then, the mixed UO_2 and Gd_2O_3 powder is directly pressed into pellet form, without co-milling, pre-pressing and granulating steps [6, 7]. Nevertheless, the incorporation of Gd_2O_3 powder to the AUC deriving UO_2 powder by the most attractive commercial method of dry mechanical blending leads to difficulties while obtaining sintered UO_2-Gd_2O_3 pellets with the minimum required density [7, 8]. This is due to the deleterious effect of the Gd_2O_3 on the traditional UO_2 sintering behaviour. The purpose of this work is to investigate the possible causes for explaining the bad sintering behaviour of the UO_2-Gd_2O_3 fuel prepared by the mechanical blending method.

Several researchers report on the sintering UO_2-Gd_2O_3 mixed oxides, a number of them pointing to difficulties in sintering fuel pellets with the minimal specified density, of around 94% of the theoretical density. Besides, a considerable disagreement between the published data can be observed. Despite the sintering conditions are not identical, the wide variation observed in the final densities of the sintered fuel pellets cannot be explained only based on this reason. The influence of the Gd_2O_3

[a] Nuclear Fuel Centre, Nuclear and Energy Research Institute — IPEN, Brazilian Nuclear Energy Commission — CNEN, São Paulo, Brazil
[b] Chemical Engineering Department, Santa Catarina Federal University, Florianópolis, Brazil

content into the fuel is evident in some sintering results, but it does not appear to be significant in the others. Figure 1 summarizes the final densities achieved by different researchers in sintering UO_2-Gd_2O_3 pellets under reducing atmosphere. A wide range of sintered densities can be observed in this Figure. Table 1 presents the main experimental conditions adopted in the sintering experiments.

The few sintering curves available in the literature show that the lower sintered densities are due to an abnormal sintering behaviour of the UO_2-Gd_2O_3 fuel, when compared with the sintering behaviour of the traditional UO_2 fuel. The dilatometric analyses show that at temperatures around 1100–1400^oC, the shrinkage of the UO_2-Gd_2O_3 pellets is delayed, the sintering rate is decreased and the densification is shifted to higher temperatures [7, 17, 18, 20]. Otherwise, sintering curves obtained in previous work [17] showed that the sintering blockage does not occur when the samples are prepared by the coprecipitation method through ADU (Ammonium Diuranate). In this case, very high sintered densities are achieved under the same sintering conditions adopted in the case of dry mechanical blending samples. The gadolinium distribution into the mixed powder is very homogeneous when the coprecipitation method is adopted. This method is mostly used in laboratories to produce homogeneous pellets [9, 21, 22].

As well as the densification results in sintering UO_2-Gd_2O_3 pellets are discrepant and contradictory, likewise are the mechanisms proposed to explain the sintering behaviour. According to Une and Oguma [15], when sintering UO_2-Gd_2O_3 fuel under reducing atmosphere, the system becomes hypostoichiometric to compensate electrically the incorporation of Gd^{3+} ions in the cubic fluorite-type structure of UO_2. Anion vacancies are formed to balance the electrical charge. In this condition, as in the case of the UO_2-PuO_2 system, the cation diffusivity decreases under hypostoichiometric conditions that prevail during sintering, which would explain the low sintered densities achieved while sintering UO_2-Gd_2O_3 fuel pellets. Davis and Potter [19] also attribute the low densities achieved in sintering UO_2-Gd_2O_3 to the hypostoichiometric situation caused by the substitution of U^{4+} ions by Gd^{3+} ions, which would reduce the cation mobility and, consequently, the densification during sintering.

In opposition to the above explanation, Ho and Radford [12] explain their high densities achieved in sintering UO_2-Gd_2O_3 fuel pellets with base in the formation of oxygen vacancies and oxidation of U^{4+} ions. According to these investigators, the electrical charge compensation due to the Gd^{3+} ions incorporation in the UO_2 fluorite structure is accomplished by the formation of oxygen vacancies and oxidation of U^{4+} ions to U^{5+} and/or U^{6+} ions. The oxidation of U^{4+} ions to U^{5+} and U^{6+} ions, which have smaller ionic radii, enhances the cation diffusion and leads to high sintered densities. Above a critical level of Gd_2O_3 addition (around 6 wt%) the diffusivity is inhibited due to the association of Gd^{3+} ions with U^{5+} or U^{6+}. In this case, the associated cations should moves only by cooperative transport, which reduces the sinterability of the system. According to Ho and Radford [12], the increase in the oxygen potential reduces the oxygen vacancies concentration and also allow the creation of oxygen interstitials, which would counterbalance the formation of the small size cations (U^{5+} and U^{6+}), reducing the diffusivity and, therefore, the sinterability. The association of cations also would be favoured.

Manzel and Dörr [7] attribute the low densities observed in sintering UO_2-Gd_2O_3 pellets to the formation of solid solution simultaneously with the densification process. During sintering, the diffusion processes lead not only to the densification but also to the formation of solid solutions. The interdiffusion processes decrease the sintering rate and shift the densification to higher temperatures. Assmann, Pehhs and Roepenack [8] complement this proposition by mentioning that the diffusion coefficients in the UO_2-Gd_2O_3 system depend in a complex manner on the U:Gd:O ratio in the generated oxide phases. Peehs, Dörr, Gradel and Maier [23] detected the presence of the $(U_{0.5}Gd_{0.5})O_2$ phase in sintered UO_2-Gd_2O_3 pellets, without, however, discuss its possible participation in the sintering blockage mechanism. In all these studies, the samples were prepared by the dry mechanical blending method, which used UO_2 powder derived from AUC. Once considered that the sintering blockage occurs during the solid solution formation, that the diffusion coefficient depends on the oxide phases formed and the observation of the $(U_{0.5}Gd_{0.5})O_2$ phase, it can be inferred that the cause proposed for the sintering blockage in the UO_2-Gd_2O_3 system is related to the formation of low diffusivity phases during the sintering process, which reduces the densification and leads to low sintered densities.

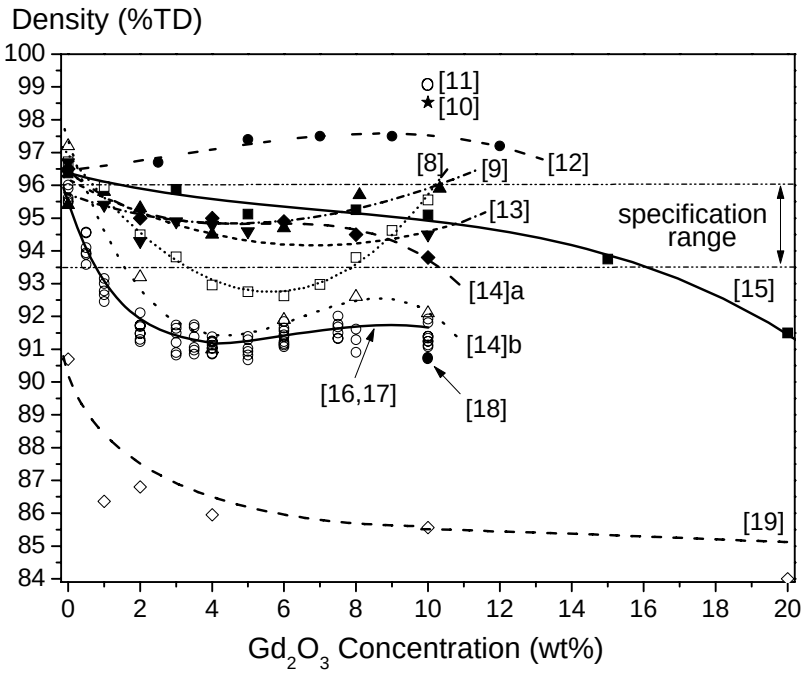

FIG. 1. Effect of gadolinia content on sintered density of UO_2-Gd_2O_3 fuel pellets. TD-theoretical density, specification range from ref. [8].

TABLE 1. MAIN EXPERIMENTAL CONDITIONS FOR THE DATA PRESENTED IN FIGURE 1

Reference	Sintering Cycle (temperature/time) °C/h	UO_2 BET (m^2/g)	Sintering Atmosphere	Method for Mixed Powder Preparation
[9]	1750/4	n.i.	$Ar/8\%H_2/H_2O$	coprecipitation
[10]	1650/4	n.i.	$N_2/8\%H_2/H_2O$	coprecipitation.
[11]	1750/4	n.i.	$25\%N_2/75\%H$	co-milling
[12]	1750/6	3.50	H_2/H_2O	co-milling
[13]	1620/3	1.60	pure H_2	co-milling
[14]	1700/2	4.37	pure H_2	co-milling
[14]	1700/2	6.65	pure H_2	co-milling
[8]	1750/2	n.i.	pure H_2	dry blend
[15]	1700/2	3.10	pure H_2	dry blend
[16,17]	1650/3	5.6	pure H_2	dry blend
[18]	1680/4	5.0	pure H_2	dry blend
[19]	1650/4	n.i.	$N_2/6\%H_2$	dry blend

n.i. — not informed.

Yuda and Une [20] proposed that the sinterability of the UO_2-Gd_2O_3 system could not just be evaluated from the viewpoint of cation diffusivity. According to these investigators the two peaks observed in their sintering rate curves correspond to the reaction between adjacent UO_2-UO_2 particles (first peak) and to the reaction between adjacent UO_2-Gd_2O_3 particles (second peak). They proposed the formation of large closed pores due to the difference in the sintering rates between UO_2-UO_2 particles and UO_2-Gd_2O_3 particles. As the large pores are formed in high temperatures, when the pore structure is already partially closed, they are difficult to be eliminated in the posterior sintering treatment. This effect is more intense in oxidizing atmospheres because the pore structure is already essentially closed when the larges pores are formed. This explains the lower density observed in UO_2-Gd_2O_3 pellets sintered under oxidizing atmospheres.

Nishida and Yuda [11] also explain the decrease in the density of samples sintered under higher oxygen potential atmosphere on basis of closed porosities formation. Despite the diffusivity of U and Gd ions is enhanced corresponding with the oxygen potential, under oxidizing atmospheres the effective diffusion length necessary to form solid solution is slightly elongated due to a barrier effect of closed porosities formation, which also results in sintered density decrease.

Song et al. [18] concluded that the sintered density of UO_2-Gd_2O_3 pellets is decreased due to the formation of new pores in the regions with high Gd concentration as the oxygen potential of the sintering atmosphere is increased. The delay of densification occurs together with the solid solution formation in the temperature range of 1300–1500 ^oC. While the formation of $(U,Gd)O_2$ progresses, new pores are produced at the original sites of Gd_2O_3 particles as a result of the directional diffusion of Gd ions into UO_2. The delay of densification is mainly attributed to the formation of new pores.

The sintering results presented in Figure 1 and the experimental conditions presented in the Table 1 indicate that the method for the UO_2-Gd_2O_3 mixed powder preparation exerts an important influence in the densification during the sintering process. This influence was confirmed by experimental results previously published, presented in Figure 2. The level of homogeneity of the gadolinium distribution in the UO_2 powder determines not only the final sintered density, as well as the form of the sintering curve. When the homogeneity of the gadolinium distribution is good, high densities are obtained during sintering and the sintering blockage is not apparent. On the other hand, when the homogeneity of the gadolinium distribution is bad, low densities are obtained after sintering and the sintering blockage is evidenced, which occurs in two stages [17]. The mechanism proposed by Une and Oguma [15] and Davis and Potter [19] to explain the sintering behaviour of the $UO_2Gd_2O_3$ fuel is not consistent with the results presented in Figure 2. When the gadolinium distribution into the fuel is good, as a solid solution (ADU coprecipitation route), high densities are achieved and no blockage is evidenced. So, the mechanism proposed by Ho and Radford [12] seems to be valid when the gadolinium distribution is homogeneous enough.

On the other hand, when the gadolinium distribution into the fuel is not homogeneous (dry mechanical blending route), the diffusion barrier formation mechanism proposed by Manzel and Dörr [7] (formation of phases with low diffusivity) seems to be possible. Also, the mechanism based on the pore formation during sintering [11, 18, 20] must be considered possible.

In this work, both the mechanisms considered possible are studied. Two hypotheses are proposed and experienced. The first one is based on the formation of low diffusivity $(U,Gd)O_2$ phase that would actuate as a diffusion barrier. The second one is based on the pore formation during sintering. An interesting observation in the UO_2-Gd_2O_3 sintering behaviour is related to the deleterious effect of the oxidizing atmosphere on the densification of UO_2-Gd_2O_3 pellets during sintering. There is a general agreement that the increase in the oxygen potential of the sintering atmosphere causes a significant decrease in the density of the UO_2-Gd_2O_3 pellets after sintering. Another interesting observation is the lower sintered densities observed by Agueda et al. [14] when UO_2 with higher specific surface is used to prepare the mixed powder (dry mechanical blending method). Based on the published data, it can be concluded that the mechanism to be proposed to explain the sintering behaviour of UO_2-Gd_2O_3 fuel pellets must consider the effect of the gadolinium distribution homogeneity into the UO_2-Gd_2O_3 powder, the effect of the oxygen potential of the sintering atmosphere and the effect of the specific surface of the UO_2 powder used to prepare de mixed powder by the dry mechanical blending method.

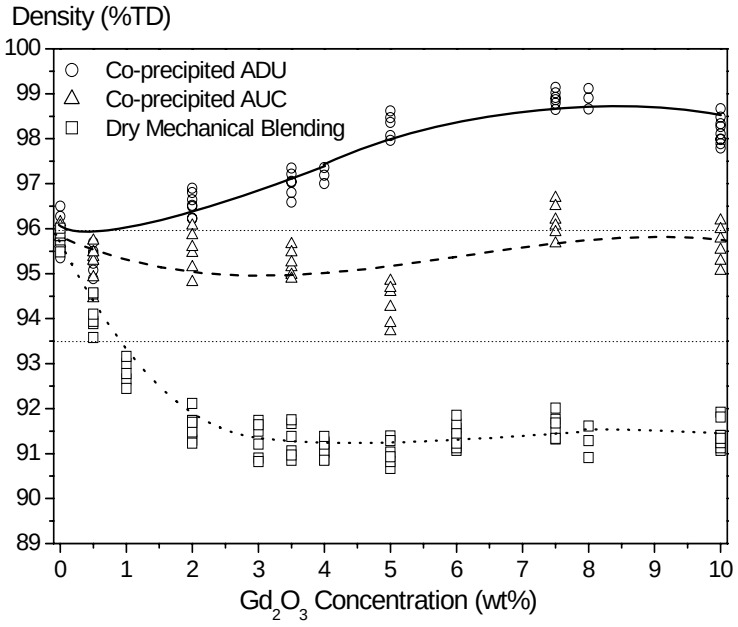

FIG. 2. Effect of the mixed powder preparation method on the sintered density of UO_2-Gd_2O_3 fuel pellets.

2. The diffusion barrier hypothesis

2.1 Phases in the UO_2-Gd_2O_3 system

Once the ADU co-precipitation method for UO_2-Gd_2O_3 powder and pellets preparation demonstrated to result in samples with a high gadolinium homogeneity degree (solid solution) [17], this method was selected for the preparation of samples containing concentrations of Gd_2O_3 from 0 to 100 wt%. These samples made possible the accomplishment of an investigation for verifying the existence of phases with low cation diffusivity in the $(U,Gd)O_2$ system, which could base the diffusion barrier hypothesis. The samples were prepared by coprecipitation from ADU, starting from mixed nitrate solutions, according to procedures previously reported [17].

The variation of the sintered densities as function of the molar fraction of gadolinium present in the sample demonstrates that exist ranges of gadolinium concentration for which the sintered densities are unequivocally decreased, as can be observed in Figure 3. An increase in the sintered density with the increase in the Gd_2O_3 concentration occurs up to 10 wt%, as presented in the Figure 2. This increase reaches a saturation starting from the composition $(U_{0.9}Gd_{0.1})O_2$, when a high densification level is maintained up to the composition $(U_{0.5}Gd_{0.5})O_2$. In this gadolinium concentration range the sintered densities remain in the range varying from 98 to 99% of the theoretical density. These high sintered densities can be explained according to the model proposed by Ho and Radford [12], in which the presence of Gd^{3+} ions causes an increase in the cation diffusivity and, therefore, an increase in the UO_2 sinterability.

When the number of Gd atoms outreaches the number of U atoms (Gd>0.5), the sintered densities decrease drastically and reach a minimum value for the composition $(U_{0.3}Gd_{0.7})O_2$. The further increase in the molar fraction of gadolinium increases the sinterability of the $(U,Gd)O_2$ system again, until reaching a maximum for the composition $(U_{0.2}Gd_{0.8})O_2$, when densities of about 93% of the theoretical density are obtained. After this densification peak, a new decrease in the sinterability is observed. Another minimum is observed in the composition $(U_{0.18}Gd_{0.82})O_2$, when the densification level rises again to reach the typical density for sintering pure Gd_2O_3 pellets (94% of the theoretical density). It is interesting to notice the behaviour of the curve presented in Figure 3 between the compositions $(U_{0.3}Gd_{0.7})O_2$ and $(U_{0.18}Gd_{0.82})O_2$, where it can be observed a peak in the sintered densities. This behaviour was confirmed through repetitions in sintering tests for the composition $(U_{0.2}Gd_{0.8})O_2$ and by sintering the intermediate compositions between Gd=0.7 and Gd=0.9.

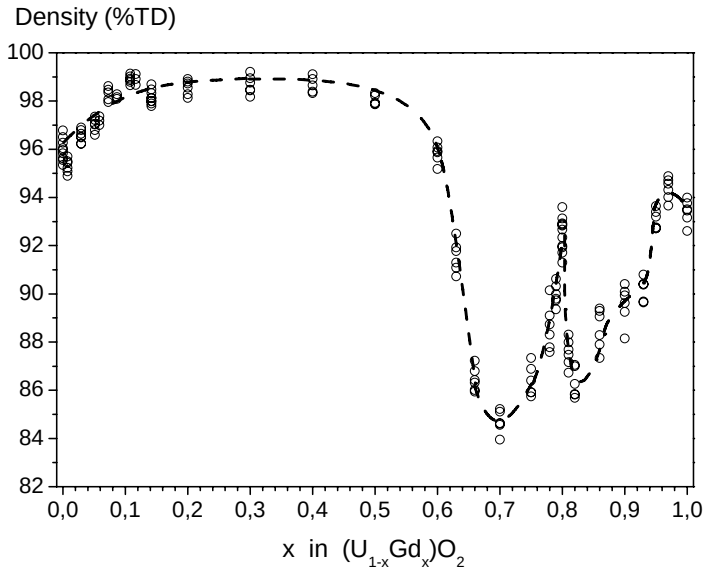

FIG. 3. Effect of the gadolinium concentration on the sintered density of (U,Gd)O_2 pellets prepared by coprecipitation.

The UO_2-Gd_2O_3 sintered pellets were milled and analyzed by X ray diffraction. The lattice parameters of (U,Gd)O_2 were determined with base on the diffractograms by analysing the 2θ position for the more intense (111) planes. Figure 4 presents the variation of the lattice parameter in function of the molar fraction of gadolinium in the sample. A linear decrease on the lattice parameter occurs for compositions up to $(U_{0.5}Gd_{0.5})O_2$, according Vegard's law. This observation indicates the presence of a single phase with fluorite type structure, with Gd^{3+} ions substituting U^{4+} (solid solution). Despite the inaccuracy of this data, a good adjustment for a line can be observed.

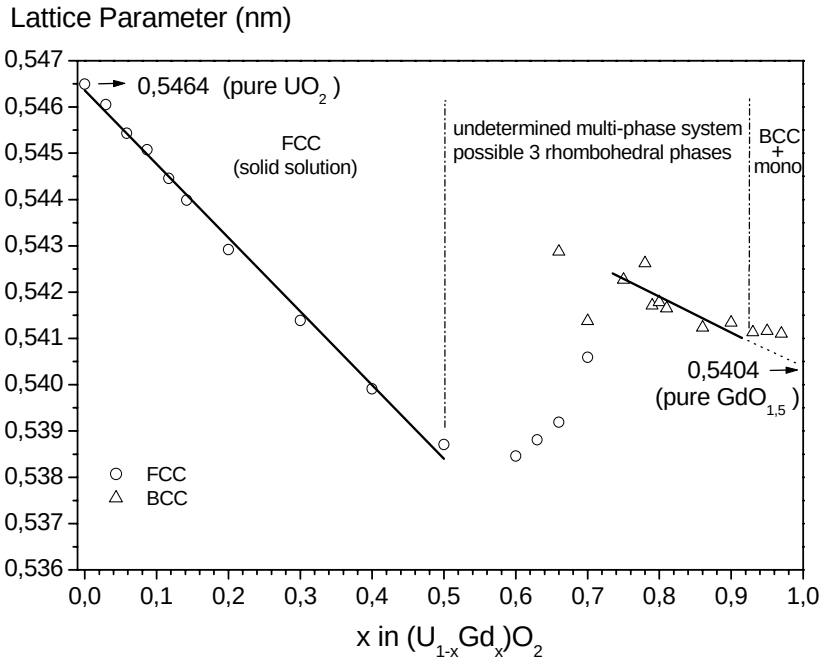

FIG. 4. Variation of the lattice parameter with dissolved gadolinium content.

When the molar fraction of gadolinium outreaches the value 0.5, the behaviour of the lattice parameter of the fluorite structure is not linear anymore, which indicates the end of the single-phase field. For compositions between $(U_{0.25}Gd_{0.75})O_2$ and $(U_{0.10}Gd_{0.90})O_2$, the diffractograms indicate only the presence of the body centered cubic structure, when a tendency to linear decrease on the lattice parameter with the molar fraction of gadolinium can also be observed. However, in this case, it is not possible to affirm that the Vegard's law is obeyed, once a bad adjustment was obtained in a linear regression from the experimental data. This observation may indicate the existence of two or more phases in that composition range. An attempt to fit a straight line to the data is illustrated in Figure 4.

In the intermediate range of composition between $(U_{0.5}Gd_{0.5})O_2$ and $(U_{0.25}Gd_{0.75})O_2$ it cannot be affirmed the simple coexistence between the FCC (face centered cubic) and BCC (body centered cubic) phases, once the lattice parameter is not constant for none of the two structures. For compositions between $(U_{0.25}Gd_{0.75})O_2$ and $(U_{0.1}Gd_{0.9})O_2$ it also cannot be affirmed that the system is single-phase with BCC structure, once cannot be affirmed that the Vegard's law is obeyed. Therefore, in that extensive composition range, where the molar fraction of gadolinium varies from 0.5 to 0.9, the results presented in Figure 4 indicate the existence of one or more phases different from the FCC fluorite structure of UO_2 and BCC structure of Gd_2O_3. For compositions over $(U_{0.10}Gd_{0.90})O_2$ the coexistence between the forms C and B of Gd_2O_3 was evidenced, with structures BCC and monoclinic, respectively.

Aitken, Bartran and Juenke [24] observed a phase with rhombohedral structure in the U-Y-O system, with composition varying in a wide range of yttrium concentration, from 51 to 86 mol%. This phase was designated RI. A second phase was observed in this system, also with rhombohedral structure, designated RII, with composition varying between 68 and 75 mol% yttrium. These two rhombohedral phases were also observed in the U-La-O system and a third rhombohedral phase, designated RIII, was detected in the concentration range varying from 55 to 67 mol% of lanthanum [25]. These rhombohedral phases were also observed in the compounds U-R-O (R=Nd, Sm, Eu, Ho, Er, Tm, Yb and Lu) and in the R-O system, where R=Ce, Pr and Tb, which can present valences +3 and +4. Kang and Eyring [26] observed that these rare earths exhibit a family of binary oxides where coexist the valences +3 and +4, resulting in oxygen deficient fluorite related structures. Among them, the composition R_7O_{12} has the same rhombohedral structure observed in the U-Y-O system. In that and in subsequent reports [27], these researchers propose the construction of crystalline structures of a group of compounds in the R-O system by assembling modules, which are unitary cells of the fluorite structure with oxygen vacancies in different positions in the unitary cell. With base in that mechanism, these researchers established and characterized 14 different phases in the R-O system. The R_7O_{12} phase is isostructural to the rhombohedral UGd_6O_{12} phase.

The experimental observation of the phases built with base in the methodology proposed by Kang and Eyring indicates that an extensive series of phases with structure based on the fluorite structure may exist, where oxygen vacancies are distributed in different ways. This is an important conclusion; once phases that are isostructural to the phases observed by Kang and Eyring in the R-O system may probably also exist in the system U-Gd-O. The U^{4+} cation can be present in these structures substituting the R^{4+} cation. Besides, with the possibility for the existence also of the U^{5+} and U^{6+} cations, the possibility for occurrence of phases more complex than the identified ones cannot be discarded.

Many researchers agree that the stoichiometry in the $(U,Gd)O_2$ system stays close to 2 up to the concentration of 40 mol% Gd_2O_3 [9,28,29,30]. It is also noticed a slight hypostoichiometry for this Gd_2O_3 concentration range. Starting from 40 mol% Gd_2O_3, Beals and Handwerk [28] observed a consistent decrease in the O/M ratio with the increase in the molar fraction of gadolinium, until the value of 1.5 is reached in the case of pure Gd_2O_3. With base in the literature, it can be considered that when Gd^{3+} cations are incorporate in the fluorite structure, U^{4+} cations may be oxidized for charge compensation. According to Ohmich et al [30], the formation of a small proportion of oxygen vacancies may also occurs, probably randomly distributed in the crystal lattice of the solid solution, which is evidenced by the hypostoichiometry. This mechanism, which would be the model 3 proposed by Ho and Radford [12], could be considered valid for Gd_2O_3 concentrations up to 50 mol%.

Above 50 mol% in Gd_2O_3, it is started a systematic formation of oxygen vacancies for charge compensation. When the number of oxygen vacancies reaches a critical value, the oxygen vacancies rearranges to form new phases that would be isostructural to the ones observed and modelled by Kang and Eyring in the R-O system, as discussed previously. The rhombohedral phase would probably be one of them. In that way, the variation on the lattice parameter as function of the molar fraction of gadolinium stops satisfying the Vegard's law. With the continuous increase in the number of oxygen vacancies, the crystalline structure develops until obtaining the BCC structure of Gd_2O_3, where 16 oxygen vacancies are present. If the straight line that represents the variation of the lattice parameter in the composition range of x = 0.75 to 0.9 is extrapolated, it intercepts the ordinate axis at the value 0.5404 nm for x = 1 ($GdO_{1.5}$), which is very close to the X ray diffraction standard value of 1.0813 nm for the Gd_2O_3 unitary cell, or 0.5407 nm for the pseudo fluorite cell of the $GdO_{1.5}$.

The beginning in the sinterability decrease in the UO_2-Gd_2O_3 system corresponds to the end of the monophase area in the system, with fluorite structure, for the composition $(U_{0.5}Gd_{0.5})O_2$ (see Figures 3 and 4). This also corresponds to the beginning of the systematic formation of oxygen vacancies, evidenced by the decrease in the O/M ratio, which was almost constant until approximately this composition, according to the literature [28]. Although the new $(U,Gd)O_2$ phases have not been observed directly in this work, the results of this work support the proposition that the beginning of the systematic oxygen vacancies formation makes possible the formation of new $(U,Gd)O_2$ phases in the system, which are different from the fluorite phase. One probable phase is the rhombohedral phase observed in the U-Y-O system, which should be isostructural to the one observed in the rare earth oxides CeO_{2-x}, PrO_{2-x} and TbO_{2-x}. This complex phase structure would be responsible for the decrease in the cation diffusivity of the system, leading to the decrease in the sinterability. The presence of some phase with good diffusivity (not detected directly in this work) could be responsible for the form of the curve presented in Figure 3, which revealed good sinterability for the composition $(U_{0.2}Gd_{0.8})O_2$.

The experimental results presented in the Figure 3 give base for the proposed Diffusion Barrier Hypothesis, once molar fractions of gadolinium higher than 0.5 results in very low sintered densities. The occurrence of phases different from fluorite for molar fractions of gadolinium higher than 0.5 was also observed, what could explain the decrease in the sinterability. However, nothing can be affirmed about the dependence of the interdiffusion coefficient in the UO_2-Gd_2O_3 system on the gadolinium concentration, which ultimately is what determines the sinterability of the system. Aiming at giving additional support for the proposed hypothesis, an interdiffusion study in the system UO_2-Gd_2O_3 was accomplished, whose results are presented and discussed in the next item.

2.2 Interdiffusion studies

The interdiffusion studies were accomplished by determining the gadolinium concentration profile (penetration curves) in a couple of sintered UO_2/Gd_2O_3. The interdiffusion coefficient was determined in function of the molar fraction of gadolinium by applying the Matano-Boltzman method [31]. The UO_2/Gd_2O_3 couple was prepared by compacting simultaneously both the UO_2 and Gd_2O_3 powders. The couple was sintered at 1650 °C for 3 hours. The couple obtained after sintering presented good mechanical resistance in the interface, which makes possible its longitudinal cut, perpendicular to the interface. The surface of the sample was prepared through conventional metallographic techniques.

Initially, a qualitative analysis was accomplished in the polished surface, where the appearance of the UO_2/Gd_2O_3 interface was revealed through scanning electron microscopy. The general form of the concentration profile was determined through qualitative analysis (EDS - Energy-dispersive X ray spectroscopy) of the gadolinium concentration over a line perpendicular to the interface. In three areas, it was accomplished a quantitative analyses for the gadolinium concentration through WDS (Wavelength dispersive X ray spectroscopy) in points spaced by 0.5 μm. The precision in the determination of the gadolinium concentration was esteemed to be 0.1%. From the penetration curves, the interdiffusion coefficient was determined through graphic integration applying the Matano-Boltzmann method. Figure 5 presents an electronic micrograph illustrating the UO_2/Gd_2O_3 interface. In general, it was observed the presence of a void between the phases, with width between 1 and 3 μm. The uranium and gadolinium concentrations were determined along the line indicated in the Figure.

The concentration profiles indicate interpenetration of approximately 16 μm after sintering for 3 hours at 1650 °C. The gadolinium penetration into the UO_2 phase is sensibly higher than the uranium penetration into Gd_2O_3 phase (higher than 2/3 of the total interpenetration distance).

An inspection was accomplished along the interface with aiming at selecting areas with good continuity between the UO_2 and Gd_2O_3 phases, where the width of the void was minimal. Three areas were selected, which presented a good continuity between the phases. In those areas quantitative analyses were performed for gadolinium concentration determination in points spaced 0.5 μm along a line normal to the UO_2/Gd_2O_3 interface line. The experimental points are presented in Figure 6. Once constructed the penetration curve, the interdiffusion coefficient in the UO_2-Gd_2O_3 system was calculated in function of the molar fraction of gadolinium by applying the data analysis method proposed by Matano [31].

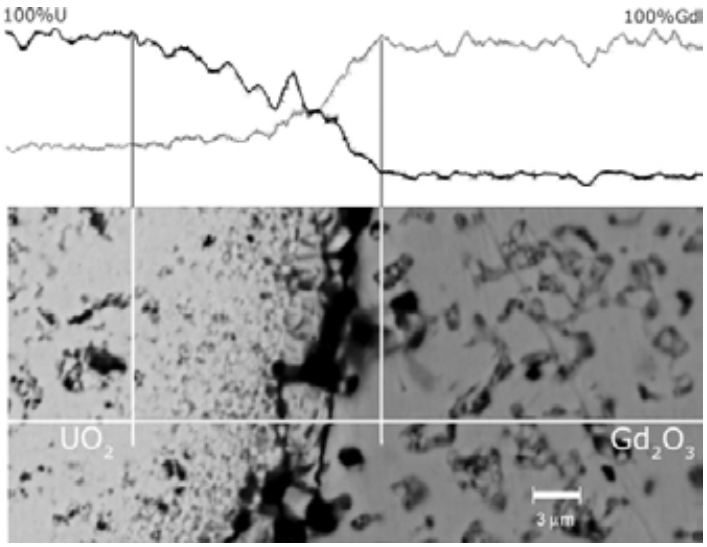

FIG. 5. Scanning electron micrograph illustrating the UO_2/Gd_2O_3 interface.

The interdiffusion coefficient was calculated for 0 to 100 mol% of gadolinium. The results are presented in Figure 7. The most important characteristic in this Figure is the sudden decrease in the interdiffusion coefficient for gadolinium concentrations above 50 mol%. It is also interesting to observe the increase in the interdiffusion coefficient value for gadolinium concentrations of about 80 mol%. These results are in good agreement with the results presented in Figure 3, and confirm in a direct way that the interdiffusion coefficient in the UO_2-Gd_2O_3 system decreases abruptly when the molar fraction of gadolinium is higher than 0.5, or when more than half of the cations presents are Gd^{3+}. Despite the imprecision of the applied method, which is evidenced by the considerable dispersion in the experimental data presented in Figure 7, it is conclusive that the UO_2-Gd_2O_3 sinterability decreases drastically starting from the composition $(U_{0.5}Gd_{0.5})O_2$ due to a sudden decrease in the interdiffusion coefficient of the system starting from that composition.

The presented results give base for the Barrier Diffusion Hypothesis. The sinterability of the system is drastically decreased for concentrations higher than 50 mol% Gd_2O_3, as is unequivocally shown in Figure 3. The cause for the sinterability decrease seems to be the sudden decrease on the interdiffusion coefficient for concentrations higher than 50 mol% Gd_2O_3, as is shown in Figure 7. Although they have not been detected directly, other unidentified phases with crystalline structure different from the fluorite probably exist for concentrations higher than 50 mol% Gd_2O_3, as is indicated by the variation of the lattice parameter presented in Figure 4. This observation is reinforced by the identification of a series of phases in the systems (Ce, Pr, Tb)-O, which probably have the same crystalline structure of the phases still not identified in the system U-Gd-O, once the model for construction of these phases in the rare earth oxides is entirely applicable for the UO_2-Gd_2O_3 system.

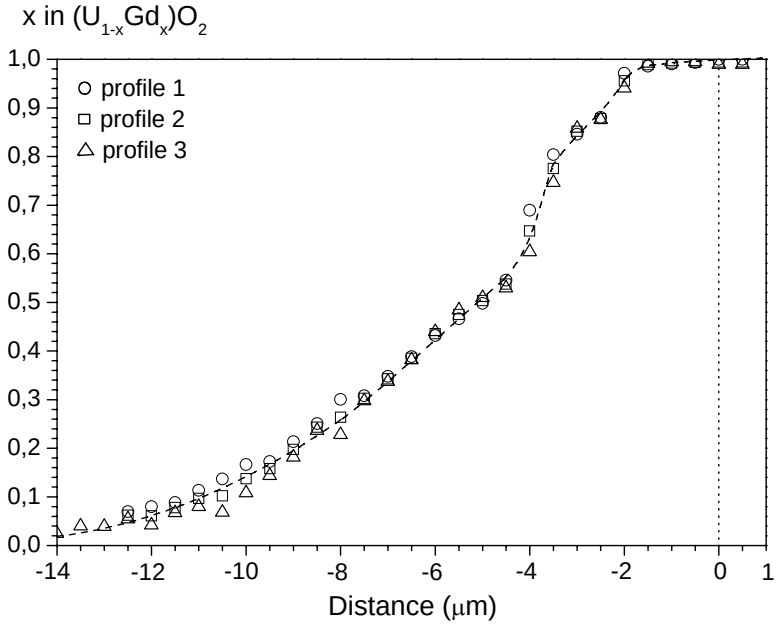

FIG. 6. Concentration profile across the UO_2/Gd_2O_3 interface.

2.3 Testing the hypothesis

The methodology adopted for testing the hypothesis is based on performing a sintering test in mixed powders where the Gd_2O_3 is incorporated to the UO_2 in such a way that guarantees the diffusion barrier is not formed. In other words, it is guaranteed that the Gd_2O_3 concentration never surpasses the value of 50 mol%. As the formation of low sinterability phases different from the fluorite just begins for Gd_2O_3 concentrations higher than 50 mol%, as previously discussed, mixed powders were prepared where the pure Gd_2O_3 powder was substituted by powders prepared by coprecipitation containing Gd_2O_3 concentrations inferior to 50 mol%. In that case, the formation of phases with gadolinium concentration above 50 mol% is not possible during the gadolinium solubilization, and the formation of the diffusion barrier also is not possible. According to the results presented in Figure 3, this new mixed powder presents sinterability higher than pure UO_2, once the presence of gadolinium in the fluorite structure favors the sintering process.

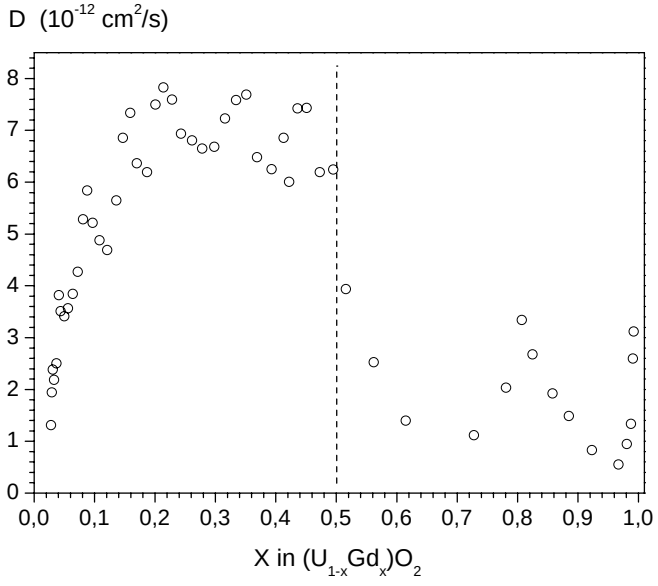

FIG. 7. Interdiffusion coefficient as function of the molar fraction of gadolinium.

Powders obtained by coprecipitation via ADU, which presents good homogeneity, were mechanically blended with UO_2 powder by homogenizing the mixture in a shaker mixer. Powders prepared by coprecipitation with compositions of 20, 30, 40, 50, 60, 70, 80 and 90 mol% of Gd_2O_3 were added to the UO_2 powder in order to always obtain the equivalent concentration of 10 wt% Gd_2O_3 (or 14,2 mol%) in the sample. The samples were compacted and sintered under the same conditions used previously (1650 °C for 3 hours under H_2 atmosphere). After sintering, the densities were determined by measuring the weight of samples immersed in xylol (Archimedes principle). The results are presented in Figure 8.

As previously mentioned, the sinterability decrease in the UO_2-Gd_2O_3 system, or the interdiffusion coefficient decrease, is probably due to the formation of phases different from the fluorite structure of UO_2 and it only happens for Gd_2O_3 concentrations above 50 mol%. Below that concentration the only one phase present is a solid solution where Gd^{3+} cations substitute U^{4+} cations in the fluorite structure, which is beneficial in terms of sinterability of the system, as it is illustrated in Figure 3. Therefore, the formation of the diffusion barrier is unable to happen when pure Gd_2O_3 powder is substituted by coprecipitated powders containing Gd_2O_3 concentrations smaller than 50 mol% in preparing the mixed oxides by mechanical blending. In this case, it becomes impossible the occurrence of areas where the gadolinium concentration exceeds 50 mol% in mol and, therefore, it becomes impossible the formation of low diffusivity phases that could act as a diffusion barrier. In that condition, the presence of gadolinium should necessarily increase the sinterability of the system, even when it is added through the mechanical blending method. The sintered density expected would be the one observed in sintering coprecipitated powder containing 10 wt% Gd_2O_3 (or 14,2 mol%). With base in the diffusion barrier hypothesis, the minimum acceptable sintered density would be the one correspondent to pure UO_2 (indicated in Figure 8), supposing that the presence of gadolinium does not affect the UO_2 sinterability. The results presented in Figure 8 show a behavior that does not support the diffusion barrier hypothesis.

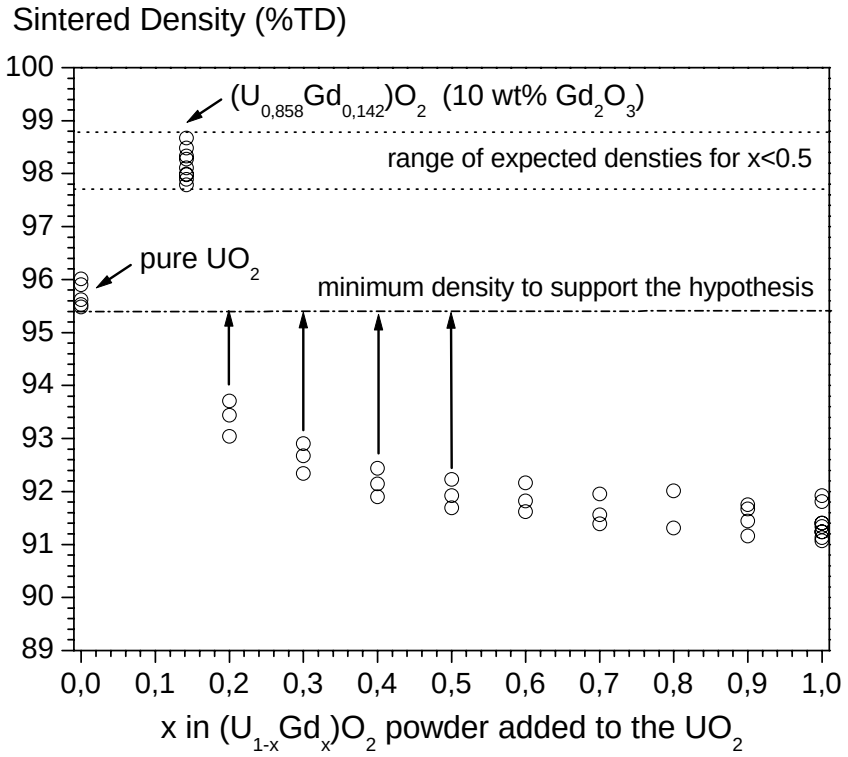

FIG. 8. Densification levels observed in sintering UO_2-Gd_2O_3 pellets prepared by mechanical blending using $(U_{1-x}Gd_x)O_2$ coprecipitated mixed powders.

If the nominal Gd_2O_3 concentration in all the sintered pellets is 10 wt% (or 14,2 mol%), it is not possible the formation of areas where the Gd_2O_3 concentration is superior to 50 mol% during sintering samples which are prepared with coprecipitated mixed powders with composition inferior to $(U_{0.5}Gd_{0.5})O_2$. As the interdiffusion coefficients stay in a constant level between the molar fractions of gadolinium varying from 0.2 to 0.5 (see Figure 7), in the range from 6 to $8x10^{-16}$ m^2/s, the final density expected after sintering mechanically blended mixed powders prepared with coprecipitated powders with compositions of gadolinium inferior to 50 mol% should necessarily be compatible with the density level observed in sintering pellets containing 10 wt% Gd_2O_3 prepared by coprecipitation (approximately 98%TD). Even so adopting an extreme hypothesis, which would consider that does not happen any gadolinium redistribution during sintering, the minimum acceptable density that would support the Diffusion Barrier Hypothesis would be the typical density obtained in sintering pure UO_2 (approximately 95.5%TD), which did not also happen. The experimental evidence that would support the hypothesis would be an abrupt increase in the sintered density obtained in the samples prepared with mixtures UO_2- $(U_{1-x}Gd_x)O_2$, with $X \leq 0.5$. Low densities should be observed only for values of X superior to 0.5 in the formula, once, in that case, the formation of low diffusivity phases is possible.

Consequently, with base in the experimental results obtained in testing the hypothesis, the formation of a diffusion barrier to explain the sintering behavior of UO_2-Gd_2O_3 fuel pellets must be rejected as a possible mechanism.

3. The pore formation hypothesis

An interesting observation on the results obtained in the interdiffusion studies presented previously is related to the shape of the penetration curve presented in Figures 5 and 6. The results indicate that the material flow is not homogeneous, with Gd^{3+} cations penetrating preferentially in the UO_2 fluorite structure. In Figure 5 is evident the largest penetration of the gadolinium in the UO_2 phase when the position of the interface UO_2/Gd_2O_3 is taken as reference. Those observations indicated that the Kirkendall effect seems to be occurring in this system.

The diffusion between the components of the mixture during sintering the UO_2-Gd_2O_3 fuel prepared by the mechanical blending method happens simultaneously. If the diffusion rate of the two species of atoms is not the same, the Kirkendall effect occurs. In other words, if the gadolinium cations diffuse more quickly into the UO_2 phase than the opposite, a larger flow of gadolinium deriving from the Gd_2O_3 agglomerates in direction to the UO_2 phase is established, when compared with the uranium flow in direction to the interior of the Gd_2O_3 agglomerates. In this case, the UO_2 phase expands for receiving the extra gadolinium cations and a void is generated at the place of the original Gd_2O_3 agglomerate. This phenomenon is commonly observed in mixed powders systems where exists an unbalanced diffusivity or solubility between the powders [32].

As the pore formation due to this effect occurs at temperatures in which the pore structure is essentially closed, during the second stage of sintering, the pore elimination is probably very difficult. The possibility of occurrence of this phenomenon in the UO_2-Gd_2O_3 system gives base for the Pore Formation Hypothesis.

3.1 Experimental evidences

The results obtained in the interdiffusion studies revealed that the penetration of the gadolinium into the UO_2 is considerably larger than the penetration of the uranium into the Gd_2O_3 (see Figure 5).

Although the individual diffusion coefficients was not determined in this work and the individual diffusion coefficients of gadolinium into the UO_2 and uranium into Gd_2O_3 have not been found in the literature, it is known that uranium diffuses very little in the cubic form of Gd_2O_3 and the diffusion of uranium in the B form of Gd_2O_3 (monoclinic) is practically null. In the UO_2-Y_2O_3 system the maximum solubility of uranium in the cubic Y_2O_3 (C form) is 7–8 mol% [33]. The maximum solubility of uranium in the B form Gd_2O_3 is 2 mol% [34, 35]. In conclusion, all the information indicates low solubility of uranium in both cubic and monoclinic forms of Gd_2O_3. On the contrary,

gadolinium diffuses easily into the UO_2 fluorite structure, as is illustrated in Figure 4, which shows a wide range of gadolinium concentration where solid solution is formed.

Therefore, the experimental results obtained in this work and the information obtained in the literature indicate that a considerable difference exists between the diffusion coefficients of gadolinium into UO_2 and uranium into Gd_2O_3 (both forms C and B), which could cause an unbalancing in material transport during the solid solution formation when sintering the UO_2-Gd_2O_3 fuel prepared by the mechanical blending method, where Gd_2O_3 agglomerates are dispersed in a UO_2 matrix before sintering. In this situation is probable the occurrence of the Kirkendall effect.

The morphology of the Gd_2O_3 powder and the pore structure developed in sintered UO_2-Gd_2O_3 pellets prepared by the mechanical blending method supports the pore formation hypothesis. The morphology of the Gd_2O_3 powder is illustrated in Figure 9. The presence of Gd_2O_3 agglomerates with large diameter (>40 μm) is evidenced. In sintered UO_2-Gd_2O_3 pellets prepared by mechanical blending, it is observed the existence of pores with diameters sensibly larger than the pore diameter typically observed in pure UO_2 sintered pellets. The curve of pore diameter distribution is shifted in the direction of larger diameters. This effect is illustrated in Figure 10. In this Figure it is observed that the pore diameter distribution in the pure UO_2 fuel pellet agrees well with the pore diameter distribution typical for the UO_2 fuel fabricated starting from TCAU, which varies between 0.5 μm and about 10 μm with average between 3 and 4 μm [6,36]. In the case of the sample containing 10 wt% Gd_2O_3, it is observed pores with diameter up to 25 μm, with the average moved to approximately 8 μm. This resulted supports the proposition of the hypothesis, once the Gd_2O_3 agglomerates existent in the system (see Figure 9) can result in the formation of pores due to the Kirkendall effect occurrence during the solid solution formation, simultaneously with the sintering process. That pores could not be eliminated (at least not totally) during the sintering stage subsequent to their formation.

With base in these observations, which already bases the hypothesis by itself, is possible to propose that during the sintering of the UO_2-Gd_2O_3 fuel prepared by the mechanical blending method occurs simultaneously the formation of the $(U,Gd)O_2$ solid solution. The formation of large pores due to the Kirkendall effect happens during the formation of the solid solution, in places where originally existed Gd_2O_3 agglomerates, due to the preferential solubilization of gadolinium into the fluorite structure of UO_2, These large pores, once formed in high temperature, are difficult to be eliminated in the subsequent sintering stages and remain in the sintered pellet in the form of stable pores, which causes the decrease of the final sintered density. The formation of stable pores during sintering (Kirkendall effect) would be responsible for the sintering behavior of the UO_2-Gd_2O_3 fuel prepared according to the mechanical blending method due to the presence of Gd_2O_3 agglomerates in the green pellets.

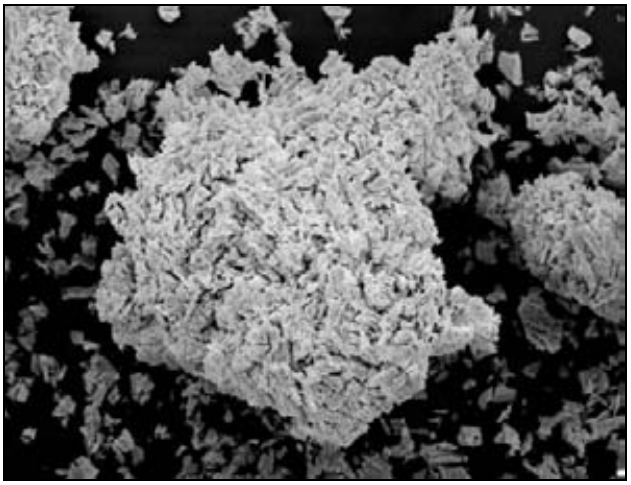

FIG. 9. Scanning electron micrography illustrating Gd_2O_3 agglomerate.

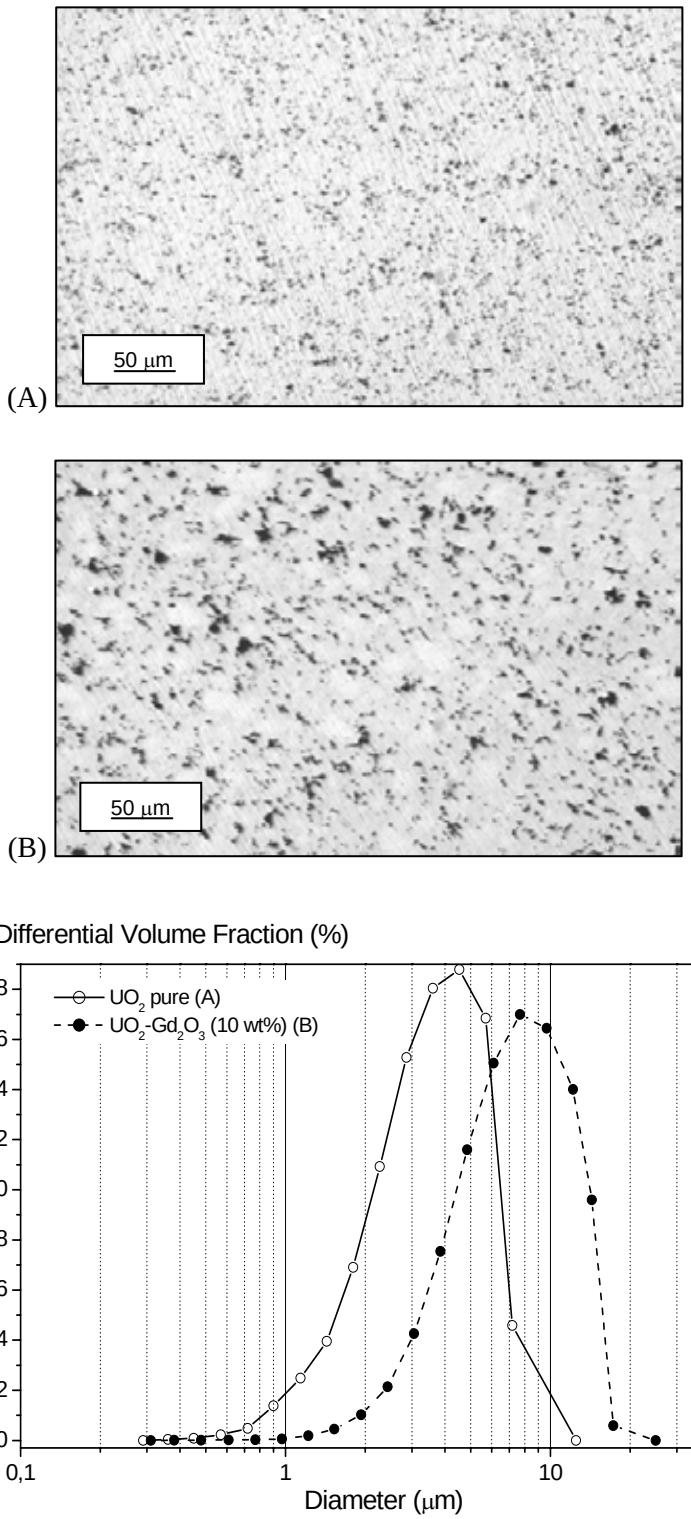

FIG. 10. Optical micrographies and pore diameter distribution curves for:A) pure UO_2 and B) UO_2-Gd_2O_3 (10 wt% Gd_2O_3)

3.2 Testing the hypothesis

The hypothesis test was accomplished through the preparation of UO_2-Gd_2O_3 pellets where Gd_2O_3 agglomerates of controlled size were added to the UO_2 powder by the mechanical blending method. The Gd_2O_3 agglomerates were obtained by compacting and granulating the original Gd_2O_3 powder. The granules were classified in the size ranges <37 μm, between 37 and 45 μm, between 45 and 53

μm and between 53 and 62 μm. The Gd_2O_3 concentration was 10 wt%. The UO_2-Gd_2O_3 mixtures prepared with Gd_2O_3 granules of different size were compacted and sintered at 1650 °C for 3 hours under H_2 atmosphere. Polished sections of the sintered pellets were observed in optical microscope and the pore diameter distributions were determined.

The micrographies presented in Figure 11 show pore structures with pore diameters superior to the range of diameters typically observed in the standard UO_2 fuel fabricated starting from AUC, which varies between 0.5 μm and about 10 μm [6,36]. In those micrographies it is possible to observe a consistent increase in the diameter of the big pores with the increase in the diameter of the Gd_2O_3 granules mixed to the UO_2 powder. In the micrographies corresponding to Gd_2O_3 granules superior to 45 μm, it is possible to observe that some granules were not totally solubilized in the UO_2 fluorite structure. A growing void around the granule perimeter can be observed. This experimental observation demonstrates that the big pores observed in the micrographies of Figure 11 were really formed at places where initially existed Gd_2O_3 granules. Those pores are responsible for the bimodal form of the pore diameter distributions presented in Figure 11. Unlike the typical monomodal distribution, which is characteristic of the standard UO_2 fuel prepared starting from AUC, it is observed that all the pore diameter distributions obtained are bimodal. It is also observed that the position of the second peak of the distributions is related to the granulometry of the added Gd_2O_3 granules. As larger are the Gd_2O_3 granules present, larger are the pore diameter corresponding to the second peak of the bimodal distribution. If the size of the Gd_2O_3 agglomerate is sufficiently small, the diameter of the pore formed due to the Kirkendall effect is incorporated in the first peak of the bimodal distribution, which results in a monomodal distribution shifted in the direction of larger diameters (see Figure 10B). The scanning electron micrograph presented in Figure 12 illustrates the formation of pores due to the Kirkendall effect. Part of the gadolinium of the Gd_2O_3 agglomerate was already diffused into the UO_2 matrix, but the solubilization is not complete. This Figure shows Gd_2O_3 agglomerate inside a pore in formation.

The correlation between the pore diameter in the second peak of the bimodal distribution and the presence of Gd_2O_3 inside pores in formation demonstrate that those pores of larger diameter are generated starting from Gd_2O_3 agglomerates by occasion of their dissolution in the crystal lattice of UO_2 during sintering, which is resulted from the Kirkendall effect occurrence. As the formation of solid solution occurs at elevated temperatures when the pore structure is probably already essentially closed, during the second stage of sintering, the pores formed cannot be eliminated, at least not entirely, resulting in a sintered body with larger residual porosity.

The mechanism based on the formation of stable pores during sintering explains the strong influence that the homogeneity of the Gd_2O_3 powder distribution in the UO_2-Gd_2O_3 mixed powder exerts on the density obtained after sintering [17]. This mechanism also explains the lowering in the sintered densities with the increase in the oxygen potential of the sintering atmosphere. In this case, as the sintering process is favored and proceeds at lower temperatures, the pore formation due the Kirkendall effect occurs in a much closed pore structure, which essentially impedes their elimination because the sintering process is almost totally finished when the pores are formed.

The pore formation mechanism also explains the influence of the specific surface of the UO_2 powder on the sintered densities of UO_2-Gd_2O_3 pellets, as pointed by the results obtained by Agueda et al. [14] (see Figure 1 and Table 1). If the specific surface of the UO_2 powder is high, the sintering process is favored and the pore structure closes at lower temperatures, which makes difficult the elimination of the pores formed due the Kirkendall effect. On the other hand, if the specific surface of the UO_2 powder is low enough, the sintering process is sufficiently delayed in order to allow the formation of pores due the Kirkendall effect in a pore structure open enough to help their further elimination. In other words, if the specific surface of the UO_2 powder is adequate, a reserve of activity for sintering in higher temperatures would be available in order to close the pores formed due the Kirkendall effect.

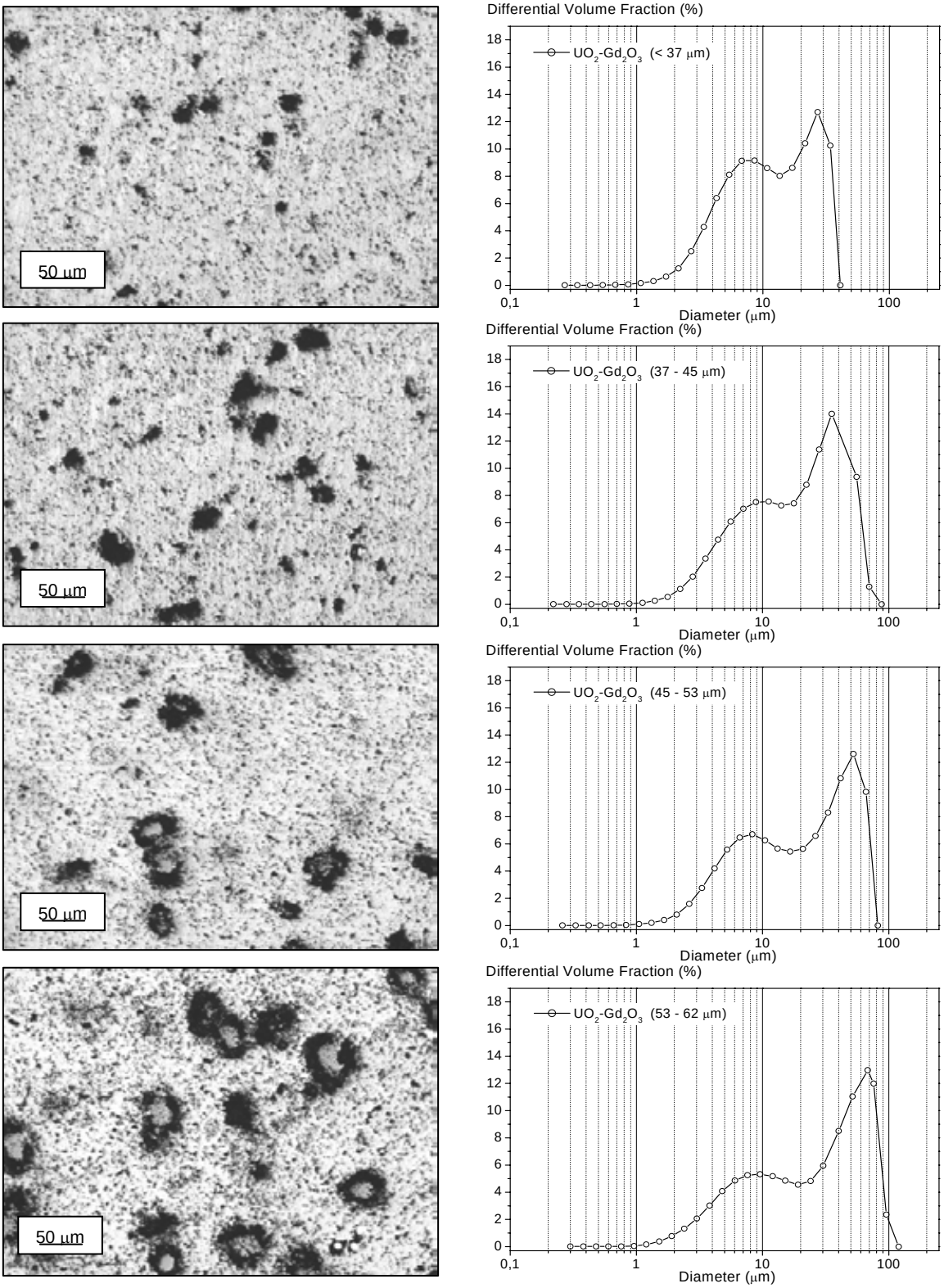

FIG. 11. Pore structure of sintered UO_2-Gd_2O_3 pellets prepared with Gd_2O_3 granules of different sizes.

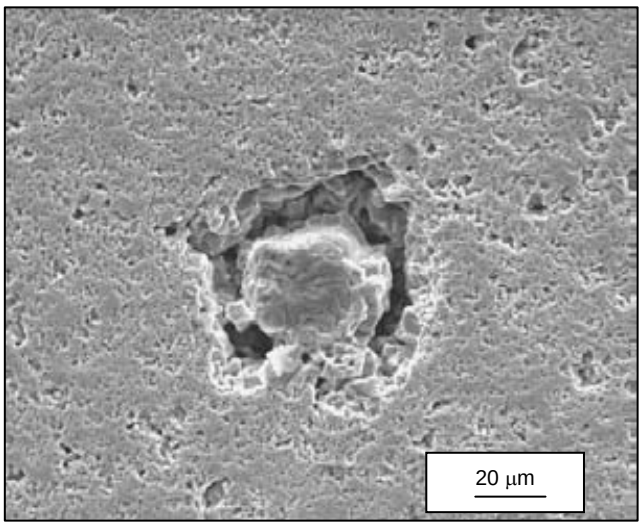

FIG. 12. Scanning electron micrography illustrating the pore formation at Gd_2O_3 agglomerate original places.

4. Conclusions

With base in the obtained experimental evidences, the hypothesis based on the formation of stable pores can be considered demonstrated. Although phases different from the fluorite were indirectly detected, which have low cation diffusivity; the hypothesis based on the formation of a diffusion barrier must be rejected. The phenomenon is better characterized as a concurrence between pore formation and elimination during sintering than as a sintering blockage.

The mechanism that explains the sintering behavior of the UO_2-Gd_2O_3 fuel prepared by the mechanical blending method and using UO_2 powder derived from the AUC technology is based on the occurrence of the Kirkendall effect. A significant difference in the interdiffusion coefficients of the gadolinium into UO_2 and of the uranium into Gd_2O_3 causes a misbalancing in the material transport during the solid solution formation. As consequence of this phenomenon, the densification during sintering occurs simultaneously with the formation of pores in places where originally Gd_2O_3 agglomerates were present. The diameters of these pores are proportional to the initial diameter of the agglomerates present and they are stable, once they have been formed in high temperature in an essentially closed pore structure. Under this situation, it is not possible the elimination of that pores after their formation, in the subsequent sintering process. That pores remain in the sintered pellet and causes the low densities observed.

ACKNOWLEDGEMENTS

The authors wish to express their gratitude to CTMSP (Navy Technological Center in São Paulo) for the permission to use its facilities. The authors also wish to express their sincere thanks to the staffs of the Nuclear Materials Laboratory of CTMSP for their helps in the course of this study.

REFERENCES

[1] BÖHM, W., KIEHLMANN, H.D., NEUFERT, A., PEEHS, M., Gd_2O_3 up to 9 weight percent, an established burnable poison for advanced furl management in pressurized water reactors, Kerntechnik **50,** (1987), p.234.

[2] HELLSTRAND, E., Burnable poison reactivity control and other techniques to increase fuel burnup in LWR fuel cycles, Trans. Am. Nucl. Soc. **40,** (1982), p.181.

[3] SKOGEN, F.B., NIELSEN, L.A., GRUMMER, R.G., Operation experience with Exxon nuclear-supplied Gadolinia in Pressurized Water Reactors, Trans. Am. Nucl. Soc. **40,** (1982), p.194.

[4] BRANDBERG, S.G., The conversion of uranium hexafluoride to uranium dioxide, Nuclear Technology **18,** (1973), p.177.

[5] ASSMANN, H., BECKER, M., Technology of UO_2 fuel fabrication by the AUC powder process, Trans. Am. Nucl. Soc. **31,** (1979), p.147.

[6] ASSMANN, H., DÖRR, W., Microstructure and density of UO_2 pellets for Light Water Reactors as Related to Powder Properties, Materials Science Monographs **16,** (1983), 707.

[7] MANZEL, R., DÖRR, W., Manufacturing and irradiation experience with UO_2/Gd_2O_3 fuel, Am. Ceram. Soc. Bull. **59,** 6, (1980), p.601.

[8] ASSMANN, H., PEEHS, M., ROEPENACK, H., Survey of binary oxide fuel manufacturing and quality vontrol, J. Nucl. Mater. **153**, (1988), p.115.

[9] FUKUSHIMA, S., OHMICHI, T., MAEDA, A., WATANABE, H., The effect of Gadolinium content on the thermal conductivity of near-stoichiometric $(U,Gd)O_2$ solid solutions, J. Nucl. Mater. **105,** (1982), p. 201.

[10] HIRAI, M., Thermal diffusivity of UO_2-Gd_2O_3 pellets, J. Nucl. Mater. **173,** (1990), p.247.

[11] NISHIDA, T., YUDA, R., Effect of particle size and oxygen potential on UO_2/Gd_2O_3 pellet sintering, Advances in Fuel Pellet Technology for Improved Performance at High Burnup, IAEA–TECDOC—**1036**, Vienna, (1998), p.73.

[12] HO, S.M., RADFORD, K.C., Structural chemistry of solid solutions in the UO_2-Gd_2O_3 system, Nuclear Technology **73,** (1973), p.350.

[13] LITTLECHILD, J.E., BUTTLER, G.G., LESTER, G.W., The production of burnable poison oxide fuel, Nuclear Fuel Performance 1973, Proc. Int. Conf. London, Vol. **1**, London, (1973), p. 65.

[14] AGUEDA, H.C., HEREDIA, A.D., AMAYA, D.C., STERBA, M. E., RUSSO, D., Efectos del oxido de Gadolínio en la sinterization de dioxido de uranio", General Congress on Nuclear Energy, Proc. Conf. Rio de Janeiro, Vol. **2**, Rio de Janeiro, (1994), p.567.

[15] UNE, K., OGUMA, M., Oxygen potential of $U_{0.96}Gd_{0.04}O_2$ (UO_2-3wt% Gd_2O_3) solid solution, J. Nucl. Mater. **131,** (1985), p.88.

[16] RIELLA, H.G., DURRAZO, M., HIRATA, M., NOGUEIRA, R.A., UO_2-Gd_2O_3 solid solution formation from wet and dry processes, J. Nucl. Mater. **178,** (1991), p.204.

[17] DURAZZO, M., RIELLA, H.G., Effect of mixed powder homogeneity on the UO_2-Gd_2O_3 nuclear fuel sintering behavior, Key Eng. Mat. **189–191,** (2001), p.60.

[18] SONG, K.W., KIM, K.S., YANG, J.H., KANG, K.W, JUNG, Y.H., A mechanism for the sintered density decrease of UO_2-Gd_2O_3 pellets under an oxidizing atmosphere, J. Nucl. Mater. **288,** (2001), p.92.

[19] DAVIS, H.H., POTTER, R.A., UO_2-Gd_2O_3 sintering behavior, Materials Science Research **11,** (1977), p.515.

[20] YUDA, R., UNE, K., Effect of sintering atmosphere on the densification of UO_2-Gd_2O_3 compacts, J. Nucl. Mater. **178,** (1991), p.195.

[21] WADA, T., NORO, K., TSUKUI, K., Behavior of UO_2-Gd_2O_3 fuel, Nuclear Fuel Performance, Proc. Int. Conf. London, (1973), p.63.

[22] MIYAKE, C., KANAMARU, M., IMOTO, S., Microcharacterization of Gadolinium in $U_{1-x}Gd_xO_2$ by means of electron spin resonance, J. Nucl. Mater. **137,** (1986), p.256.

[23] PEEHS, M., DÖRR, W., GRADEL, G., MAIER, G., Zur Wärmleitfähigkeit und Plastizität von UO_2 mit Gd-Zusätzen, J. Nucl. Mater. **106,** (1982), p.221.

[24] AITKEN, E.A., BARTRAM, S.F., JUENKE, E.F., Crystal chemistry of the rombohedral $MO_3.3R_2O_3$ compounds, Inorg. Chem. **3,** (1964), p.959.
[25] GSCHNEIDER Jr, K.A., EYRING, L. Handbook on the physics and chemistry of rare earths. Non-Metallic compounds-I, Vol. **3**, North-Holand Physics Publishing, Amsterdam (1979), p.444.
[26] KANG, Z.C., EYRING, L., A Compositional and structural rationalization of the higher oxides of Ce, Pr, and Tb, Journal of Alloys and Compounds **249,** (1997), p.206.
[27] KANG, Z.C., EYRING, L., The prediction of the structure of members of the homologous series of the higher rare earth oxides, Journal of Alloys and Compounds **275–277,** (1998) p.30.
[28] BEALS, R.J., HANDWERK, J.H., Solid solutions in the system urania-rare-earth oxides, J.Am. Ceram. Soc. **48,** (1965), p.271.
[29] UNE, K., OGUMA, M., Thermodynamic properties of nonstoichiometric urania Gadolinia solid solutions in the temperature range 700–1100 ^oC, J. Nucl. Mat. **110,** (1982), p.215.
[30] OHMICHI, T., FUKUSHIMA, S., MAEDA, A., WATANABE, H., On the relation between lattice parameter and o/m ratio for uranium dioxide–trivalent rare earth oxides: I, UO_2-$GdO_{1.5}$, J. Nucl. Mat. **102** (1981) 40.
[31] MATANO, C., On the relation between diffusion-coefficients and concentration of solid metals (the nickel-copper system), Japanese Journal of Physics **8,** (1933), p.109.
[32] GERMAN, R.M., Sintering theory and practice, John Willey and Sons, New York, (1996).
[33] GSCHNEIDER Jr, K.A., EYRING, L., Handbook on the physics and chemistry of rare earths. Non-Metallic Compounds–I, Vol. **3**, North-Holand Physics Publishing, Amsterdan (1979), p.444.
[34] BEALS, R.J., HANDWERK, J.H., WRONA, B.J., Behavior of urania-rare-earth oxides at high temperatures, J.Am. Ceram. Soc. **52,** 11, (1969), p.578.
[35] KELLER, C., Ternäre und polynäre Oxide des Urans, Gmelin Handbuch der Anorganischen Chemie, Springer-Verlag, Berlin, (1975).
[36] ASSMANN, H., DÖRR, W., PEEHS, M., Oxide fuels with controlled microstructure, J. Am. Ceram. Soc. **67,** (1984), p.631.

Evolutionary Design Studies of PHWR Fuel Rods

S. Castañiza[a], L. Alvarez[b]

Abstract. Argentina has two nuclear power plants (PHWR) and currently it is in its final stage the construction of a third reactor of the same type: Atucha–2. Over the years the designs of their fuel assemblies have been improved product of operational experience, fabrication evolution and technical-economic needs. The changes have been evolving in some cases, such as increasing the uranium mass in the fuel rods. Other changes have represented a total conversion of the nuclear reactor operation; like the use of slightly enriched uranium (0,85%). At the present the initial design of the Atucha–2 fuel assembly is completed and the first core is currently under construction. Future evolution of this fuel might be based on the previous experience and also will consider the information from the operation. To study the changes that could be implemented on the Atucha–2 fuel rod the effects of some design parameters have been calculated. Aspects like pellet density, pellet porosity, pellet geometry, dishing volume, pellet-cladding gap size and initial pressurization were considered and their effects on the thermo-mechanical behavior of the entire fuel rod in terms of safety and performance were analyzed. In this paper are presented the studies of the evolutionary design changes proposed for Atucha–2 fuel rod and the analysis for their eventual implementation. Safety limits that might be affected are identified and safety margins evaluated.

1. Introduction

Argentina has two nuclear power plants, Embalse (CANDU 6, 600 MW(e)) and Atucha–1 (PHWR, 357 MW(e)). Both reactors operated originally with natural uranium fuel in the form of uranium dioxide (Atucha 1 fuel was later converted to slightly enriched uranium) and are moderated and cooled with pressurized heavy water. Currently, and after a delay of more than twenty years, it is in its final stage the construction of a third reactor, Atucha–2, that will bring 700 MW to the interconnected system of Argentina. It is placed within the line of pressure vessel heavy water reactors developed by KWU/Siemens, of which only the MZFR prototype (57 MW(e)) in Germany and Atucha–1 were constructed.

Each fuel assembly has a diameter of 103 mm, and consists of 37 fuel rods of approximately 5560 mm of length arranged in three concentric circles and a central fuel rod. Each fuel rod consists essentially of a zircaloy–4 tube containing the stack of fuel pellets, with top and bottom plugs hermetically welded to the tube. The cladding is self standing (non collapsible) during the fuel assembly lifetime. Pellets are made of sintered uranium dioxide, with natural enrichment. Pellets have dishings at both ends and chamfered edges to accommodate the axial expansion of the pellet stack during irradiation. Atucha–2 fuel assemblies are based on Atucha–1 design, in fact it has the same diameter and the same fuel rod distribution, but the fuel rod diameter is 1 mm larger in Atucha–2.

Fuel assemblies for Atucha–2 will be manufactured in Argentina. Over the years the designs of the fuels for the Argentine power plants have been improved as a result of operational experience, fabrication evolution and technical-economic needs. The changes in fuel designs have been evolving in some cases, such as increasing the uranium mass of the fuel rods Atucha–1 and Embalse power plants. For example the mass increment program (MASU) for Atucha–1 included several changes in pellet, cladding and fuel rod design that have the aim of increasing the content of uranium for a total of 6.3% [3]. Other design changes have represented a total conversion of the nuclear reactor operation; this is the case of the slightly enrichment uranium (ULE) program that was applied to Atucha–1 since 2001. This program consisted in enrich the fuel from natural to 0.85% of U-235, duplicating the fuel burnup and allowing an important reduction on fuel consumption [4].

[a] Fuel Engineering Department, National Atomic Energy Commission of Argentina.
[b] Fuel Engineering Department, National Atomic Energy Commission of Argentina.

One of the most important motivations for these changes has been to reduce the generation cost. It is desirable to apply this experience to Atucha–2 fuel. At the present the initial design of the Atucha–2 fuel assembly is completed and the first core is currently under construction. Future design evolution of this fuel might be based on design studies like this work, the previous knowledge and naturally will consider the information from the fuel operation, fuel tests and fuel performance evaluation.

In this paper are presented the studies of the change of some design parameters for Atucha–2 fuel rod, to provide information for the eventual redesign of the fuel rods. Safety limits that might be affected are identified and safety margins evaluated.

2. Design modifications for Atucha–2 fuel rods

The design parameters of the fuel rods for Atucha–1, Atucha–1 MASU (increase of U content) and Atucha–2 are showed in table 1. The aim for the modification of fuel rod design in Atucha–1 was the increase of uranium mass to increase the residence time and reduce operative cost while maintaining the suitability and safety. This could be a possible aim for future design modifications of Atucha–2 fuel rods, but the main motivation of this work is to know the capabilities and limits of the fuel rods to maintain the suitability and safety of future modifications, or in case of necessity increase margins for some occurrences. Anyway the information generated will provide a better understanding of the behavior of the Atucha–2 fuel rod.

TABLE 1. DESIGN CHARACTERISTICS OF ATUCHA TYPE FUEL RODS

	Atucha–1	Atucha–1 MASU	Atucha–2
Pellet length (mm)	12	13	14
Pellet diameter (mm)	10.62	10.74	11.57
Length-diameter ratio	1.13	1.21	1.21
Pellet density (g/cm^3)	10.55	10.60	10.55
Dishing deep (mm)	0.3	0.23	0.25
Cladding outer diameter (mm)	11.90	11.92	12.90
Cladding inner diameter (mm)	10.80	10.92	11.81
Min clad thickness (mm)	0.505	0.460	0.495
Minimum gap (mm)	0.13	0.13	0.18
Maximum gap (mm)	0.23	0.23	0.30

The studied design changes are:

- Fuel pellet density
- Fuel pellet diameter
- Fuel pellet length
- Helium initial pressurization of the fuel rod

The first three are about an increase of the uranium mass in the fuel rod and are based on the MASU program for Atucha–1, and the fourth is to reduce end of life internal pressure of the rods. There is no proposed change in the cladding outer diameter to maintain the hydraulic characteristics of the fuel assembly.

3. Design and safety limits

Any change to the Atucha–2 fuel design must take account the established design limits. These limits are according to [2]. The most relevant limits for this work are the limits related to cladding strain, fuel temperature and fuel rod internal pressure.

The cladding strain limit is set up to reduce the impact of failures by pellet-cladding interaction in the case of fast power transients. In these cases the cladding strain (elastic + plastic) shall not exceed 1% after pellet-cladding hard contact and cladding stress reversal.

The maximum temperature of the center of the fuel pellet should be less than the melting temperature of UO_2 (≈2800ºC).

The maximum internal pressure of the fuel rod, in power transients and at end of life, must be less than the pressure required to increase the fuel/clad gap; this is the coolant pressure: 115 bar. Also the initial helium pressurization must preclude the possibility of cladding collapse.

Also an important consideration while establishing the guidelines for this work was to keep the external design of the fuel rod to maintain the hydraulic behavior of the fuel channel and the structural design of the fuel assembly.

4. Methodology

The procedure in this work consisted in make calculations with variations in selected fuel rod parameters. These calculations were done using a fuel rod code, developed by KWU/Siemens and transferred to the National Commission of Atomic Energy of Argentina (CNEA). The fuel rod code was developed for the numerical and analytical treatment of the in-reactor behavior of fuel rods during progress in burnup and accumulated neutron dose. The code comprises the whole rod in its radial and axial extensions. The individual power history of the rod under consideration during its total in-reactor lifetime can be followed; this includes power changes due to refueling.

The fuel rod code is deterministic and conservatism of the calculations is to be provided by a proper selection of the input since this characteristic is not intrinsic to the code. This selection includes the power histories, fabrication tolerances, and model parameters. For this work all values of strain, temperature and pressure were calculated conservatively because is in this way that the design will be later evaluated and approved for use.

4.1 Operational conditions

The calculations were performed using two input power histories, one is a ramp from zero to the design maximum linear heat generation rate (LHGR) of 640 W/cm. This value comes from multiplying the maximum LHGR by safety factors that arise from neutronic and thermal-hydraulic analysis of the core. The maximum LHGR comes from the neutronic simulation of the core [1]. Summarizing:

Average core LHGR = 237.7 W/cm
Maximum LHGR = 468.7 W/cm,
Design maximum LHGR = 640 W/cm

The other power history is a simulated one selected from a data bank in [1] for been the most demanding in terms of average power and burnup (it has a rod average burnup of 9 MW•d/kgU), and correspond to a fuel rod from the external ring of rods of a fuel assembly that start in the periphery of the core for approximately 90 days and was later moved to the center of the core. Smaller variations on the power indicated the movement of other fuel elements in the surrounding area. This power history was extended conservatively to reach an average rod burnup of 15 MW•d/kgU (the design burnup) and adapted for input to the fuel rod code. The power history is showed as LHGR in function of time and in function of average burnup in Figure 1.

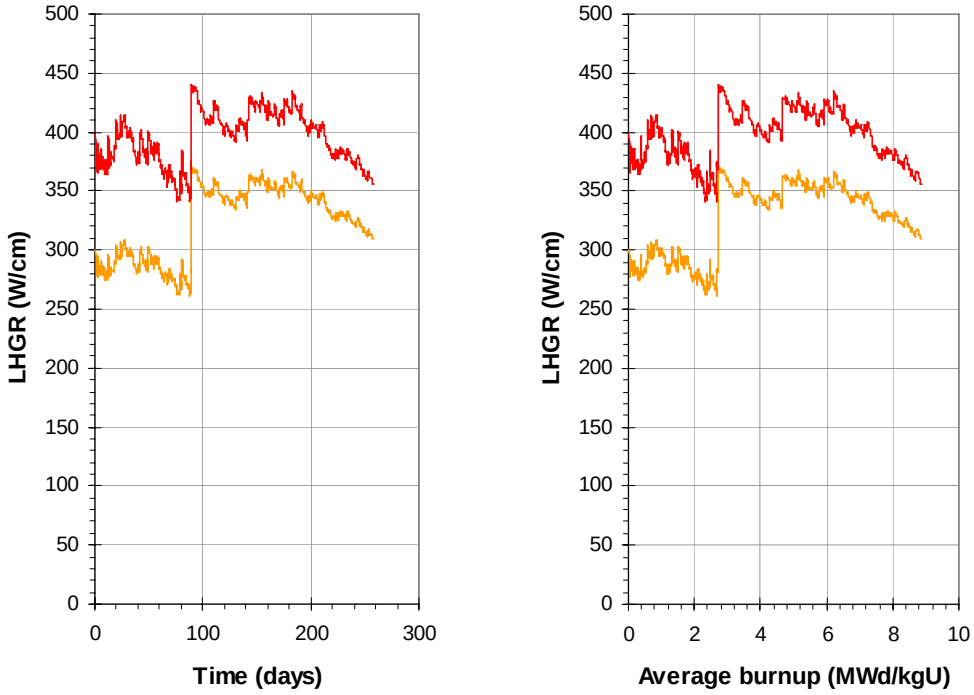

FIG. 1. Power history used in the end of life calculations.

These two power histories cover in principle the conditions for a feasibility analysis of the proposed design modifications in the fuel rod. They are hot channel with the maximum power for beginning of life and end of life conditions with the maximum burnup. The maximum local power is located approximately in the middle of the rod, and there is also located the maximum fuel temperature and cladding strain.

Along with these two power histories there is a time dependent input of the fast neutron flux (E > 821 keV) that is used in the irradiation damage model of fuel rod. And also others hydraulic operation conditions of the core like:

Primary system pressure (Coolant) = 115 bar
Coolant channel inlet temperature = 277.8 ºC
Mean coolant channel outlet temperature = 314.6 ºC

4.2 Evaluation of pellet thermal expansion by finite elements method

For the evaluation of fuel pellet length, the radial temperature distribution of the pellet calculated with the fuel rod code was used as input in a 3D finite element model of the thermal expansion of the fuel pellet implemented in a commercial platform of finite element analysis. The thermal expansion curve of the UO_2 was taken from the source code of the fuel rod code. This finite element model allowed evaluating the different amount of strain at pellet end and middle at maximum power.

5. Study of pellet density increase

Current density for Atucha–2 fuel pellet is 10.55 g/cm^3, but natural uranium pellet with a central value of 10.60 g/cm^3 has been already introduced for Atucha–1 pellets in MASU program. By shifting the density to 10.60 g/cm^3 there is a little improvement on the overall fuel performance due to the reduced pore content (from 3.7% to 3.1%), and also the uranium content is increased. This improvement is likely to be applied to Atucha–2 fuel in short term. All the calculations in this report have been done using a pellet density of 10.60 g/cm^3.

6. Study of pellet diameter change

The influence on the thermo-mechanical behavior of the Atucha–2 fuel rod by modifying the diameter of the fuel pellet was studied. The geometry of the cladding remains unmodified

6.1 Hot channel calculations

Calculations for hot channel were performed using the fuel rod code with power ramp from zero to the design maximum LHGR for a range of pellet diameter from 11.56 mm to 11.73 mm. According to the international experience a pellet-cladding gap on the order of 1.5 to 2.5% of the fuel diameter is recommended for a satisfactory performance at LHGR of 330 W/cm or greater. This range for Atucha–2 pellet will be from 17 mm to 29 mm.

The determination of the maximum strain of the cladding and the maximum temperature and gas release were obtained with different sets of model parameters in order to get conservative results.

Figure 2 shows the cladding strain due to power increase for various pellets diameters. As power increases the cladding strain raises by cladding thermal expansion, rod internal pressure increases and pellet expands. In this graph are marked three LHGR's, the core average LHGR, the maximum LHGR and the design maximum LHGR. For diameters smaller than 11.61 mm the pellet-cladding hard contact occurs for LHGR's above the maximum LHGR, and for diameters larger than 11.61 mm it occurs for smaller values.

Figure 3 shows the maximum strain of the cladding due to pellet expansion (after pellet cladding hard contact) as a function of pellet diameter. As pellet diameter increases, the maximum strain increases and reaches the stated limit of 1% for 11.66 mm. In the same Figure is represented the LHGR necessary to reach hard contact between fuel pellet and cladding and, the LHGR necessary for stress reversal, that is reverse the elastic stress produced by the coolant pressure.

In Figure 4 is showed the maximum fuel temperature and the maximum internal pressure in function of pellet diameter. Both maximum pellet temperature and maximum internal pressure decrease with diameter increase.

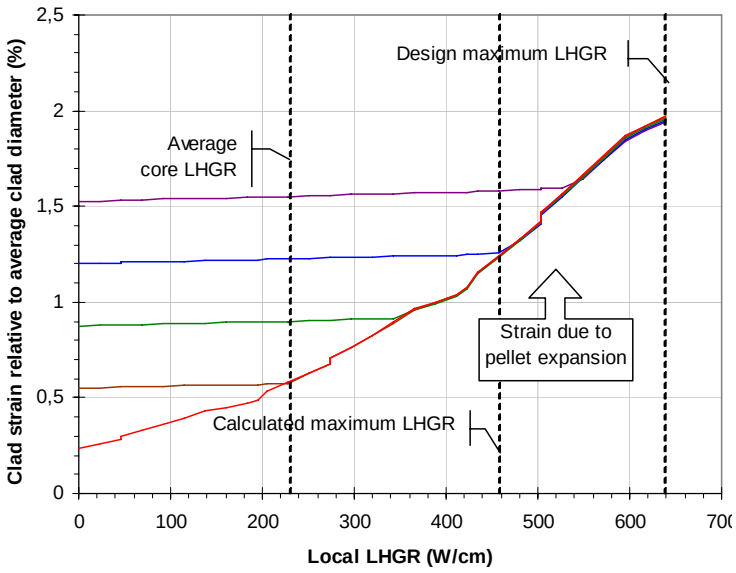

FIG. 2. Cladding strain for different pellet diameters at hot channel.

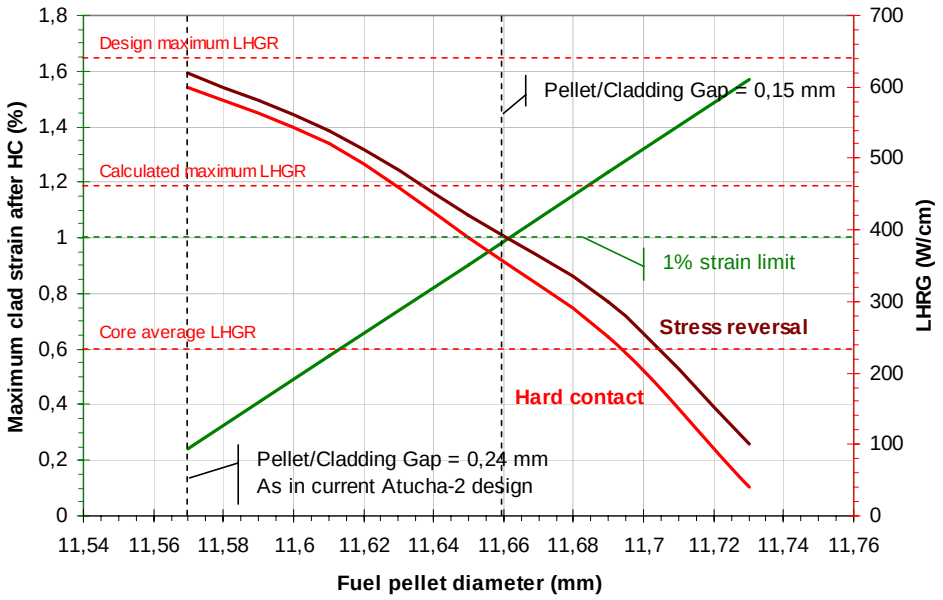

FIG. 3. Strain and hard contact for different pellet diameters at hot channel.

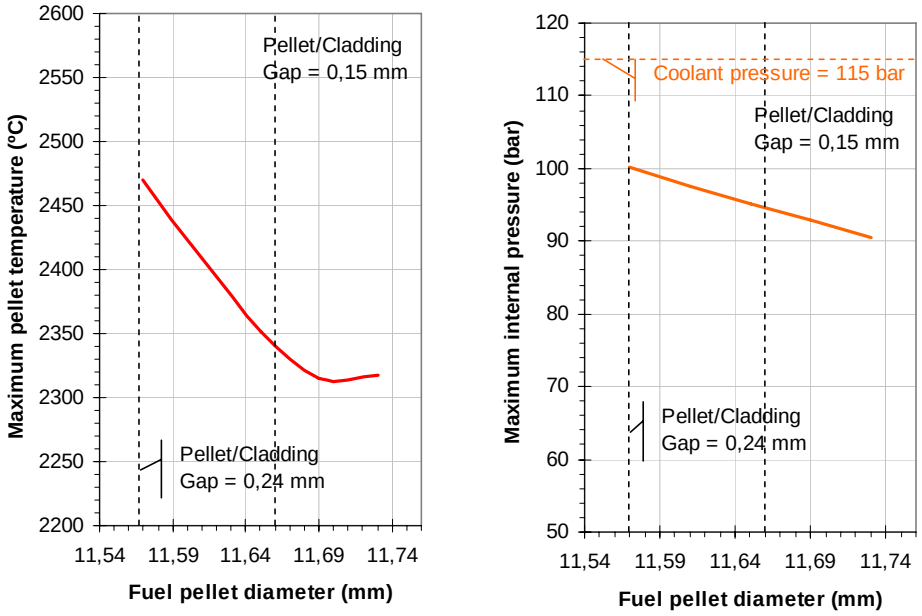

FIG. 4. Maximum pellet temperature and rod pressure for different pellet diameters at hot channel.

In these Figures can be observed that strain; temperature and pressure are in accordance with the design limits for pellets diameters up to 11.66 mm. A pellet diameter of 11.63 mm which means a pellet-cladding gap of 0.18 mm keeps within the limits with a security margin. Additionally hard contact for this diameter occurs for LHGR's between the calculated maximum and the design maximum.

6.2 End of life calculations

Calculations for end of life were done with the power history of Figure 1, for a range of pellet diameter from 11.56 mm to 11.73 mm.

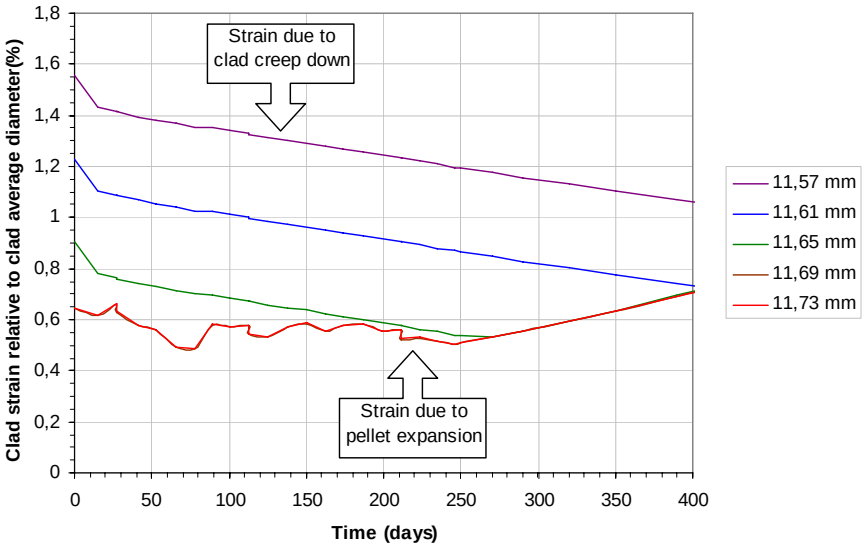

FIG. 5. Strain and hard contact for different pellet diameters at end of life.

Figure 5 shows the cladding strain for various pellets diameters as function of fuel rod average burnup. The cladding creeps down by the coolant overpressure as time pass. Once the fuel pellet thermal expansion and cladding creep are enough hard contact between both is established. As with higher pellet diameter the cladding contact the pellet earlier. For the pellet diameters equal or higher than 11.69 mm the hard contact occurs immediately after start up the fuel, and the cladding strains with the pellet thermal expansion from the beginning of the power history.

Figure 6 shows the cladding strain after hard contact as function of pellet diameter. For pellet diameters below 11.61 mm cladding strain is zero since hard contact doesn't occur. For pellet diameter between 11.61 mm and 11.65 mm there is a small amount of strain well below to the 1% limit. For diameter above 11.65 mm the cladding collapse at start up but the amount of strain is below the 1% limit in all cases. In the same Figure is represented the end of life internal pressure in function of pellet diameter. It decrease with the increase of pellet diameter and in all cases lies well below the coolant pressure.

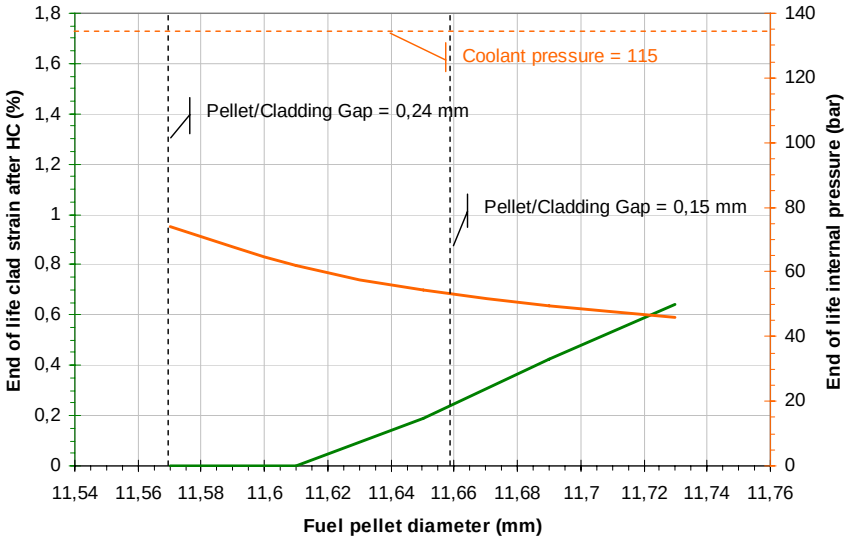

FIG. 6. Cladding strain and rod pressure for different pellet diameters at end of life.

7. Study of Pellet Length Increase, and Dishing Depth Modification

The influence on the thermo-mechanical behavior of the Atucha-2 fuel by modifying the length of the fuel pellet was studied.

Calculations for pellet length and dishing modification were done using a power ramp from zero to the design maximum LHGR for a range of pellet length from 11 mm to 17 mm, while keep the current pellet diameter. This implies a range of length-diameter ratio from 0.95 to 1.40. The value of displacement of the pellet surface at pellet ends and at middle was used to indicate the pellet deformation.

Results are in Figure 7, where are plotted the axial displacement of the pellet surface at dishing and the radial displacement of the pellet surface at middle and at edge. For all cases the influence of pellet geometry in the deformation of the pellet is very low.

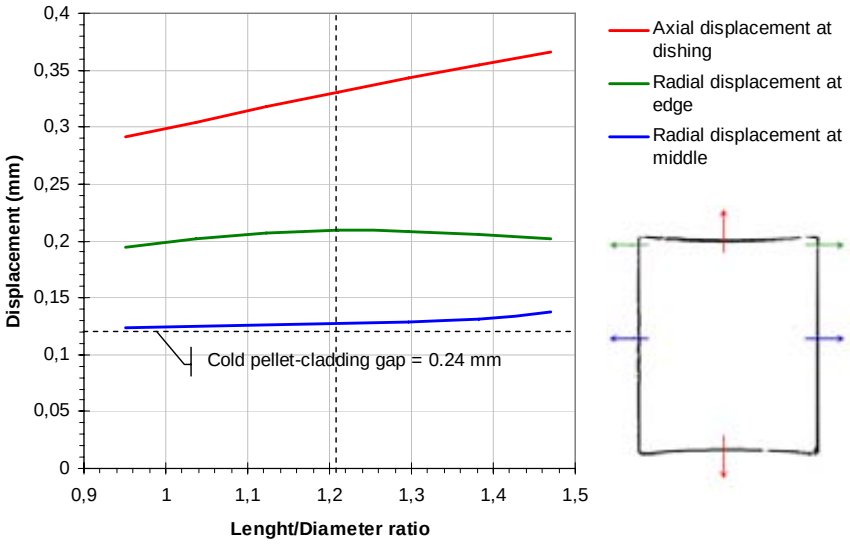

FIG. 7. Pellet thermal expansion for different length/diameter ratios at hot channel.

8. Study of initial pressurization change

In this section the influence on thermo-mechanical behavior of the Atucha–2 fuel rod of modifying the initial helium pressurization was calculated. In the current design of Atucha–2 fuel rod is initially pressurized with helium (with argon traces) up to 22.5 bar. Residual gas (mainly nitrogen) from fabrication is limited by the fuel pellet specification.

8.1 Hot channel calculations

Calculations for hot channel were done using the fuel rod simulation code with power ramp from zero to the design maximum LHGR for a wide range of initial pressure from 10 bar to 35 bar.

Figure 8 shows the maximum pressure and temperature reached at the design maximum LHGR in function of the initial pressurization. The internal pressure exceeds the coolant pressure for initial pressurizations higher than 30 bar. In the same Figure is represented the maximum pellet temperature, which decrease with higher pressures.

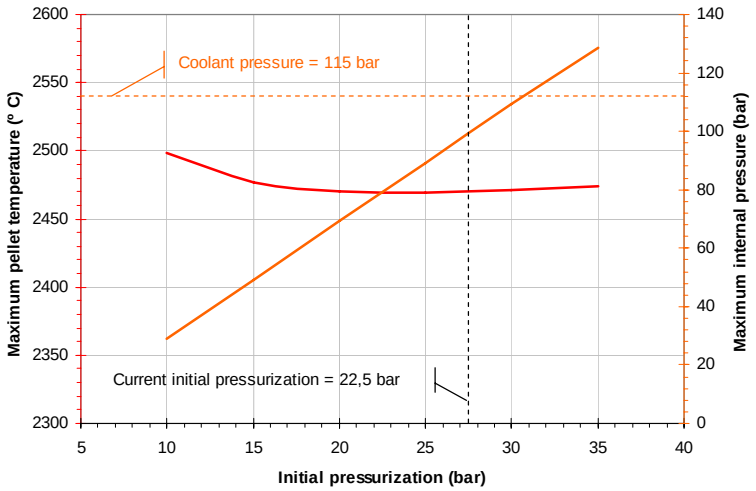

FIG. 8. Maximum temperature and rod pressure for different initial pressurizations at hot channel.

8.2 End of life calculations

Calculations for end of life were done with the power history of Figure 10, for a wide range of initial pressure from 10 bar to 35 bar

The next Table shows the end of life pressures for the power history, and all end of life pressures resulted less than the coolant pressure for all the initial pressurizations.

Initial Pressurization (bar)	10.00	15.00	20.00	25.00	30.00	35.00
End of life pressure (bar)	19.32	35.10	50.44	65.03	79.01	92.48

Figure 9 shows the cladding strain for various initial pressurizations in function of fuel rod average burnup. The cladding creepdown by the coolant overpressure increases as initial pressurization decrease. Hard contact between fuel pellet and cladding occurs only for initial pressurizations lower than 15 bar.

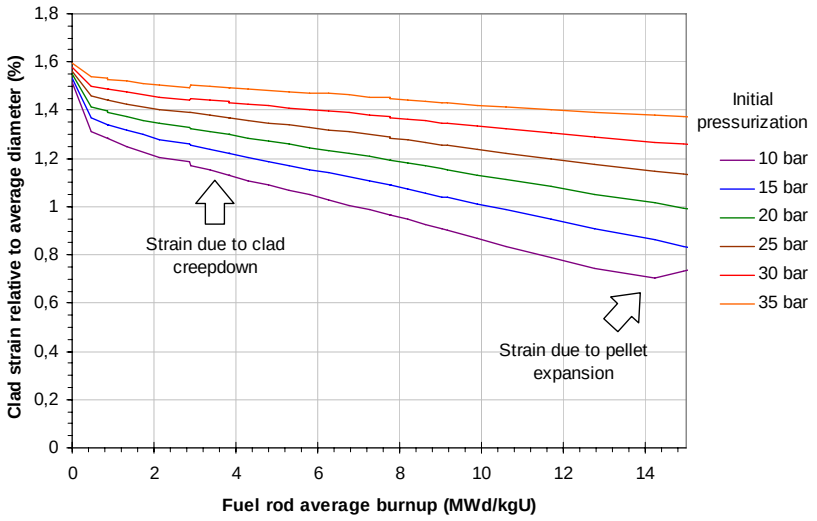

FIG. 9. Rod pressure for different initial pressurizations at end of life.

9. Conclusions

Some limits for future changes in the Atucha–2 fuel rod design with respect to pellet-cladding gap, pellet length and fuel rod initial pressurization were established.

In the case of pellet-cladding gap it was found that the minimum value that causes not to meet the design limit for maximum strain (1%) for the design maximum value of LHGR is 0.11 mm. The safety margin for the studied range of pellet-cladding gap with respect to this criterion can be also calculated from Figure 3. In addition the amount of reduction of pellet maximum temperature and end of life internal pressure associated with the reduction of pellet-cladding gap was estimated.

The pellet thermal strain for a range of pellet length was characterized. According to these result there is a margin for pellet length increase without significative deviations in the cladding strain from current design.

For the initial pressurization it was identified that the value for which the internal pressure limit is reached for the design maximum power is 30 bar. The cladding creepdown with lower initial pressurizations was calculated and used as a reference for the lower limit of internal pressure.

This information obtained is relevant for the future development of the Atucha–2 fuel rod design. The next step on this subject should include calculation of the fuel rod behavior with other fuel rod codes to compare results and studies on others fuel parameters like rod plenum and rod diameter.

REFERENCES

[1] NUCLEOELECTRICA ARGENTINA, S.A, CNA–2 Historias de irradiación de las barras combustible en las condiciones más desfavorables esperables durante la operación normal, (2009).

[2] US REGULATORY COMMISSION, Standard review plan, Chapter 4.2: Fuel system design, NUREG–0800.

[3] CNEA, Análisis del diseño de la barra combustibles para incremento de la masa de uranio de la BC CNAl, Internal Report, (1999).

[4] NOTARI, C., A PHWR with slightly enriched uranium, Annals of Nuclear Energy, Vol. **31**, Issue 3, (2003), p.303–309.

Application of Probabilistic Methods to Fuel Rod Design Evaluation

A. Wensauer[a], I. Distler[b]

Abstract. The safety concept of nuclear power plants relies on a system of multiple barriers to preclude the release of fuel containing uranium and/or plutonium or highly radioactive solid and gaseous fission products generated during operation of the reactor. The gas-tight welded fuel rods (FRs) represent a first and important barrier of this concept. As a consequence, FR design must demonstrate that systematic failures are precluded by applying appropriate codes and methods. In particular, this means that critical physical quantities (e.g. temperatures, strains, internal pressure) must not exceed their design respectively defect limits. Traditional proofs in the field of nuclear engineering are based on a conservative-deterministic approach which makes use of an unfavorable combination of input parameters with respect to interesting quantities. However, there have been significant drivers during the last years which triggered the advancement of more realistic methodologies. For instance, power uprates of plants, increased enrichments and burnups, and the pertaining challenging experience feedback from PIE and pool measurements push forward to regimes which were not preconceived when the traditional concepts in FR design evaluation were established. Thus, all stakeholders of the licensing process started to reflect the potential of the traditional approaches in the light of current and future demands, i.e. in particular to improve fuel utilization and reduce the amount of radioactive waste: What is the degree of conservatism of the conservative-deterministic approach? Is it over-conservative, are sufficient margins left at more challenging demands, or might there even be a lack of conservatism possible? Is the selection of input parameters within the deterministic approach still justified? Are there — dependent on the situation — other combinations conceivable with more unfavorable results? Is it possible to map the possible nonlinear response of state-of-the-art codes? To answer these questions it was proposed to apply an advanced approach based on the combination of probabilistic methodologies, best-estimate codes, and a comprehensive, reliable database what allows for a controlled way to approach the technical limits by a realistic assessment (‘best-estimate scenario’) as well as by a conservative result with a well defined degree of conservatism in terms of an appropriate quantile. Thus, the advanced approach is able to fulfill all requirements of licensing scenarios and, thus, can be used as a direct licensing tool or as a benchmark for the traditional methods.

1. Introduction

The safety concept of nuclear power plants relies on a system of multiple barriers to preclude the release of fuel containing uranium and/or plutonium or highly radioactive solid and gaseous fission products generated during operation of the reactor. The gas-tight welded fuel rods (FRs) represent a first and important barrier of this concept. As a consequence of the significance of this barrier, FR design must demonstrate that systematic failures are precluded by applying appropriate codes and methods. In particular, this means that critical physical quantities (e.g. temperatures, strains, internal pressure) must not exceed their design respectively defect limits. FR design was one of the first fields in nuclear industry where probabilistic methods were applied to normal operation of plants to cope with advanced demands. It had been developed by the predecessor of today’s AREVA NP GmbH, the Siemens AG, [1–9] and applied to licensing issues in FR design since 1995 where it proved to be a very stable, powerful, and flexible tool.

Thus, probabilistic methods in FR design provide an ideal example to illustrate the potential and benefit associated to this advanced approach. Moreover, the probabilistic approach is a tool whose application range can be extended to other areas of interest as well, and, therefore the description includes some fundamental mathematical aspects, too.

This Paper is organized as follows: The second section deals with the evolution of demands imposed on FR design. In the third and fourth section it is investigated how traditional and probabilistic approaches perform with respect to the advanced requirements. The Paper ends with a brief conclusion and outlook.

[a] AREVA NP, Erlangen, Germany.
[b] AREVA NP, Erlangen, Germany.

2. Evolution of demands

During the last years there has been a combination of significant drivers which triggered the advancement of more improved methodologies to be applied in the nuclear industry. The most important reason originates from the operators' wish to economically optimize plant and fuel utilization of existing nuclear power plants. To achieve this goal several measures (or even a combination of them) are possible to be applied. The typical scenarios are power uprates of plants (up to 20% in thermal power) what is associated to a corresponding increase of core average linear heat generation rate (LHGR). Another option is an increased enrichment approaching and reaching the limit of 5 w/o U^{235} for commercial LWRs. Those high enrichments allow for extended rod burnups up to 75 MW•d/kg(HM). Moreover, the impact of improved fuel utilization with reduced reload and discharge batches is not only restricted to economical aspects, but can be transferred to ecological aspects as well. Advances in fuel economics lead to a decreased amount of spent fuel what can be directly related to the average fuel assembly burnup of discharge batches depicted in Figure 1.

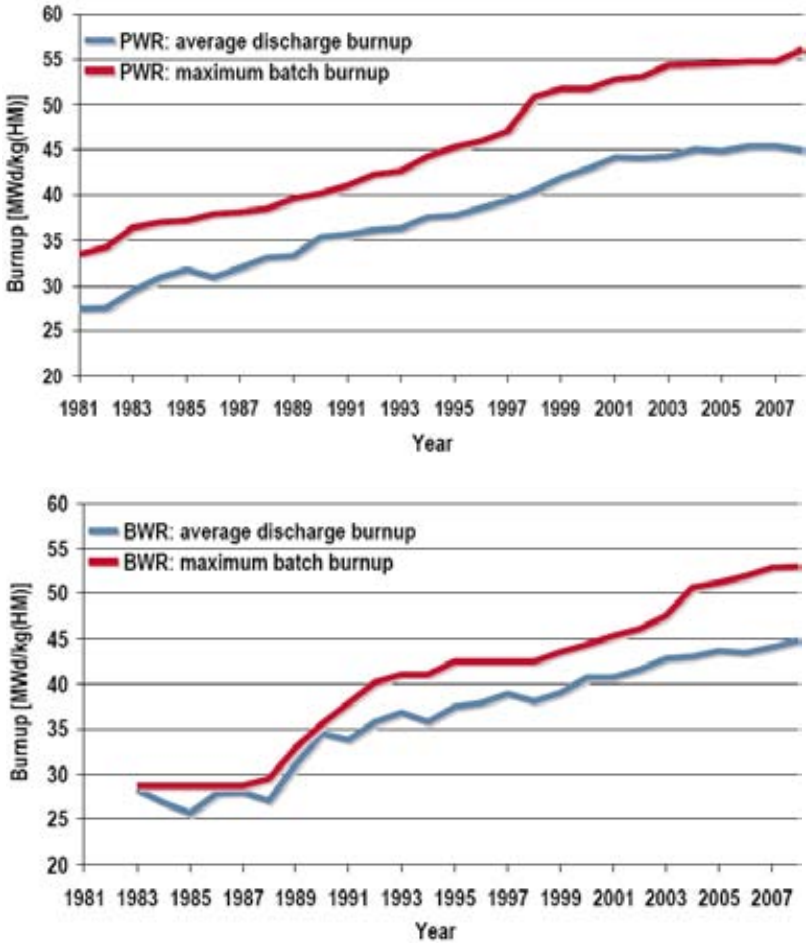

FIG. 1. Increase in average and maximum discharge burn-up over the last decades for PWR and BWR

Of course, this development is strongly correlated with increasing technical demands. Focusing on FR design aspects the most important challenge originates from the combination of high burnup and high power for UO_2 fuel with high enrichment or MOX fuel with high fissile plutonium content. These new regimes were continuously approached by the irradiation of lead test assemblies accompanied by comprehensive inspection campaigns enclosing pool measurements and post irradiation examination. The latest experience for FRs turned out to be very challenging yielding results which could not be preconceived from the application of established codes and methods in FR design evaluation. This trend is impressively illustrated in Figure 2 schematically showing the range of the fission gas release database for UO_2 rods irradiated in commercial PWRs in the mid 1990s and today.

Facing the new challenges all stakeholders of the licensing process were prompted to reflect the potential of the traditional approaches in the light of current and future demands.

3. Traditional approaches

Traditional proofs in the field of nuclear engineering are based on a conservative-deterministic approach which makes use of an unfavorable combination of input parameters with respect to interesting quantities.

In the field of FR design this kind approach was well founded within the frame of the boundary conditions of the past. Due to low enrichments the achieved maximum rod burnups were well below 40 MW•d/kg (HM) and the decrease of reactivity led to decreasing rod powers as well. Moreover, the fuel at that time did not provide today's dimensional stability. Under these conditions with a minimum of dependencies and interactions between different models (and a still unknown degradation of fuel thermal conductivity) verifications turned out to be straight forward: For example the highest fuel temperature in the core could be easily identified at the rod position with maximum LHGR which occurred for a rod with low burnup due to reactivity reasons and in an open-gap situation.

With the introduction of fuel with increased enrichment up to 5 w/o U^{235} and MOX fuel the burnups were significantly increased to 70 MW•d/kg (HM) and beyond while simultaneously the higher reactivity allows for high LHGR even in the medium- and high-burnup range. In combination with an increased knowledge on fuel properties, for example degradation of fuel thermal conductivity with burnup (e.g. [20]), the situation is more complex. Figure 3 demonstrates the basic sensitivity of fuel temperature on LHGR and irradiation: a certain decrease of LHGR has to be assumed to keep the temperature constant with increasing burnup.

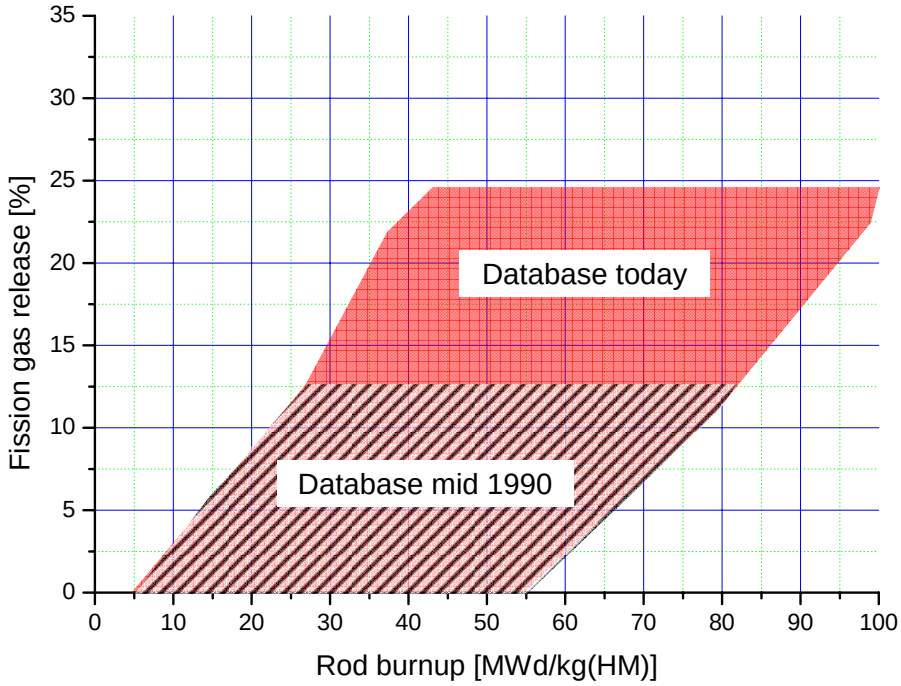

Figure 2. Schematic range of the fission gas release database for UO_2 rods irradiated in commercial PWRs: comparison between the mid 1990s and today

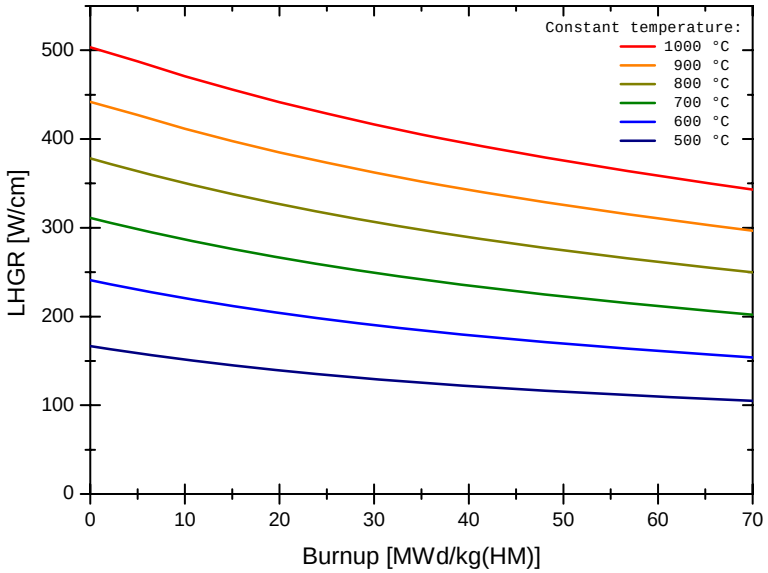

FIG. 3. Necessary decrease of LHGR which has to be assumed to keep the average fuel temperature constant with increasing burnup (example for UO_2)

When the LHGR exceeds the threshold sketched in Figure 3 the original conservative-deterministic approach shows a lack of conservatism due to continuously changing boundary conditions without reviewing the original assumptions. Of course, this example illustrates an extreme case, however, even in less severe situations it can be questioned whether the degree of conservatism remains unchanged in an analysis considering all aspects.

In contrast, the opposite case might be also possible that the existing methods exhibit a degree of conservatism which is not required to comply with the safety guidelines. In this case there would be sufficient margins left to realize a more economical fuel management with reduced reload batches, and consequently, a reduced number of spent fuel assemblies.

Considering the recent experience is not only associated to changed material properties but also impacts the mathematical complexity of FR codes. On the other hand, however, the positive experience with lead test assemblies showed the technical feasibility of new economically optimized fuel management schemes. Consequently, developers were prompted to manage the challenges arising for FR codes from the new database. For example, as pointed out in the previous section for the experimental data on fission gas release the latest data does not only indicate the well known dependence on burnup but, moreover, reveals a pronounced sensitivity on LHGR (or fuel temperature) as well. This kind of experience feedback for high power and high burnup was not included in the validation database of older FR codes and could not be anticipated either. Thus, the effect of LHGR is not mapped in the models of older FR codes causing partly inconservative predictions for fission gas release and rod internal pressure. Introducing the temperature sensitivity into a FR code means that the non-linear effect in the fission gas release model of state-of-the-art-codes will be additionally stressed. Please recall that fission gas release is a mainly diffusion-driven process with a strong non-linear dependence caused by Arrhenius type diffusion coefficients.

Consequently, it has to be reviewed whether error propagation assuming linear dependence on parameters is still an appropriate approach for FR code models with increased complexity. The relevance of this question is demonstrated by the following two simple examples. Let be $f_1 : (x_1, x_2) \mapsto 0.5 \cdot x_1 + 0.8 \cdot x_2$, $f_2 : (x_1, x_2) \mapsto 0.5 \cdot x_1 + 0.8 \cdot x_2 + x_1 \cdot x_2$ two functions depending on two normally distributed ($\mu = 0, \sigma = 1/3$) parameters x_1, x_2. Obviously, $f_1(x_1, x_2)$ is a linear function of x_1, x_2, and, thus, the simple error propagation for the 95%-quantiles $x_1(0.95) = x_2(0.95) \approx 0.545$ of the input parameters yields a 95%-quantile of 0.51 for the

distribution of $f_1(x_1, x_2)$. This is in agreement with the result which can be obtained by direct integration of the problem which is feasible for such an easy case. Turning to $f_2(x_1, x_2)$ it seems to be linear when the tests are restricted to the x_1 or x_2 axis although it includes a nonlinear element. Therefore, the result of the error propagation method remains unchanged with 0.51, however, the result of the direct integration is 0.61. This example shows that the potential of error propagation methods assuming linear dependence is limited whenever the model response is governed by nonlinear effect which cannot be properly addressed in this approach.

Due to this higher degree of complexity of models in FR codes it can be questioned in general whether a certain set of input parameters (roughly 10 to 20 for models and geometry and, in addition, the state-points defining the power history) can be still justified to be conservative in all cases conceivable within the deterministic approach for one certain criterion. The huge variety of situations could allow for other possible combinations to yield more unfavorable results.

Thus, in summary the basic questions to be answered by probabilistic methods are:

- What is the degree of conservatism of the conservative-deterministic approach?
- How to achieve a compromise which allows for an appropriate consideration of the combination of economical, ecological and technical requirements?

4. Probabilistic methods

To answer these questions in the area of FR design it had been proposed [1–9] to apply an advanced approach based on the following combination of elements:

- Best-estimate codes validated against a comprehensive, representative, reliable database
- Analysis of the uncertainty of input parameters
- Probabilistic methodologies

As results will be obtained:

- A realistic assessment (‘best-estimate scenario’) when omitting the uncertainties
- A conservative assessment with a well defined degree of conservatism in terms of an appropriate quantile (safety and confidence level)

In the following the probabilistic approach is demonstrated at the example FR design at AREVA NP.

The first important element of a probabilistic approach requires a best-estimate code which is validated against a comprehensive, representative, reliable database. AREVA NP is in the comfortable position to have a database of its disposal which can be called unique in the world. It comprehends data from pool campaigns and post-irradiation examination originating from test and power reactors. This data encloses all important validation parameters (e.g. temperatures, strains, fission gas release, etc.) which are required to fulfill today’s and future demands like:

- Traditional and modern fuel management schemes
- High power densities
- High enrichments up to 5 w/o U^{235}
- High burnups up to 100 MW•d/kg(HM)
- UO_2, MOX, and UO_2/Gd_2O_3 fuel
- Modern fuel types

Beyond the best-estimate validation there are additional requirements arising from the intended application within the frame of a probabilistic approach:

- Excellent run-time to be able to perform up to 10^3 … 10^5 calculations in several hours on a Linux cluster or multi-processor workstation
- Excellent numerical stability without any aborts
- Reliable error management to detect numerical problems and warn users if any problems should occur

Currently AREVA NP has two codes available and licensed fulfilling the above requirements for probabilistic methods:

- CARO-E3 for PWR and BWR application in Europe (Erlangen market)
- RODEX4 for BWR application in USA

In the near future COPERNIC3 [16] will serve as AREVA NP advanced global FR code for PWR and BWR application. It will replace the current codes used for probabilistic methods whereby all the international experience is accounted for which has been gained with the advanced method for more than 14 years.

Concerning the uncertainties entering into the FR code it has to be distinguished between fabrication and model uncertainties. Probability distributions of fabrication uncertainties can be easily derived from an analysis of manufacturing procedures including specifications and processes. In most of the cases it will be possible to show that typical input parameters of FR codes as pellet diameter, clad inner and outer diameter are normally distributed. The analysis of model parameter uncertainties requires a more thorough analysis as they depend on the model sensitivity. Finally, the resulting model parameter probability distributions have to map the probability of a code over-prediction or under-prediction.

The principles of AREVA NP's probabilistic methodology in FR design are outlined in the following paragraphs. A detailed mathematical description can be found e.g. in [11].

The objective of the method is the estimation of the fraction of FRs in a population (e.g. core, reload or discharge batch) not exceeding the given limit by n simulations. The random selection of a FR is implemented in two steps (Figure 4).

Let us consider the j^{th} simulation (or calculation) ($1 \le j \le n$). In the first step one FR (we assume the k^{th} FR) out of N FRs in the population is randomly selected. Thus, all rod-specific quantities (power history, materials, input parameter distributions) are uniquely determined. The probability for each rod to be selected is 1/N as we are dealing with a Laplace experiment.

In the second step the parameters are randomly selected with respect to the underlying distribution. The randomly chosen parameter combination will yield a value $y \le y_L$ with probability p_k (FR does not exceed the limit, $V_j = 1$) and a value $y > y_L$ with probability $1-p_k$ (FR exceeds limit, $V_j = 0$). V_j is the random variable describing the result of the j^{th} simulation. According to the random selection of the method the probabilities are

$$p := P(V_j = 1) = \sum_{k=1}^{N} \frac{1}{N} p_k \quad \text{and} \quad P(V_j = 0) = 1 - \sum_{k=1}^{N} \frac{1}{N} p_k = 1 - p\,. \tag{1}$$

Therefore, we can identify $V = V_1 + \ldots + V_n$ as a Bernoulli chain with probability p, length n and expected value

$$E(V) = n \cdot p\,. \tag{2}$$

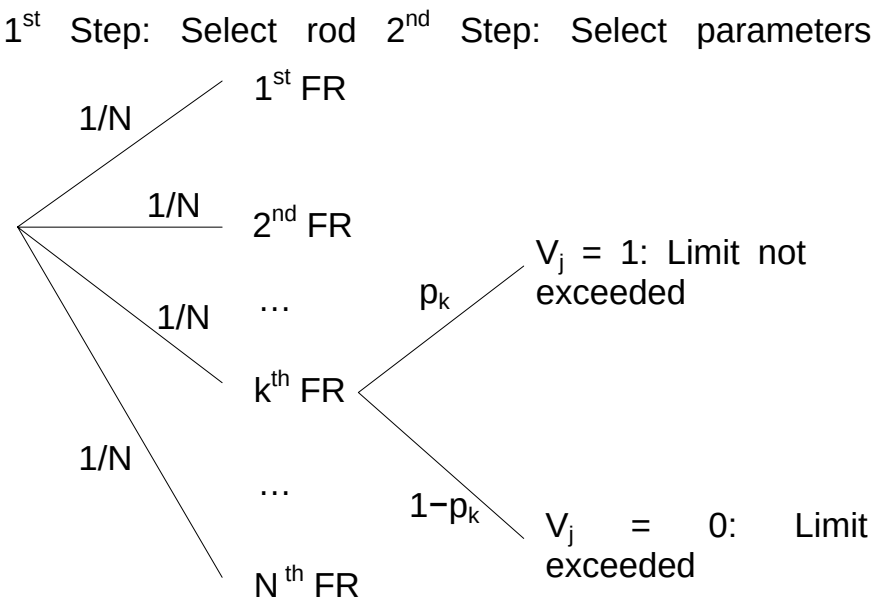

FIG.4. Random selection of a FR and rod-specific parameters in two steps.

From n simulations we obtain v/n as an estimator for p. The confidence interval $[p_L,1]$ corresponding to the confidence level (1-α) is given by

$$p_L = \frac{v}{v + (n - v + 1)\cdot F_{2(n-v+1),2v;1-\alpha}} \tag{3}$$

according to [17]. $F_{a,b;1-\alpha}$ are the quantiles of the Fisher distribution.

Consequently, the interpretation of the result reads: "The fraction of FR in the population not exceeding the given limit is at least p_L with a confidence level of at least (1−α)." Using the relation

$$E(V) = \sum_{j=1}^{N} p_j = Np \geq Np_L \tag{4}$$

we find an alternative interpretation: "The expected value of the number of FR in the core not exceeding the given limit is at least $N\cdot p_L$ with a confidence level of at least (1−α)."

Solving Equation (3) for n we are able to derive the number of required simulations as a function of p_L, (1−α), and v (respectively z = n−v)

$$n = z + \frac{p_L}{1 - p_L}(z+1)\cdot F_{2(z+1),2(n-z);1-\alpha} \approx \frac{1}{1 - p_L}(z+1)\cdot F_{2(z+1),\infty;1-\alpha}\,. \tag{5}$$

The approximation is correct in the limit of large n and small z. Examples for p_L = 99.9% and (1−α)=0.95, i.e. the 95%/99.9% quantile, or, p_L = 1−1/N and (1−α)=0.95, i.e. 95%/1−1/N quantile (so-called 'one-rod quantile'), are given in Table 1.

TABLE 1. REQUIRED NUMBER OF SIMULATIONS

	z=0	z=1	z=2	z=3	z=4
p_L = 0.999	n≈3000	n≈4750	n≈6300	n≈7750	n≈9200
p_L = 1-1/N	n≈3.0N	n≈4.7N	n≈6.3N	n≈7.8N	n≈9.2N

The above mathematics reveals another interesting feature of probabilistic methods: the number of required calculations depends only on the desired quantile, but not on the number of input parameters. Consequently, this approach can very well deal with a huge number of input parameters (even with non-linear dependencies or non-Gaussian distributions). In contrast to traditional approaches tedious sensitivity analysis of parameters and combinations of parameters are not required. The relevance of input parameters and their sensitivity with respect to all different output parameters is inherently mapped onto the resulting distributions. It is a non-intuitive, advantageous feature of the concept that it works truly unbiased and does not have to rely on any existing knowledge. Moreover, the same set of calculations can be used to analyze all interesting output parameters (e.g. rod internal pressure, strain, temperature) simultaneously.

After reviewing the mathematical basics of the probabilistic approach the focus is shifted back to the physical interpretation of the results. The crucial objective of verification in FR design is to preclude systematic FR failures. This means that for licensing purposes an appropriate combination of underlying population, quantile, and pertaining criterion has to be identified which fulfills this basic objective. This means that there in not only one unique constellation which complies with the requirements. Due to historical reasons licensing boundary conditions developed differently and this effect can be still observed today. The following two examples show combinations which, both, fulfill the requirement and are established in FR design licensing with respect to internal pressure in Germany [11] and the USA [15]:

- Germany:
  Population: complete core
  Quantile: 95%/1−1/N (‘one-rod quantile’) [10, 12]
  Criterion: Preclude rod failure by thermal feedback by limitation of the reopening of the gap due to internal overpressure; criteria derived from rod overpressure experiments [18, 19]

- USA:
  Population: reload batch
  Quantile: 95%/99.9%
  Criterion: system pressure plus 55 bar

It is noticeable that the above interpretation can be mathematically extended. The additional statements which can be derived can be found in [13, 14]. They underline that the new approaches are consistent and target-oriented to preclude systematic fuel failures. Moreover, it was proved that the probabilistic approach can be also applied to a mixed core situation which is often realized in plants, i.e. one part of FRs is treated by new and another part by traditional methods.

Before closing this section an example of a rod internal pressure distribution is presented in Figure 5. The underlying population consists of all the rods (UO_2, UO_2/Gd_2O_3, and MOX) contained in the core of a German 16 × 16 PWR. The probabilistic assessment was performed applying the FR code CARO-E3. The total number of 136110 calculations is sufficient to evaluate quantiles up to the one-rod quantile with a confidence level of 95%. The internal pressure values pertaining to the 95%/99.9% and the 95%/99.9978% quantile are 126 bar and 154 bar. Moreover, these results clearly proof that any risk for systematic FR failure can be precluded as the majority of FRs in the core are far away from calculated maxima. This crucial information is new compared to the traditional conservative-deterministic approaches which only provide knowledge on extreme values irrespectively how many FRs are in the vicinity of those extremes.

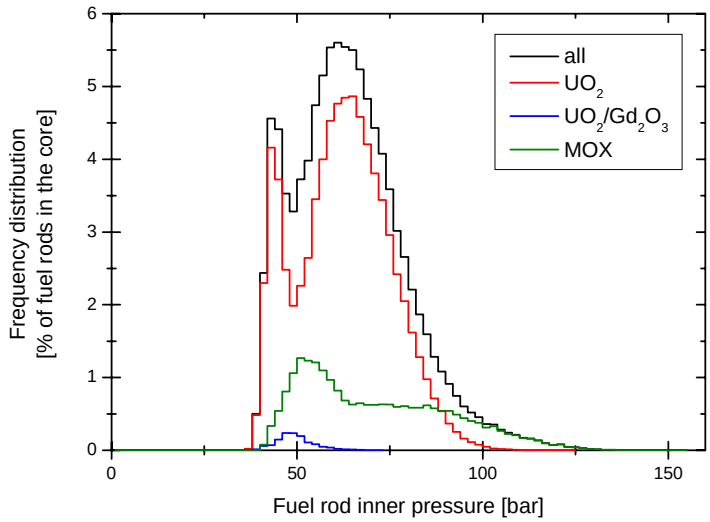

FIG.5. Resulting distribution of rod internal pressures in the core of a German 16×16 PWR with 45370 FRs containing UO_2, UO_2/Gd_2O_3, and MOX fuel

In summary, the new approach is able to fulfill all requirements of licensing scenarios and, thus, can be used as a direct licensing tool or as a benchmark for the traditional methods. Moreover, due the provided high information density it defines a controlled path to approach the technical limits, e.g. in lead test assembly programs, at a well controlled and monitored risk.

5. Conclusions and outlook

This Paper proofs that probabilistic methods enclose an enormous mathematical potential with respect to their applicability in the context of nuclear safety. They provide two main elements which are crucial for today's demands. First of all they include a best-estimate approach which yields the realistic result, and second, they allow for a systematic consideration of uncertainties which can be quantitatively controlled. Moreover, the number of calculations depends on the safety and confidence level only which are appropriately adapted to the objective of verification, however, it does not depend on the number of input parameters or requires linear response. Thus, probabilistic methods are ideal tools to be applied to today's problems with high complexity depending of an increased number of input parameters.

Thus, the new approach has the capability to fulfill all requirements of licensing scenarios. It is well established and has been used as a direct licensing tool in fuel rod (FR) design for many years (e.g. in Germany, Scandinavia, Sweden, Finland, Netherlands, Spain), and was recently approved by NRC in the USA. Moreover, probabilistic approaches are available as a benchmark for the traditional methods to prove that sufficient margins are still available. Their growing relevance is indicated by the extension of their application to other areas as analysis of LOCA or hold-down springs as well.

In conclusion, probabilistic methods turn out to be the answer how to adequately address economical, ecological, and technical safety-related aspects in nuclear industry and beyond.

REFERENCES

[1] HEINS, L, GROSS, H., NISSEN, K., WUNDERLICH, F., Statistical analysis of QC data and estimation of fuel rod behaviour, J. Nucl. Mat. **178**, (1991), p.287.

[2] HEINS, L, SCHIEDEL, R., Probabilistic fuel rod design applied to maximum rod internal pressure criterion of PWR fuel rods, Jahrestagung Kerntechnik, Stuttgart, (1994).

[3] EBERLE, R., HEINS, L, SONTHEIMER, F., Fuel rod analysis to respond to high burnup and demanding loading requirements: probabilistic methodology recovers design margins narrowed by degrading fuel thermal conductivity and progressing FGR, IAEA Techn. Comm. Meeting on Water Reactor Fuel Element Modeling at High Burnup and its Experimental Support, (1994).
[4] SCHIEDEL, R., DISTLER, l., HAHN, T., Probabilistische Methoden in der Brennstabauslegung, Jahrestagung Kerntechnik, (1996).
[5] HEINS, L., Improved fuel rod design by statistical methods, Technical Meeting of the "Fuel Assembly" and "Reactor Physics and Calculation Methods" Groups of the German Nuclear Society (KTG), (1998).
[6] HEINS, L, LANDSKRON, H., Fuel rod design by statistical methods for MOX fuel, International Symposium on MOX Fuel Cycle Technologies for Medium and Long-Term Deployment, (1999).
[7] HEINS, L, Fuel rod design by statistical methods for increased demands, TOPFUEL '99, (1999).
[8] ARIMESCU, V.I., HEINS, L., Nonparametric order statistics method applied to uncertainty propagation in fuel rod calculations, IAEA TCM on Nuclear Fuel Behavior Modeling and its Experimental Support, (2000).
[9] ARIMESCU V.I., HEINS L., Statistical methodology to quantify uncertainties of best-estimate fuel rod design calculations, International Meeting on Best-Estimate Methods in Nuclear Installation Safety Analysis, (2000).
[10] RSK-Bericht, Erhöhung der thermischen Leistung des Kernkraftwerks Grafenrheinfeld (RSC report, Enhancement of the thermal power of the reactor Grafenrheinfeld (KKG)), in German, (2003), www.rskonline.de.
[11] WENSAUER, A., DISTLER I., HEINS, L., Probabilistic uncertainty analysis applied to fuel rod design, Probabilistic Safety Assessment and Management, PSAM 7–ESREL '04, Volume **5**, Springer, (2004).
[12] RSK-Bericht, Gestaffeltes Sicherheitskonzept, (RSC report, Multi-Level Safety Concept), in German, (2005), www.rskonline.de.
[13] FALK, M., HEINS, L., WENSAUER, A., Safety assessment of fuel rods via generalized Bernoulli chains, IEEE Transactions on Reliability **55,** (2006), p.393–396.
[14] FALK, M., HEINS, L., WENSAUER, A., Verification of rod safety via confidence intervals for a binomial proportion, Nuclear Engineering and Design **237**, (2007), p.1055–1059.
[15] ARIMESCU, V.I., Best-estimate BWR fuel thermal-mechanical analysis based on non-parametric order statistics, Water Reactor Fuel Performance Meeting, (2008).
[16] GARNIER, CH., SONTHEIMER, F., MAILHE, P., LANDSKRON, H., DEUBLE, D., ARIMESCU, V.I., BELLANGER, PH., Validation of advanced fuel performance COPERNIC3 code on AREVA, Global Database up to 100 GW•d/tHM, Proceedings of Top Fuel 2009, (2009).
[17] DIN 53804/Teil 4, Statistische Auswertung; Attributmerkmale, Beuth Verlag, (1985).
[18] SONTHEIMER, F., NISSEN, K.L., Evaluation of the stress reversal creep experiment IFA-585 in the HBWR and the lift-off experiment ROPE-I in the R2 Studsvik using the Siemens/KWU clad creep model, Enlarged HPG Meeting in Bokesjø, (1994).
[19] SONTHEIMER, F., BILLAUX, M.R., Mechanical analysis for the Siemens rods during ROPE-II start-up with a new advanced Siemens fuel rod code, Enlarged HPG Meeting in Loen, (1996).
[20] WIESENACK et al., Assessment of UO_2 conductivity degradation based on in-pile temperature data, OECD Halden Reactor Project, HWR-469 (1996).

Fuel Element Designs for Achieving High Burnups in 220 MW(e) Indian PHWRs

P.N. Prasad [a], R.M. Tripathi [b], A.N. Kumar [c], S. Ray [d], K.P. Dwivedi [e]

Abstract. Presently 19-element natural uranium fuel bundles are used in 220 MW(e) Indian PHWRs. The core average design discharge burnup for these bundles is 7000 MW•d/Te U and maximum burnup for assembly goes upto of 15 000 MWD/Te U. Use of fuel materials like MOX, Thorium, slightly enriched uranium etc in place of natural uranium in 19-element fuel bundles, in 220 MW(e) PHWRs is being investigated to achieve higher burnups. The maximum burnup investigated with these bundles is 30 000 MW•d/Te U. In PHWR fuel elements no plenum space is available and the cladding is of collapsible type. Studies have been carried out for different fuel element target burnups with different alternative concepts. Modification in pellet shape and pellet parameters are considered. These studies for the PHWR fuel elements/assemblies have been elaborated in this paper.

1. Introduction

Presently, India has 17 Nuclear Power Plants (NPPs) in operation with a total installed capacity of 4120 MW(e), which includes PHWRS[f] of two 540 MW(e) capacity and 13 number of 220 MW(e) capacity and two BWR reactors of General Electric make. Indian nuclear power programme is guided by the limited available natural uranium and the vast amount thorium resources available. Therefore the fuel design, development and fuel utilization are planned accordingly and fuel bundle design using higher fissile content fuel materials like SEU, MOX, Th etc which can be irradiated to burnups of 20 000 to 30 000 MW•d/Te HE[g] are being developed. The fuel bundle design in use at present is limited to irradiation up to 15 000 MW•d/Te U burnup. The high burnup fuel element development studies for the PHWR fuel elements/assemblies and subsequent irradiations have been elaborated in this paper.

2. Design studies

Presently 19- element natural uranium fuel bundles are used in 220 MW(e) Indian PHWRs[1]. Figure 1 shows the fuel bundle and the element details. The core average design discharge burnup for these bundles is 7000 MW•d/Te U and maximum burnup for the bundle assembly goes upto of 15 000 MW•d/Te U.

Increase in fuel burnup beyond 15 000 MW•d/Te U using higher fissile content materials like slightly enriched uranium, Mixed Oxide and Thorium Oxide in place of natural uranium in fuel elements used in 220 MW(e) PHWRs is being investigated. Performance of these fuel bundles at high burnup is studied. Due to higher fissile content these bundles will be capable of delivering higher burnup than the natural uranium bundles. The maximum burnup studied with these bundles is 30 000 MW•d/Te U.

In PHWR fuel elements no plenum space is available and the cladding is of collapsible type. The additional fission product swelling and gas release due to use of high burnup fuels in PHWRs, needs to be accommodated within the fuel elements taking into account these factors.

---

[a] Nuclear Power Corporation of India Limited, Mumbai, India.
[b] Nuclear Power Corporation of India Limited, Mumbai, India.
[c] Nuclear Power Corporation of India Limited, Mumbai, India.
[d] Nuclear Power Corporation of India Limited, Mumbai, India.
[e] Nuclear Power Corporation of India Limited, Mumbai, India.
[f] Pressurised heavy water reactors.
[g] Burnup of MOX bundles is specified in MW•d/Te HE (tonne of heavy element).

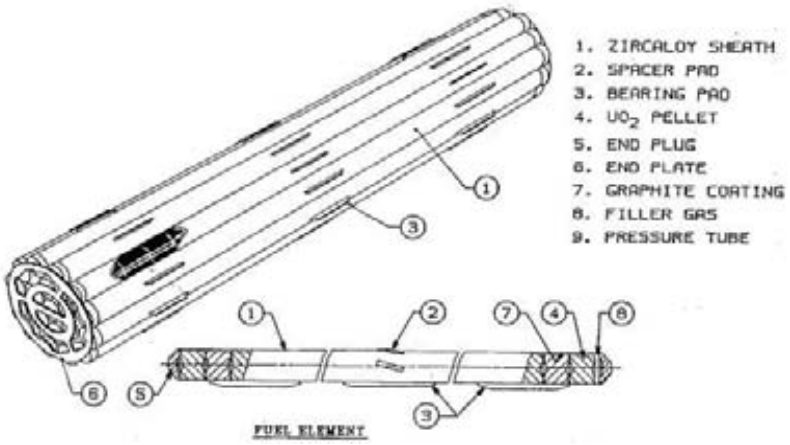

FIG. 1. 19–Element fuel bundle for 220 MW(e) reactors.

Studies have been carried out for different fuel element target burnups with different alternative concepts. Modification in pellet shape and pellet parameters are considered.

R&D works for design of full core of Indian 220 MW(e) PHWRs with high burnup fuels are being carried out. Fuel design issues in respect of the higher fissile content have been reviewed [2,3]. Studies on reactor physics characteristics like reactor control, shut down margin, fuel and other systems thermal-hydraulic and material compatibility have been studied. Large scale utilisation of such bundles leads to substantial reduction in the volume of fuel bundles required. The core average discharge burnup increases with this scheme. Due to this, the fuelling rate comes down from 9 bundles / FPD in the case of Natural Uranium core to less number of bundles/FPD in the proposed high burnup cores and so consequently it is planned to go for 2/4 bundle shift scheme instead of 8 bundle shift..

The element power envelope upto the design burnup for different fiffile contents generated by reactor physics calculations are utilized for fuel design. The peak LHR (linear heat rate) of the element is maintained same as current natural U elements, to avoid any thermal hot spots. This has led to increase in residence period corresponding to higher burnups.

2.1 Fuel swelling

Fuel swelling occurs at high burnups. To accommodate higher burnups upto 30 000 MW•d/Te, it is proposed to reduce fuel density by 1 to 2%.

2.2 Residence period

The bundle residence period increases for high burnup fuel. For central channels it is 3 years and for outer most channels it is 5 years compared to 2.5 years presently. This increases oxidation of cladding. The higher residence period has effect on 1) low cycle fatigue behaviour of fuel cladding and end plate, 2) corrosion and hydriding behaviour of the fuel cladding and end plate 3) fretting damage of fuel bundle and 4) power ramps at higher burnups. The fuel bundle flux depression factors across the elements are higher compared to natural U bundle. The zircaloy corrosion, hydriding and irradiation embrittlement behavior for the bundle for their residence period in core was estimated and is satisfactory for these extended burnups and powers.

2.3 Power ramp effect

The PHWR fuel bundle cladding inner surface is coated with graphite layer to provide resistance to power ramp SCC failures. The proposed 2/4 bundles refuelling shift for high burnup fuels will lead to power ramp on the bundles when bundles in the channel are shifted from 4 to 6^{th} location in the channel. This happens at a relatively high burnup of about 7500 MW•d/Te U, The ability of graphite coating to provide resistance to power ramp at these burnups is one of the main concern.

2.4 Thermo mechanical analysis

Thermo-mechanical analysis of the fuel element is carried out for the power histories reaching 30 000 MW•d/Te respectively. The fuel material (namely SEU, MOX, ThO_2) properties are included in the code data base. The resultant thermo-mechanical parameters, such as fuel temperature, internal fission gas pressure etc, for these high burnup bundles were compared with respect to bundle with current burnups. The fuel element design analysis has been carried out using Fuel Design Analysis code FUDA[4] to check the limiting parameters at higher burnups like fission gas release, internal gas pressures, plenum volume requirements, centre temperature, sheath strains etc,.

The fuel pellet density, grain size and dish depth of the pellet and element LHR parameters, are the one which could be modified in order to limit the fission gas pressure without putting much difficulty in manufacturing. Hence a parametric study was undertaken for these parameters, while keeping the other geometric and operating conditions same as that of the present 19-element fuel bundle used in 220 MW(e) PHWR. The different designs are studied for burnups of 25 000 to 30 000 MW•d/Te. One of the case study is further explained.

Maximum center line fuel temperatures are found to be 2040^0C and 1670 ^{0}C for 19-element fuel bundle at 58 kW/m Linear Heat Rate(LHR) and 22-element fuel bundle at 50 kW/m LHR respectively. The analysis results are given Table 1. The maximum fission gas pressures reduces with increase in dish depth, with annular pellets and also for low LHR. Decrease in density results in more porosity. More porosity accommodates more gas. However it also decreases the thermal conductivity, which is found to result in enhanced fuel temperature in present study, and consequent more gas release. The net effect is found to be decrease in fission gas pressure by about 11% with the decrease in density from 10.6 g/cc to 10.5 g/cc. The strain in clad decreases by 17%.

TABLE 1. 19-ELEMENT AND 22-ELEMENT

Sl. No	Bundle	LHR	Variable parameter	Burnup	Center	Fisson Gas	Internal gas
	Power (KW)	KW/M		MW•d/TeHE	Temperature (Celsius)	Rel (%)	Pressure (Mpa)
	19–element fuel bundle peak power element						
1	483	58	Normal parameters	25 000	2040	15.3	9.8
2			Double dish pellet	25 000	2040	14.8	5.5
3			Fuel p. grain size 40 μm	25 000	2040	14.7	8.9
4			Low fuel density	25 000	2080	18.4	7.4
5			Pellet central hole	30 000	1950	14.2	6.4
	22–element fuel bundle peak power element						
6	483	50	Normal parameters	30 000	1670	3.7	6.4

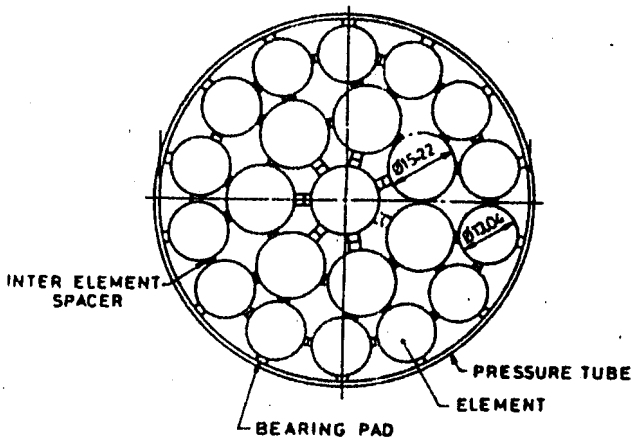

FIG. 2. Element fuel bundle.

The centerline temperature and radial temperature profile are found to be independent of dish depth increment. Fission gas pressure was found to be decreased with dish depth increment on account of more space availability for accommodation of fission gas. Reduction in gas pressure leads to decreased clad strain for increased dish depth pellets.

The studies indicated that, present fuel design is suitable upto 25 000 MW•d/Te U with minor modifications like use of higher grain size, more dish depth etc with decrease in density. For burnups beyond that either annular pellets or the earlier developed 22-element fuel bundle (Ref. 4) with lower LHR, shown in Figure 2 is being considered.

3. Fuel bundle irradiation to high burnup

To investigate fuel behavior at high burnup with regard to fission gas release, fuel swelling and sheath material behavior, fuel bundle integrity and power ramp performance; it was decided to irradiate few high burnup fuel bundles of different types including natural uranium bundles in the operating PHWRs. Short length fuel bundles and on-power refueling provision in PHWRs provides flexibility to use variety of fuel types and consequently permits optimum use of fuel in the reactor. Following paragraphs cover the alternative fuel design concepts in use or under consideration for use in Indian PHWRs.

3.1 Natural uranium fuel bundles

It was planned to prolong irradiation of few natural uranium bundles present in core, to higher burnups. For this purpose natural uranium bundles in two channels (H-13 and O-08 of KAPS-2[a] core) were selected and fuel irradiated upto a discharge burnup of 20 000 MW•d/Te U. Bundles in these channels were irradiated to about 1100 FPD which is about 35% more compared to normal irradiation time[2]. Performance of these channels was assessed by Delay Neutron Monitoring (DNM) system and by comparing the measured Channel Outlet Temperature (COT) with the estimated values by the fuel management code TRIVENI. The variation of DN counts of these channels during this period and also during refueling of these channels indicated successful performance of the fuel bundles including the power ramps seen during operation at high burnup. Fourteen fuel bundles of these two channels have seen burnups more than 15 000 MW•d/Te U, the maximum being 22300 MW•d/Te U.

[a] Kakrapar Atomic Power Station Units 1 and 2.

3.2 Thorium bundles

It was planned to use Thorium bundles for flux flattening in the initial core such that the reactor can be operated at rated full power in the initial phase. The Thorium bundle is a 19–element fuel bundle with Thorium dioxide as fuel in pellet form [6]. The pellet shapes used are both flat and single dish type. As shown in Figure 3 the bundle power of these bundles gradually increase with irradiation exposure time due to production of fissile isotope U^{233} [5]. The fuel element Thermo-mechanical analysis was carried out for elements operating on such an envelope. The elements are designed for a peak Linear Heat Rating of 57.5 KW/M and burnup of 15 000 MW•d/Te Th. The Thorium dioxide pellet specification was evolved which consists of chemical content, density, shape specifications. High density ThO_2 pellets suitable for PHWR were developed at BARC[a] [7]).The fuel element axial and radial gaps have been suitably specified. By carrying out minor modification in their bearing pad positions, proper identification of these bundles was provided. The fuel bundles were fabricated by NFC[b].

Initially four lead thorium bundles were irradiated in MAPS -1[c] reactor during the eighties. Subsequently, 35 Thorium bundles have been used as a part of initial charge fuel in the 220 MW(e) PHWRs for flux flattening in the initial core such that the reactor can be operated at rated full power in the initial phase. These bundles are distributed throughout the core in different bundle locations, both in the high power and low power channels. This loading was successfully demonstrated in KAPS–1 and subsequently adopted in the initial reactor loading of KAPS–2, KGS–1 and 2[d] and RAPS 3 and 4[e]. So far, 232 thorium dioxide bundles have been successfully irradiated in different reactors [8]. The maximum fuel bundle power and burnups seen are 408 kW and 13 000 MW•d/TeTh respectively. These bundles withstood the power ramps normally experienced in reactor while the typical power envelope of thorium fuel is such that power increases with irradiation.

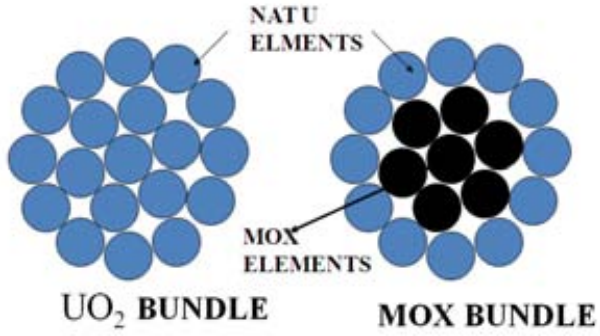

FIG. 3. Natural uranium and MOX–7 fuel bundles.

3.3 MOX–7 bundles

MOX–7 bundle design has been evolved, which is a 19–element cluster, with inner seven elements having MOX pellets consisting of Plutonium dioxide mixed in natural uranium dioxide and outer 12 elements having only natural uranium dioxide pellets[9]. Figure 4 shows typical MOX fuel bundle.

Based on detailed studies, an optimised loading pattern and refuelling scheme has been evolved for loading initially 50 lead MOX bundles in an existing operating reactor. The LHR for these elements are maintained similar to the 19–element natural uranium bundle outer elements. Subsequently For initial trial irradiation 50 number of MOX–7 bundles have been fabricated by BARC and NFC. Unlike natural uranium bundles, elements of these bundles are seal welded by TIG welding. The pellets are of

---

[a] Bhabha Atomic Research Centre, Mumbai, India.
[b] Nuclear Fuel Complex , Hyderabad, India.
[c] Madras Atomic Power Station Units 1 and 2.
[d] Kaiga Generating Station Units 1 and 2.
[e] Rajasthan Atomic Power Station Units 3 and 4.

single dish pellets. Fifty number of MOX bundles were loaded in the KAPS–1 reactor in different locations in the year 2004 [9]. In each refueling four MOX, bundles are loaded in the bundle locations 5 to 8 of the channel. In few channels MOX bundles were loaded in 4th location and subsequently shuffled to 8th location in the same channel. In order to obtain higher bundle power production from MOX bundles and achieve desired burn up at the earliest, bundles producing about 300 KW in low power channels like K–03 were recycled to central channels at a burnup of about 2000 MW•d/Te HE. These bundles successfully withstood the power ramps. Forty six bundles, after 16 months of irradiation and accumulating a burnup of about 11 000 MW•d/Te HE, have been discharged as a part of normal refuelling. Four bundles were irradiated to a burnup of 20 000 MW•d/Te HE in one chanel. The performance is good. The DN counts of these channels were steady, indicating good fuel performance of these bundles. All the discharged bundles were sniffed in spent fuel bay and found nondefective.

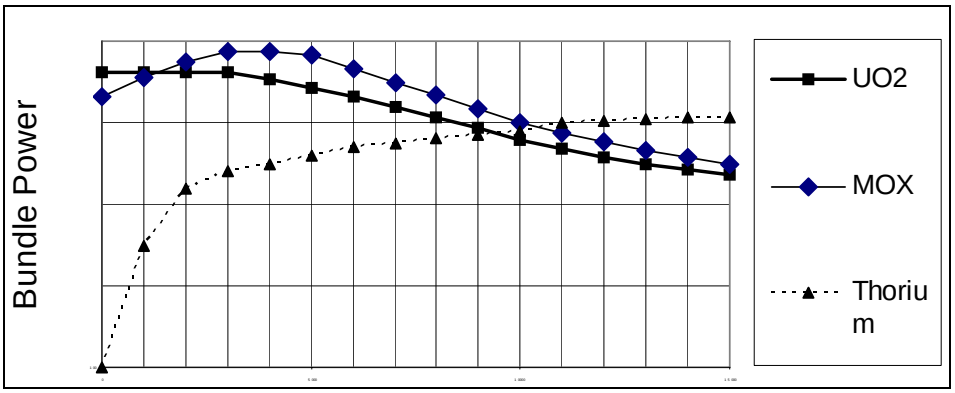

FIG. 4. Bundle power envelopes for different fuel types.

3.4 SEU fuel bundles

India has also started analysis and design works for PHWRs using slightly enriched uranium. This offers higher burnup and consequently less annual fuel requirement and spent fuel inventory. R&D works for design of full core of PHWRs with SEU are completed. Fuel design issues in respect of 0.9% to 1.1% U–235 isotopic content have been reviewed. The core average discharge burnup increases to 14 000 MW•d/Te U with 1.1% enrichment, thermo mechanical analysis of 19–element fuel bundle up to 25 000 MW•d/Te U burnup was carried out for 0.9% EU envelope. The void volume inside the fuel element is increased by increasing the dish depth to maintain low internal fission gas pressure. To accommodate Fuel swelling at higher burnups upto 25 000 MW•d/Te U, fuel (UO_2) density is maintained at about 96 to 97% theoretical density. Few SEU bundles were fabricated by NFC and are loaded in MAPS–2 unit recently for trial irradiation. The channels in which EU bundles are loaded are kept under watch and the DN Counts of these channels are closely observed. The performance of these bundles in core is satisfactory so far.

4. Conclusions

Indian nuclear power programme is based on optimum utilisation of available uranium and thorium resources in the country. The fuel designs and fuel usage strategies are evolved based on this objective. As part of this, high burnup fuel design and irradiation studies have been takenup. Few natural uranium bundles in KAPS–2 were irradiated upto 3.5 years. Also the MOX bundles in KAPS–1 were irradiated upto 2.5 years. This experience gives confidence that the high burnup fuel behaviour in core is satisfactory without any deterioration due to corrosion and irradiation embrittlement. The irradiation performance of both the graphite coated natural U and MOX bundles in the reactors gives the confidence that the graphite coating works at the burnups experienced by them and the bundles can withstand the power ramps due to neighboring channel fuelling.

REFERENCES

[1] BHARDWAJ, S.A., et al, Fuel design evolution in Indian PHWRs, International Symposium on improvements in water reactor fuel technology and utilization, IAEA, Stockholm, (1986).

[2] BHARDWAJ, S. A., Kumar, A.N., Prasad, P.N., Ravi, M., Fuel performance, design and development in Indian reactors, International Conference on CANDU fuel, (2003).

[3] TRIPATHI, R.M., PRASAD, P. N., DWIVEDI, K.P., Thermo-mechanical parametric studies on high burnup bundles for 220 MW(e) PHWRs , CQCNF–2009, (2009).

[4] FUDA MOD–2 manual,"NPC–500/DC/37000/08–Rev–0", (1996)

[5] BHARDWAJ, S.A., SIVASUBRAMANIAN, S., LEE, S.M., Current status and future possibilities of thorium utilisation in PHWRs and FBRs, Annual Conference of Indian Nuclear Society–2000, Mumbai, (2000).

[6] DAS, M., et al, Design and irradiation experience with torium bsed fuels, Thorium Cycle Activities in India, Bombay (1990).

[7] VIJAYAEAGHAVAN, R., et al., Development and fabrication of high density Thoria pelltets, Presented at the Thorium cycle activities in India, (1990).

[8] KUMAR, A.N., et al, Experience with Kakrapar atomic power plants with Thorium loading", Annual Conference of Indian Nuclear Society–2000, Mumbai, (2000).

[9] BAJAJ, S.S., PRASAD, P.N., RAVI, M., KUMAR, A.N., Fuel design and performance in Indian reactors, The International Conference on Characteristics of Quality Control of Nuclear Fuels, Hyderabad, (2003).

[10] PARIKH, M.V., et al., Status report on MOX–7 bundles loaded in KAPS–1 core, (2008), NPCIL Internal Report.

Research on Defects of Pressure Resistance Welding for HWR Fuel Element

E. Wang[a], S. Wang[b], S. Shi[c]

Abstract. Qinshan Phase 3 HWR in China uses Canadian CANDU–6 technologies, noted for 2×728MW total capacities, and the design capacity factor for 85%, life expectancy is 40 years. The project formally started on June 8th 1998. The first load supplied by ZPI (Zircatec Precision Industries Inc.), and formally put into commercial operation on December 31st 2002. In order to meet the reload demand, BNFP (Baotou Nuclear Fuel Plant) and ZPI signed CANDU–6 technology transfer contract in December 1998, the fuel plant was completed and put into operation in December 2002, the first reload made by BNFP was put into reactor on 27th March 2003. Until to June 30th 2009, 56,209 fuel assemblies manufactured by BNFP have been loaded, 49,059 fuel assemblies have been unload and among them 19 fuel assemblies have leakage. All the leaking fuel assemblies were manufactured before 2005. From October 2005 to June 2009, there was no leakage for 45 months, which proved that the fuel assemblies manufactured by BNFP have good performance in reactor. This article introduces BNFP pressure resistance welding process, and classifies the defects into different types, then analyzes the root causes for the welding defects with abnormal phenomenon, by making artificial defects to simulate some defects conditions to further verify the causes, and then it draws the conclusions of the major causes of the defects. During the formal production, precautions for decreasing the defects are implemented, thus gained valuable practical manufacturing experience which could improve the fuel quality and determine the direction of control and improvement for HWR fuel element end plug welding with pressure resistance welding process.

1. Introduction

Qinshan Phase 3 HWR in China uses Canadian CANDU–6 technology, noted for 2×728MW total installed capacity, and the design capacity factor for 85%, life expectancy is 40 years. The project formally started on June 8th 1998. The first load supplied by ZPI (Zircatec Precision Industries Inc.), and formally put into commercial operation on December 31st 2002. In order to meet the reload demand, BNFP (Baotou Nuclear Fuel Plant) and ZPI signed CANDU–6 technology transfer contract in December 1998, the fuel plant was completed and put into operation in December 2002, the first reload was put into reactor on 27th March 2003. This article will introduce BNFP pressure resistance welding process, analyze the welding defects with abnormal phenomenon found during production and in the simulation test samples, which may cause the fuel leakage in the reactor, thus gained valuable practical manufacturing experience to further improve the fuel quality and determine the direction of control and improvement for CANDU fuel assembly manufacturing with upset welding process.

2. Introduction for HWR pressure resistance welding process

2.1 The welding joint form

End plug welding is one of the critical processes in HWR fuel element manufacturing, in this process pellets are sealed in the tube, and formed the first safety barrier for the reactor. The plugs are welded with pressure resistance welding process, welding joint form (see Figure 1). When the current passes through a close contact surface and its adjacent area of the resistance interface, the material is heated to plastic state, forging with the combination of heat and pressure, by the action of recrystallization, diffusion, the connection between atoms are achieved. The welding cycle mainly divided into steps as preheating, heating, forging, maintaining and cooling, in which preheating, heating, forging in three successive stages formed resistance welding joint. Details of the welding joint see Figure 2 and 3, metallographic structure see Figure 4.

[a] China North Nuclear Fuel Co. Ltd., Baotou, China.
[b] China North Nuclear Fuel Co. Ltd., Baotou, China.
[c] China North Nuclear Fuel Co. Ltd., Baotou, China.

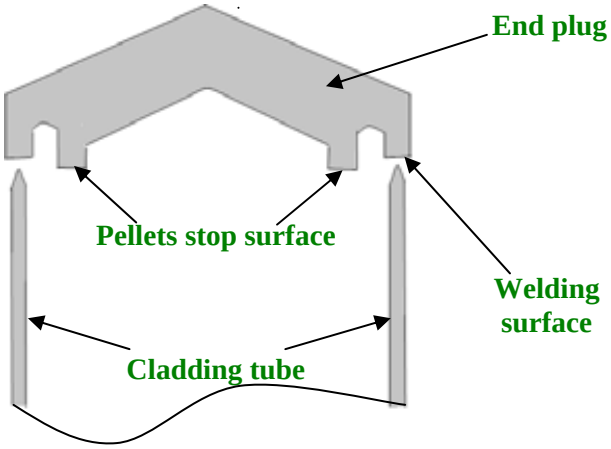

FIG. 1. Welding joint

FIG. 2. End plug welding section

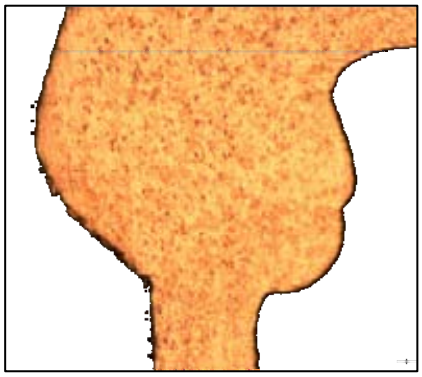

FIG. 3. End plug welding joint

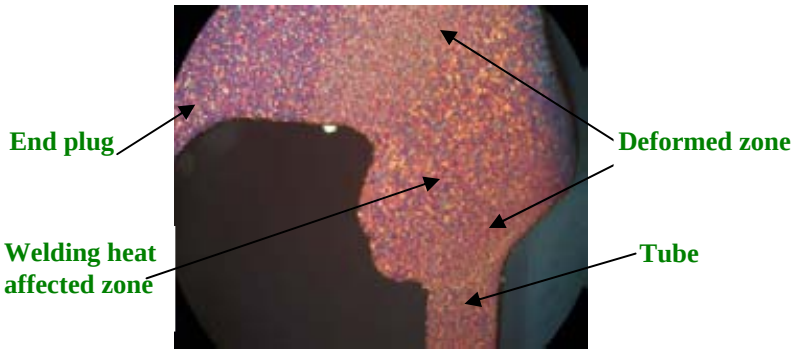

FIG. 4. End plug weld metallographic structure

2.2 The requirement for the welding process

2.2.1 The requirements for the welding joint

The ultimate goal is to weld the plug with tube in the circumference and form a complete joint without defect, it has to ensure the weld seam a uniform consistency welded profile, and should contain the equal quantities of material from the end plug and tube, in the welding seam foreign materials are not permitted, no oxidation and cracks etc.

2.2.2 Process technical parameters

The main technical parameters are: extrusion, welding current and time, forging pressure, upset, tube and plug concentricity and so on.

- Extrusion: the distance of the tube end extruded out of the welding collets, to be controlled by the extrusion gauge.
- Welding current: to be divided into preheat and heat current.
- Time: by pulse, welding time is very short, large current intensity with short welding time is applied.
- Pressure: due to welding face is too small, the squeeze force should be accurately controlled.
- End plug and tube concentricity: should be controlled strictly.
- Upset: upset is used as an indirect welding quality control measure, defined as reduced length for the welding work piece, which is compared with a known standard to feedback the welding heat effect.

2.2.3 Qualification requirement

Among all the parameters, welding time, extrusion, and the plug and tube concentricity are only adjusted slightly, welding current, extrusion pressure, upset have to be qualified, the purpose is to achieve the applicable scope of parameters, within these parameter scopes. The required inspection items are as following:

A. Visual examination, including upset size, irregular welds, splash, discoloration, foreign material inclusion etc;

B. Metallographic examination, the length of sound welding line is more than 80% of the minimum wall thickness in the preferential section (worst situation position), The welding joint metallographic section see Figure 5;

C. Tensile test, broken section doesn't occur in the welds, as shown in Figure 6;

D. Burst test, broken section doesn't occur in the weld seams, as shown in Figure 7;

E. Corrosion test, uniform color, no abnormal discoloration, as shown in Figure 8;

F. Eddy current inspection, to check the welds with uniform material after flash removal;

FIG. 5. Welding joint metallographic section

FIG. 6. Tensile test samples

FIG. 7. Burst test sample

FIG. 8. Corrosion test sample

3. Potential defect analysis and verification

3.1 Potential leaking defects analysis

Even the inspection items are all acceptable, potential welding defects are still possible, because all the test items are sampled from the production run, any element may have leakage. According to Canada ZPI and AECL operating experience, damage of fuel in the reactor are mainly concentrated in the position of weld due to the manufacturing reasons. On condition of end plug bar used in BNFP had been ultrasonic detected twice, the possibility of holes in the plug remains very low, that means if the element has leakage in the reactor, leaking points may occurs mainly in the welds. And QS–3 HWR has also caught some leakage successfully, see Figure 9 and Figure 10:

FIG. 9. Photographs of fuel leakage in welding joint in the reactor

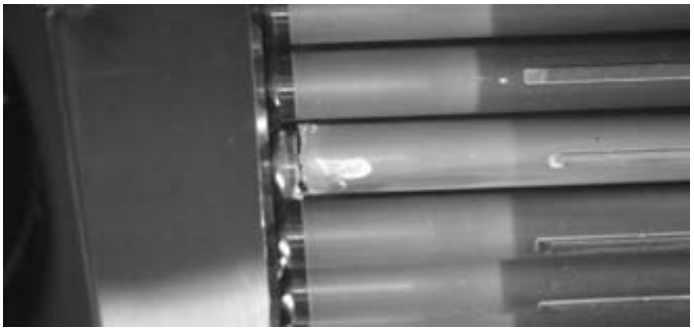

FIG. 10. Photographs of fuel leakage in welding joint in the reactor

So the abnormal phenomenon in the manufacturing process should be strictly considered, through visual inspection and destructive testing methods for abnormal joint, main defects are: joint discoloration, irregular shapes of upset, materials splash, low joint combination intensity (inner welding line existing), internal defects (foreign material inclusion) and superficial defects etc.

3.2 Production defect data analysis

Starting from 2003 to 2009, the qualified parameters are strictly implemented, BNFP adopted a tightened sampling plan, and BNFP has established more strict internal control criterion. But under all these efforts, welding defects are still frequently detected in production under the condition of sampling; therefore, we have to continue doing a lot of simulation experiments and sample more fuel element to detect the root cause of defects. Here one point should be emphasized, it is seldom to found failure for the burst and tensile test during the production and it is also rare to find the defects for splash and upset with irregular profile with the welding electrodes are well prepared. The main defects are welding joint discoloration (see Figure 11) and internal welding line (see Figure 12, 13, 14).

3.2.1 Welding discoloration test and analysis

At the first stage of production, the quality of the discolored welds are suspected, we took 345 accumulated samples and classified them into 3 groups with different level of discoloration, then made statistical analysis for different test (detailed as Figure15,16,17). The sample test distribution see Table 1.

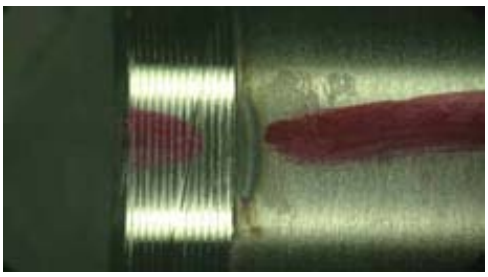

FIG. 11. Welding joint discoloration

FIG. 12. Discontinuous welding lines in the welding joint

FIG. 13. A continuous thin welding line in the welding joint

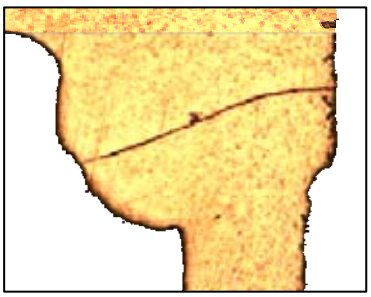

FIG. 14. A continuous thick welding line in the welding joint

TABLE 1. THE SAMPLE TEST DISTRIBUTION

Inspection items	Discoloration line (long)	Discoloration line (middle)	Discoloration line (short)	Total	Test result
metallographic	68	122	110	300	acceptable
tensile	5		5	10	acceptable
burst	5		5	10	acceptable
corrosion	10		15	25	acceptable
total	88		257	345	acceptable

All the samples listed in Table 1 are accepted and meet the inspection requirement, so the fuel element with discoloration weld should not cause rejection to the product. But by analyzing all the metallographic section, we found it is common that an indentation exists on the inner upset opposite to the discoloration position, it is lack of material in this area compared with elsewhere on the inner upset, and the longer of the discoloration line, the probability for this appearance is increasing. See Table 1I and Figure 18 for details.

FIG. 15. Discol. lines long

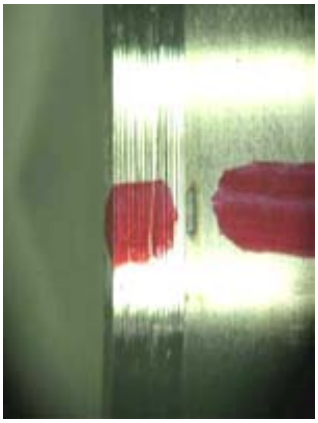

FIG. 16. Discolocation line middle

FIG. 17. Discoloration lines short

TABLE 2. THE RELATION OF DISCOLORATION LINE AND INNER UPSET INDENTATION

Discoloration line	Long	Middle	Short
Sample quantity with discoloration line	68	122	110
Quantity of sample with indentation	56	95	67
Percent	82%	78%	61%

FIG. 18. Photo of the inner upset indentation

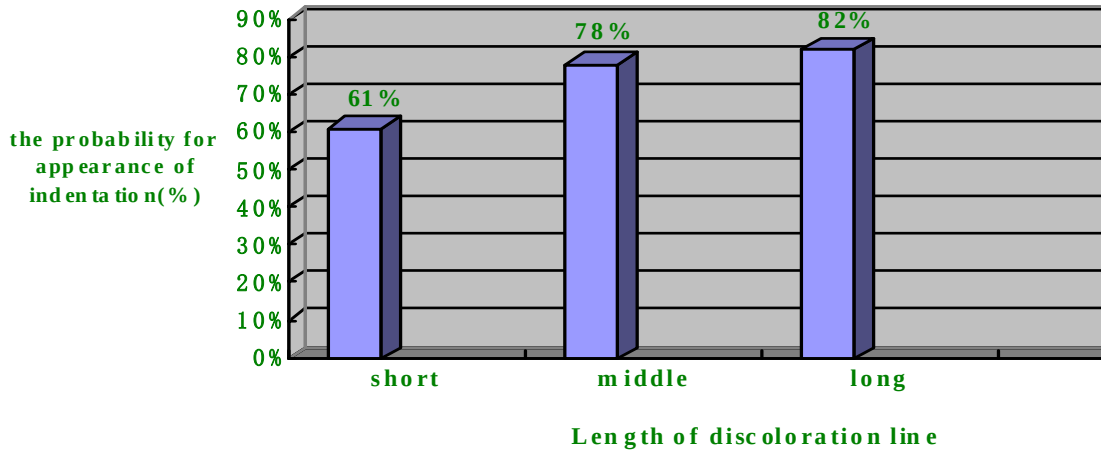

FIG. 19. Discoloration line and inner upset indentation relationship

Analyzed reason for discoloration line: the heat source of upset welding is resistance heat; the change of resistance heat affects the form of welds. If there are small particles on the surface of the tube, or the chamfer of electrode collets are worn, the resistance of this area is increased, and the current intensity is decreased here, local heat decreases relatively, the material is not well heated up and then cause the lack of material in the position when welding; the small particles of this part or the wearing out of the collets impedes the heat spreading, then the heat generated has accumulation effect, oxidation of the surface and discoloration line are formed. Judging from the required inspection results, the phenomenon has no evidently influence to the performance and strength of the welds. But anyway the discoloration line is not a good phenomenon, and it should be kept as low as possible.

3.2.2 Internal welding line simulation test and analysis

The internal welding line displayed in Figure 12, 13, 14 are a kind of defect, we think when the fuel is in high temperature and high pressure and after long-time service in the reactor, the defect is able to spread, if it becomes large enough, it will low the welding joint strength, then potential leakage passage in the fuel element welds is formed. And under normal production condition, it is hard to reproduce this defect, therefore in order to find the root cause of the defect, artificial simulation process samples are used and intend to find the expected defect. Detailed test plan is as follows:

- Cleanliness conditions of welding preparation

Condition A: Graphite contamination samples: 20 PCS (Process Control Sample). Contamination sources: the graphite slurry used for graphite coating.

Condition B: UO2 contamination samples: 20 PCS. Contamination sources: UO2 pellets.

Condition C: Oil contamination: 20 PCS. Contamination sources: mechanical oil.

Condition D: Oxidation film: 10 PCS. Contamination sources: tube surface with slight oxidation film.

Condition E: Oxidation film: 10 PCS. Contamination sources: tube surface with serious oxidation film.

Condition F: Normal samples: normal samples used for process control.

- Welding chamfer damaged

Condition G: Slight damage of chamfer: 10 PCS. Use a knife to cut slight groove;

Condition H: Serious damage of chamfer: 10 PCS. Use stainless steel edge to perform serious damage to the chamfer.

The test results see Table 3 below, the percentage of reject to test samples see Figure 20.

TABLE 3. THE TEST RESULTS FOR ARTIFICIAL SIMULATION PROCESS SAMPLES

Sample Number	Sort of test	Quantity of samples	Quantity of reject	Reject percentage
A1—A20	graphite contamination	20	18	90%
B1—B20	UO2 contamination	20	15	75%
C1—C20	Oil contamination	20	4	20%
D1—G10	Slight oxidation film	10	0	0%
E1—E10	Serious oxidation film	10	1	10%
F1—F20	Normal PCS	20	0	0%
G1—G10	Slight damage of chamfer	10	1	10%
H1—H10	Serious damage of chamfer	10	1	10%

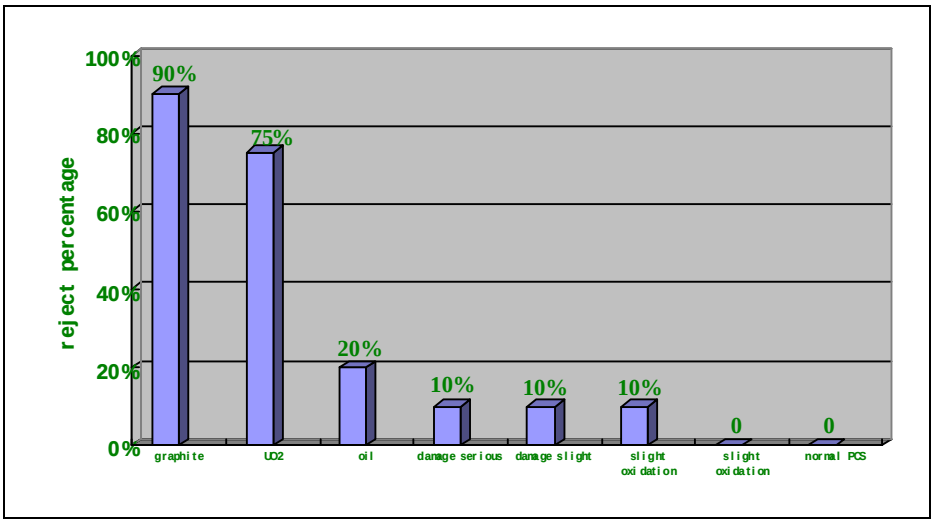

FIG. 20. The percentage of reject to test samples

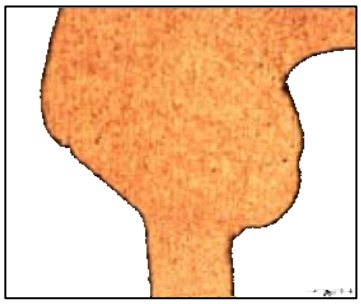

FIG. 21. Normal PCS

FIG. 22. Graphite contamination

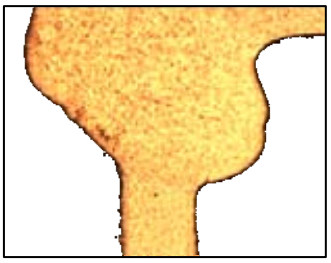

FIG. 23. UO_2 contamination

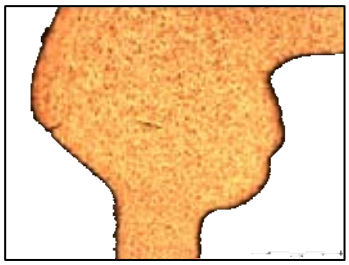

FIG. 24. Oil contamination

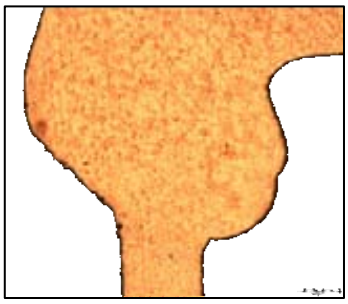

FIG. 25. Slight damage of chamfer

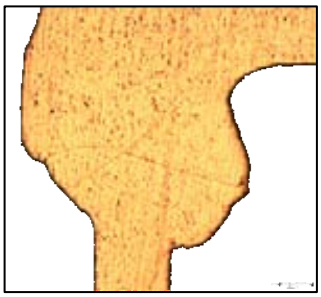

FIG. 26. Serious damage of chamfer

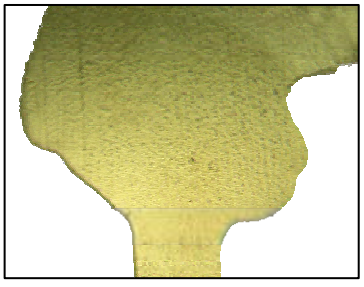

FIG. 27. Slight oxidation film

FIG. 28. Serious oxidation film

Now we can see the major rejected reason is with welding line in the seams, so we focus our efforts on the factors which cause the problem, relatively graphite and UO2 contamination are more easily cause the welding line in the seam, and we divide the welding line defect into thick welding line and thin welding line to analysis.

The analysis of internal thick welding line: through Table 3 and Figure 20, judging from the test results, both the contamination and damage of welding chamfer have effect on the quality of weld. And we picked out some typical samples with welding line to scan them by electronic microscope, see Figure 29 and 30 for details.

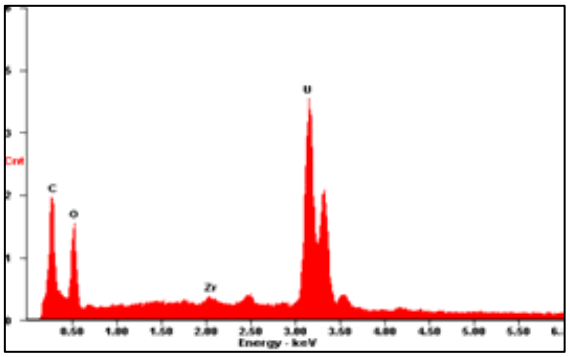

Element	*Wt%*	*At%*
CK	08.10	30.29
OK	19.85	55.73
ZrL	01.25	00.62
UM	70.79	13.36
Matrix	Correction	ZAF

FIG. 29. The electronic microscope scanning result for thick welding line

From Figure 29, through magnifying the thick welding line 1000 times and the scan analysis of inclusion, we can see that the uranium content is 70.79% , carbon content is 8.1% and oxygen content is 19.85%. The main content of the inclusion is uranium and a small amount of carbon, so the cause of thick welding line is the uranium contamination of the welding chamfer, compare with graphite contamination, the contamination of UO2 has more obvious effect to cause the thick welding line.

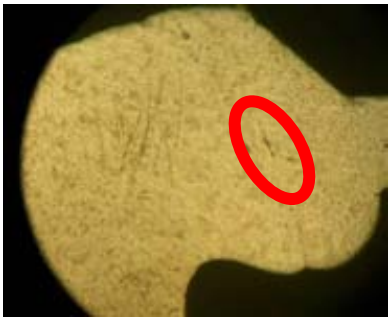

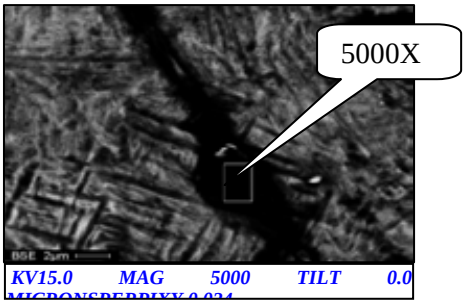

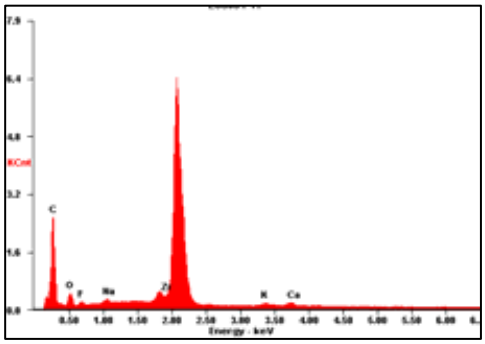

Element	*Wt%*	*At%*
CK	71.51	83.20
OK	13.02	11.37
FK	02.92	02.15
NaK	01.28	00.78
ZrL	07.36	01.13
KK	01.53	00.55
CaK	02.40	00.84
Matrix	Correction	ZAF

FIG. 30. The electronic microscope scanning result for thin welding line.

From Figure 30, through magnifying the thin welding line 5000 times and the scan analysis of inclusion, we can see that the carbon content is 71.51% and oxygen content is 13.02%. The main content of the inclusion is carbon, so the cause of thin welding line is the graphite contamination of the welding chamfer; compare with UO_2 contamination, the contamination of graphite has more obvious effect to cause the thin welding line. The analysis of thin welding line caused by welding chamfer damaged and oxidation film: The influence of chamfer damage and residual oxidation film on tube surface is not remarkable. During the welding process, the oxidation film and inclusion of the interface causes uneven distribution of the welding surface resistance, with the temperature and pressure combined action can cause the radial expansion and moving for the inclusion and film with the material, the oxidation film and inclusion are squeezed out of the welded seam or move to the outside of welded seam edge. The oxidation film and inclusion which is not squeezed out of the interface formed internal defective welding line after upsetting. In the resistance welding, incomplete penetration is defined the phenomenon of inadequate melt in the joint, the possible theoretical reason for incomplete penetration which appears as another kind of thin welding line are as following:

A. the preheating time is too short or the preheating temperature is too low;

B. the upset speed is too low;

C. the interface is not clean or the contacting face is not flat.

Above A and B are process parameters, and they keep constant during the test. The samples which are made during the test are all accepted, that means the process condition is stable and the process test samples are not contaminated. So we can exclude condition A and B in such condition for the system contamination. The welding interface of end plugs and tubes are probably damaged during the operation by accident before welding, which will lead to the thin welding line. The electron microscopic scanning result for this kind of welding line is not sensitive to the foreign material, so we think it is due to the flatness of the contacted interface.

3.3 The treatments and precaution for welding abnormality and defects

3.3.1 Treatment and precaution

Through systematic analysis of welding abnormality and defects, and combined with practical experience in the operation, the following treatment Table is made. These treatments are carried out during the daily production. The weld defects which are trapped by sampling decrease obviously in the normal production. This approved that the product quality trends up.

3.3.2 The feedback running data in the reactor for fuel assemblies manufactured by BNFP

The first reloading fuel assemblies manufactured by BNFP were loaded in reactor on March 27th 2003. Until to June 30th 2009, 56209 fuel assemblies manufactured by BNFP have been loaded, 49059 fuel assemblies have been unload and 19 fuel assemblies have leaking. All the leaking fuel assemblies were manufactured before 2005. From October 2005 to June 2009, there was no leakage for 45 months. The current leakage rate is 0.038%. It is proved that the fuel assemblies manufactured by BNFP have good performance in reactor and the quality of fuel assemblies trends up, see Figure 31 for the trend.

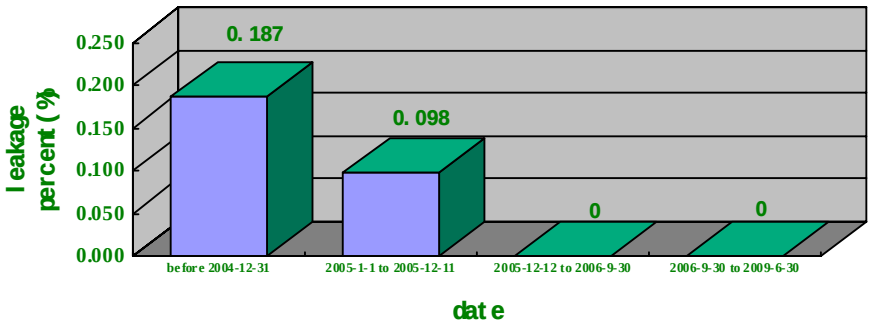

FIG. 31. The leakage trend for the assemblies made by BNFP.

4. Conclusion

- With present process condition, the main causes of weld defect for CANDU–6 fuel element are the contamination of weld interface by graphite and UO_2 contamination, by controlling the cleanliness of the production environment and reducing the contamination level, the quality of the product could be improved and the welding abnormality and defects get decreased.
- The discoloration of welding joints should not be used as a reject criterion, but which could affect the shape of welding joints in some extent.
- The treatments to the welding defects are effective.

TABLE 4. TYPES OF WELD ABNORMALITY DEFECTS AND TREATMENT

No.	Defect type	Treatment and precaution
1	Discoloration	Improve distribution of shielding gas, clean welding electrode and welding preparation
2	Irregular upset	Adjust the concentricity of end plug and tube
3	Splash	Check the tube extension, and annular contact interface of tube and end plug
4	Intensity of welded joints is too small. (internal thin welding line)	a. improve the condition of the contact surface of end plug and tube for the resistance. b. check the contact condition of the electrode and tube, electrode and end plug; c. strictly control the welding upset; d. monitor and increase the welding current; e. check the wear condition of connecting cables and welding circuit;
5	Foreign material inclusion(including the internal thick and thin welding line)	a. check the defect of electrode; b. control the cleanliness UO_2 pellets; c. reduce thickness of graphite coating and 100% control the diameter of pellets; d. reduce helium blowing pressure; e. inspection straightness of outer tubes after brazing f. increase exhausting system capacity; g. strictly control the cleanliness of welding equipment, work piece and environment;

REFERENCES

[1] WENHUI, S., The performance of CANDU fuel assemblies in Qinshan III reactor, (2003).
[2] QA, The quality statistics report of BNFP, Department of BNFP, (2003).
[3] AECL, Root cause investigation of BNFP fuel failures in Qinshan unit 1 and 2, (2006).
[4] XIHUA, Z.,The resistance welding, Mechanical Industry Press.
[5] GACESA, M., Canadian fuel development program, Third International Conference On CANDU Fuel, (1992).
[6] HYUN–TAEK PARK, Fuel defect root cause investigation at WOLSONG–1, Fifth International Conference on CANDU Fuel, (1997).
[7] ALVAREZ, L.A., CASARIO, J.A., VALESI, J., OLEZZA, R., Nuclear fuel performance in EMBALSE NPP, design optimizations and manufacturing improvements, 5th International Conference On CANDU Fuel, (1997).

Current Status of R&D of Nuclear Fuel Elements for PWR in Indonesia

B. Briyatmoko[a], M. Rachmawati[b], T. Yulianto[c]

Abstract. The Experimental Fuel Element Installation (EFEI) of PTBN — BATAN was designed for PHWR fuel element of CIRENE type. Currently the R and D in EFEI have trend to modify the installation for PHWR and PWR fuel fabrication in one place. It has been initiated with modification of equipment necessary for PWR prototype fuel PIN fabrication. Modification is includes in pelletizing area, PIN fabrication area, and criticality nuclear safety and health physics protection. Based on the existing CIRENE pelletization technology, development is carried out by modifying the replaceable punch and dies of the compaction machine and pellet blade of the grinding machine. R and D of PWR fuel pellets with improved characteristics for high burn-up application by adding dopant / additive (TiO_2, Nb_2O_5, V_2O_5) and burnable poison (Gd_2O_3, Er_2O_3) in pellets. Low enriched UO_2 is simulated using natural UO_2 via ADU and depleted UO_2 via AUC. The powder is compacted in 11 mm dies using hydraulic press. The compacting process parameters are determined based on both the compressibility and compactibility as indicated consecutively by the density and mechanical strength of the green pellets. The compacting pressure is chosen based on the condition that gives the UO_2 pellets a maximum green strength with a density within the specification requirement. The selected pressure is 4.0 ton/cm^2 for standard pellet, and 3.5 ton/cm^2 for UO_2 + additive and UO_2 + burnable poison. The sintering parameters for UO_2 pellet: temperature sintering 1700 ^{0}C, heating rate of 250 ^{0}C/h and soaking time of 4 hours. The sintering parameters for UO_2 with dopant / additive (TiO_2, Nb_2O_5, V_2O_5): temperature 1200 ^{0}C, heating rate of 250 ^{0}C/h and soaking time of 3 hours. The sintering parameters for UO_2 with burnable poison (Gd_2O_3, Er_2O_3): temperature of 1200 ^{0}C, heating rate of 250 ^{0}C/h and soaking time of 3 hours. In the manufacture of PIN, welding box should be modified so that it is compatible with TIG welding machine. Due to unfinished modification, PIN fabrication is done in BATAN BANDUNG. The result of this experiment indicates that 15 seconds of post purge time produce weld surface which is accepted on visual control quality process. The 7.5 rpm velocity of the weld and by using argon as shielding gas can reduce the cost of welding so that this condition is chosen on first end plug welding of the fuel pin.

1. Introduction

Long term national energy problem has correlation with energy security of supply and its sustainability to support long term development in Indonesia. On the other hand, short term national energy problem that should be solve immediately to prepare alternative source energy to substitute fossil fuel in fulfill society and industrial consumption. Electrical energy consumption growth up to 2025 is about 7% per annum. The energy need of Indonesia is increasing due to the population growth and for the economic progress. Fossil fuel as primary energy source for electrical energy generation is still big enough. While limited potential of fossil energy source, deployment of non fossil energy sources is not optimize yet. The government of Indonesia intends to apply an optimum energy mix comprising all viable prospective energy sources. Indonesia is seeking alternative energy by considering various aspects (availability, safety, social aspect, economic and environmental). The Government Regulation No.5 year 2006 indicates the target of energy mix until 2025 and the share of nuclear energy is about 2% of primary energy or 4% of electricity (4000 MW(e)) [1] . The first two units of NPP is expected to be operated before 2020 as stated in Act No. 17 year 2007 on National Long Term Development Planning of 2005–2025. PWR and PHWR (the leading NPP design in the world proven to be safe, reliable, environmental clean, economic advantage) is technically feasible for Indonesia's future NPP. However, for the first NPP to be built in Indonesia is PWR type.

[a] Nuclear Research Center, Jakarta, Indonesia.
[b] Nuclear Research Center, Jakarta, Indonesia.
[c] Nuclear Research Center, Jakarta, Indonesia.

R and D activities on PWR fuel has been started directly after building the Power Reactor Experimental Fuel Element Installation (EFEI) 1986 that was originally designed as an experimental facility to develop PHWR fuel, CIRENE. The collaboration has been carried out with an Italian company to study the possibility modification of EFEI to be able to prepare PWR PIN specimen and completed in the end of 1996. The most important result is a document for engineering work for modification of the fuel fabrication laboratory.

2. Engineering work for modification of the fuel fabrication

Laboratory (FFL) of PHWR fuel to PWR

The FFL plant is design to yield, on laboratory scale, a PHWR fuel element with specification limits that this type of reactor requires. The laboratory is divided into two main section i.e. ceramic area and rod area.

Ceramic area :

1. Blending
2. Precompacting or Predensification
3. Granulation
4. Condotioning/Lubrication
5. Pelletizing
6. Crushing and Sieving
7. Sintering
8. Wet Grinding and Drying Pellets
9. Hard Scraps Oxidation
10. Pellets Storage

Rods area :

1. Plug Machining (top and bottom)
2. End Facing
3. Degreasing, Picking, Ultrasonic Cleaning and Drying
4. Plugging
5. First Welding Magnetic Force Welding (MFW)
6. X Ray or Ultrasonic Control
7. Cutting
8. Pellets Loading
9. Second Welding MFW
10. He Pressurization and Hole Welding

The ceramic area is used to yield UO_2 pellet of PHWR with critical parameter as follow:

- Chemical composition (hydrogen and moisture, O/U, contaminants that might have ended in the pellets during manufacturing);
- Density;
- Grain size;
- Surface roughness;
- Pellet diameter;
- Face perpendicularity and profile;
- Surface imperfections (see below);
- Cleanliness and workmanship.

The change of critical parameter of UO_2 pellet of PHWR to UO_2 pellet of PWR, i.e. a smaller pellet diameter, requires a modification in the main equipment of ceramic area, i.e. replaceable punch and dies of compacting machine and UO_2 pellet blade. The modification inevitably changes the pelletization process parameters of both compacting and sintering, and hence a comprehensive qualification of the process parameters should be conducted.

In rod area, modification of welding box of fuel filling is done so that compatible with TIG welding machine. The activity has not finished yet. Hence the welding process optimization of fuel PIN is done by working coordination within BATAN facility, Nuclear Research Center in Bandung [13].

3. The current status

We have modified some of the main equipments in the existing pelletizing area such as replaceable punch and dies of compaction machine and UO2 pellet blade of grinding machine with the exception of the criticality nuclear safety and health physics protection.[2-4] R and D of PWR fuel pellets starts with UO2 pellet standard[5,6] and UO_2 pellet with improved characteristics by adding dopant / additive (TiO2, Nb2O5, V2O5)[8,9,10,11] and burnable poison (Gd_2O_3, Er_2O_3)[11,12,13,14,15] for high burn-up application and fuel fabrication economically. Low enriched UO2 used for PWR fuel have been simulated using natural UO_2 via ADU and depleted UO_2 via AUC.

The welding process optimization of fuel PIN is done by working coordination within BATAN facility, Nuclear Research Center in Bandung[16].

3.1 R&D of UO_2 pellet standard

The UO_2 powder via ADU and AUC is compacted in 11 mm dies with the range of compaction pressure (3–5) ton/cm^2. Compacting process parameters are determined based on both the compressibility and compactibility as indicated consecutively by the density and mechanical strength of the UO_2 green pellets. The compacting pressure is chosen based on the condition that gives the UO_2 pellets maximum green strength with density within specification requirements. The qualification results of the compacting process at a pressure 4 ton/cm^2 consistently give green pellet density within the specification requirement — 5.31 g/cm^3 for UO_2 green pellets via ADU and 5.62 g/cm^3 for UO_2 via AUC. The sintering parameters are chosen at a temperature of 1700 ^{0}C, a heating rate of 250 ^{0}C/h and soaking time of 4 hours. The sintered density of UO_2 pellets via ADU (10.51 g/cm^3) is higher than that of sintered UO_2 pellets via AUC (10.53 g/cm^3).

3.2 R&D of UO_2 pellet with dopant/additive

Based on literature studies, the addition small amount of a certain substance (called additive agent) on pure UO_2 powder will improve pelletizing by decreasing temperature and time of sintering without decreasing quality of pellets. These conditions could affect manufacturing cost and production rate positively. In this paper will be discussed the effect of additive on pelletizing process, particularly emphasis on micro structural mechanism of sintering process. The aim of discussion is to obtain some characteristic of substance required for additive agent. The result of discussion show that characteristic of the substance is that the substance should form solid solution with UO_2, although the solubility should be low. Other requirements are that the substance should have higher electropositive than

uranium and low neutron absorption cross section. The substance fulfill those requirement among other thing include TiO_2, Nb_2O_5, $CaO–TiO_2$ and V_2O_5.

3.2.1 R&D of UO_2 pellet with dopant / additive V2O5

In correlation with V_2O_5, we studied the UO_2 fuel pellet microstructure modification by the addition of small amounts of V_2O_5 for improving fuel performance in-pile stability in reactor. The investigation has been done by comparing the grain size and fine pore of UO_2 sintered pellet and UO_2 sintered pellet with the addition of V_2O_5 in the range of 0.1 wt%–0.3 wt%. The result of the observation is that the addition of small amount of V_2O_5 is greatly increased the grain size and decrease the size of fine porosity, but also reduce the sintered density. This matter offer substantial benefits in terms of in-pile performance requirements, reduce the total path length to free surface for the removal of fission-induced vacancies, reducing the fission gas release from the pellet, and increase the probability of trapping of the vacancies at these larger pores. An irradiation experiment for examining these properties and their relevance to irradiation behavior would have to be established so that the benefits of the additions could be weighed.

3.2.2 R&D of UO_2 pellet with dopant / additive TiO_2

We also studied about the effects of compacting pressure and sintering temperature on the characteristic of UO_2 + 0.25% TiO_2 sintered pellets. An experiment has been conducted to investigate such effects by varying the compacting pressure and the sintering temperature in the production of UO_2 + 0.25% TiO_2 sintered pellets. The objective of the experiment is to seek for the optimum operational conditions of compacting pressure and sintering temperature to obtain pellets that fulfill fuel specifications. The variation of compacting pressure is from 2.8 up to 5.1 ton/cm^2, while the sintering temperature is varied from 1000 until 1200 °C with a heating rate of 250 °C/ hour and a sintering time of three hours. Experiment results show that a rise in sintering temperature increase density and grain size, but it decreases hardness and O/U ratio. At the highest sintering temperature in the experiment (1200 °C), the density and the grain size of the pellets are the highest at 95% theoretical density and 8.97 µm respectively. The hardest pellet is 777 Hv that resulted from sintering temperature of 1050 °C and compaction pressure of 3.9 ton/cm2. The pellet with the best value of O/U ratio of 2.04 is resulted from 1200 °C sintering temperature.

3.3 R&D of UO_2 pellet with burnable poison

3.3.1 R&D of UO_2 pellet with burnable poison Gd_2O_3

The influence of Gd_2O_3 addition on green strength and density of pellet UO_2 have been investigated. The work is done using UO_2 powder from Cameco mixed up with ZnSt lubricant and Gd_2O_3 prior to the compaction. The fraction of Gd_2O_3 is varied in the range of 2% up to 12%. The applied compaction pressure is 3 Mpa for all mixture. The measurement of density and green strength is done to all UO_2 pellets. The green strength test is done using diametral compression strength test with loading rate 0.1 mm/mm. The green strength of UO_2 pellet is increased and reached its maximum value at 4.6% of Gd_2O_3 addition. The phenomenon does work for the density of UO_2 pellet, however its maximum value is at 2.7% of Gd_2O_3 addition. Any addition of Gd_2O_3 more than 2.7% will give a result that the density of UO_2 pellet will be even lower than the density of UO_2 pellet without addition of Gd_2O_3. From this experiment, the maximum interval fraction of optimal addition of Gd_2O_3 can be predicted as 5%.

3.3.2 R&D of UO_2 pellet with burnable poison Er_2O_3

The influence of compacting pressure, Er_2O_3 composition and low-sintering temperature on the density, microstructure, hardness and O/U ratio of UO_2 + Er_2O_3 pellet was investigated to determine the optimum condition of compacting pressure, Er_2O_3 composition and sintering temperature to obtain good quality pellets. UO_2 powder of <150µm in size was mixed with Er_2O_3 of 0–1.0% and zinc stearat of 0.4% and then compacted at pressures of 2.9–5.23 ton/cm^2. The green pellets were sintered at temperatures of 1000, 1100 and 1200 °C with a heating rate of 250 °C/hour and soaking time of

3 hours in argon atmosphere. The density of the pellets was determined, also to be determined the microstructure using optical microscope, the hardness using Vickers hardness tester and the O/U ratio using gravimetric method. The results showed that compacting pressure of 2.93–4.68 ton/cm^2 on UO_2 + Er_2O_3 pellets with Er_2O_3 composition of 0–1.0% could enhance green pellet density in the order of 45.45–51.68% TD (Theoretical Density), while increasing sintering temperature between 1000–1200 °C enhanced sintered pellet density to 95.66% TD. Sintered pellet density of 92–95% TD which conform to the specification was obtained at sintering temperature of 1200 °C, compacting pressure of 4.10–4.68 ton/cm2, and Er_2O_3 composition of 0–1.0%. At temperature of 1000 and 1100 °C the density of the pellets obtained was <92% TD. The microstructure observation which has been done on UO_2 + Er_2O_3 samples with Er_2O_3 composition of 0–1.0%, compacting pressure of 4.68 ton/cm2 and sintering temperature of 1200 °C showed the presence of equi-axial grains. Changes in Er_2O_3 composition resulted in different grain sizes and hardness. Higher Er_2O_3 composition increased the size of sintered pellet grain to 8 μm and decreased its hardness. Increasing Er_2O_3 composition at sintering temperature of 1200 °C enhanced the O/U ratio up to 2.12

3.4 R&D of the welding process of fuel PIN

To minimize the cost of the fuel pin welding, regulating the post purge time and the welding velocity and replacement of the shielding gas have been done. The result of this experiment indicates that 15 seconds of post purge time produce weld surface which is accepted on visual control quality process. The 7.5 rpm velocity of the weld and by using argon gas as shielding gas can reduce the cost of welding so that this condition is chosen on the first end plug welding of the fuel pin.

4. Result and discussion

There is a discussion in the case of UO_2 pellet with improved characteristics by adding dopant / additive (TiO_2, Nb_2O_5, V_2O_5)[4-7]. Researcher from Republic of Korea[14], prefer to take normal sintering temperature (as used for UO_2 pellet without additive), 1700 °C during 4 hours, to obtain pellet with higher grain size to increase high burn up. Other researchers, include from Indonesia [4-7] prefer to chose UO_2 pellet with additive to reduce sintering temperature and soaking time (1200 °C, 1 hour) without to increase the grain size (as grain size of UO_2 pellet without additive). With reducing sintering temperature and soaking time, production rate will increase and production cost will reduce.

5. Conclusion

The modified of punch and dies of compacting machine and UO_2 pellet blade of grinding machine can be qualified to produce UO_2 pellet from UO_2 powder with additives and burnable poison with the result as follow:

1. The addition of small amount of additive of TiO_2, Nb_2O_5, V_2O_5 on UO_2 powder has improved pelletizing process. In compaction process, certain amount of additives will improve compressibility and compactibility of UO_2. In sintering process, certain amount of additives will improve sintering process by decreasing temperature and time of sintering without decreasing quality of the pellets.

2. The addition of small amount of burnable poison (Gd_2O_3, Er_2O_3) on UO_2 powder has improved pelletizing process. In compaction process, certain amount of additives will improve compressibility and compactibility of UO_2.

3. The sintering parameters for UO_2 pellet: temperature sintering 1700 ^{0}C, heating rate of 250 ^{0}C/h and soaking time of 4 hours. The sintering parameters for UO_2 with dopant / additive (TiO_2, Nb_2O_5, V_2O_5): temperature 1200 ^{0}C, heating rate of 250 ^{0}C/h and soaking time of 3 hours. The sintering parameters for UO_2 with burnable poison (Gd_2O_3, Er_2O_3): temperature of 1200 ^{0}C, heating rate of 250 ^{0}C/h and soaking time of 3 hours

4. The welding experiment has been done and the welding parameter has been resulted. The result of this experiment indicates that 15 seconds of post purge time produce weld surface which is accepted on visual control quality process. The 7.5 rpm velocity of the weld and by using argon gas as shielding gas can reduce the cost of welding so that this condition is chosen on the first end plug welding of the fuel pin.

REFERENCES

[1] ADIWARDOYO, Preparation of NPP Establishment and Operation.

[2] LATIEF, A., LANGENATI, R., RACHMAWATI, M. BADRUZZAMAN, M., WIDJAKSANA, Revitalization and modification of experimental fuel element facility, Proceeding of Scientific Presentation on Nuclear Fuel Cycle.

[3] YULIANTO, T., Preliminary study on modification of fabrication equipment for fuel element fabrication of HWR and LWR, Proceeding of Scientific Presentation on Nuclear Fuel Cycle, PEBN.

[4] LATIEF, A., LANGENATI, R., RACHMAWATI, M. BADRUZZAMAN, M., WIDJAKSANA, Revitalization and Modification of Experimental Fuel Element Installation, Proceeding of Scientific Presentation on Nuclear Fuel Cycle–II, PEBN–BATAN, Jakarta, (1996), ISSN 1410–1998.

[5] RACHMAWATI, M., SAPUTRA, T.T., KISWORO, D., Characterization and comparation of UO2 powder from ammonium diuranate and ammonium uranyl carbonate process during compacting process, Proceeding of Scientific Presentation on Nuclear Fuel Cycle.

[6] RACHMAWATI, M., SURYANA, R.A., HIDAYAT, N., WIDJAKSANA, Analysis of pellet defects on fabrication process, Technical Report of Nuclear Fuel Element.

[7] RACHMAWATI, M., HIDAYAT, N., WIDJAKSANA, Effect of additive on UO2 pellet performance to optimize operation cost, Proceeding of Seminar of Nuclear Fuel Technology and Radioactive Waste Treatment, Deputy of Research and Development of Nuclear Industry.

[8] RACHMAWATI, M., SAPUTRA, T.T., KISWORO, D., UO2 pellet microstructure modification using V2O5 additive, Proceeding of Seminar of Basic Research of Nuclear Science and Technology, Advance Technology Research and Development Center.

[9] RACHMAWATI, M., LANGENATI, R., SAPUTRA, T.T., MAHPUDIN, A., SUTARYA, D., ZAHEDI, Characteristic of UO2 powder compacting process and effect of TiO2 on density and mechanical strength of UO2 pellet, Proceeding of Seminar of Nuclear Fuel Cycle.

[10] LATIEF, A., ADHI, A.S., SAPUTRA, T.T., KISWORO, J., PURNOMO, B.T., Effect of compacting pressure change and sintering temperature on characteristic of UO2 + 0.25% TiO2, Proceeding of National Seminar of Nuclear Apparatus Management Research, Advance Technology Research and Development Center.

[11] LANGENATI, R., RACHMAWATI, M., Preliminary analysis of effect of Gd2O3 additive on mechanical strength and density of UO2 green pellet, Proceeding of Seminar of Technology and Safety of NPP and Nuclear Facility.

[12] LATIEF, A., RACHMAWATI, R., SAPUTRA, T.T., SUTARYA, D., MAHPUDIN, A., ZAHEDI, Effect of compacting pressure and Gd2O3 additive in UO2 powder on quality of UO2.

[13] LATIEF, A., SAPUTRA, T.T., KISWORO, D., PRIBADI, S., ADHI, A.S., Effect of compacting pressure, Er2O3 composition and low sintering temperature on quality of UO2 + Er2O3 pellet, Center for Nuclear Fuel Technology and Recycle.

[14] LATIEF, A., Effect of burnable poison Er2O3 additive and sintering temperature on density, microstructure, hardness and O/U ratio of UO2 + Er2O3 sintered pellet, Research Collection of Nuclear Fuel Technology.

[15] LATIEF, A., Combination effect of compaction and sintering temperature on Quality of UO2 + 5% Gd2O3 sintered pellet, Proceeding of Seminar of Nuclear Fuel Cycle.

[16] UMAR, E., HIDAYAT, S., GANDANA, Welding process optimization on nuclear fuel element, Proceeding of Seminar of Nuclear Reactor Utilization for Society Prosperity, PPTN.

[17] YOO, H.S., KIM, H.S., Effect of Nb2O3 and UO2 powder type on sintered density and grain size of the UO2 pellet, Journal of the Korean Nuclear Ssciety, Volume **29**, Number 3, p.196.

ADVANCED FUELS (ADV)

(Session 2)

Chairperson

P. Blanpain

France

High Burnup UO_2 Fuel Pellets with Dopants for WWER

A.V. Lysikov [a], E.N. Mikheev [b], V.V. Novikov [c],Y.V. Pimenov [d]

Abstract. The currently achieved level of design and technology developments provided for the implementation of the fuel cycle (4×1) in WWER at the maximal design burnup of 56 MW·day/kgU per FA. Presently in Russia the program is under way to improve the technical and economic parameters of WWER fuel cycles characterized by an increased fuel usability. To meet the requirements placed on the new fuel that ensures the reliable operation under conditions of higher burnups complex activities are under way to optimize the composition and microstructure of fuel pellets as applied to WWER. This paper describes a general approach to providing the stimulated composition and microstructure of fuel via introducing various dopants. Aside from this, the paper presents the experimentally results of studies into the main technologic and operational characteristics of dopant containing fuel pellets including higher grain sizes, pores distribution and oxygen to metal ratio. The results of the experiments made it possible to work out the pilot commercial process of the modified fuel fabrication, to manufacture pellet batches to be semi-commercially operated at NPP with WWER.

1. Introduction

At present time nuclear power is primarily based on thermal neutron reactors — light water pressurized and boiling ones. The serviceability of a reactor, feasibility of NPP as a whole and also the behavior of a reactor under accident conditions depend to a significant extent on the quality and reliability of fuel rods. Generally a fuel rod comprises a leak-tight cladding that contains nuclear fuel and retains active fission products.

The main type of fuel used in stationary power facilities at nuclear power plants (NPP) is uranium dioxide. For the most efficient generation of electric power at NPP nuclear fuel (UO_2) has to be enriched in U-235 to the mass fraction of 5%. The currently achieved level of design and technology development provided for the four-year fuel cycle in WWER at the average burnup of ~ 50 MW·day/kgU. At present time ROSATOM is executing the program of activities aimed at improving the feasibility of fuel cycles that feature higher burnups and an effective use of fuel.

It is known that as the burnup increases at the periphery of a pellet, a specific microstructure begins to form with subgrains (the effective size of a grain decrease) and coarser gas bubbles along grain boundaries (the so-called ‘rim’ structure) remain results in larger releases of fission gas products (FGP) even under conditions of a lower linear load, Fig. 1 [1]. As a result, the pellet-cladding interaction (PCI) (mechanical effect of thermally expanding fuel on cladding) becomes stronger.

This dictates the need in further improvements of the design and technology of fuel rods to ensure the serviceability of fuel in a five-year fuel cycle at the burnup > 70 MW·day/kgU [2].

The likely way of resolving the problem is to use fuel having coarser grains and the optimized pore structure, capable of retaining FGP within a pellet with no releases under a fuel cladding. It is known that one of the effective ways of opposing the formation of a rim-structure is to increase grain sizes. Some researchers, e.g. [3,4], have demonstrated that increased grain sizes reduce FGP releases, practically completely suppress the formation of a rim-structure and lower down the swelling of fuel.

[a] JSC ‘VNIINM’, Moscow, Russian Federation.
[b] JSC ‘VNIINM’, Moscow, Russian Federation.
[c] JSC ‘VNIINM’, Moscow, Russian Federation.
[d] JSC ‘TVEL’, Moscow, Russian Federation.

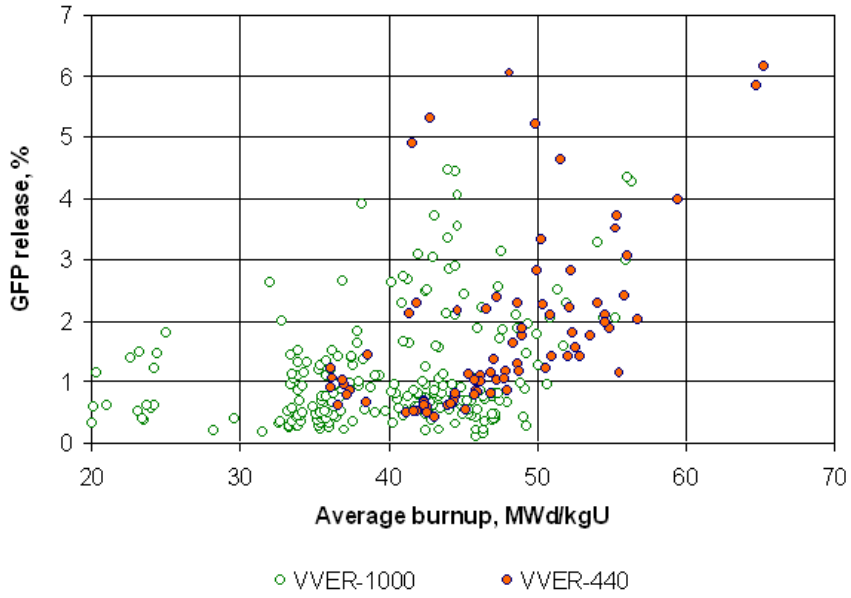

FIG. 1. FGP release vs burnup [1]

The introduced microadditives also increase the fuel pellet ductility [5], i.e. the yield strength becomes lower and the creep rate of fuel pellets increases. In the end the tensile strength of a fuel cladding (reduced PCI) effected by the interaction on the pellet side decrease at significant burnups and the lower increase.

At JSC 'VNIINM' the design analysis was implemented [6] to study the influence produced by the initial characteristics of fuel pellets on the pressure of gases available in a fuel rod of PWR in the fuel cycle (Fig. 2) as well as the design analysis of the contradiction made by thermal diffusion and low temperature mechanisms of gas releases available in mixed gases under cycle pertaining to the fuel produced by the standard and promising processes (Fig. 3).

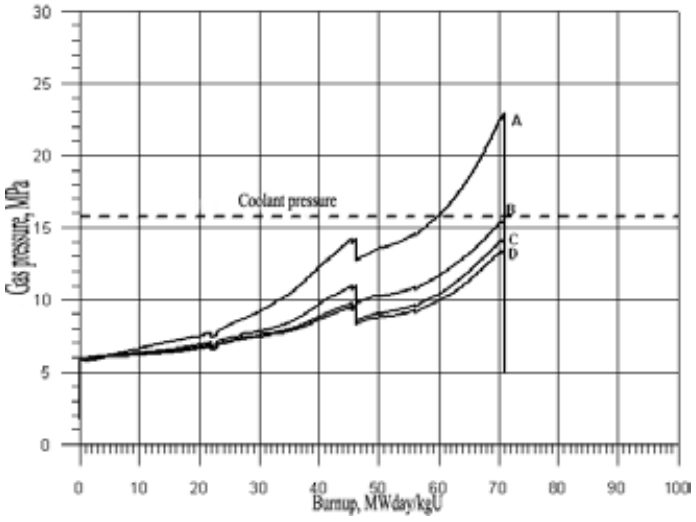

A — standard fuel *(dg=8 mkm, Popen=1%, x=0.003)*
B — modified fuel *(dg=25 mkm, Popen=1%, x=0.003)*
C — modified fuel *(dg=25 mkm, Popen=1%, x=0.001)*
D — modified fuel *(dg=25 mkm, Popen=0.05%, x=0.001)*

FIG. 2. Design analysis of influence produced by initial technologic characteristics of fuel material on gas pressure in fuel rod.

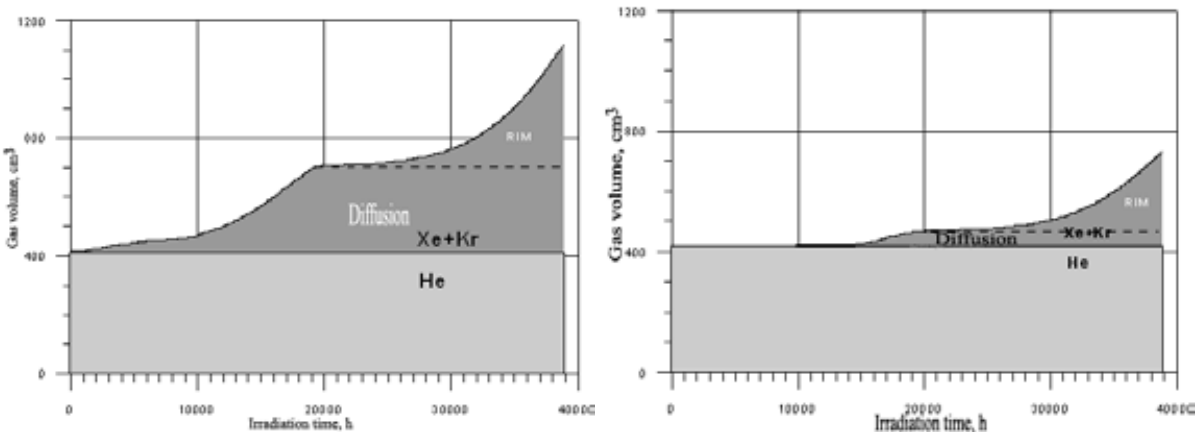

FIG. 3. Design analysis of contribution made by thermal diffusion and low temperature mechanisms of gas releases into composition of mixed gases under fuel rod cladding for fuel produced by standard (a) and promising processes (b).

The analysis has shown that to reduce gas releases as the burnup increases the mean tentative grain size has to be not less than 20 μm and the volume fraction of open pores has to be not more than 0,5% (or not less than 10% of the total quantity).

The standard fuel has grains 10–15 μm in sizes and no technological procedures (rises of sintering temperatures, time of sintering, etc) are capable of increasing substantially their sizes without inflicting significant economic losses (consumption of expensive electric energy, drastically reduced output). However, through the application of microadditives that accelerate the growth of grains the desirable aim might be reached. In this case uranium dioxide might not be alloyed with a great many of additives sense, first, it shall reduce the load of a fuel rod with UO_2, second, it might impact the reactor physics, third, it might lead to affecting other most important properties of fuel.

For many years JSC 'VNIINM' has been engaged in alloying UO_2 with the aim of reducing the pellet-cladding interaction and possible increases of density as well as in studying the influence of additives on the properties of pellets [7, 8] which certainly reduced the time of putting in practice the stated problem.

The complex of work implemented by JSC 'VNIINM' in search for microadditives, their preparation, the technological procedures of introducing them into UO_2, the studies of the novel fuel as well as the methods of control made it feasible (i.e. without overriding the requirements for the impurity contents given in the specifications in force) change the fuel microstructure as it is needed not to do recommend the processes to manufacture novel fuel pellets.

2. Investigations

Proceeding from the analysis of various microadditives for uranium fuel several types of oxide additives and the method of their introduction were chosen. It follows from the review of the existing process from sheet used to manufacture uranium fuel pellets that microadditives might be introduced either during the manufacture of uranium dioxide powder or during the preparation of press feed. In this particular work the microadditives were introduced during the press feed manufacture (the preparation of the blend), Figure 4.

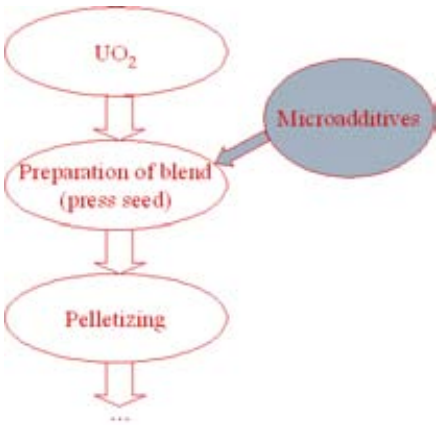

FIG. 4. Schematic presentation of introducing microadditives.

TABLE 1. DENSITY AND RESINTERING OF SAMPLES UNDER IVESTIGATION

Parameter	Standard	+ dopants 1 (Al-Si-Fe-O)	+ dopants 2 (Al-Si-O)	+ dopants 3 (Al-Nb-O)
Density, g/cm^3	10,55	10,52	10,54	10,56
Resintering, %	0,215	0,175	0,121	0,113

First of all the important properties of fuel such as its density and thermal stability (resintering) were investigated, Table 1.

The density of fuel pellets was studied by immersion technique.

The results given in Table 1 evident from above given results that the selected additives that meet the specified requirements for fuel pellets and do not result in substantive changes in their properties. The lower resintering of the pellets having the additives as compared to that of standard pellets is explained by the influence effected by larger sizes of grains.

The sintered pellets were visually controlled for their appearances. Their appearances placed on the standard fuel pellets, Figure 5.

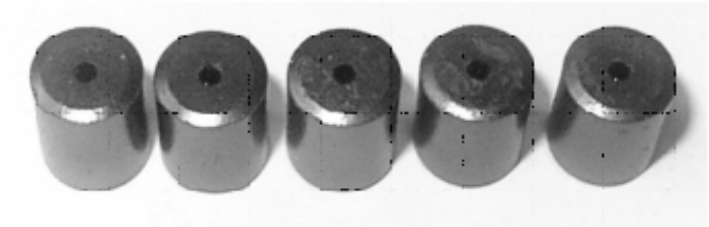

FIG. 5. Appearances of sintered pellets containing microadditives.

The manufactured fuel pellets containing microadditives were subjected to microstructure examination. The particular attention was focused on grain sizes and the volume distribution of microadditives. Grain sizes were investigated by metallographic analysis. The distribution of microadditives in the fuel pellets was studied by X raying. The results are illustrated in Figures 6,7 and tabulated in Table 2. Table 2 gives a linear grain size.

TABLE 2. LINEAR GRAIN SIZES IN EXAMINATED SAMPLES

Composition	Standard	+ dopants 1 (Al-Si-Fe-O)	+ dopants 2 (Al-Si-O)	+ dopants 3 (Al-Nb-O)
Linear grain size, mkm	10	25	28	37

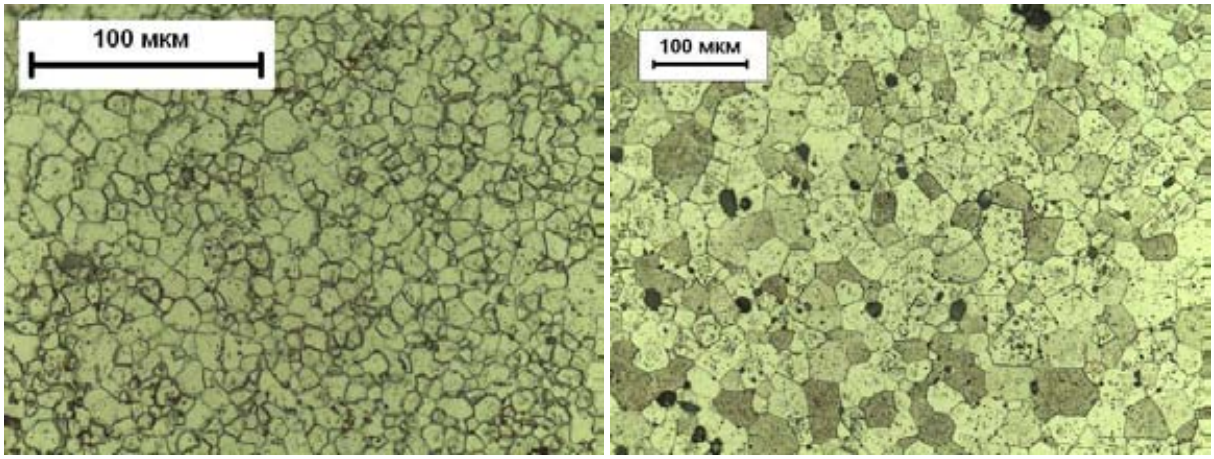

a) b)

FIG. 6. Grain microstructure of pellets (a) standard pellets (b) pellets with alumosilicate additives.

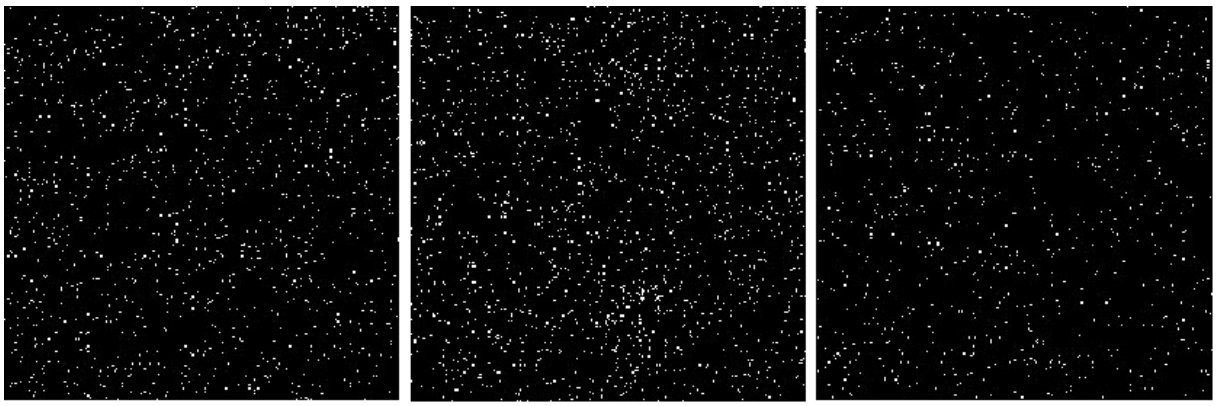

a) b) c)

FIG. 7. Image of scanned surface in characteristic X ray radiation: (a) sample with added Al-Si-Fe-O, (b) sample with added Al-Si-O, (c) sample with added Al-Nb-O.

The carried out investigations reveal that the introduced additives make it possible to increase the grain size to more then 25 μm. Beside, it follows from the accomplished X ray examinations (see Fig. 7) that the mircoadditives are uniformly distributed within UO_2 matrix. In terms of providing the uniform distribution of an additives within a pellet volume the given results evidence the optimal character of the developed process of mixing uranium dioxide with oxide additives.

To assess the characteristics of fuel pellet swelling under irradiation and behavior of a fuel pellets-cladding gap as well as to calculate the mechanical pellet-cladding interaction data are needed on the thermal expansion and the thermal conductivity of the pellets.

To investigate the thermal expansion was made of samples in the form of sleeves 10 mm in diameter and 22–25 mm high. The thermal expansion of the samples was measured by the dilatometric technique in the temperature range of 293–1775 K in purified helium.

The analytic dependence of the linear thermal expansion of fuel pellets in range 293–1775 K is described by polynomial expression with constants derived on basic of experimental data by the least square method:

$$\left(\frac{\Delta L(T)}{L_{293}}\right) = A + BT + CT^2, \qquad (1)$$

where L_{293} — length of sample at room temperature;

T — temperature of investigations;

L(T) — length of sample at temperature of investigation;

$\Delta L(T)=L(T)-L_{293}$ — elongation of sample at temperature of investigation.

The linear thermal expansion coefficient was found from the ratio:

$$\alpha = \frac{1}{L_{293}}\left(\frac{dL(T)}{dT}\right) = \frac{d\left(\Delta L(T)/L_{293}\right)}{dT} = B + 2CT. \qquad (2)$$

The results of the thermal expansion of the fuel pellets containing additives are illustrated in Figures 8, 9.

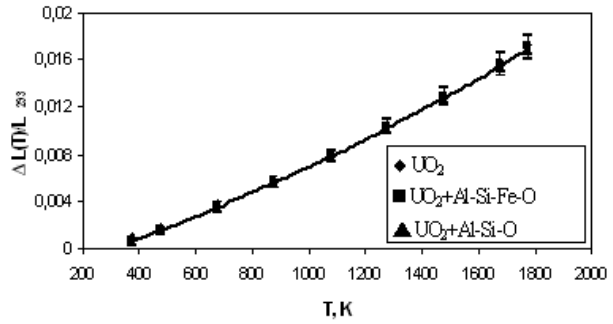

FIG. 8. Linear thermal expansion vs temperature

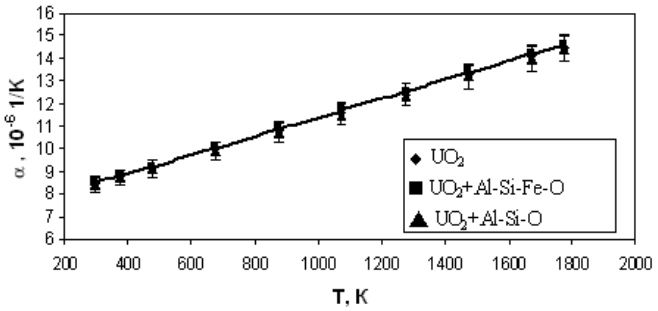

FIG. 9. Linear thermal expansion coefficient vs temperature

The thermal conductivity of the fuel pellet samples having microadditives was investigated by the laser burst method (Parker pulse method) [9], that involves measurements of a time interval during which. a thermal energy impulse passes through a thin sample (thin discs in our case). The results are shown in Figure 10.

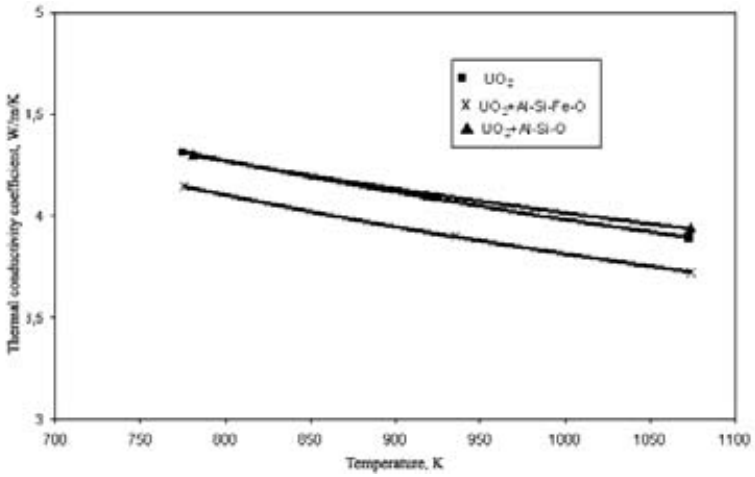

FIG. 10. Thermal conductivity coefficient vs temperature

It follows from the available results the thermal expansion and the thermal conductivity coefficient of fuel pellets with and without microadditives are the same. The difference in the thermal conductivity coefficient is within an error of the method of measurements.

The corrosion resistance of the fuel pellets containing microadditives was investigated under the condition corresponding to the water-chemistry of WWER-1000 [10]. Thus, the tests simulated the conditions under which a fuel rod becomes leaky and the pellets interact with an environment. The data of the tests of that kind might be used to assess the quantity of a fissionable substance that enters a coolant during an accident.

According to the program of the tests the pellets were exposed to a corrosive environment for 50, 100, 500, 1000 h. After each exposure the pellets were removed from an autoclave and dried to reach the constant mass; changes in the masses of the pellets and their appearances were assessed.

After testing for 500 and 1000 h the microstructures of the pellets containing microadditives were investigated by the metallographic method. Their corrosion resistance was compared to that of the pellet not containing microadditives.

The investigations have shown that the process of a fuel pellet fracture in the tests for corrosion resistance is explained by the process of UO_2 oxidation to U_3O_8 as well as by the formation of uranium compounds with corrosion environment elements.

The investigations (ceramography) of fuel pellets have been revealed that the oxidation process proceeds differently, Fig. 11. As applied to the standard fuel pellets having grain size of ~ 10 μm, the intergranular oxidation process proceeds at a higher rate and penetrates a fuel pellet more deeply than the process of the oxidation of fuel pellets doped with microadditives. Consequently, the corrosion resistance of these fuel pellets is higher in comparison with standard samples.

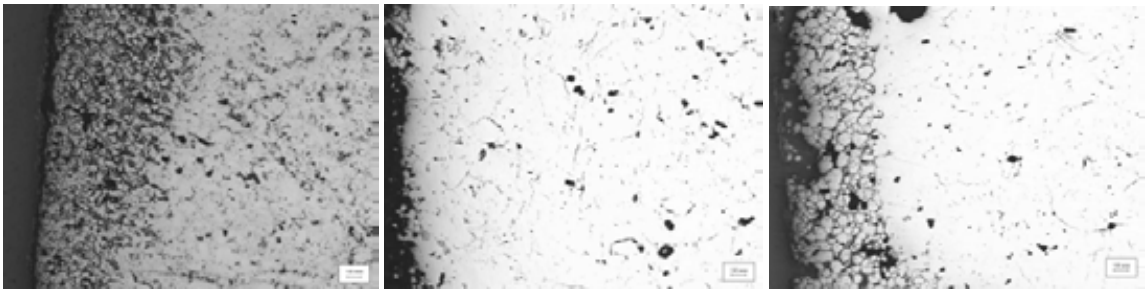

Non-doped UO_2 + Al-Si-O UO_2 + Al-Si-Fe-O

FIG. 11. Surfaces of pellet microsections as tested for 500 hours.

JSC ‘VNIINM’ together with JSC ‘SSC RIAR’ have investigated the properties of the high burnup fuel in the research reactor ‘MIR’ at a power ramp [11].

The power ramp tests of the fuels involved a preliminary irradiation stage to reach the specified burnup and a ramp of the power followed by holding it at a higher level.

This experiment made use of the RIAR designed procedure of testing WWER-1000 fuel rods under power transient conditions [11]. The device with the fuels to be tested was installed into the loop facility channel where the coolant parameters corresponding to WWER were maintained. The reactor was set up to the power level that ensured the needed initial conditions of the experiments in the loop channel.

In this case the controllers that are nearest to the loop channel were in the lower position. After all, the parameters were stabilized and the equilibrium power was increased in ramp of the needed amplitude. To achieve this, the nearest controllers were withdrawn and the introduced positive reactivity was compensated via inserting controllers into the other parts of the core. Figure 12 schematically illustrates experimental fuel rods and an irradiation device, Table 3 tabulates the design values of the maximal linear rating of the fuels.

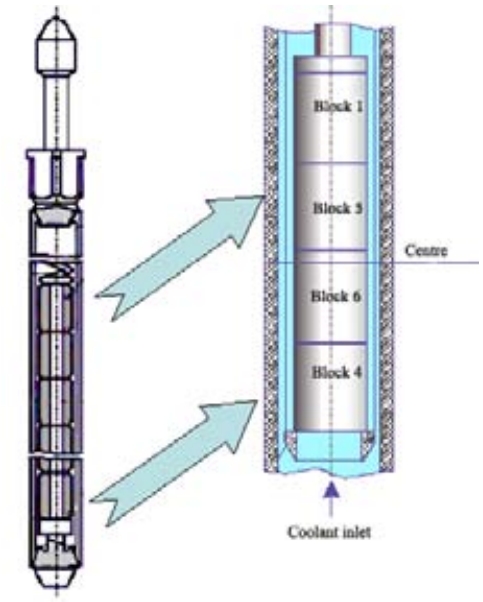

a) b)

FIG. 12. Schematics of experimental fuel rod a) and irradiation device b).

TABLE 3. DESIGN VALUES OF MAXIMAL LINEAR RATING OF FUELS

Point number	$T_{inlet,}$ K	$T_{outlet,}$ K	ql_5, kW/m	ql_6, kW/m
1	528	551	31,4	24,2
2	546	576	58,3	44,8
3	554	589	61,1	47,0
4	562	593	47,2	36,0
5	567	597	45,0	34,1

In the particular experiment the fuel containing an aluminosilicate microadditives did not result in a loss of tightness by the fuel. The fuel having this fuel composition remained serviceable under conditions of the experiment.

The acquired data also evidence a lower xenon diffusion coefficient which indicates that it is feasible to apply an alumosilicate microadditives to reduce fission gas reveals and fuel swelling. Larger grain sizes also have to promote those effects.

3. Conclusions

- Activities were implemented to study the properties that involved in-pile investigations of fuel pellets with microadditives that increase the grain size to more then 25 μm.
- The process was designed to manufacture fuel pellets with microadditives that increase the grain size to more than 25 μm.
- The properties of fuel pellets containing microadditives have been studied.
- The implemented investigations of the microstructure of the modified fuel evidence that the selected additives increase grain sizes and are uniformly distributed in the fuel pellet volume.
- The carried out investigations of the thermal physics properties of the modified fuel (linear thermal expansion, thermal conductivity) have demonstrated that the introduced microadditives do not deteriorate those properties.
- The corrosion resistance of the fuel pellets containing microadditives was investigated under the conditions have shown that the modified fuel pellets containing microadditives have a higher corrosion resistance when interacting with coolant.
- Optimal additives were selected (aluminum silicates that comply with the requirement specified for fuel pellets and do not lead to substantive changes in their properties).
- The acquired experimental results allowed the development of semi-commercial process of modified fuel fabrication, the manufacture of pellet batches to semi-commercially operated in NPP with WWER.
- Batches of pellets were manufactured to be semi-commercially operated at NPP with WWER.
- Since 2005 the semi-commercial operation of the fuel containing microadditives has been commenced in NPP with WWER–1000 (Kalinin NPP, Balakovo NPP), WWER–440 (Kola NPP). The burnup of 56 MW·day/kgU was reached.

REFERENCES

[1] PIMENOV Y.V. , SMIRNOV V.P., MARKOV D.V. et al, PIE results of high-burnup WWER FA. IAEA Technical Co-ordination Meeting High burnup Experience and Economics. Sofia, (2006).

[2] NOVIKOV V., DOLGOV A., MOLCHANOV V. WWER nuclear fuel trends. (Proc.: Int. Topical Meeting TopFuel Germany, (2003), CD-Rom, paper 301–f.

[3] UNE K., HIRAI M., NOGITA K. et al., Rim structure formation and high burnup fuel behavior of large-grained UO2 fuels. J. of Nucl. Mater. **278**, (2000), p.54–63.

[4] YUDA R., HARADA H., HIRAI M. et al., Effect of pellet microstructure on irradiation behavior of UO2 fuel. J. of Nucl. Mater. **248**, (1997), p.262–267.

[5] DAVIES J.N., VAIDYANATHAN S., RAND R.A. Modified UO2-fuel for high burnups. (Proc.: International Topical Meeting TopFuel'99 France, (1999), p.385–395.

[6] KHVOSTOV G., NOVIKOV V., MEDVEDEV A., BOGATYR S., Approaches to modeling of high burn-up structure and analysis of its effects on the behaviour of light water reactor fuels in the START–3 fuel performance code. Proc. 2005 Water Reactor Fuel Performance Meeting Kyoto, (2005). p.992–1009.
[7] LYSIKOV A.V., NOVIKOV V.V., KULESHOV A.V. et al., Modified fuel for WWER–1000 reactors to assure high burn-up and optimization of fuel cycles. Nuclear and Radiation Physics Proc. 6th Int. Conf. Almaty, (2007).
[8] NOVIKOV V.V., BIBILASHVILI Yu.K., RESHETNIKOV F.G. et al., Development of low-strain resistant fuel for power reactor fuel rods. IAEA. Technical Committee Meeting on Improved Fuel Pellet Materials and Designs. IAEA–TECDOC–**1416**. Vienna, (2003) p.297–306.
[9] FINK J.K., Thermophysical properties of uranium dioxide. J. of Nucl. Mater. **279/1**, (2000), p.1–8.
[10] LYSIKOV A.V., NOVIKOV V.V., SAMOKHALOV A.N., Corrosion resistance of doped pellets, Proc. 2008 Water Reactor Fuel Performance Meeting. Seoul, 2(008), CD-Rom, Paper No. 8017.
[11] NOVIKOV V.V., BIBILASHVILI Yu.K., MIKHEEV E.N. et al., WWER fuel behavior with additive elements. Atom Energy **105/4**, (2008), p.205–210.

Westinghouse Advanced Doped Pellet — Characteristics and Irradiation Behaviour

K. Backman [a], L. Hallstadius [b], G. Rönnberg [c]

Abstract. There are a number of trends in the nuclear power industry, which put additional requirements on the operational flexibility and reliability of nuclear fuel, for example power uprates and longer cycles in order to increase production, higher burnup levels in order to reduce the backend cost of the fuel cycle, and lower goals for activity release from power plant operation. These additional requirements can be addressed by increasing the fuel density, improving the fission gas retention, improving the Pellet Cladding Interaction (PCI) resistance and improving the post-failure performance. In order to achieve that, Westinghouse has developed ADOPT (Advanced Doped Pellet Technology) UO_2 fuel containing additions of chromium and aluminium oxides. The additives facilitate pellet densification during sintering, enlarge the pellet grain size, and increase the creep rate. The final manufactured doped pellets reach about 0.5% higher density within a shorter sintering time and a five times larger grain size compared with standard UO_2 fuel pellets. Fuel rods with ADOPT pellets have been irradiated in several light water reactors (LWRs) since 1999, including two full SVEA Optima2 reloads in 2005. ADOPT pellets have been investigated in pool-side and hot cell Post Irradiation Examinations (PIEs), as well as in a ramp test and a fuel washout test in the Studsvik R2 test reactor. The investigations have identified three areas of improved operational behaviour: Reduced fission gas release (FGR), improved properties pertinent to PCI performance, and higher resistance against post-failure degradation. The better FGR behaviour of ADOPT has been verified with a pool side FGR gamma measurement performed at 55 MW•d/kgU, as well as transient tests in the Studsvik R2 reactor. Creep measurements performed on fresh pellets show that ADOPT has a higher creep rate which is beneficial for the PCI performance. ADOPT has also been part of a high power Halden test (IFA–677). The results from these tests are presented in this paper.

1. Introduction

Pellet additives, ‘dopants’ can provide an enhancement of key properties, adding value and reliability to the nuclear fuel (Refs. 1–3). Westinghouse has developed ADOPT (Advanced DOped Pellet Technology) UO_2 fuel containing additions of Cr_2O_3 and Al_2O_3. The additives facilitate densification and diffusion during sintering, which results in about 0.5% higher density within a shorter sintering time, and about five times larger grains, compared with standard UO_2 fuel. While attaining the desired properties, the amount of chromium has been kept low in order to minimize the parasitic neutron absorption. Aluminum has a very small cross section for thermal neutrons, similar to that of Zr. Data shows that Al_2O_3 enhances the grain size enlarging effect of Cr_2O_3, i.e., there is a synergy between the two additives (Fig 1). Beside the increased pellet density, enabling higher energy-density fuel, which permits more energy production per fuel assembly, poolside, hot-cell and test reactor investigations have demonstrated significant performance advantages of ADOPT pellets: Reduced fission gas release (FGR), increased margin to Pellet Cladding Interaction (PCI), and improved resistance against post-failure degradation. Fuel with ADOPT pellets has been irradiated in commercial LWR reactors to a burn up of more than 60 MW•d/kg. Two full SVEA Optima2 reloads with ADOPT pellet were loaded in 2005.

[a] Westinghouse Electric Sweden, Västerås, Sweden.
[b] Westinghouse Electric Sweden, Västerås, Sweden.
[c] OKG AB, Oskarshamn, Sweden.

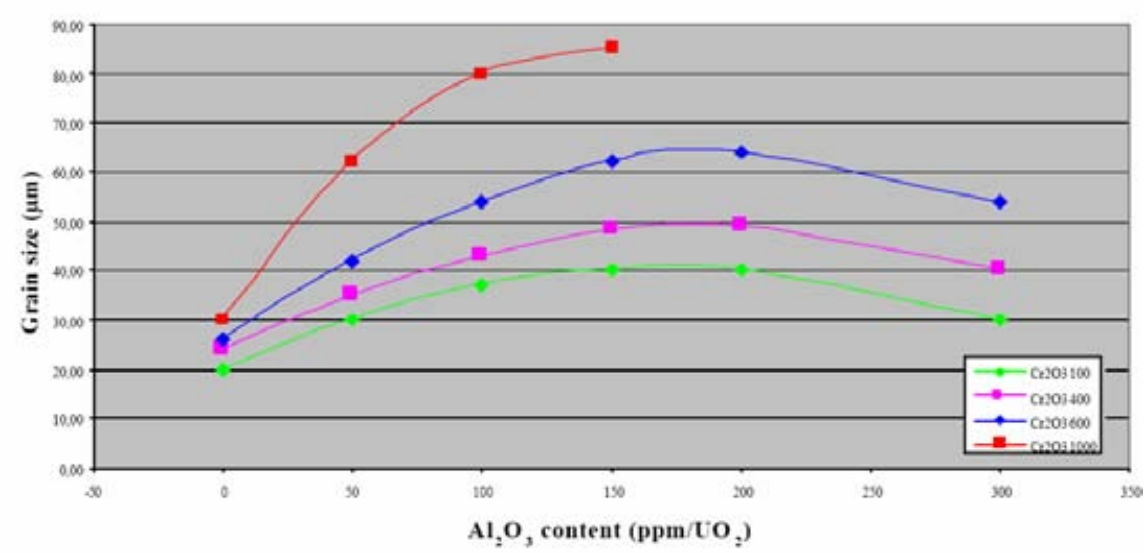

FIG. 1. Grain size of ADOPT pellets as a function of alumina and chromia content.

1.1 Densification and swelling behavior

The densification of ADOPT in a re-sintering test at 1700ºC is only about 20% of that of standard pellets. This will give an earlier pellet cladding contact which results in a somewhat higher rod length increase. Poolside measurements of rod growth have shown that after the initial densification the swelling rates of the different pellet types are the same, see Fig 2.

2. Fission gas release

2.1 FGR measured with gamma scanning after irradiation in commercial reactor

Two assembles that both consist of a mixture between ADOPT and standard pellets have been subject to FGR pool side gamma scanning. Measurements have been performed at burnups up to 55 MW•d/kg U, after irradiation in a commercial reactor. The results, shown in Figure 3, indicate an improvement of the order of 30% over standard UO_2 at the highest burnups. At lower burnups, before the thermal diffusion component of fission gas release is active, we see a similar gas release of the two fuel types.

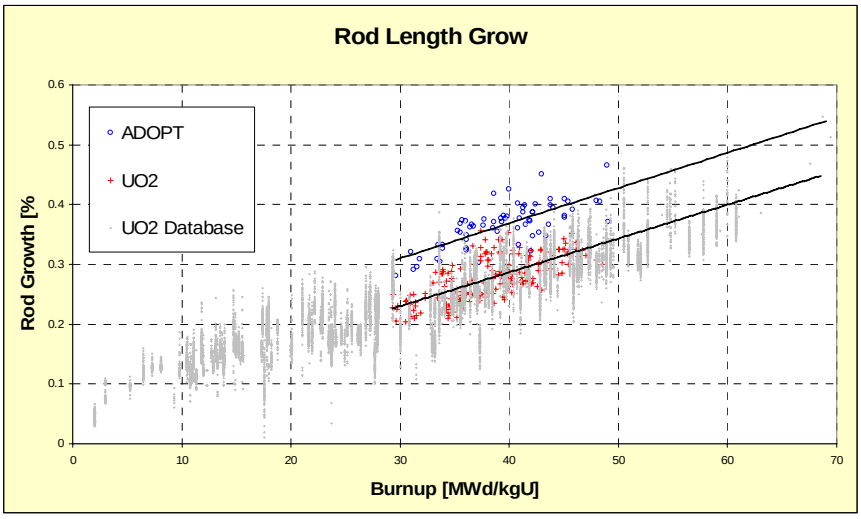

FIG. 2. Rod growth vs burnup for ADOPT and standard pellet.

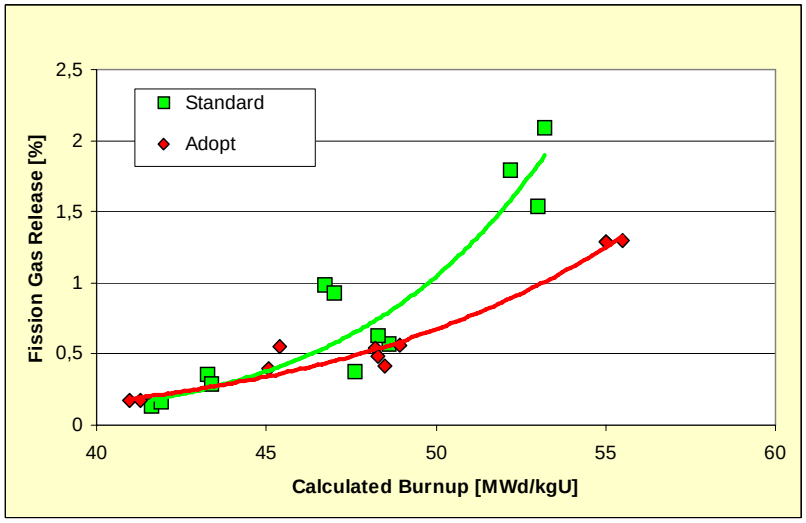

FIG. 3. Fission gas release vs burnup for for ADOPT and standard UO_2.

2.2 FGR measured after a PCI ramp test and a bump test

Furthermore, fission gas release was measured after a PCI ramp test, and after a 'bump' test (an extended period of enhanced power). Segmented lined fuel rods were irradiated in a commercial BWR to a burnup of about 30 MW•d/kgU under normal operating conditions. All pellets were enriched to 4.2%. Subsequent to the base irradiation, ramp and bump tests were performed under BWR conditions (90 bar, 285 °C) in the R2 reactor at Studsvik, Sweden. The power ramp sequence started at 22 kW/m for 12 hours followed by an increase in steps of 5 kW/m with a holding time of 1 hour at each step, reaching a maximum of 57 kW/m. The bump test irradiation was initiated by a conditioning power of 22 kW/m for 9 hours, followed by 46 kW/m for 17.5 days.

Since both the doped pellet rodlet and the reference UO_2 rodlet survived the ramp test, the FGR of the two fuel types could be measured: 17.2% and 30.2%, respectively. Ceramography in the peak power region of the segments, see Figure 4, showed that the doped pellets had formed a central hole, in contrast to standard UO_2, i.e., a small fraction of the central pellet region had been displaced to the pellet pellet interface.

For the standard UO_2 pellets, some small fission gas bubbles were found inside the grains at mid radius position, but the larger bubbles had mainly precipitated at the grain boundaries, see Figure 5. For the doped pellets, the majority of bubbles were found inside the grains, which is consistent with a lower rate of fission gas release. Furthermore, there is a higher degree of ^{137}Cs migration to pellet-pellet interfaces in standard UO_2, which is also likewise consistent with a higher FGR.

2.3 FGR after high initial rating test in Halden

The high initial rating test IFA–677 was running under BWR conditions in the Halden reactor between December 2004 and September 2007. The rig achieved an average burnup of ~26.3 MW•d/kgUO_2. The test rods were fitted with pressure transducers, fuel stack elongation detectors and fuel centerline thermocouples (at both ends of the fuel stack). The primary aim of the experiment was to investigate the performance of modern fuels subjected to a high initial rating, with specific attention paid to thermal behavior, dimensional changes (densification and swelling), fission gas release (FGR) and pellet clad mechanical interaction (PCMI) [4].

Three of the six tested rods contain pellets manufactured by Westinghouse. The three pellet types supplied by Westinghouse were ADOPT with 900 ppm Cr_2O_3, ADOPT with 500 ppm Cr_2O_3 and standard UO_2 pellets. The FGR from the two fuel types was comparable (22% and 17% for the ADOPT rods and 19% for standard UO_2 fuel), see Figure 6.

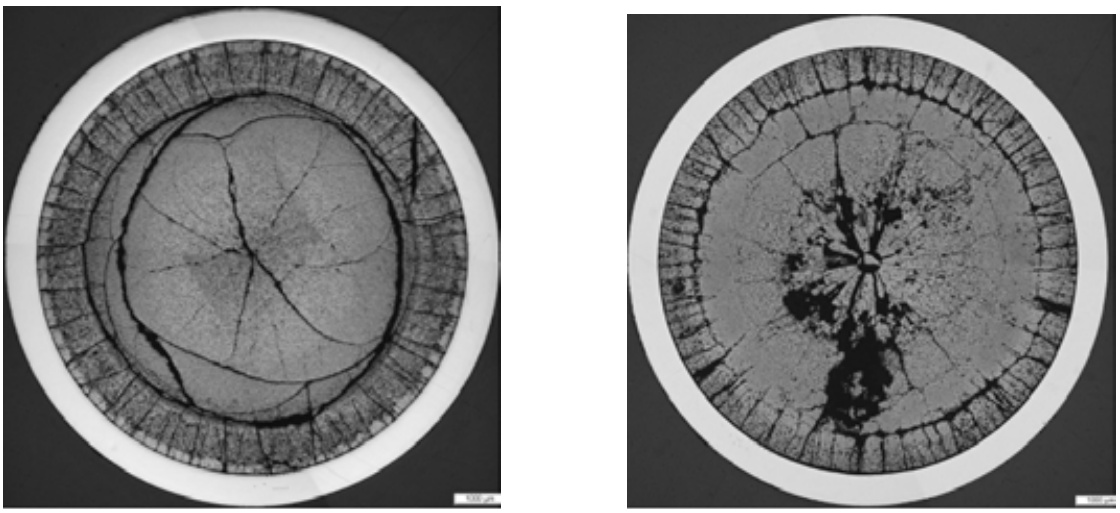

FIG. 4. Ceramograhy after ramp testing to 57 kW/m of standard UO_2 (left) and doped fuel (right).

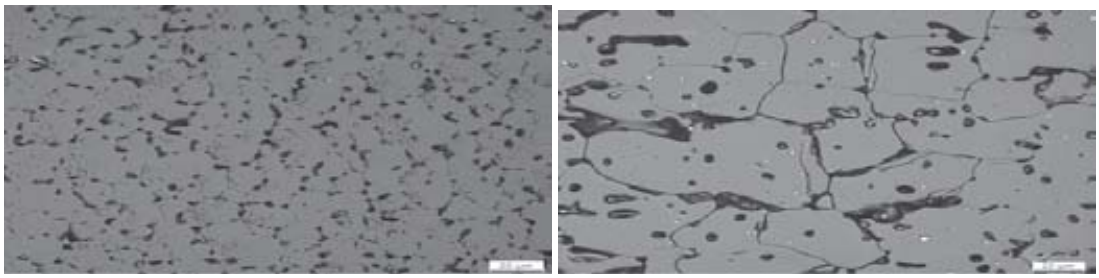

FIG. 5. Magnification of ceramography after ramp testing, about 2 mm from pellet center. The bar at lower right represents 20 μm. Left: standard UO_2, right: doped fuel.

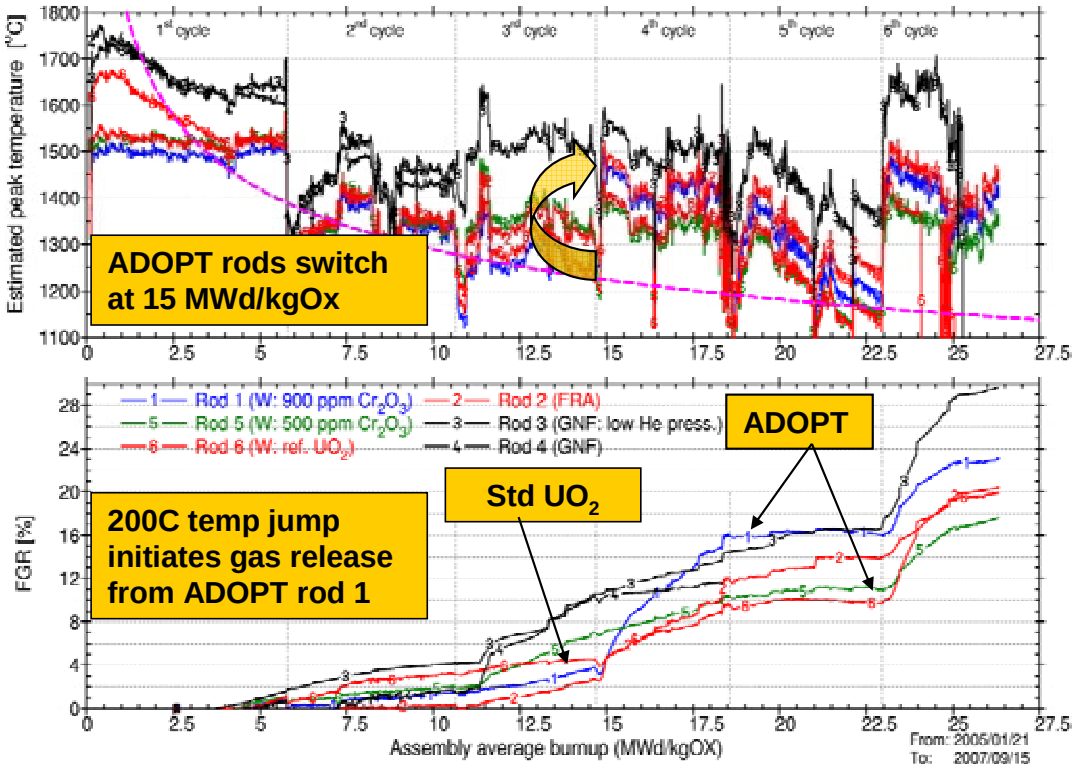

FIG. 6. Estimated peak temperatures and FGR as a function of assembly average burnup for the tested rods in IFA 677. The Figure 39 is taken from [4].

IFA–677 has been operated in a way that is unfortunately not representative for commercial reactor operation since

– The power was very high (>35 kW/m) throughout the experiment
– In the beginning of the second part of the experiment a change in local core environment induced a radial power tilt. This tilt caused a major increase in rod power and initiated fission gas release. The ADOPT rod with the highest FGR was also the rod that experienced the highest increase in rod power and highest temperatures in the last cycle of irradiation see Figure 6.
– There are generally a lot of transients and steps in the power history.

The fission gas release data have been evaluated by Westinghouse fuel performance code STAV7 using the power histories supplied by Halden. All calculations have been performed with pellet properties as if they would have been standard pellet to be able to compare the results from the ADOPT pellets with standard pellets. The conclusion from these calculations is that STAV7 can predict the behavior of the UO_2 rod very well, see Figure 7, and the calculated fission gas release from the ADOPT rods is in the same range as if they would have been UO_2 rods, see Figure 8 and 9. However it should be noted that IFA–677 experiment featured a significant numbers of fast ramps up to high LHGR's. This can present difficulties for a steady state fuel performance code, like STAV7: Rapid steps and transients are known experimentally to stimulate gas release, which cannot be reproduced by such a code. This means that the calculations presented here performed using standard UO_2 pellet properties may very well represent under-predictions of the FGR, and in particular for ADOPT.

Ceramograhy examinations of the three rods, which contain pellets manufactured by Westinghouse, have been performed. Photos are shown in Figs. 10 to 12 below. The results are consistent with earlier ADOPT experience, for example, the ADOPT pellets have a larger number of small cracks in the periphery and more pores precipated inside the grains.

3. Pellet-Cladding Interaction (PCI)

3.1 PCI ramp test

A PCI ramp test was performed as described in the previous section, using lined fuel irradiated in a commercial power plant to about 30 MW•d/kg U. Both rodlets, i.e., containing doped and standard UO_2 pellets, survived the test.

Figure 4 shows ceramographic cross sections after the test. The near absence of large cracks in the central region of the doped pellet indicates a more visco-plastic behavior at high temperature, which is consistent with an improved PCI performance. The doped pellet shows a larger number of smaller cracks around the periphery, compared to standard UO_2, a feature which is understood to further mitigate PCI by distributing cladding stress/strain more uniformly.

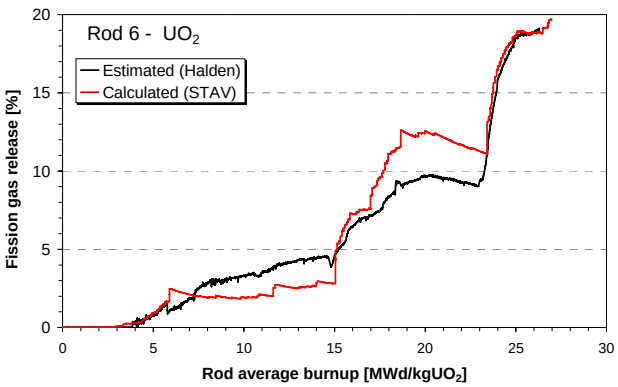

FIG. 7. Comparison between FGR estimated by Halden and FGR calculated by STAV7 using standard UO_2 properties for rod 6 containing standard UO_2 pellets.

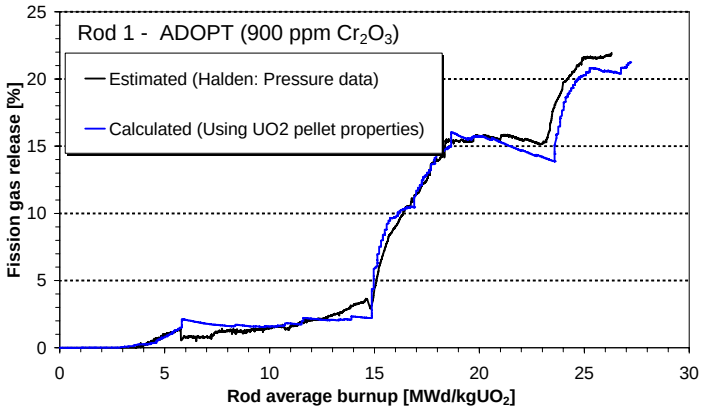

FIG. 8. Comparison between FGR estimated by Halden and FGR calculated by STAV7 using standard UO_2 properties for rod 1 containing ADOPT pellets doped with 900 ppm Cr_2O_3.

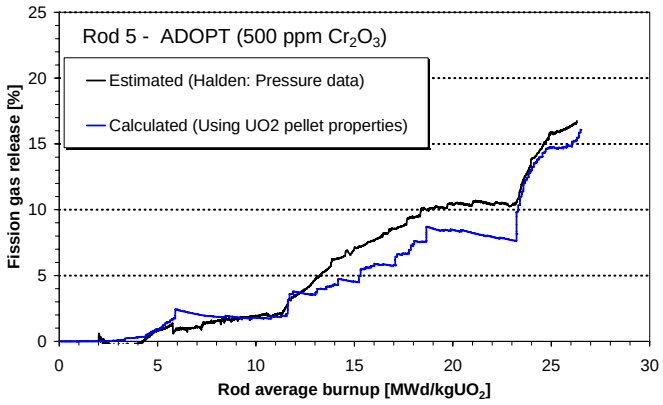

FIG. 9. Comparison between FGR estimated by Halden and FGR calculated by STAV7 using standard UO_2 properties for rod 5 containing ADOPT pellets doped with 500 ppm Cr_2O_3.

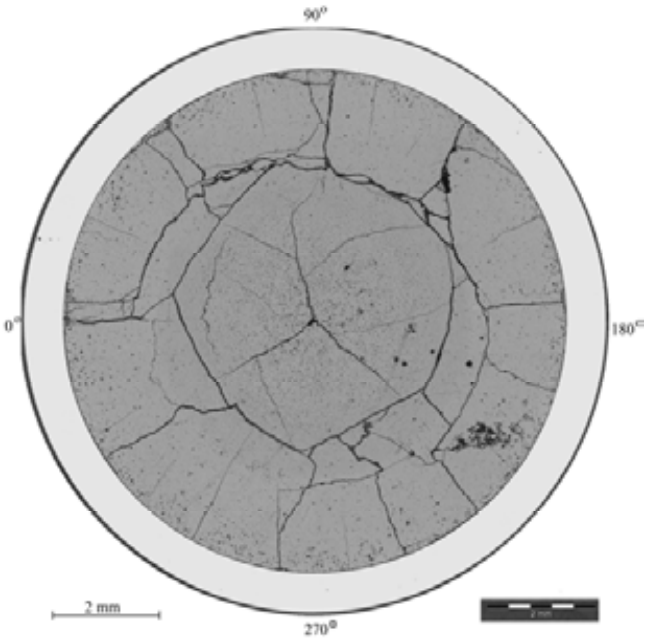

FIG. 10. Macrograph presenting the cross section in polished condition for rod 1 containing ADOPT pellets with 900 ppm Cr_2O_3.

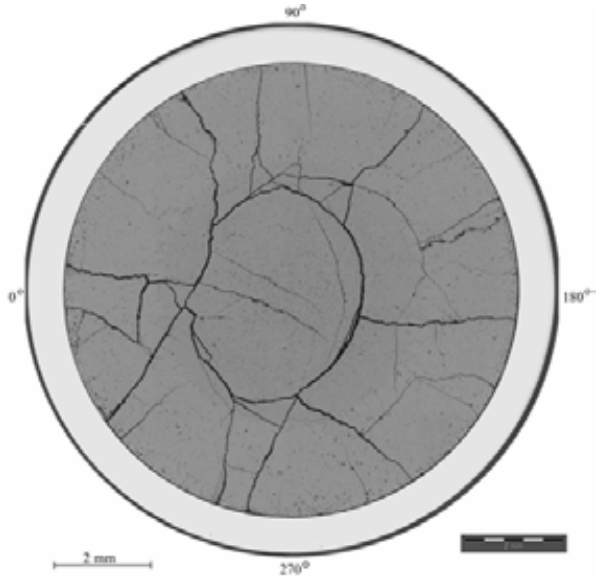

FIG. 11. Macrograph presenting the cross section in polished condition for rod 5 containing ADOPT pellets with 500 ppm Cr_2O_3.

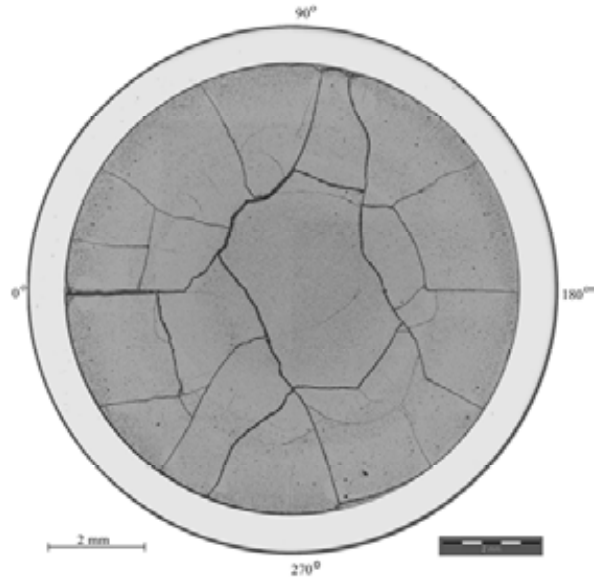

FIG. 12. Macrograph presenting the cross section in polished condition for rod 6 containing standard pellets.

3.2 Creep and ductility

In order to compare the viscoplastic behavior of standard UO_2 and ADOPT at high temperatures, creep and hardening tests were performed using unirradiated pellets. Both types of tests were performed in an atmosphere of dry hydrogen. The deformation versus time was measured at constant load and temperature in the creep test, and the load versus deformation was measured at constant strain rate and temperature in the hardening test.

The creep tests show a strong temperature dependence (in the range of 1300 °C–1700 °C) and a higher viscoplasticity for the ADOPT fuel compared to the standard UO_2 fuel, see Figure 13.

The hardening tests, Fig 14, show that for strains up to about 1%, ADOPT requires less or similar compressive stress than standard UO_2 to attain a given strain rate. This indicates more plasticity for ADOPT in the strain range relevant for PCI.

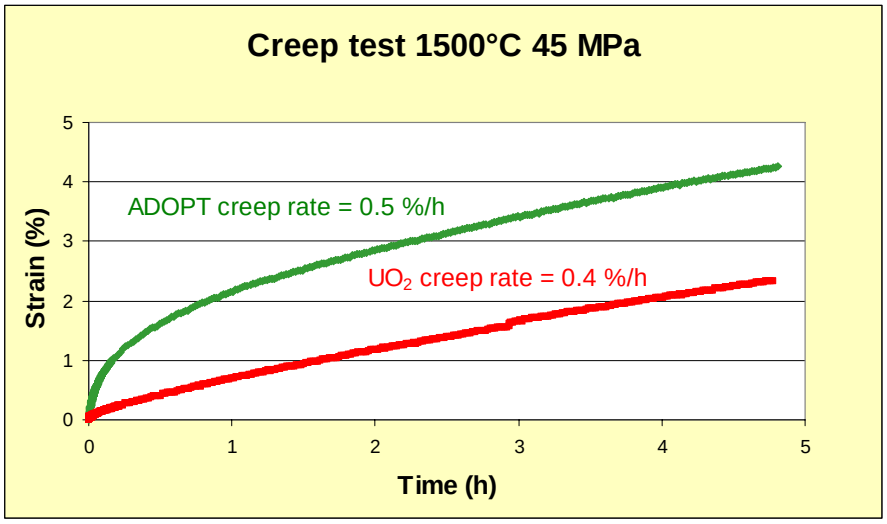

FIG. 13. Creep test at 1500 °C and 45 MPa of unirradiated ADOPT and standard UO_2 pellets.

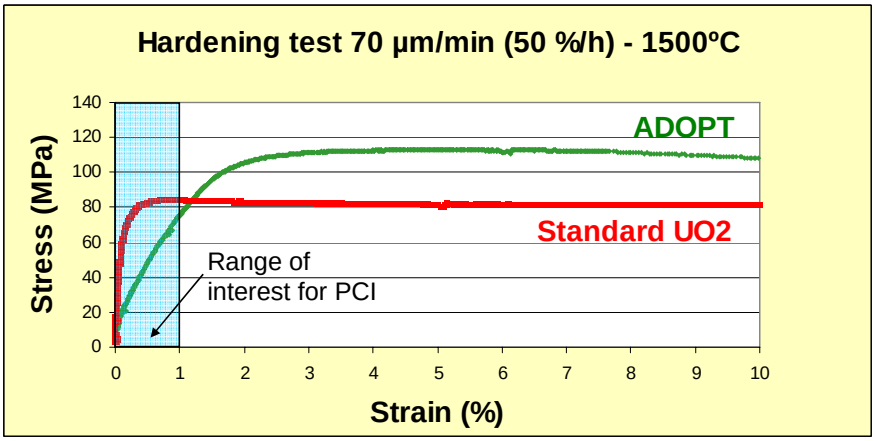

FIG. 14. Hardening test at 1500 °C and 70 µm/min of unirradiated ADOPT and standard UO_2 pellets.

4. Secondary degradation

In a fuel failure scenario, e.g., caused by debris fretting, UO_2 washout from the leaking rod can lead to contamination of the core, increased radiation doses to personnel, and for BWRs, ultimately to costly mid-cycle outages to remove the failed fuel.

4.1 Oxidation test of unirradiated pellets

An oxidation test performed as a thermal-microbalance test was performed on fresh pellets in order to quantify the corrosion resistance. Samples of standard UO_2 and ADOPT pellets were tested under a highly oxidizing atmosphere while their weight increase were measured on-line. The pellets were exposed to a temperature of 400ºC for 20 hours. The oxidizing atmosphere was produced by moisturized argon at room temperature. Evaluation of the test results shows that the oxidation rate for ADOPT is about half of that for standard UO_2 pellets, see Figure 15.

4.2 Pellet dissolution/erosion test

The resistance against post failure fuel washout for standard UO_2 and ADOPT pellets were investigated in an in-pile pellet dissolution/erosion test performed in the Studsvik R2 test reactor. The rodlets, which had slots open to the coolant, were irradiated for about 70 days at a rod power between

25 and 35 kW/m. The intention with the open slots was to simulate a secondary failure situation. The rather large slot size implies that the washout mechanism could be dominated by erosion, i.e., boiling at the pellet surface. After end of irradiation the fuel loss were determined by gammascanning. By using regression analysis of the results it was concluded that the fuel loss increases with power and decreases with density. Hence, the ADOPT pellet is more resistant against this fuel wash-out mechnism as well, thanks to the higher density.

Ceramographic investigations of the rodlets show that the shape and distribution of fuel loss is similar to a real post-failure situation see Figure 16.

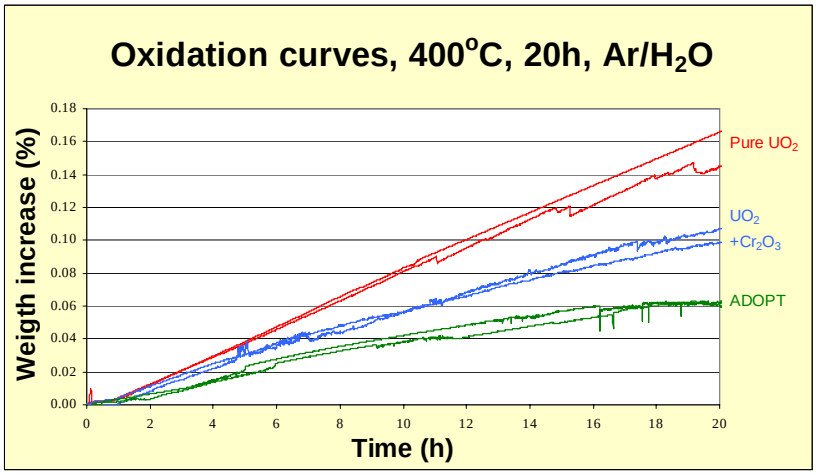

FIG. 15. Weight gain in 400 °C steam, of fresh doped and undoped pellets.

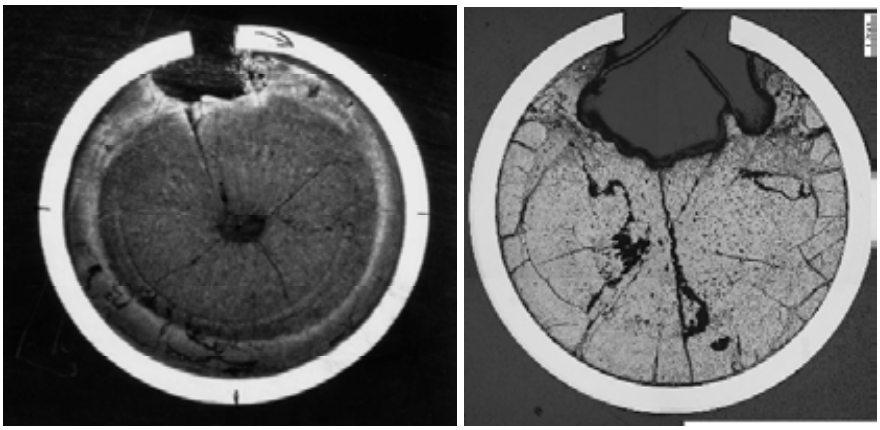

FIG. 16. Micrograph showing the cross-section of a BWR rod with a large secondary defect (long slit) and significant fuel loss (left) and micrograph showing the cross section of one of the pellets types that were tested in the pellet dissolution/erosion test.

4.3 Summary secondary degradation

Secondary degradation is a complex phenomenon that is at least a combination of oxidation and erosion. ADOPT pellets have been tested for both, and found to be more resistant against both phenomena.

5. Physical characteristics

The heat capacity C_p, thermal expansion coefficient α, melting temperature T_m and thermal diffusivity, of unirradiated standard UO_2 and ADOPT pellets have been measured and compared. No measurable differences in these physical properties have been found [1].

6. ADOPT operating experience

The first ADOPT rods were loaded in a commercial power plant in 1999 and current operating experience includes two full commercial reloads of ADOPT fuel. Several sets of lead test rods are running in different plants.

7. Conclusions

Small amounts of additives have a great, beneficial impact on the densification and grain growth during sintering, while physical properties remain the same. ADOPT pellets have shown improvements of in-reactor properties compared to standard UO_2 pellets such as reduced FGR during operating running under conditions representative for a commercial reactor, improved properties pertinent to the PCI behavior, and improved corrosion resistance. The ADOPT pellet program will focus on investigation of high burnup properties in the near future.

The amount of chromium has been kept low in the ADOPT pellet in order to minimize the parasitic neutron absorption. Aluminum has a very small cross section for thermal neutrons, similar to that of Zr.

REFERENCES

[1] ARBORELIUS, J., BACKMAN, K., HALLSTADIUS, L., LIMBÄCK, M., NILSSON, J., REBENSDORFF, B., ZHOU, G., KITANO, K., LÖFSTRÖM, R., RÖNNBERG, G., Advanced doped UO_2 pellets in LWR applications, Water Reactor Fuel Performance Meeting, Kyoto, (2005).

[2] ZHOU, G., ARBORELIUS, J., HALLSTADIUS, L., LIMBÄCK, M., NILSSON, J., BACKMAN, K., REBENSDORFF, B., HEDE, G., KITANO, K., RÖNNBERG, G.,Westinghouse advanced UO_2 fuel behaviors during power transient, Water Reactor Fuel Performance Meeting, Kyoto, (2005).

[3] KITANO, K., LOSIN, C., ARBORELIUS, J., LIMBÄCK, M., Study on incipient cracks at inner surface of cladding after high power irradiation test, Water Reactor Fuel Performance Meeting, Kyoto, (2005).

[4] JOSEK, R., The high initial rating test IFA–677.1: final report on in-pile results, OECD, Halden Reactor Project, (2008).

Washout Behaviour of Chromia-doped UO_2 and Gadolinia Fuels in LWR Environments

C. Delafoy [a], M. Zemek [b]

Abstract. To enhance the efficiency of their plants, nuclear utilities have requirements for power uprate, or operating cycle extensions and increase of fuel average discharged burnups. This general trend is accompanied with uncompromising towards safety margins. In this context, the AREVA chromia-doped UO_2 fuel proved to bring significant margins in mitigation of Pellet-Clad Interaction risk of clad failure as well as to the reduction of Fission Gas Release and induced rod internal pressure at the end of life. The optimized Cr_2O_3-doped fuel characteristics provide additional fuel robustness by a reduced pellet chipping susceptibility and reliability features. This latter concerns fuel washout behaviour in case of defective rods after the occurrence of primary defects occasionally observed under operation. This paper presents results of the testing program carried out to clarify the washout behaviour of both chromia-doped UO_2 and chromia-doped gadolinia fuel pellets with comparison to non-doped standard fuels. The pure reaction with oxygen has been first investigated by thermogravimetry studies under dry conditions. For a better understanding, pellets with different chromia additions and grain sizes were tested. Distinctly, increasing the matrix grain size and additionally the fuel density improved the fuel oxidation resistance. For non-doped fuels, optical examinations revealed the phenomenon proceeded by surface oxidation quickly followed by intergranular cracking and spalling of oxidized grains. On the contrary, with the AREVA large grain chromia-doped fuels, the formation of an outside layer delays oxygen diffusion and decelerates the oxidation rate. In a second study, fuel corrosion behaviour was studied by means of autoclave leaching tests under representative LWR conditions. The washout rate of the Cr_2O_3-doped pellets has been shown to be reduced up to a factor of 5 in comparison to non-doped fuel types. The doped sample surface remains nearly intact following the formation of a compact surface layer. The entire testing program clearly establishes the improved resistance to oxidation and corrosion of the AREVA optimized chromia-doped UO_2 and gadolinia fuels. Such an enhanced operational behaviour is desired to struggle against disintegration of the fuel in case of defective rods and combined consequences to LWR primary coolant contaminations.

1. Introduction

In order to make the nuclear power generation more economical and more competitive, different action lines have been established and are continuously reviewed. Their translation into operating practices focuses on upgraded power operating with high burn-up and extended fuel cycles. Also in some specific context, improvement in nuclear plant availability and flexibility are desired to sustain the management of operating hazards (e.g. load-follow all along fuel cycles, extended low power operations, fast return to power, etc.) [1]. According to that general background, AREVA have been researching advanced fuel materials with higher performance for LWR's applications. Focussing on fuel pellets, the key improvement features concern fission gas release and pellet-clad interaction resistance. The AREVA optimized chromia-doped UO_2 fuel proved to be an efficient product to mitigate the consequences of these two phenomena up to high burnup level [2].

In parallel to performance enhancement, the fuel reliability constitutes a substantial lever for improving the availability factor of nuclear plants. Nowadays, nuclear fuel operating feedback in light water reactors is globally satisfactory; nevertheless some unexpected events can induce fuel failures. Failed fuel degradation after the occurrence of primary defects can significantly affects the reactor operation or the planned outages and increases workers exposure. Namely, not only high release of fission products to the reactor coolant occurs leading to high offgas levels, but also fuel washout is observed due to the direct contact of the fuel pellets with the coolant. Fuel dissolution is a critical issue since it may take up to 10 years to clean a core from the tramp uranium which will result in increasing the background activity level [3]. Previous experiments and observations showed that UO_2 is readily oxidized since the oxygen diffusion rate in UO_2 is very fast [4]. The oxidation process is controlled by

[a] AREVA, Lyon, France.
[b] AREVA, Erlangen, Germany.

the surface reactions of the fuel, i.e. at the solid/gas interface. According to Lewis [5], oxidation of UO_2 progresses along grain boundaries causing the grains to be separated from the bulk of the pellet. This was confirmed by Verrall et al. [6] who reported that UO_2 oxidation proceeds more rapidly along grain boundaries than within the grains themselves, allowing islands of grains throughout the oxidation phase. Accordingly, the fuel pellet characteristics may have a crucial impact on its dissolution tendency. In particular, improved oxidation resistance of the grain boundaries or a reduction in the grain boundary specific surface might reduce the risk of fuel dissolution in a degraded rod.

To assess the behaviour of the AREVA large grain chromia-doped fuel in a defective fuel rod, out-of-pile lab testing was performed with comparison to non-doped fuels. First, the pure reaction with oxygen has been investigated by thermogravimetry. For a better understanding of the mechanisms involved, variants with different density and grain size characteristics were tested. In a second study, fuel corrosion behaviour was investigated by means of autoclave leaching tests under representative LWR conditions. Here, Cr_2O_3 doping applied to UO_2 and also to gadolinia fuel pellets.

2. Experimental details

2.1 Experimental means

The test program consists of two parts characterizing first the oxidation behaviour of the fuel pellet samples by means of thermogravimetry under dry conditions and second, the corrosion behaviour by means of autoclave leaching tests of the fuel under representative conditions for in-reactor operation (pressure, temperature and oxygen potential).

2.1.1 Thermogravimetry

Thermogravimetry tests were carried out in a Netzch STA409C device under an Ar-oxygen atmosphere with well defined oxygen contents up to 40 h at 380 °C. The samples have been heated-up under pure Ar and then the desired amount of oxygen has been admixed to the gas stream. For each fuel variant, the absolute mass change and the kinetics of the mass change during a test have been evaluated and compared. The penetration depth of oxygen (reaction front) was determined by means of ceramographic examinations and the corresponding O-U phase was clarified by X ray diffractometry.

2.1.2 Autoclave testing

Data from the thermogravimetric study are not sufficient to describe the situation under wet conditions. Therefore, autoclave leaching tests have been performed to simulate a long-term exposure of the fuel pellets to the in-reactor environment in the case of a cladding failure.

The autoclave tests have been performed in a refreshing autoclave with a steel pressure vessel having a volume of 2.3 l and a water/steam flow rate of 1.5 kg/h (see Figure 1). All along the tests, the autoclave and feed water temperatures were monitored, as well as the autoclave pressure and the pH, oxygen and conductivity values in the feed water tank. De-ionized water has been used as the basis of the feed water.

The autoclave leaching tests included two runs under simulated BWR conditions –in water and in steam with very pure water chemistry and higher oxygen content and two runs under simulated PWR conditions –in water with boron and lithium additions and in steam at elevated temperatures for accidental case simulation. The typical BWR and PWR conditions under which the tests were carried out are summarized in Table 1. The samples have been exposed to these conditions for 6 days. After the test the samples have been dried at 60 °C in vacuum for 24 h and the absolute mass change was measured and compared. As for thermogravimetry, the penetration depth of oxygen was determined by ceramographic examinations and the evolution of fuel phases by X ray diffractometry.

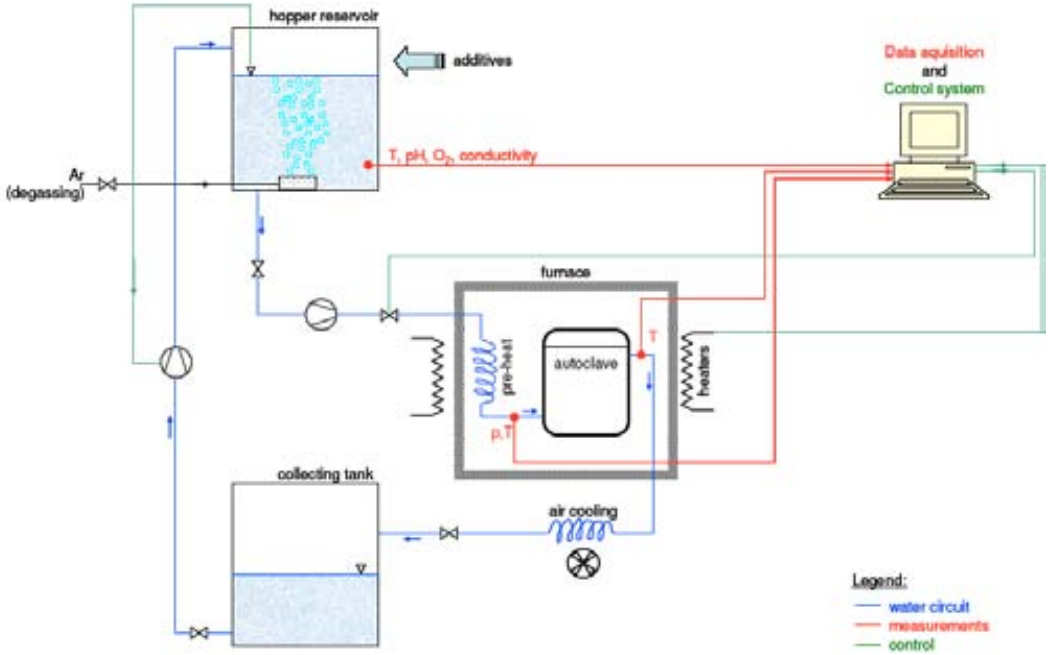

FIG. 1. Schematic view of the autoclave testing equipment.

TABLE 1. TYPICAL BWR AND PWR AUTOCLAVE TESTING CONDITIONS

Study case	Pressure (bar)	Temperature (°C)	Water chemistry
BWR	70	290 (water)	70 ppm H_2O_2
	70	360 (steam)	70 ppm H_2O_2
PWR	180	360 (water)	650 ppm B by H_3BO_3, 2 ppm Li by LiOH (pH ~7.4)
	100	400 (steam)	No additives

2.2 Fuel specimens

The AREVA chromia-doped UO_2 fuel was developed in order to combine a large grain microstructure with improved viscoplastic fuel characteristics [7]. This goal is achieved with an optimum chromium oxide concentration of 0.16 wt% and fine tuned manufacturing conditions. The AREVA Cr_2O_3-doped UO_2 fuel is characterized by a matrix grain size of 50 to 60 µm (linear intercept method). As a consequence of the grain growth activation, a better densification of the matrix occurs what allows reaching high densities as well as very stable UO_2 fuel. Otherwise, no large Cr_2O_3 free particles are observed in the fuel matrix since the additive content selected is compatible with the solubility limit of chromium in UO_2 [8].

Following the chromia-doped UO_2 fuel technology, AREVA has also launched the development of Cr_2O_3-doped UO_2 gadolinia fuel. At first, the influence of chromia doping on the sinter kinetic of (U-Gd)O_2 was determined by means of dilatometric tests. Compared to pure UO_2, the densification curves of the (U-Gd)O_2 fuels are shifted to higher temperatures due to the formation of the (U-Gd)O_2 solid solution at about 1100–1300 °C. This shift is all the more important than the gadolinia content is high. Compared to non-doped (U-Gd)O_2, significant enhanced densification behaviour is present with Cr_2O_3 doping. Whereas, the sintering begins ~ 100–200 °C later, a significant acceleration of the

densification rate takes place above ~ 1600 °C, in particular for chromia addition larger than 0.075 wt%. Such trends are typical of chromium oxide doping effect as already observed with UO_2 fuel [9]. However, with very high Cr_2O_3 contents (> 0.3 wt%), detrimental effects are noticed: decrease of fuel density due to solarization effect [10] and dopant precipitations. Figure 2 shows that no significant influence of the chromia doping on the U/Gd phase structure is observed and accordingly on the formation of $(U–Gd)O_2$ solid solution. On the other hand for the higher Cr_2O_3 additions tested, an increase of dopant precipitates is seen. This reveals a clear excess of dopant with regard to its solubility limit into the fuel matrix.

Microstructural examinations of the samples show a significant development of the gadolinia fuel matrix polycrystalline structure from a chromia addition of 0.16 wt% with average grain sizes larger than 40 µm (see Figure 3). Considering these positive trends and by reference to the chromia-doped UO_2 product, a doping level of 0.16 wt% Cr_2O_3 has been also selected for the gadolinia fuel.

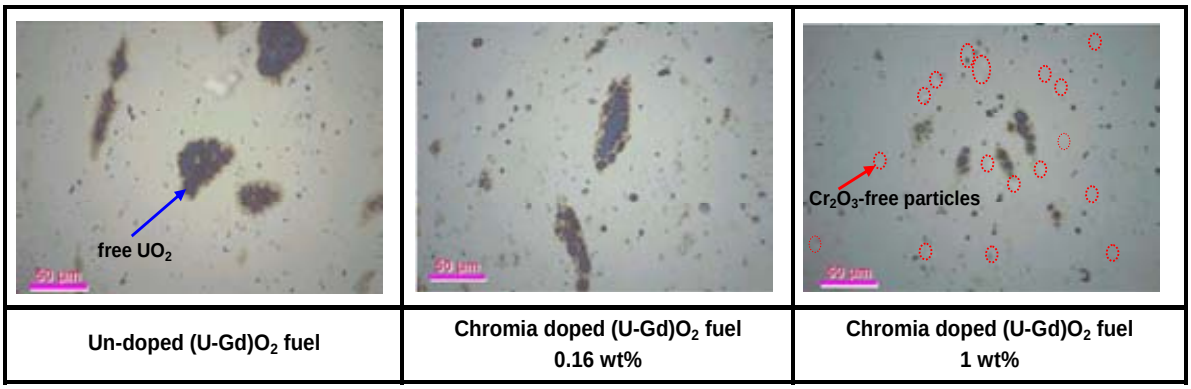

FIG. 2. Cr_2O_3 doping effect on the U/Gd phase structure revealed by colour etching.

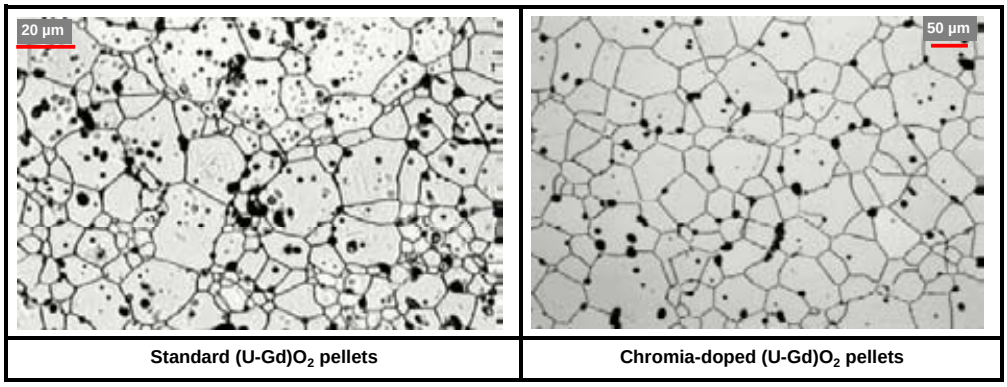

FIG. 3. Microstructure of the Cr_2O_3-doped $(U-Gd)O_2$ fuel in comparison to standard $(U-Gd)O_2$ fuel.

The Cr_2O_3-doped gadolinia fuel thermal conductivity was determined by means of laser flash method up to 1500 °C under controlled atmosphere to avoid phase transformation. As commonly reported in the literature, it was found that the addition of Gd_2O_3 deteriorates the thermal conductivity of UO_2 [11]. On the other hand, Cr_2O_3 doping has no significant influence on the thermal conductivity of the $(U-Gd)O_2$ fuel within the margin of measurement uncertainty. Finally, the viscoplastic properties were characterized by creep testing means at high temperature (1500 °C) and compression stresses in the range of 30 to 60 MPa. Compared to non-doped $(U-Gd)O_2$, doping with chromia allows enhancing distinctly the fuel plastic behaviour with an improvement factor up to 10 on the deformation rate.

This effect, also observed in case of chromia-doped UO_2 fuel, is attributed to grain size enlargement what allows compensation of the matrix hardening which results from a solid solution formation [7].

The Cr_2O_3 addition leads to an increase in the density of mobile dislocations what provides a lower-stress resistance capability to the fuel and accordingly faster strains rates. As-fabricated data of all pellet samples tested in the present study are summarized in Table 2. For a better understanding of the mechanisms involved variants with and without dopant having different density, grain size characteristics or UO_2 powder source have been prepared in the lab in addition to the industrially produced pellets. Allowing for exceptions, the chromia doping level is of 0.16 wt%.

TABLE 2. FUEL SAMPLE CHARACTERISTICS FOR THERMOGRAVIMETRY AND LEACHING TESTING

Pellet type	Pellet density (% TD)	Pellet grain size[a] (μm)	Remark
Non-doped UO_2	94.6	10	DC powder
	96.5	14	DC powder
	97.0	12	DC powder
	96.7	13	ex-AUC powder
	96.7	19	ex-ADU powder
Cr_2O_3-doped UO_2	97.1	57	DC powder
	98.2	55	DC powder
	96.8	28	ex-AUC powder — 0.07 wt% Cr_2O_3
Non-doped (U-Gd)O_2	95.9	25	DC powder — 6 wt% Gd_2O_3
Cr_2O_3-doped (U-Gd)O_2	95.9	44	DC powder — 6 wt% Gd_2O_3

[a] Linear intercept method.

3. Oxidation behaviour

3.1 Definition of the test atmosphere

Under the dry conditions, the pure reaction of pellets with oxygen has been investigated. The appropriate test conditions were defined so as to achieve a sufficient oxidation for representative measurements but without a bulk oxidation of pellets. This was done by a test series with standard UO_2 at different oxygen partial pressures in argon inert atmosphere.

Standard UO_2 pellets were subjected to four atmosphere variants made of argon with oxygen content from 0.01% to 1%. After 20 h testing it was observed that the atmosphere containing 0.1% oxygen already led to a significant attack of the pellet, at 1% oxygen, the pellet was almost completely pulverized. The pellets tested in atmospheres above 0.05% oxygen have shown already a significant amount of U_3O_8 powder on their surfaces, whereas the pellet tested in the atmosphere with 0.01% oxygen show more or less intact surface with only few traces of oxidation (U_3O_8 grey structures in white UO_2 phase). Figure 4 shows the polished cross-sections of the samples. In all atmospheres, the oxidation took place in an intergranular mode, where the oxygen attacked the grain boundaries first. The consequent volume increase of the matrix when oxidizing produced stresses in the structure leads to propagation of cracks and to strip deeper grain layers.

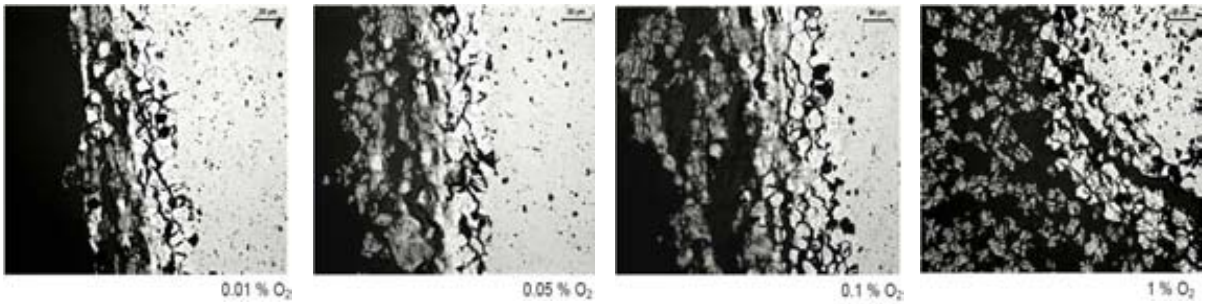

FIG. 4. Ceramography of UO_2 samples tested under [Ar-O_2] atmospheres (×300).

The thermogravimetric records on Figure 5 show that the weight gain logically increases when rising the oxygen concentration in Ar. It is also observed that the oxidation kinetic varies according to the oxygen concentration. Under Ar+0.01% O_2, a period of low weight gain, often called induction period, is followed by a rapidly accelerating rate up to a linear portion. The induction period reveals that the oxidation is governed by surface processes mainly. For the other test conditions, the oxidation process is initiated faster and the kinetic is continuously linear. The dependence of the oxidation rate on the oxygen partial pressure was of potential character with an exponent ~0.72. This result is consistent with that obtained by Tucker [12] who determined values of 0.65 and 0.68 at 350 and 400 °C respectively. The total sample weight change after 20 h indicated that an atmosphere with 1% oxygen led to an almost complete oxidation of UO_2 to U_3O_8.

Based on these series, further tests were performed applying an Ar atmosphere containing 0.01% O_2. Under this condition, the mass changes are reliably measurable, the pulverization of the pellet surface occurs relatively late so the ceramographic examinations are less affected by the loss of material. Moreover, such low oxygen content allows distinguishing, possible behavioural differences of samples during the initial surface oxidation process, before the bulk oxidation begins.

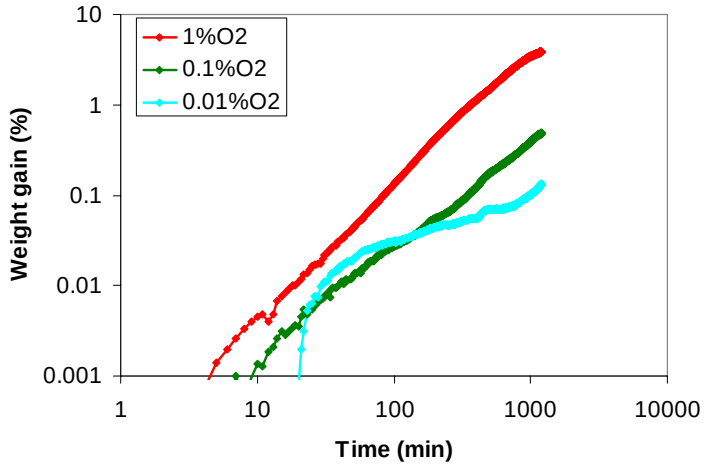

FIG. 5. Thermogravimetric records of UO_2 samples tested under Ar-containing different oxygen concentrations.

3.2 Influence of pellet characteristics

3.2.1 Influence of UO_2 powder source

In this series, all variants have a sintered density of ~96.5% TD and an average grain size of about 15 µm. From one sample to the other, the initial oxidation phases are only slightly different. Despite,

some kinetic changes during the oxidation process, all samples reached the same final linear-rate curve; with comparable final weight changes (see Figure 6). All together, one can conclude that the type of UO_2-source powder doesn't deeply affect the long-term oxidation behaviour of pellets The variability observed in the oxidation kinetics is difficult to explain a posteriori. One hypothesis to put forward is the respective impurity amounts for each UO_2 powder source. Impurities can concentrate up to high amounts in grain boundaries due to local favourable atomic structure. On these locations the grain boundary oxidation rate can thus slow down more or less temporarily.

3.2.2 Influence of pelletdensity

Whatever is their initial density, the UO_2 variants exhibit a very slow non-linear oxidation in the early 250 min followed by a fast linear mass increase and roughly the same final weight change (see Figure 7). In the domain investigated, the pellet density doesn't play a fundamental role in the fuel oxidation.

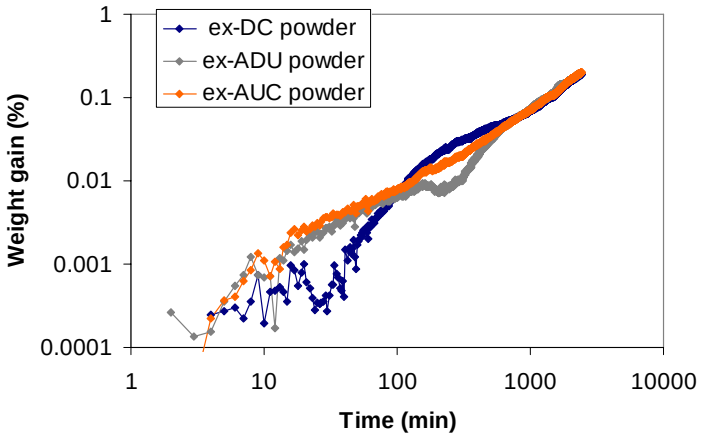

FIG. 6. Influence of the powder source on the oxidation behaviour of UO_2 samples (Ar+0.01% O_2 — 380 °C).

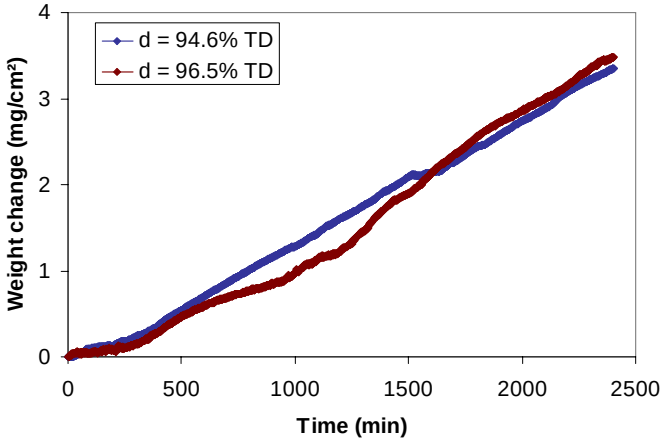

FIG. 7. Influence of pellet density on the oxidation behaviour of UO_2 samples (Ar+0.01% O_2 — 380°C).

The ceramographic examinations performed after testing indicate that the behaviour is again an intergranular oxidation mode. XRD examination of the material spalled and scrapped-off from the surface revealed three phases: U_3O_8, U_3O_7 and UO_2 phases (see Figure 8). This is consistent with the broad consensus for which the oxidation of uranium dioxide below 400 °C is a two-step reaction [13]: $UO_2 \rightarrow U_4O_9/U_3O_7 \rightarrow U_3O_8$. Moreover, on the microphotographs, the different oxide phases can be identified by colour variation: dark U_3O_8 layer on the outer surface, bright U_4O_9/U_3O_7 as intermediate layer and the grey UO_2 meat. Bringing together the phase identification and thermogravimetric records indicated that the formation of intermediate U_4O_9/U_3O_7, i.e. UO_{2+x} corresponds to the initial non-linear oxidation before intergranular cracks formation [14].

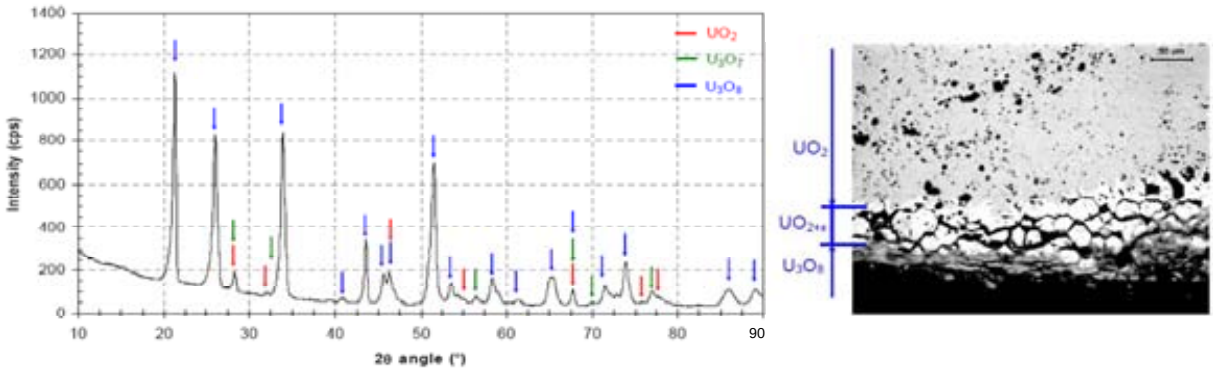

FIG. 8. Identification of phases involved during the oxidation of UO_2 (Ar+0.01% O_2 — 380 °C).

3.2.3 Influence of chromia doping

From the thermogravimetric records of Figure 9 it appears that chromia doping distinctively enhances the resistance of fuel pellets against oxidation. Similar to trends observed above with non-doped fuel, increasing the density of doped pellets leads to some limited improvement. On the other hand, it appears that the matrix grain size has a more decisive effect on the oxidation behaviour. This is clearly revealed by the result obtained for the doped sample having a grain size of 26 µm which exhibits roughly a similar behaviour to non-doped UO_2. On the contrary, 33% is gained on the resistance to oxidation with an average grain size of 55 µm what is typical of the AREVA 0.16 wt% Cr_2O_3-doped UO_2.

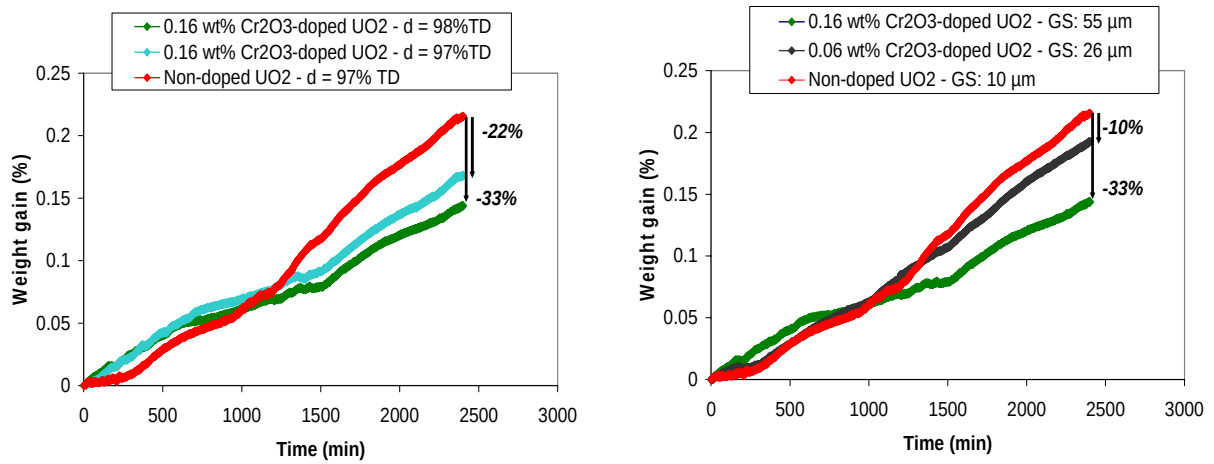

FIG. 9. Influence of chromia doping on the oxidation behaviour of UO_2 samples (Ar+0.01% O_2 — 380 °C).

The ceramographic examinations on Figure 10 reveal different features in the oxidation modes of doped and non-doped samples. For pure UO_2 pellets, the surface oxidation is followed by intergranular cracking and later spallation of oxidized grains [15]. No intergranular cracks are formed with the chromia-doped samples and the oxidation proceeds by a surface mode. Here the oxidized layers offer a certain protection for oxygen diffusion and decelerate so the oxidation rate. However, it is still not clear, why the initial oxidation period is short with the high dense and large-grained doped fuel compared to standard UO_2. This goes contrary to general understanding for which longer induction times are observed with doped fuels due to a lower rate of U_3O_8 formation [14]. In the case of the chromia-doped fuel, the total thickness of the attacked layer is thinner by a factor up to 2.5 compared to the standard pellets. A separation of the individual grains did not occurred in the doped UO_2, but the stresses induced by the lattice changes on the pellet surface were released in the form of a few deep cracks. Close to the pellet surface, big pores due to calibrated poreformer addition seem to promote those cracks. However, their contribution to the oxidation is limited to the nearest region of the crack and the surface.

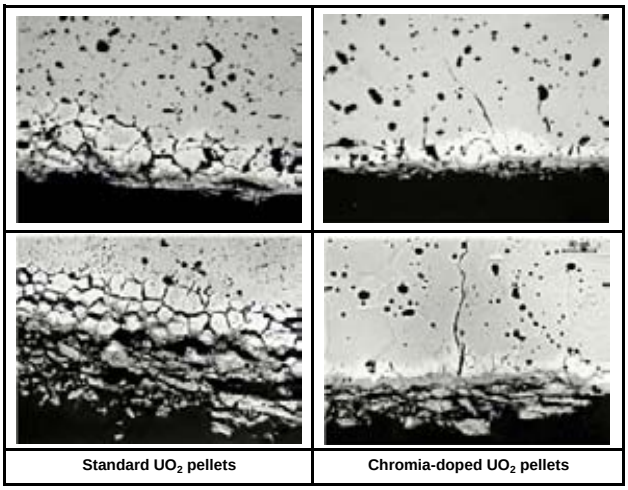

FIG. 10. Oxidation modes of Cr_2O_3-doped and non-doped UO_2 samples tested under Ar+0.01% O_2 at 380 °C (×300).

4. Washout behaviour

4.1 Autoclave leaching tests — PWR conditions (water and steam)

After 30-day leaching, a continuous weight increase can be recorded but a washout of the samples, UO_2 and Cr_2O_3-doped UO_2 was not achieved. The ceramographic examinations revealed oxidized surface layer only. The thickness of this layer increased with prolonging leaching time, however, no material loss was observed. According to the weight change and layer thickness, the composition of this layer was identified to be formed by U_3O_7. This phase corresponds with the intermediate oxidation step found in case of thermogravimetric tests (see § 3.2.2). The XRF spectrum of the pellet surface evidenced UO_2 and traces of U_3O_8 and U_3O_7. The SEM examinations showed a restructuring of the pellet surface in a similar way for all variants (Figure 11). A formation of new crystal has been seen — the EDX and XRD spectra confirmed, that they are formed by uranium and oxygen; no foreign compounds were found.

From these results, one can conclude that the leaching of non-irradiated UO_2 fuel pellets in water or steam undergoes an intermediate oxidation step. Therefore the washout depends strongly on the oxygen concentration in the medium. Since the PWR conditions are rather reducing (very low oxygen concentrations in the primary coolant) the rate of corrosion is low. This conclusion is in agreement with the work of Une et al. [16] who identified that a dissolved oxygen concentration of at least 3 ppm is required for a noticeable corrosion on UO_2 fuel pellets.

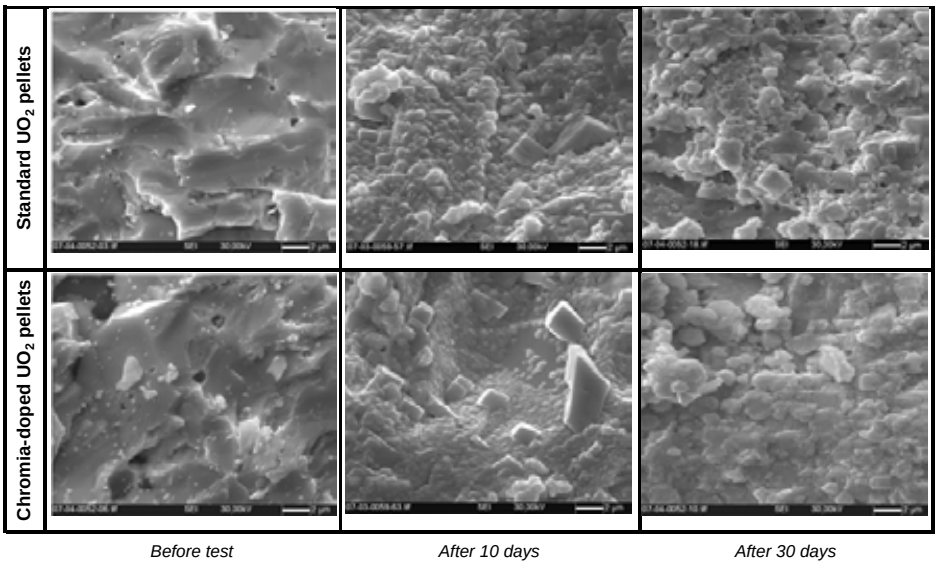

FIG. 11. SEM examinations of samples after leaching tests in PWR conditions

4.2. Autoclave leaching tests — BWR conditions

4.2.1 Six-day testing at T = 290 °C / p = 70 bars / 70 ppm H_2O_2

No noticeable washout occurred; the conditions in this case were too weak to cause a corrosion of the pellets and to show significant differences between the variants. The visual inspection showed a yellow-coloured surface formed by needle-like crystals. The ceramography of the near-surface region showed only a slight intergranular oxidation without any significant bulk formation of secondary phases.

4.2.2 Six-day testing at T = 360 °C / p = 70 bars / 70 ppm H_2O_2

These more severe conditions allowed a real washout of the pellet surface and to evidence significant differences between un-doped and chromia-doped UO_2 and (U-Gd)O_2 pellets. After a 6-day testing, the non-doped UO_2 pellets have lost ~4.6 wt%, and the chromia doped UO_2 pellets lost less than 1 wt%. In the same way, whereas the non-doped gadolinia pellets have lost ~15 wt%, the mass loss of the chromia-doped gadolinia samples is only ~3 wt%. Moreover, it was observed that the mass loss of the non-doped gadolinia samples begun after 2 days of testing while at least 5 days are required in case of the chromia-doped gadolinia fuel.

Accordingly, the AREVA chromia-doped fuels: UO_2 and (U-Gd)O_2 present an improved resistance to washout by a factor up to 5. This improvement can be attributed to the grain size enlargement of the doped pellets what provides a lower outer surface area for the propagation of the oxidation line. Similar trends were found by Lysikov et al. [17] with silicate and chromate of alumina as dopant for some U-Gd fuel. The visual inspection of UO_2-based samples (see Figure 12) showed an oxidized surface formed by cracked oxidized grains and a few needle-like crystals in the case of the non-doped pellets. This appearance called ‘popcorn’ or ‘cauliflower’ results from the volume expansion associated with the conversion to U_3O_8. On the other hand with the chromia-doped UO_2 fuel, the surface is partially intact. The ceramographic examinations of the near-surface region showed a similar structure as in the case of the thermogravimetric testing (see § 3.2.2.). However, the composition of the outer layer was changed to a $UO_3 \cdot 2H_2O$ hydrate and U_3O_8 composition. The outer layer seems to protect the pellet meat from the environment and to decelerate effectively the further oxidation and disintegration of the material. In case of non-doped UO_2 fuel, the intergranular oxidation and disintegration of the surface leads to the loss of this layer and the oxidation can further proceed. Here, the resistance of the chromia-doped UO_2 is of high advantage, because the slower and non-disintegrating oxidation lets the hydrate oxide layer remain and further protect the material.

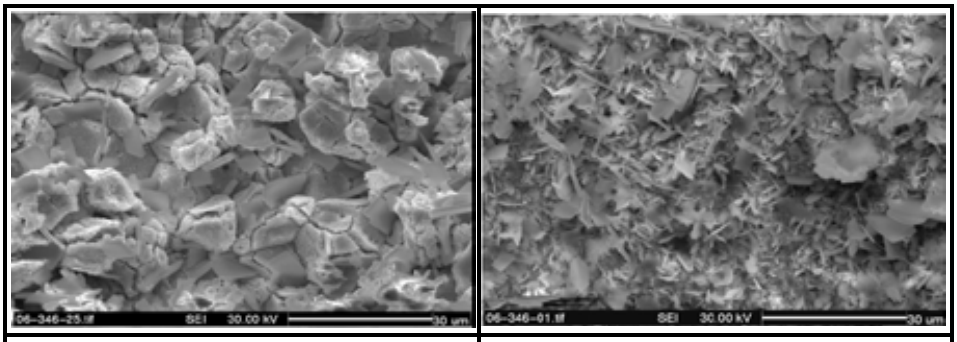

FIG. 12. SEM examinations of the UO_2-based pellet surface conditions after autoclave leaching tests.

For the (U-Gd)-based samples, the visual inspection showed an oxidized surface formed by cracked oxidized grains and grey/brown to yellow layer formed by dendritic crystals in the case of the non-doped pellets and a grey-colored layer on the surface of the chromia-doped samples (see Figure 13). On the leached broken-out area on the pellet edges, a difference in the structure was found: on the grain boundaries of the chromia-doped pellets, 'channels' were found likely a residue of a layer, that was leached away. This was not observed in case of the non-doped samples. This observation would indicate a layer of a secondary phase coating the grains of the fuel polycrystalline structure, which possibly contributes to the better corrosion resistance.

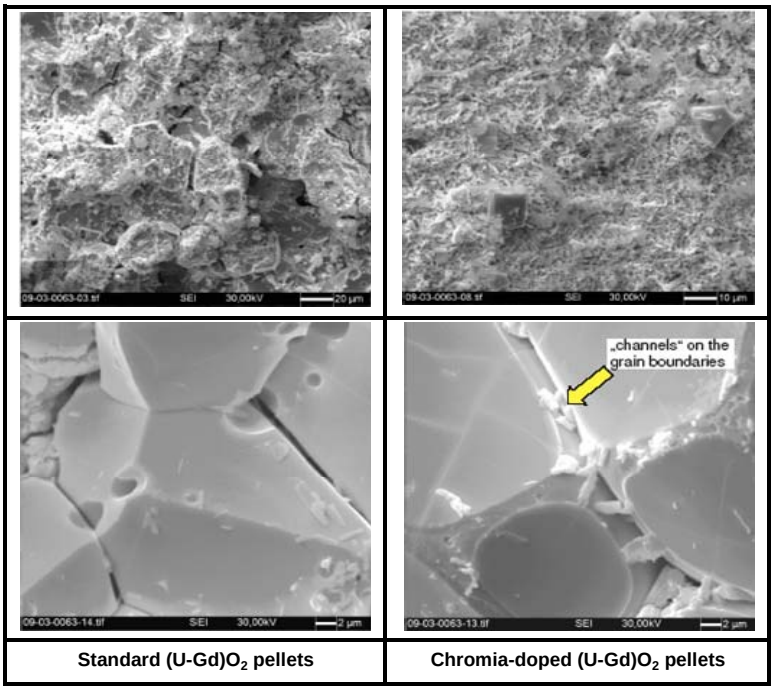

FIG. 13. SEM examinations of the gadolinia tested pellet variants leached in steam.

Here, the outer layer is composed by $UO_2.(OH)_2$ hydrate and U_3O_8. It was almost impossible to detect the gadolinium oxide in the UO_2 matrix, because no Gd was free but in the form of the solid solution in consistency with the observations made before tests (see § 2.2.). The microstructural examination showed in both cases an intercrystalline oxidation mode. In case of the standard gadolinia pellet, the original fuel surface was already gone.

5. Conclusion

The oxidation and washout behaviour of unirradiated non-doped and chromia-doped UO_2 and $(U,Gd)O_2$ fuel pellets have been analyzed by thermogravimetry and by autoclave leaching tests simulating LWR conditions. The entire testing program demonstrates that chromia doping enhances the corrosion resistance of the fuel pellets.

From the sensitivity studies carried out, it was shown, that the main driver of improvement is the grain size enlargement of the fuel matrix, the density playing only a minor role. The optimum doping amount of 0.16 wt% Cr_2O_3 proved to be especially efficient. In that case, matrix grain sizes higher that 40 and 50 µm for UO_2 and $(U\text{-}Gd)O_2$ fuels respectively are obtained leading to an improved washout behaviour by a factor up to 5 compared to non-doped fuels. Such an enhanced operational behaviour is desired to struggle against disintegration of the fuel in case of defective rods and combined detrimental consequences to LWR primary coolant contaminations. In perspective of the zero by ten initiative defined by the INPO, the AREVA chromia-doped UO_2 and doped $(U\text{-}Gd)O_2$ fuels present high reliability and robustness features. Both fuel types are currently under irradiation in commercial nuclear plants to meet future more demanding operating requirements.

REFERENCES

[1] THIBAULT, X., et al., EDF PWR fuels — EDF operation experience, Water Reactor Fuel Performance Meeting, Proc. TopFuel Paris, (2009), p.2153.

[2] DELAFOY, C, AREVA NP Cr_2O_3-doped fuel development for BWRs, Light Water Reactor Fuel Performance Meeting, Proc. ANS Conf. San Francisco, (2007), p.1071.

[3] RUDLING, P., INGEMANSSON, T., BWR fuel failure management handbook, Report ANTI **04**–0023R, (2004), p.3–33.

[4] CARTER, R., LAY, K., Surface controlled oxidation — reduction of UO_2, Journal of Nuclear Material **36,** (1970), p.77–86.

[5] LEWIS, B.J., Fundamental aspects of defective nuclear fuel behaviour and fission product release, Journal of Nuclear Material **160,** (1988), p.201–217.

[6] VERRALL, R.A., et al., Characterization of fuel oxidation in rods with clad-holes, Journal of Nuclear Material **344,** (2005), p.240–245.

[7] DELAFOY, C. DEWES, P., AREVA NP Cr_2O_3-doped fuel development and qualification, Annual Meeting on Nuclear Technology, Proc. KTG Karlsruhe, (2007), p.504.

[8] LEENAERS, A., On the solubility of chromium sesquioxide in uranium dioxide fuel, Journal of Nuclear Materials **317,** (2003), p.62–68.

[9] BOURGEOIS, L. et al., Factors governing microstructure development of Cr_2O_3-doped UO_2 during sintering, Journal of Nuclear Materials **297**–3, (2001), p.313–326.

[10] ASSMANN, H., Control of UO_2 microstructure by oxidative sintering, Journal of Nuclear Materials, **140**–1, (1986), p.1–6.

[11] INTERNATIONAL ATOMIC ENERGY AGENCY, Thermophysical properties database of materials for light water reactors and heavy water reactors, IAEA–TECDOC–**1496**, Vienna, (2006), p.160–172.

[12] TUCKER, P.M., The effect of the oxygen partial pressure on the kinetics of unirradiated UO_2 oxidation, Proc. Worksh. Berkeley Nuclear Laboratories, (1987) p.49–84.

[13] ROUSSEAU, G., et al., A detailed study of UO_2 to U_3O_8 oxidation phases and the associated rate-limiting steps, Journal of Nuclear Materials **355,** (2006), p.10–20.

[14] McEACHERN, R.J., TAYLOR, P., A review of the oxidation of UO_2 at temperatures below 400 °C", Journal of Nuclear Materials **254,** (1998), p.87–121.

[15] BAE, K.K. et al., Oxidation behaviour of unirradiated UO_2 pellets, Journal of Nuclear Materials **209,** (1994), p.274–279.

[16] UNE, K., et al., Corrosion behaviour of unirradiated oxide fuel pellets in high temperature water, Journal of Nuclear Materials **227,** (1995), p.32–39.

[17] UNE, K. et al., Fuel oxidation and irradiation behaviours of defective BWR fuel rods, Journal of Nuclear Materials **223,** (1995), p.40–50.

[18] LYSIKOV, A.V., et al., Corrosion resistance of doped $(U,Gd)O_2$ pellets, Water Reactor Fuel Performance Meeting, Proc. TopFuel Seoul, (2008), p.8017.

Development of Burnable Neutron Absorber BNA Pellets

H. Hamilton[a], C. Simister[b], S. Livingstone[c]

Abstract. Certain fuel designs require the presence of burnable neutron absorbers (BNA). Historically, BNA have been added to the UO_2 fuel meat to control reactivity in fresh fuel but, in AECL's Advanced CANDU Reactor®[1] fuel design, BNA are used to achieve a reduced coolant void reactivity. For this application it is desirable to have the BNA separate from the uranium. Zirconium oxide was chosen as a candidate inert matrix material to host the BNA due to its irradiation stability, compatibility with the BNA oxides, and material properties. This paper documents AECL's fabrication development activities and gives preliminary results of irradiation testing.

1. Introduction

Addition of Burnable Neutron Absorbers (BNA) to UO_2 to control reactivity in fresh fuel is a well-proven technology. In CANDU®[1] reactors, a need was identified for incorporation of BNA into the fuel design, but not in the UO_2. The coolant-void reactivity in a CANDU reactor can be modified by manipulation of the fuel design. Addition of BNA to the central element of a CANDU 'type' bundle has been proven effective for this purpose. The first generation of these 'Low-Void Reactivity Fuels' (LVRF) used BNA in UO_2 since the satisfactory performance of such fuel was already established. Follow-on work established that incorporation of BNA in a non-fissile matrix was advantageous. Since the only function of the matrix is to host the BNA, experience from Inert-Matrix Fuel research was applicable. A review of the candidate materials resulted in Zirconium Oxide (Zirconia — ZrO_2) as a most promising candidate.

1.1 Zirconia as an inert-matrix host for BNA

A considerable amount of research has been done on zirconium oxide. Zirconium oxides have been studied in a wide variety of applications from diamond substitutes to thermal barrier coatings. ZrO_2 is considered a potential inert fuel matrix due to its low neutron capture cross-section, irradiation stability and solubility with lanthanides and actinides. Zirconium oxide has been studied as a means to disposition plutonium in a non-fertile matrix [1] and as a medium for the transmutation of minor actinides.

Pure zirconia has three polymorphic phases, with the following phase transitions [2]:

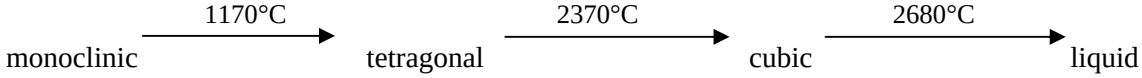

Pure zirconia pellets cannot be fabricated because zirconia undergoes a temperature-induced phase change while cooling from the sintering process. The volume change associated with the phase change causes cracking. Zirconia can be 'stabilized' in the cubic phase to prevent any phase transition by doping it with various materials; e.g., Y_2O_3, CaO or MgO [2]. It is generally accepted that at least 8 mol.% Y_2O_3 in ZrO_2 is required for a stable cubic phase at room temperature. The cubic phase has a fluorite-type structure and is isomorphous with uranium dioxide and thorium dioxide. Stabilized ZrO_2 has shown no amorphization under neutron or ion radiation to a high damage level [3], and negligible swelling under fast-neutron irradiation [4] which is characteristic of the fluorite structure.

[a] Atomic Energy of Canada Limited, Chalk River, Canada.
[b] Atomic Energy of Canada Limited, Chalk River, Canada.
[c] Atomic Energy of Canada Limited, Chalk River, Canada.

The addition of dysprosia (Dy_2O_3) and/or gadolinia (Gd_2O_3) also has a stabilizing effect for the cubic phase of zirconia due to their chemical similarity to Y_2O_3. Dysprosia and gadolinia have high neutron absorption cross-sections, which make them ideal candidates as BNA. Hafnium is also present as a neutron absorber in BNA pellets, due its natural occurrence in ZrO_2 powder, at approximately 2 wt.%.

2. Fabrication development

Several experiments were performed in the development of BNA pellet fabrication. These tests explored different powder blending methods, pellet compositions and sintering cycles. All pellets were fabricated with ZrO_2 powder with a surface area of approximately 25 m^2/g. All sintering was performed using a Rapid Temperature Air Sintering Furnace.

2.1 BNA powder blending

Four different fabrication methods to blend the powders were tested: milling, low-intensity blending, high-intensity blending and a combination of milling and low-intensity blending. For all four blending methods Composition 6, as discussed in [5] and identified in Table 1, was used.

For the low- and high-intensity blended powders, slugs were initially pre-pressed to a green density of approximately 50% of the target-sintered density. For each of the four fabrication methods, two different sizes of pellets were produced, in the range 10 to 20 mm diameter. Both pellet sizes were pressed using a hydraulic press and direct die lubricant. All pellets were sintered at approximately 1600ºC.

The percent theoretical densities are given in Table 2. The milled powders and the high-intensity blended powder gave pellets with the highest percent theoretical densities. The pellets from milling/low-intensity blended and low-intensity blended powders achieved sintered densities approximately 10% lower than the other two methods.

TABLE 1. BNA PELLET COMPOSITIONS

Composition	mol% BNA	Total mol% Rare Earth Oxide
1	Nominal	Nominal
2	None	Nominal
3	Low	Nominal
6	Nominal	Low
7	High	High

TABLE 2. SINTERED BNA PELLET DENSITIES

Blending Method	% Theoretical
Milled	88.8
Low Intensity Blended	79.8
High Intensity Blended	88.7
Milled/Low Intensity Blended	82.2

For microstructure analysis, one pellet for each blending method was cut axially, mounted and polished to a sub-micron finish. The polished surface was thermally etched using the Rapid Temperature Air Sintering Furnace and examined by optical microscopy. The microstructure analysis showed that all pellets contained a large amount of porosity. The pellets made from milling/low-intensity blended and low-intensity blended powders also contained large agglomerates and had brown spots visible to the naked eye. All microstructures are shown in Figure 1. The pellets were also analyzed by Scanning Electron Microscopy/Backscattering Electron Image (SEM/BEI) (Figure 2). This analysis showed that the pellets fabricated by milling/low-intensity blending and low-intensity blending were not homogenous. The inhomogeneity of the pellets was also demonstrated by line scan analysis performed by the Scanning Electron Microscopy/ Energy Dispersive X ray (SEM/EDX). Figure 3 presents the comparison between the line scans for the milling, milling/low-intensity blending and high-intensity blending. This analysis again showed that the milled and high-intensity blended pellets are homogenous and the milling/low-intensity blended pellet is not. The agglomerates present in the low-intensity blended pellet were analyzed by SEM/EDX spot analysis. This analysis showed that the agglomerates consisted of various concentrations of Dy2O3 and Gd2O3 and the majority of the matrix was ZrO2 (Figure 4).

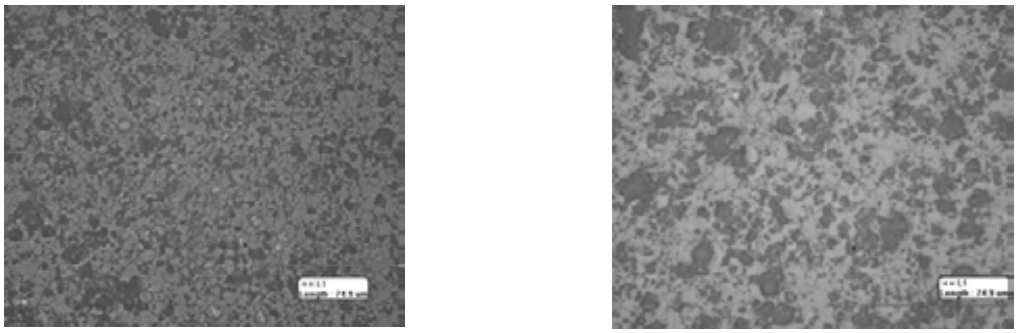

(a) 800× (b) 800×

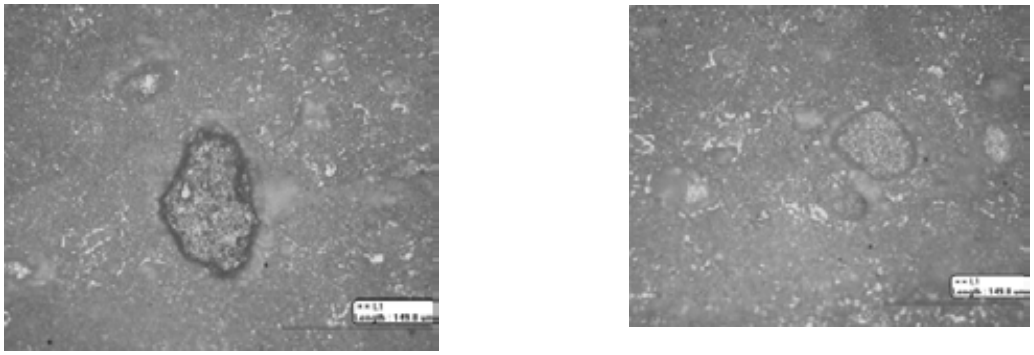

(c) (i) 400× (c) (ii) 400×

(d)i (ii)

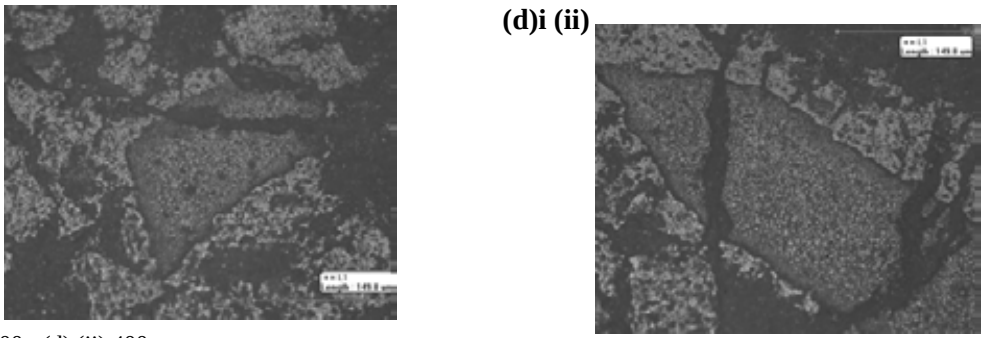

(d) (i) 400× (d) (ii) 400×

FIG. 1. Microstructure analysis a) milled b) high-intensity blending c) milled/low-intensity blending d) low-intensity blending.

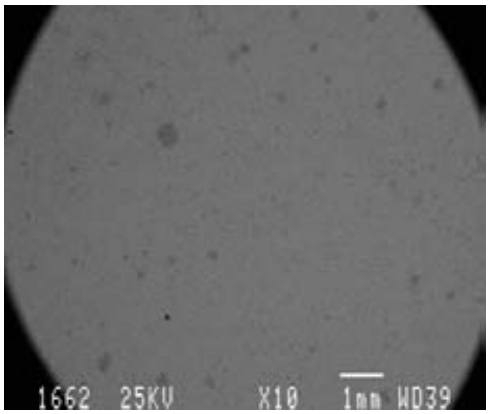

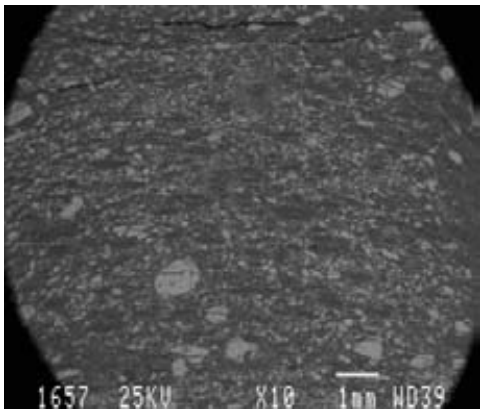

(a) (i) (b) (i)

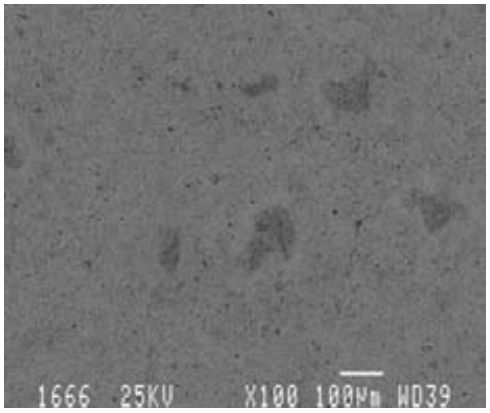

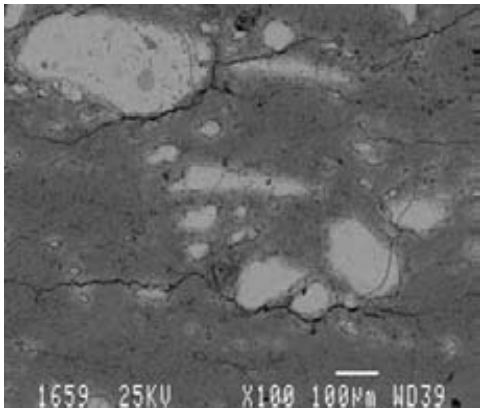

(a) (ii) (b) (ii)

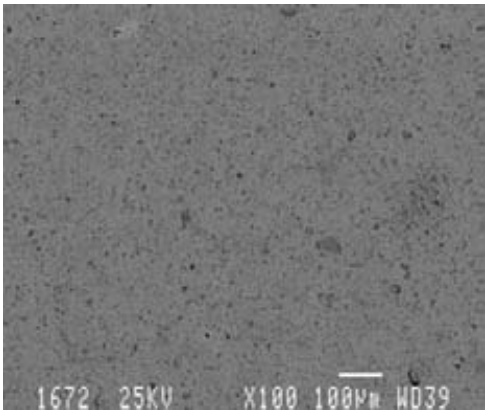

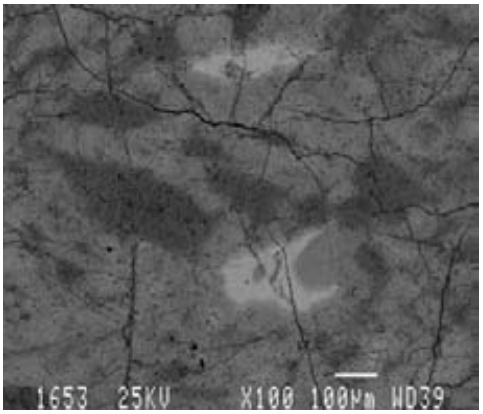

(c) (d)

FIG. 2. SEM/ BEI analysis: a) milled b) milled/low-intensity blended c) high-intensity blended d) low-intensity blended.

a)

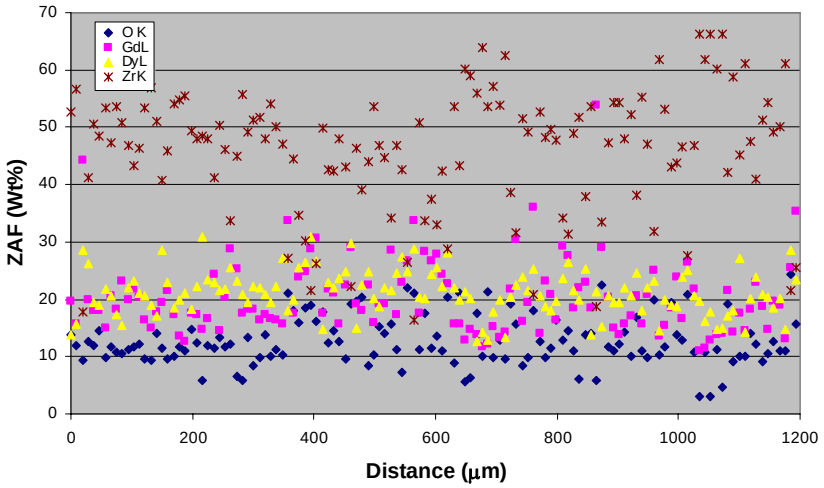

b)

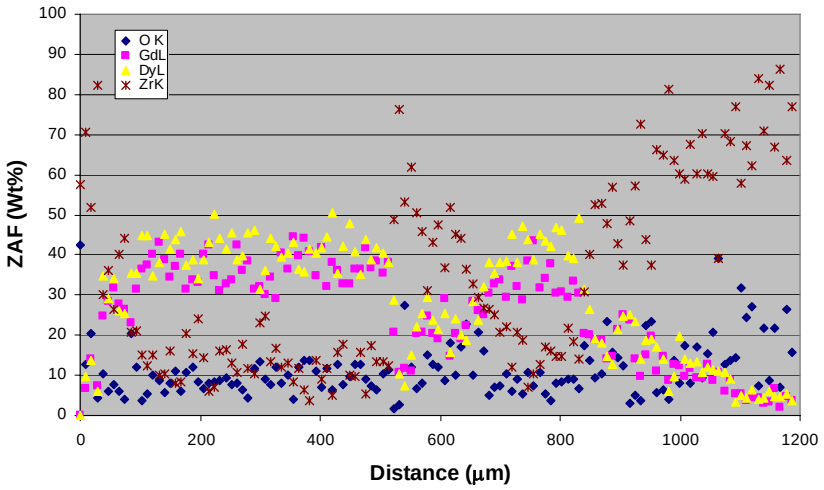

c)

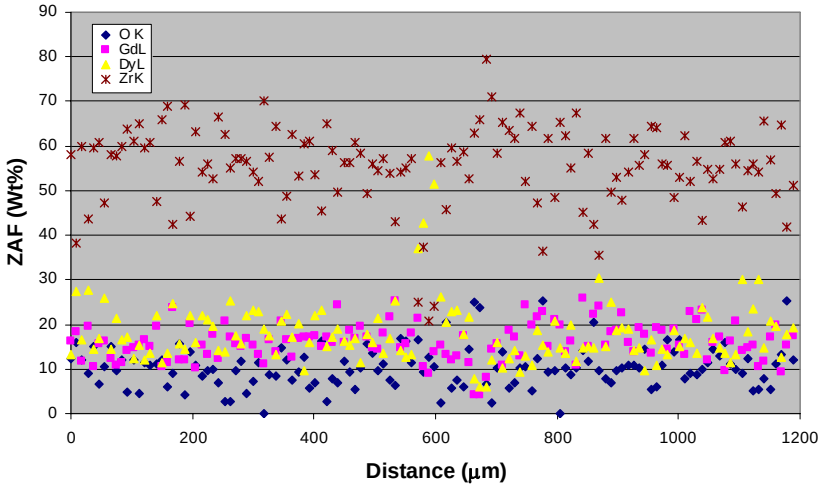

FIG. 3. SEM analysis: line scan a) milled b) milled/low-intensity blending c) high-intensity blending.

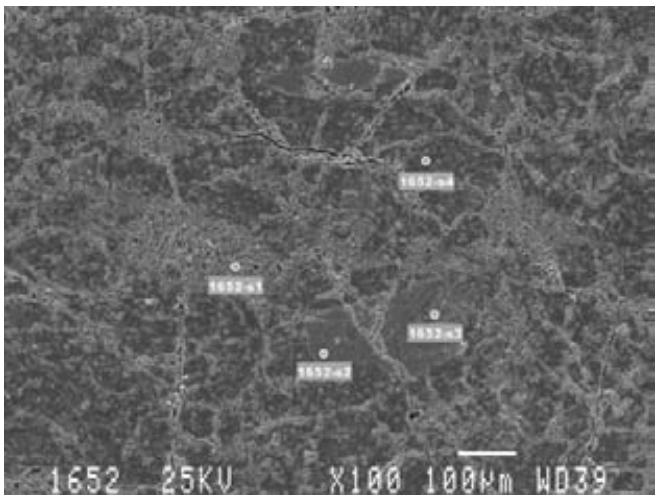

Spot/area	Element (Wt.%)							
	O	Al	Si	Ca	Gd	Dy	Zr	Total
1652–s1	19.49	---	---	---	---	---	80.51	100
1652–s2	5.17	---	---	---	1.17	89.88	3.78	100
1652–s3	8.73	1.22	10.85	3.83	2.74	72.63	---	100
1652–s4	8.29	---	---	---	34.72	21.2	35.79	100

FIG. 4. SEM/ EDX analysis for low-intensity blended pellet.

Since there is little heat generation in a BNA pellet under normal operating conditions, achieving a high pellet density, in order to maximize the thermal conductivity, is not an important criteria for success. The degree of homogeneity of the BNA in the pellet was seen as a significant factor. Reactor Physics modeled the behaviour of the BNA element based on a homogeneous distribution of the BNA and requested this be the target for pellet fabrication. Large agglomerates of BNA could result in self-shielding and a deviation of actual performance from predicted performance. Based on the microstructure and SEM analysis, it was concluded that low-intensity blending, even with prior milling of the BNA powders, was not able to intimately mix the powders to the degree necessary to form a solid solution during sintering. Both milling and high-intensity blending produced homogenous, high density pellets.

2.2 BNA pellet compositions

Several different compositions (Table 1), as discussed in [5], were fabricated by high-intensity blending and sintering at 1600ºC.

Pellet sizes from 4 mm to 20 mm in diameter were fabricated for each composition. Percent theoretical densities achieved varied depending on pellet size and composition (Table 3). All microstructures of the pellets were uniform and homogeneous, and contained significant porosity. The percentage of porosity present appeared to increase as the concentration of BNA and yttria increased, and as the size of the pellet increased. The grain size achieved ranged from 5–9 μm depending on the composition. An X ray diffraction (XRD) analysis was performed on one pellet for each composition. The XRD analysis for all compositions confirmed the majority of the structure was in the cubic phase.

TABLE 3. PERCENT THEORETICAL DENSITIES ACHIEVED

Pellet Diameter	% Theoretical
Composition 1	
20 mm	74.4
11.5 mm	74.4
8 mm	77.0
4 mm	79.3
Composition 2	
13.5 mm	74.5
11.5 mm	78.0
Composition 3	
20 mm	76.4
11.5 mm	77.2
8 mm	80.7
4 mm	84.3
Composition 6	
20 mm	82.3
11.5 mm	83.5
8 mm	84.6
4 mm	85.2
Composition 7	
11.5 mm	69.7
8 mm	71.9
4 mm	75.7

2.3 BNA pellet sintering

During the fabrication of BNA pellets, it was observed that the densities of the BNA pellets decreased significantly when the furnace was fully loaded (many pellets stacked on-top of one another) compared to a test run consisting of only 5–10 pellets. It was also observed that the pellets on the periphery of the fully loaded pellet stack sintered to a higher density than the pellets in the middle of the furnace. Various sintering atmospheres were investigated; the highest percent theoretical densities achieved were in air.

The BNA pellets were also sensitive to the cooling rate following sintering. Micro-cracking was observed when pellets were cooled at too high a rate. The effect of the sintering cycle (e.g., holds at temperatures below the peak sintering temperature) was examined. For Composition 7, variations in sintering cycle resulted in a significantly increased density, while Compositions 1 and 6 were unaffected.

The maximum temperature required to sinter the BNA pellets was also investigated for two compositions: Composition 6 and Composition 7. Both compositions were sintered at three different temperatures. A similar result was observed for both; the highest percent theoretical density was achieved by sintering at 1600 ºC, and this temperature was used as the 'nominal' sintering temperature for all of the samples manufactured in the work reported in this paper.

3. Irradiation testing of BNA pellets

While irradiation data exists for zirconia containing lanthanides and actinides, these pellets usually contained a fissile component. The presence of the fissile component greatly increases the operating temperature of the zirconia matrix compared to the application with BNA alone. For this reason, an irradiation testing program was developed to verify the satisfactory performance of BNA pellets.

The main thrust of this plan involved the irradiation of CANDU DeMountable Elements (DME) containing BNA in the experimental loops of the National Reactor Universal (NRU) reactor.

Supporting irradiations were also performed on zirconia pellets containing yttria only (no BNA) in the Multi-Capsule Rod (MCR) facility in the NRU reactor.

3.1 BNA element irradiations

The light-water cooled experimental loops in the NRU simulate CANDU power reactor conditions. The vertically-oriented test sections accommodate full-scale CANDU bundles and have similar water temperature, pressure, chemistry and flow to CANDU power reactors. BNA pellets of various compositions were loaded into elements and irradiated on a DME bundle. A DME bundle contains a fixed core of intermediate ring elements and inner and outer rings of demountable elements. Only a limited number of BNA elements could be loaded into a bundle due to the large amount of strong neutron absorbing material present per element. The arrangement of the BNA elements and the reference stabilized zirconia element are shown in Figure 5.

During January–May 2009, the DME test was irradiated for 47 days in a high flux position. Phase 1 of the experiment requires approximately 120 Full Power Days (FPD) of irradiation. An interim non-destructive examination of the experimental elements was performed after 21 FPD in the Chalk River Shielded Facilities; the DME BNA elements were profiled and visually examined, and no anomalies were detected. There was no evidence of pellet swelling. This experiment is scheduled to operate for approximately 1000 FPD.

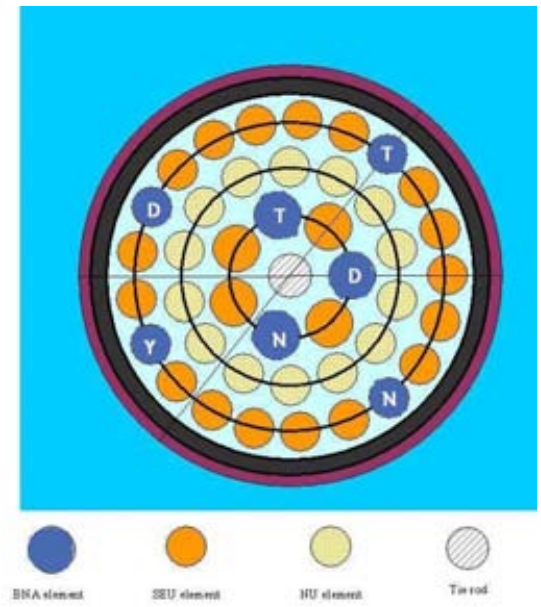

FIG. 5. Schematic of Zr-BNA DME bundle #1. For Zr-BNA elements (blue), D = Dy only; Y = Y stabilized (no BNA); T = BNA + Yttria; N = BNA — no Yttria. Slightly Enriched Uranium (SEU) elements (orange) in the outer and inner rings are 2 wt.% U–235 (in total U). Intermediate ring elements (yellow) are Natural Uranium (NU).

3.2 Multi-capsule rod (MCR) irradiations

The MCR occupies a single fuel position in the NRU and is capable of holding six strings of MCR capsules (see Fig. 6) within a 6-barrel conFiguration. The MCR facility is routinely used for isotope production, and provides a cooled high-flux radiation position. Unlike the DME loop experiment, the samples in the MCR were not exposed to high CANDU coolant pressures (~ 10 MPa), and therefore there was no sheath collapse.

3.2.1 Specimen and experiment description

The specimens were irradiated in mini-elements that were fabricated according to standard techniques for CANDU fuel elements (i.e., Zircaloy-4 sheathing, 13.5 mm diameter, He filling gas, no CANLUB coating on the inner bore, standard end-caps welded on each end, no brazed-on appendages), but were significantly shorter (~55 mm in length) in order to fit in the MCR capsule. While the MCR capsule is exposed to the coolant flow, the mini-element inside the MCR capsule is in a static air environment. FIG. 6.6 shows three images of the specimens, including a schematic and pre-irradiation photographs of the mini-element and an MCR capsule.

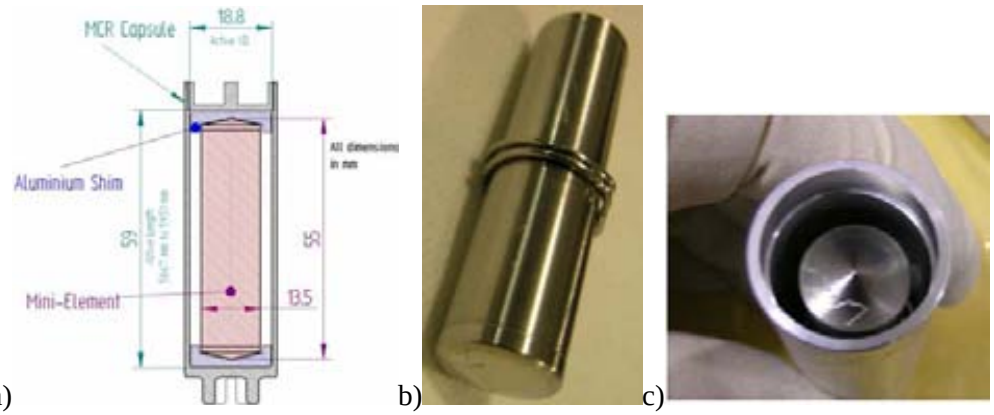

a) b) c)

FIG. 6. a) Schematic of the mini-element and capsule, b) Mini-element (pre-irradiation, including flux wire), c) Mini-element in a capsule (pre-irradiation).

As shown in FIG. 6. b), flux wires were wrapped around the mini-elements in order to provide a measurement of the thermal and fast neutron flux. The MCR capsule and mini-element arrangement was installed in the MCR facility in three strings of three samples each. The first string (ZY-1,2,3) was irradiated for 15 days in April 2008, the second string (ZY-4,5,6) was irradiated for 3 months during April–August 2008, and the final string (ZY-7,8,9) was irradiated for 9 months during April 2008 to April 2009.

3.2.2 MCR capsule — Post-Irradiation Examinations

The post-irradiation examination (PIE) of the samples in the Chalk River Shielded Facilities will include visual examinations, profilometry, flux measurements, oxide thickness measurements, ceramography and metallographic examinations. The PIE and analysis are on-going.

3.2.3 Flux measurements

The flux measurements were performed by measuring the activities of the flux wires after irradiation. These measurements were then compared with the values predicted by the NRU reactor physics codes. IV shows reasonable agreement between the measured and calculated values. Due to the design of the MCR facility, the thermal flux experienced by the mini-elements is an order of magnitude higher than that expected in an ACR bundle, and the fast flux is an order of magnitude lower. This is expected, as there is no fuel in the lattice position where the MCR rod is installed in the NRU reactor.

Table 4: Summary of Flux Measurements

Sample	Neutron Energy	Average MCR Flux [$n.cm^{-2}.s^{-1}$]	
		Measured	Calculated
ZY-1,2,3	0.0253 eV	$(2.25 \pm 4\%) \times 10^{14}$	$(2.28 \pm 4\%) \times 10^{14}$
ZY-1,2,3	> 1 MeV	1.1×10^{12}	(> 0.625 eV) 2×10^{13}
ZY-4,5,6	0.0253 eV	-	$(1.70 \pm 4\%) \times 10^{14}$
ZY-4,5,6	> 1 MeV	1.5×10^{12}	(> 0.625 eV) 2×10^{13}
ZY-7,8,9	0.0253 eV	-	$(2.54 \pm 4\%) \times 10^{14}$
ZY-7,8,9	> 1 MeV	-	(> 0.625 eV) 2×10^{13}

4. Conclusions

BNA pellets were successfully fabricated having a homogeneous distribution of BNA. A solid solution with the cubic phase was achieved for various compositions of dysprosia, gadolinia and/or yttria. The sintered densities varied depending on composition, blending method, and sintering cycle. The percent of theoretical densities achieved was as high as 89%. For one composition the percent theoretical densities achieved were improved as much as 20% by changing the sintering cycle; for other compositions this improvement was not observed. The sintering cycle and atmosphere present during sintering also appear to have a large role in the densification of the BNA pellets.

Based on the results available to date, BNA pellets do not appear to have exhibited any swelling attributable to irradiation damage. Continued irradiation of full-scale CANDU elements containing BNA pellets to ~ 1000 days is planned. PIE of BNA mini-elements irradiated in the MCR facility is ongoing.

REFERENCES

[1] DEGUELDRE, C., PARATTE, J.M., Basic properties of a Zirconia-based fuel material for light water reactors, Nuclear Technology **123**, (1998).

[2] SATTONAY, G., THOME, L.,Phase transformation induced by ion implantation in cubic stabilized Zirconia, Journal of Nuclear Materials **348**, (2006), p.233–227.

[3] SICKAFUS, K.E., et al., Radiation damage effects in cubic-stabilized Zirconia irradiated with 72 MeV I^+ ions, Nuclear Instruments and Methods in Physics Research, Vol. **B141**, (1998), p.358–365.

[4] CLINARD Jr., F.W., et al., Neutron irradiation damage in MgO, Al_2O_3, and $MgAl_2O_4$ ceramics, Journal of Nuclear Materials **108**/**109**, (1982), p.655.

[5] CHANG, J., et al., Updated BNA pellet material properties test program in support of ACR–1000 fuel design, Proceedings of 10th Canadian Nuclear Society International Conference on CANDU Fuel, Ottawa, (2008).

INNOVATIVE FUEL DESIGNS

(Session 3)

Chairperson

R. POMIRLEANU

USA

Zirconia Inert Matrix for Plutonium Burning in Reactors

C. Degueldre[42]

Abstract. The radiotoxicity of the UO_2 spent fuel is dominated by plutonium and minor actinides (MA): Np, Am and Cm, after decay of the short live fission products. Zirconia ceramics containing Pu and MA in the form of an Inert Matrix Fuel (IMF) could be used to burn these actinides in Light Water Reactors. Optimisation of the fuel designs dictated by properties such as thermal, mechanical, chemical and physical must be performed with attention for their behaviour under irradiation. Zirconia must be stabilised by yttria to form a solid solution such as $MA_zY_yPu_xZr_{1-y}O_{2-\zeta}$ where minor actinide oxides are also soluble. MA may act as a burnable poison reducing the reactivity at the beginning of live and yielding fertile nuclides improving the reactivity at the end of live. These zirconia cubic solid solutions are stable under heavy ion irradiation. The retention of fission products in zirconia, under similar thermodynamic conditions, is a priori stronger, compared to UO_2, the lattice parameter being larger for UO_2 than for $(Y,Zr)O_{2-x}$. $(Er,Y,Pu,Zr)O_{2-x}$ in which Pu contains 5% Am was successfully irradiated in the Proteus reactor at PSI, in the HFR facility, Petten as well as in the Halden Reactor. These tests support potential irradiations of such IMF in a commercial reactor. This would allow later a commercial deployment of such a zirconia fuel for Pu and MA utilisation in a last cycle. The fuel forms namely pellet-fuel, cercer, cermet or coated particle fuel are discussed considering the once through strategy. For this strategy, low solubility of the inert matrix is required for geological disposal. As spent fuels these IMFs are demanding materials from the solubility point of view, this parameter was studied in detail for a range of solutions corresponding to groundwater under near field conditions. Under these conditions the IMF solubility is about 10^6 times smaller than glass, which makes the zirconia material very attractive for deep geological disposal. The desired objective would be to use IMF to produce energy in reactors, opting for an economical and ecological solution.

1. Introduction

During the last ten years, several research organisations have devoted work to the transmutation of plutonium and minor actinides (MA: Np, Am, Cm) in thermal reactors by applying an Inert Matrix Fuel (IMF) concept e.g. [1,2,3] based on uranium-free fuel studies e.g. [4,5,6]. This situation is a consequence of the aim of eliminating the current excesses of plutonium and minor actinides. These efforts are made because of the energetic value of plutonium and of the MA's, the Pu proliferation risks and also because these nuclides contribute to the largest radiotoxicities of conventional spent fuels after some 100 years.

IMF projects initially dealt with excess plutonium produced as a result of civil nuclear electricity production. In addition, discontinuation of the nuclear weapon programs and increasing production of reprocessed plutonium from the electronuclear programs yield surplus in the stocks of the order of 200 tons weapon grade plutonium and 1000 tons civilian plutonium respectively at the end of the last century. Simultaneously, several tons of MA's are currently estimated for the world nuclear park.

The management of plutonium and MA's inventories may have suffered a major setback due to the postponement of fast breeder reactor programmes. In effect, the former goal to produce more plutonium had to change to a plutonium reduction strategy while some countries continue to produce these actinides to use them in the next generation of reactors. However, energy production remains the most desirable disposition and to solve the problem of plutonium surplus in the short and medium term it is suggested to burn [2], as quickly and completely as possible, excess plutonium in existing Light and Heavy Water Reactors (L and HWRs). Since today's practice of mixed oxide (MOX) fuelling in LWR (with up-to 40% core loading) does not allow a real reduction of plutonium and MA stockpiles, the replacement of uranium dioxide by an inert matrix and an extension of the nuclear fuel cycle have been recommended.

[42] Paul Scherrer Institute (PSI), Villigen, Switzerland.

Clearly, the current rebirth of such programmes worldwide has taken place in a new context. A new generation of IMF activities gained momentum with the first Inert Matrix Workshop held at the Paul Scherrer Institute beginning in September 1995 followed by other IMF workshops elsewhere [7,8,9,10]. Synthesis of philosophy and specific scientific programs were presented and discussed in an IAEA TECDOC report [11].

This study represents a comprehensive summary of the recent activities of the organisations directly or indirectly involved in the 'Initiative for Inert Matrix Fuel'. The contributions and country profiles are reviewed on the basis of studies that are today integrated into national or international projects. This paper presents an overview of the philosophy and current directions of IMF in the nuclear fuel cycle.

2. Zirconia based IMF candidates

The original aim of IMF development was the destruction of plutonium. Consequently one has to eliminate the source of these nuclide productions in the fuel that corresponds to the original concept of uranium-free fuel. The inert matrix fuel concept proceeds one step further: the elements and/or isotopes of the inert matrix are selected according to their transparency for neutrons.

Until recently, the basic strategy for IMF application has been to use a once-through irradiation prior to geological disposal. However, the IMF concept may also be extended by using additional fuel recycling steps. Multi-reprocessing is particularly compatible with IMF when the inert matrix can be partitioned from the actinides. The IMF concept has thus been extended for use in 'sustainable' fuel cycles proposed for fourth generation nuclear power plants. In order to define IMF candidates that meet all requirements for a particular fuel cycle, the properties are investigated systematically.

In order to select suitable IMF candidates, the following factors are initially considered:

– neutronics properties (reactivity effects),

– the compatibility of inert matrix components with coolant and structural materials,

– the fissile vector (first generation, second generation or weapon grade Pu, or Am) produced, and

– in advanced concepts, a suitable burnable poison and/or a fertile additive introduced in order to improve the neutronic characteristics of the fuel.

The first requirement in the material selection is guided by the neutronic properties. If the neutronic requirements of a particular reactor type cannot be met or are severely compromised by an element it is excluded. Next, the physico-chemical properties of the material are considered. These are of prime importance for understanding the fuel behaviour in reactor. The desired properties of the material(s) are: high melting point, good thermal conductivity, good compatibility with the cladding, low solubility in the coolant, good mechanical properties and high density. In all cases, the IMF candidate is compared to UO_2 as the reference. Material screening studies should be first carried out on the basis of literature reviews and knowledge gained in spent fuel and waste management studies but new experimental work are required. A list of candidate IMF materials for various applications is given in Table 1. Included are elements (metals, carbon), oxides, nitrides and carbides.

The addition of burnable poisons is dictated by the neutronic requirements; these can be used to make the neutronic reactivity as constant as possible with values somewhat above 1.0. In addition, for safety reasons, small quantities of resonant absorber may be added to the fuel. Finally, a stabiliser may be used to fully stabilise the solid solution in an adequate thermodynamic phase. Table 1 shows some IMF additive types and formula examples.

The evaluation process has been carried out for a range of matrix candidates, and the initial IMF selection process for burning plutonium in the current fleet of water-cooled reactors has been largely completed based on these scoping studies.

TABLE 1. EXAMPLES OF INERT MATRIX, ADDITIVE CANDIDATES AND THEIR DESIGN AS CONSIDERED IN THIS STUDY

Inert Matrix components	*Inert Matrix formula*
Elements	C, Al, Si, Zr
Carbides	SiC, TiC, ZrC
Binary oxides	MgO, CaO, Y_2O_3, ZrO_2
Oxide solid solutions	$Ca_xZr_{1-x}O_{2-x}$, $Y_yZr_{1-y}O_{2-y/2}$,
Additive type	*Additive formula*
Burnable poison	B, Gd, Er, Np or Am
Stabiliser	Y_2O_3, MgO in ZrO_2
Design	*Example*
Solide solution	$Y_yPu_xZr_{1-y}O_{2-y/2}$*
Cercer	MgO - $Y_yPu_xZr_{1-y}O_{2-y/2}$*
Cermet	Zr - $Y_yPu_xZr_{1-y}O_{2-y/2}$*

*Fissile material phase.

3. The potential of Zirconia IMF

An important criterion, for the choice of materials for IMFs, which needs to be explicitly mentioned, is that of the destination of the burnt fuel. Here: the spent IMF is sent for geological storage. Such a choice can be envisaged because the residual Pu is of very poor quality following the large reduction of the fissile isotopes (239Pu and 241Pu). The consequences of this choice are: the combustion of Pu must be as high as possible, in order to reduce the toxicity and the heat source in the storage, and the material which forms the IMF must be chemically very stable, such as to satisfy the criteria for long term storage (adequate immobilization of radioactivity in geological disposal).

Commercial L&HWRs are the only worldwide available candidate facilities in the mid-term to effectively transmute the excess plutonium and utilize its energy content. In this application, the IMF must be compatible (non-soluble and unreactive) with the coolant: H2O or D2O. In practice, this condition limits the choice of IMF quite significantly. Schematic illustrations of IMF implementation into a Light Water Reactor (PWR) and High Temperature Reactor (HTR) are given in Figure 1.

The fuel in the rods/kernels themselves can be homogeneous, for instance as a solid solution of oxides of plutonium and other elements, e.g. zirconium, or a heterogeneous concept may be used to overcome the relatively low thermal conductivity of the ceramics employed. If the candidate is a homogeneous material, it may be a solid solution or an alloy. If the candidate materials are employed heterogeneously, they can either be cercer or cermet. Figure 1 shows some design examples. The introduction of IMF rods into a UO2 fuel assembly may be somewhat complex because of the large differences in the neutron spectra of the two cell types and their interaction with each other.

The core loading options (Figure 1) chosen by the different groups who work on IMFs vary from one organisation to another [12,13,14]:

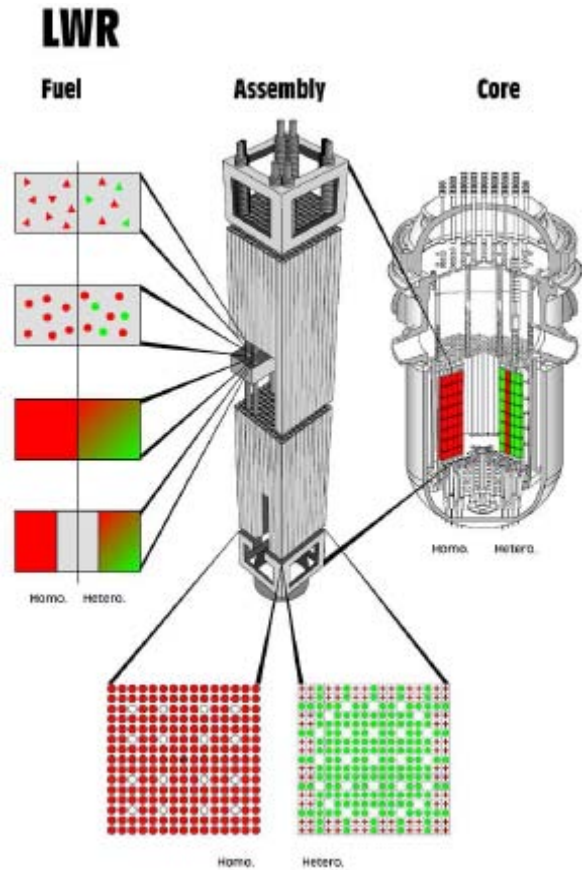

FIG. 1. The three levels for IMF utilization in LWR considering homogeneous/heterogeneous systems at the pellet/kernel level, the assembly level and the core level, for details see [9].

Some groups have studied the behaviour of 100% IMF cores (homogeneous). Other concepts foresee the partial loading of IMF assemblies in UO2 cores (heterogeneous), in an analogous way to present-day MOX fuel assemblies. The fuel assemblies themselves may be homogeneous, i.e. all fuel rods in a given assembly contain IMF, or heterogeneous with the IMF rods distributed among UO2 rods.The application of IMF in PHWR's has focused on studies of IMF full-cores for the purpose of Pu-annihilation (with Pu from either reprocessed PWR fuel, or ex-weapons Pu [15]).

4. Advantages of Zirconia IMF

In order for inert matrix fuel fabrication to be economically attractive, it should make use of fabrication technology similar to today's standard fuel or MOX fabrication process. In reactor, the fraction of the core devoted to IMF is smaller than that required with MOX to balance the Pu production by the rest of the UO2 loaded core. Consequently, for a similar fuel production cost, the lower IMF loading in core makes IMF economically competitive.

Pu disposition using IMF obviously addresses the ecological problem of radiotoxicity connected to the inventory of plutonium in the spent fuel. First, the reduction in actinide inventory helps to achieve this goal. Second, IMF can be specifically designed to provide long-term retention of actinides in spent fuel. For example zirconia solid solution forms a single phase with actinide dioxides or rare earth sesquioxides, and fission products such as earth alkaline elements may also be soluble up to the at%. Specific environmental studies are required for each IMF to understand the long-term behaviour of the spent IMF with regard to the conditions of a geological disposal. Such questions need to be addressed by specific investigation concerning the matrix solubility and corrosion rate in typical near field and far field environments and by suitable natural analogue studies.

There are two safety aspects to be discussed: one concerns the utilisation of the IMF in reactor, and the other is the material handling itself. Particular work addressing the high burn-up objectives and the core behaviour with respect to transient and accident conditions must also be noted to complete the IMF conceptual studies. The reactivity coefficients must be considered in the context of all applicable accident scenarios. The IMF material handling prior and after irradiation must be safe compared to the classical UO2 or MOX fuel case. As there do not appear to be any significant differences, this point applies more to the ecological impacts of spent fuel storage.

The non-proliferation aspects concern the safety through the IMF extension of the nuclear fuel cycle with regards to fissile material diversion. The characteristics that make the IMF an effective non-proliferation concept lie principally in its ability to utilise excess plutonium while producing no additional weapons usable material. IMF provides an efficient method for rapid destruction and degrading of the isotopic composition of weapons plutonium, which will minimise the likelihood of excess defence material returning to military application. It is likewise an efficient method to consume and reduce the quality with regard to isotopic composition of excess civil separated plutonium. IMF designed for a once-through cycle can also be made difficult to dissolve. Plutonium separation from fresh or spent fuel material is thereby made more difficult. Low leaching potential in aqueous solutions, brine, acidic, or basic heated or super-heated, molecular or ionic liquids such as molten salts is important in this regard.

The underlying incentives for all points developed above are common in that IMF could provide the option of balancing fissile material production and consumption in the current fuel cycle, negating the need and expense of long-term monitored storage of this material, contributing to the sustainability of the nuclear enterprise.

5. Program status

Current IMF programs focus on specific work in the areas of fabrication, characterisation, irradiation with accelerators or in research reactors, and development of models for predicting behaviour in commercial reactors. IMF fabrication with optimised densities is carried out prior to characterisation. The fabrication of ceramic IMF powder can be performed following either a wet or a dry preparation route. The wet route starts with nitrate solutions of all components and coprecipitates the oxi-hydroxides from concentrated or highly concentrated solutions. The latter is required in case of microsphere production by gelation. The products are dried and calcinated. Hydrated salts thermolysis has also been occasionally applied. The dry route involves mixing and milling of powders. Milling is performed in batch in a discontinuous way using ball milling or by a continuous process utilising attrition milling. Pelletising is carried out prior to sintering at a given temperature and for a given time. For cermet fuels, hot extrusion is also occasionally used.

Characterisation of the pellet or of the material is carried out at both macroscopic and microscopic levels. The ‘geometrical’ density is first measured and the porosity is deduced from the theoretical density, which itself may be derived from X ray diffraction analysis. At the microscopic level, optical microscopy and scanning electron microscopy are used to study pore or grain structure. The IMF characterisation is completed by irradiation studies using research institute facilities such as accelerators and research reactors. Prior in pile testing fuel characterisation requires also thermal conductivity quantification (Figure 2). This allows evaluation of the fuel temperature during irradiation in reactor.

Accelerators have been used to study microstructural changes during irradiation. To complete the basic knowledge gained using accelerator irradiation, in-pile tests irradiation are done in research reactors. The first series of IMF irradiations in Japanese, French, Dutch, Canadian, American and Russian reactors have already been performed and irradiations were also performed in the OECD Halden reactor as well as in the framework of joint programs in the High Flux Reactor at Petten. Emphasis is given to energy production and transport in the fuel (temperature measurements in the pin), the mechanical behaviour and the fission product release. Irradiations are also planned in the ATR reactor in Idaho Falls.

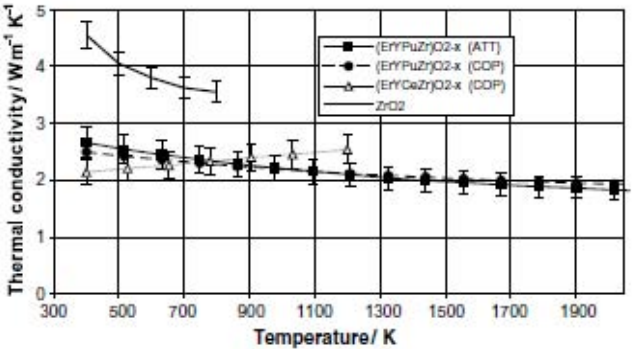

FIG. 2. Comparison of bulk thermal conductivities for ZrO_2 and $Er_xY_y(Pu/Ce)_zZr_{1-x-y-z}O_{2-(x+y)/2}$ as a function of temperature. Conditions: the relative densities of the samples $Er_{x0.07}Y_{y0.10}Ce_{0.15}Zr_{0.68}O_{1.913}$ (COP), $Er_{0.04}Y_{0.14}Pu_{0.09}Zr_{0.73}O_{1.91}$ (ATT), and $Er_{x0.04}Y_{y0.14}Pu_{0.08}Zr_{0.74}O_{1.91}$ (COP) are 0.900, 0.944 and 0.863 respectively and the thermal conductivity was corrected for the porosity. ATT stands for prepared by attrition (dry route) and COP co-precipitation (wet route).

However the fuel by itself is the first retention barrier of fission products. Their diffusivity is compared Figure 3 for Zr IMF and for UO_2. Clearly at the same temperature the retention in zirconia is better this is due to the smaller lattice parameter of zirconia (see Table 2) which compared to UO_2 allow less space for fission product bulk diffusion.

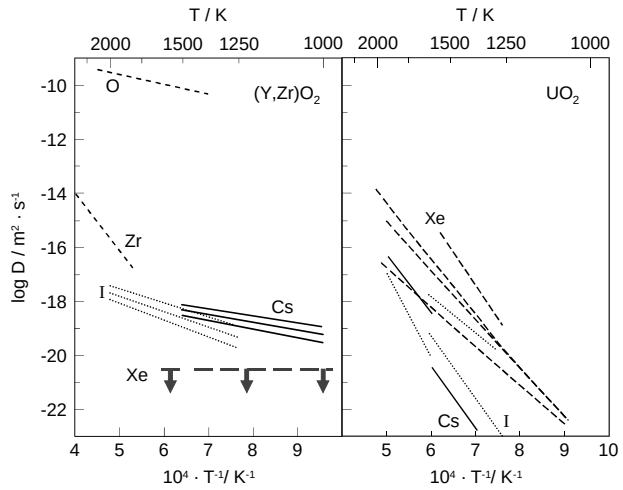

FIG. 3. Comparison of diffusion coefficients (D) for various elements (relevant fission products) with the intrinsic ion diffusion in zirconia. Note, for (Y,Zr)O2, Cs and I follow Arrhenius law, the diffusion coefficient of Xe is below the detection limit. Data for UO2 from:[21,22].

TABLE 2. COMPARING LATTICE PARAMETERS OF CUBIC STABILISED ZIRCONIA INERT MATRIX, WITH ACTINIDE DIOXIDES (IMF 20–30 PM LOWER *A* VALUES (LATTICE PARAMETER) ENHANCING FP RETENTION)

AnO_2 or ZrO_2-IMF	*Lattice parameter / pm*	*Ref.*
UO_2	547.0	[16]
PuO_2	539.5	[17]
AmO_2	538.8	[18]
ZrO_2	512.0	[19]
$(Er,Y)_yPu,Zr_{1-y}O_{2-y/2}$,	517.9-520.8	[20]

Neutronic modellings studies at the fuel, assembly and core levels have been carried out for conceptual studies to ensure the feasibility of IMF application in research reactors prior deployment in commercial reactors. The components: fissile (weapon or civilian plutonium from UOX or MOX reprocessing) / fertile in certain cases / burnable poison and inert matrix components of the IMF are selected and their respective concentrations are optimised according to the neutronic characteristics. Plutonium consumption is optimised in IMF because of the absence of ^{238}U (Figure 4). The MA (e.g. ^{241}Am) consumption is also significant in thermal flux as calculated in detail for thermal and fast neutron flux (see Figure 5).

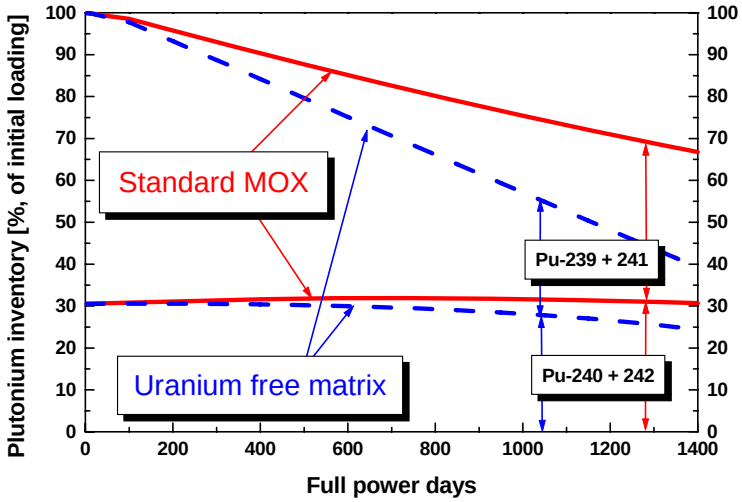

FIG. 4. Plutonium inventory as a function of IMF irradiation time in PWR.

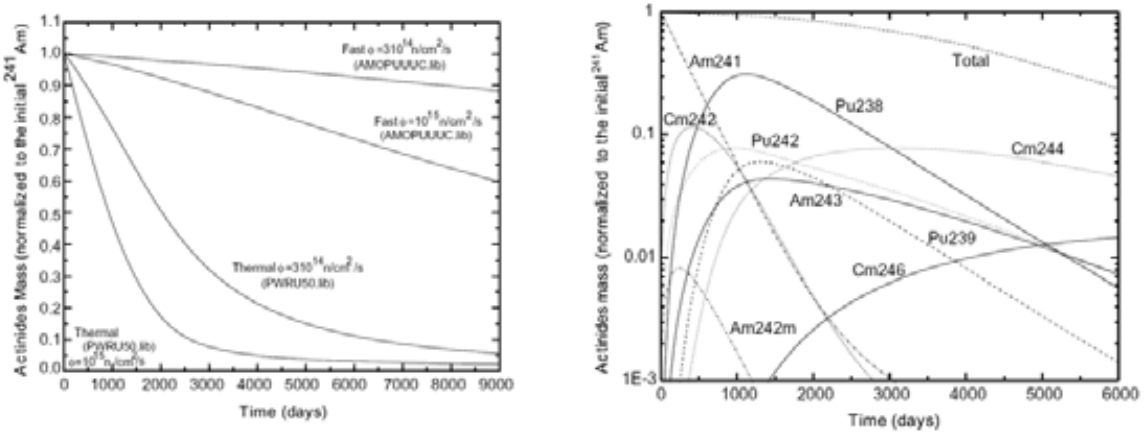

FIG. 5. : a) Total actinide mass as function of time for different neutron spectra and fluxes; b) isotopic evolution in a thermal spectrum with a constant neutron flux of 3× 10^{14} cm^{-2} s^{-1}. Actinide mass normalised to the initial isotope mass.

In pile studies of the fuel have been carried out in the frame of the of IMF feasibility tests in the HFR, Petten, NL and in the Halden, N, research reactors. The IMF: fissile (reactor grade plutonium) / burnable poison and inert matrix components ($Er_{0.04}Y_{0.14}Pu_{0.09}Zr_{0.73}O_{1.91}$ (ATT), and $Er_{x0.04}Y_{y0.14}Pu_{0.08}Zr_{0.74}O_{1.91}$ (COP) both with 5% Am Vs Pu) of the IMF were selected and their respective concentrations are optimised according to the neutronic characteristics. The tests including comparison of 2 pilot MOX's with the BNFL standard MOX and with 3 IMF materials (1 COP and 2 ATT) were carried out in the Halden reactor with full instrumentation. The fuel temperatures and fission gas releases were measured (Figure 6).

At the beginning of the life the temperature in the MOX was of the order of ~900 ^{o}C while in the IMF it reached ~1200 ^{o}C. This is due to the difference of thermal conductivity (MOX larger than IMF) that reduced the fuel temperature of the MOX Vs the IMF. At end of live the temperatures are comparable. With the burn up, the increase of fission product concentrations makes the MOX thermal conductivity decrease, increasing consequently the MOX fuel temperatures. For IMF solid solution material with already four components the addition of further components such as fission product does not significantly decrease the thermal conductivity and consequently does not increase the temperature of the fuel that is meanwhile more depleted in fissile components than the MOX.

For the fission gas release (Figure 6), it should be noted that gas releases in IMF was observed quite early. This was mainly due to the thermal shocks induced by transients in the early cycles. This was corrected later (re-sintering) and at end of live it must be noted that the fission gas release was comparable for all tested samples (IMF or MOX). This is mostly due to the fact that the temperatures (a bit higher for IMF than MOX) and the fission product diffusion coefficients (a bit higher for UO_2 or MOX than for IMF see Figure 3) are comparable.

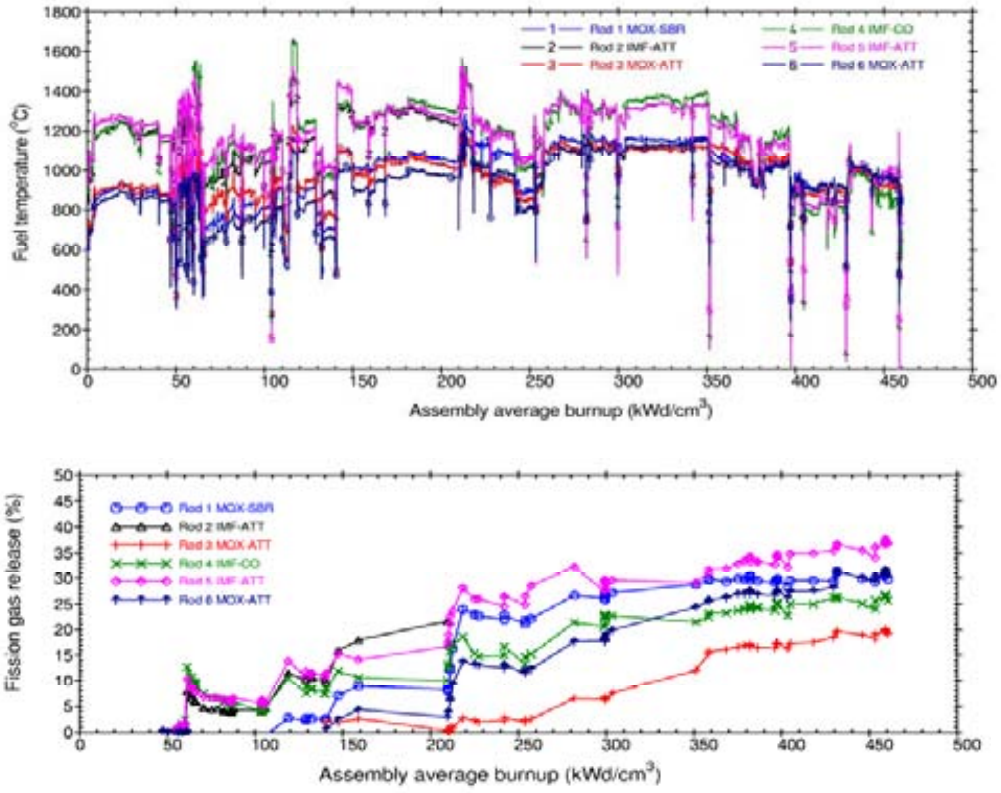

FIG. 6. Central fuel temperature and fission gas released of IMF and MOX during burn-up within the Halden reactor.

Waste management issues are relevant from a sustainability point of view. The limited evidence from the literature suggests that baddeleyite may be more resistant to the effects of alpha-decay damage from ^{232}Th and ^{238}U atoms incorporated in dilute solid solution e.g.[23]. This evidence is consistent with previous ion irradiation studies and is also supported to a certain extent by the case study presented above. However, the TEM results described in the case study document the potential modification of the microstructure of baddeleyite under intense alpha-particle irradiation by an adjacent actinide-rich phase. In this example, the bombardment by alpha-particles apparently caused the development of a domain structure and fine scale modulations, but otherwise did not significantly degrade the crystalline structure of the material.

For this strategy, low solubility of the inert matrix is required for geological disposal. As spent fuels these IMFs are demanding materials from the solubility point of view, this parameter was studied in detail for a range of solutions corresponding to groundwater under near field conditions. Under these conditions the zirconia IMF solubility is 10^6 times smaller than glass [24,25,26,27](see Figure 7). Even in carbonate solution the zirconia solubility is very low which makes the zirconia material very attractive for deep geological disposal.

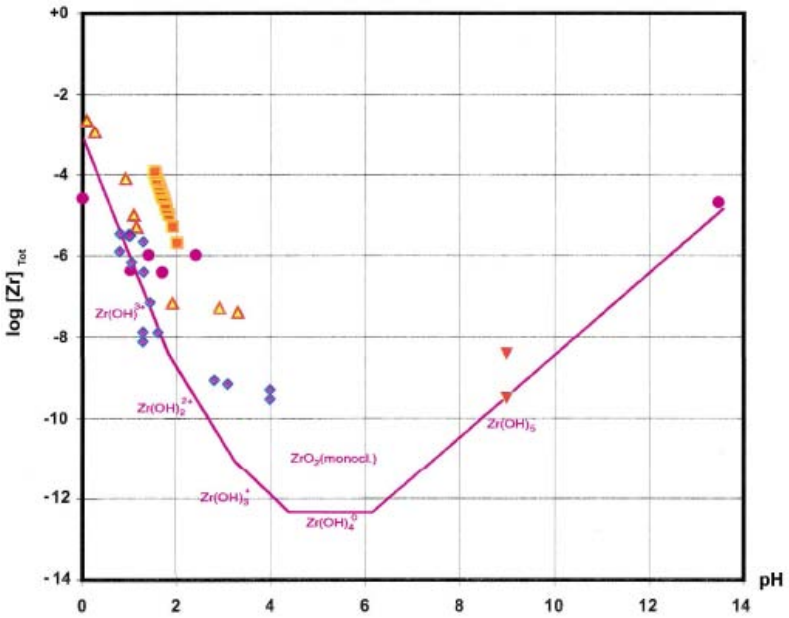

FIG. 7. Solubility (M/L) of monoclinic zirconia and oxy-hydroxide precipitate as a function of pH. Note the Zr solubility ranges from 10^{-9} to 10^{-8} M. Data from: ■ Kovalenko et al., 1961,[28]; ● Adair et al., 1961 [29]; ▼ Pouchon et al., 2001 [30], ▲ Egberg et al., 2004 [31], ♦ Michel, 2005 [27].

Internationalisation of the IMF programs has induced collaborative work among several organisations. Work has been carried out or is currently in progress in Canada, at the Atomic Energy of Canada Limited; in France, at the Commissariat de l'Energie Atomique, Saclay, Cadarache and Grenoble and at the University of Paris; in Italy at the Politecnico di Milano, the ENEA and the University of Trento; in Japan at the Japanese Atomic Energy Research Institute, at the Japan Nuclear Cycle development institute, at the University of Tohoku and at the University Kyushu; in Republic of Korea, at the Korean Atomic Energy Research Institute; in the Netherlands, at the Nuclear Energy Centre of Petten and at the University of Delft; in Russia, at the IPPE and A. Bochvar Institute, Moscow; in Switzerland, at the Paul Scherrer Institute, at the Ecole Polytechnique Fédérale, Lausanne and at the University of Geneva; and in the USA, at the University of Ann Arbor, the Massachusetts Institute of Technology, Idaho National Laboratory, Argonne National Laboratory, Los Alamos National Laboratory, and Oak Ridge National Laboratory. At the multinational level, the OECD Halden project, Norway and the European Joint Research Centre, Karlsruhe, Germany devote substantial activities for the IMF projects.

6. Conclusions

The more than 400 reactors around the world produce about 100 tonnes of plutonium and about 10 tonnes of minor actinides annually, in spent fuel, some of which are separated through reprocessing. While the recycling of plutonium as MOX fuel derives additional energy from this resource, it does little to address the issue of growing plutonium inventories. If a societal objective is to reduce the amount of plutonium, then IMF provides an attractive option for plutonium destruction. More generally, the utilization of plutonium in IMF provides flexibility in balancing the quantity of

plutonium production and consumption by enabling either the net burning of plutonium or a balanced production and consumption. This approach is viable in existing cores that already utilize MOX fuel. In addition, Zircaloy form spent fuel assemblies could be reused in the form of zirconia reducing consequently the waste stream. Due to the added dimensions in managing the fuel cycle that IMF allows, it can play an important role in the future of nuclear energy.

Another important application of IMF is the destruction of minor actinides, with or without plutonium. IMF can also be used both to manage to address the long-term radiotoxicity of the spent fuel by minor actinide destruction. Because of its economics, safety features, sustainability, and application to waste minimization from a closed fuel cycle, IMF could be used to complete recycling by a last one through then out strategy.

Several promising candidate materials have been identified for thermal reactors: ZrO_2 solid solutions or composite with MgO or Zr alloys; some of these fuel candidates have undergone test irradiations and PIE. Modelling calculations of IMF fuel performance and safety analysis as well as tests have progressed. Fabrication methods have also been developed or adapted from existing technologies. System studies have identified strategies for both implementation of IMF fuel in existing reactors in the shorter term, as well as in new reactors in the longer term.

The work to date has established the feasibility of specific IMF materials such as zirconia, and core loadings and reactor strategies for utilizing these fuels. Further development is required before commercial deployment of IMF, which will require additional resources. Additional in-pile irradiations are required, both for normal operating and accident conditions. Further safety analysis and safety testing is required. Some development is needed in the area of analysis tools and fuel performance codes. Irradiations in commercial reactors should be undertaken in a staged approach as soon as possible, beginning with segments in pins, full pins, then finally, lead test assemblies.

The desired objective would be to use IMF to produce energy in reactors, opting for an economical and ecological solution. The Swiss IMF results are reported in the proceedings of the IMF workshops published in several issues of J. Nucl. Mater. (1999, 2003, 2006) [8.10.11] and Prog. Nucl. Energy (2001) [9].

REFERENCES

[1] AKIE, H., MUROMURA, T., TAKANO, H., MATSUURE, S., Nucl. Technol. **107,** (1994) p.182.
[2] DEGUELDRE, C., KASEMEYER, U., BOTTA, F., LEDERGERBER, G., Mat. Res. Soc. Proc. **412,** (1996), p.15.
[3] FERGUSON, K., Trans. Am. Nucl. Soc. **75,** (1996), p.75.
[4] PARATTE, J.M., CHAWLA, R., Ann. Nucl. Energy **22,** (1995), p.471–481.
[5] LOMBARDI, C., MAZZOLA, A., Ann. Nucl. Energy **23,** (1996), p.1117–1126.
[6] PORTA, J., BALDI, S., GUIGON, B., Proc. ARWIF'98, OECD-NEA workshop (PSI-Villigen, (1998).
[7] DEGUELDRE, C., PARATTE, J.M., Eds., Proceedings of the 4th IMF workshop, J. Nucl. Mater. **274,** (1999), p.227.
[8] DEGUELDRE, C., PORTA, J., Eds., Proceedings of the 6th IMF workshop, Prog. Nucl. Energy, **38**, 3–4, (2001), p.250.
[9] C. DEGUELDRE, T. YAMASHITA,., Eds. Proceedings of the 8th IMF workshop, J. Nucl. Mater. **319,** (2003), p.225.
[10] DEGUELDRE, C., SCHRAM, R., Eds., Proceedings of the 10th IMF workshop, J. Nucl. Mater., (2006), in press.
[11] DEGUELDRE, C., *et al* IMF IAEA TECDOC **1303**, (2006).
[12] NITANI, N., AKIE, H., TAKANO, H., OMICHI, T., MUROMURA, T., Proc. Workshop Advanced Fuel Cycles, Paul Scherrer Institut (1995), p.118.
[13] LOMBARDI, C., MAZZOLA, A., Nucl. Sci. Eng. **122**, (1996), p.229.

[14] PUILL, A., BERGERON, J., Nucl. Technol. **119,** (1997), p.123.
[15] CHAN, P.S.W. , CAGNON, N.J.N., BOCZAR, P.G., Reactor physics analysis of plutonium annihilation and actinide burning in CANDU reactors, Proc. ARWIF workshop, NEA, PSI, Villigen, (1998).
[16] SPINO, J., PAPAIOANNOU, D., J. Nucl. Mater. **280,** (2000), p.146–162.
[17] YAMASHITA, T., MUTO, H., TSUJI, T., NAKAMURA, Y., J. Alloy Comp. **271–73**, (1988), p.404–407.
[18] RAISON, P., HAIRE, R., Proceedings of the 6th IMF workshop, Prog. Nucl. Energy **38,** (2001), p.251–254.
[19] KIM, D.-J., J. Am. Ceram. Soc. **72,** (1989), p.52.
[20] BURGHARTZ, M., LEDERGERBER, G., INGOLD, F., HEIMGARTNER, P., DEGUELDRE, C., Proceedings of the 6th IMF workshop, Prog. Nucl. Energy **38**, (2001), p.247-250.
[21] BUSKER, G., GRIMES, R.W., BRADFORD, M.R., J. Nucl. Mater. **279,** (2000), p.46.
[22] PRUSSIN, S., OLANDER, D., LAU, W., HANSSON, L., J. Nucl. Mater. **154**, (1988), p. 25.
[23] LUMKIN, G.R., J. Nucl. Mater. **274**, (1999), p.206.
[24] POUCHON, M., CURTI, E., DEGUELDRE, C., TOBLER, L., Progr. Nucl. Energy **38**, (2001), p.443.
[25] CURTI, E., DEGUELDRE, C., Radiochim. Acta, **90**, (2002), p.801.
[26] EKBERG, C., KÄLVENIUS, G., ALBISSON, Y., BROWN, P.L., J. Sol. Chem. **133**, (2004), p.47.
[27] MICHEL, N., Etude de la solubilité des oxides et oxohydroxydes de zirconium caractérisé, Thèse de Doctorat de l'Université de Nantes, (2005).
[28] KOVALENKO, P.N. , BAGDASAROV, K.N., Russ. J. Inorg. Chem. **6**, (1961), p.272.
[29] ADAIR, J. H. , DENKEWICZ, R. P., ARRIAGA, F.J., Ceram. Trans **1**, (1987), p.135.
[30] POUCHON, M., CURTI, E., DEGUELDRE, C., TOBLER, L., Progr. Nucl. Energy **38**, (2001), p.443.
[31] EKBERG, C., KÄLVENIUS, G., ALBINSSON, Y., BROWN, P.L., J. Sol. Chem., **133**, (2004), p.47.

Designing a Thorium Fuel Irradiation Experiment

J.F. Kelly[1], V. Fhager[2]

Abstract. A Norwegian company, *Thor Energy*, has been planning an irradiation experiment in which a thorium-plutonium oxide fuel will be tested in the Halden reactor in Norway. As part of this project a set of specifications has been prepared to govern the manufacture of the test batch of thorium-plutonium oxide fuel pellets. Composition, microstructural and shaping parameters were considered carefully — as outlined in this paper. Establishing specifications for the fuel ceramic stoichiometry and for certain impurity limits proved to be of specific importance for the thorium-plutonium test pellets.

1. Introduction

The Company: *Thor Energy* is a small Norwegian company in the '*Scatec'* group of renewable energy enterprises. Among its portfolio of business activities *Scatec* has major solar and wind energy interests — including single-crystal silicon production and off-shore wind power planning. *Scatec* founded *Thor Energy* in early 2006 after recognising that nuclear power is a necessary component in the low-emission energy mix for many countries. High public awareness of the large thorium resource in Norway has led to a supportive environment in which to conduct an initiative aimed at exploiting this energy source.

Nordic Feasibility Studies: between mid–2007 and mid–2008, *Thor Energy* undertook a comprehensive study of the feasibility of using thorium-based fuels in current-generation power reactors. The study was done in partnership with a large Nordic utility as a one-year, multi-million NOK exercise aimed at identifying:

- a broad conclusion as to whether thorium fuelled nuclear power generation will be feasible.
- technical challenges associated with bringing thoria-based nuclear fuels into service.

The heart of the study involved modelling the in-reactor performance of candidate thorium fuels in the PWR, BWR, HWR and HTGR systems. The fissile driver materials considered were [3]; reactor grade Plutonium, Uranium-233, and Uranium enriched to 20% in U-235 ('MEU'). Reactor safety, proliferation resistance, waste management aspects and environmental credentials were also closely assessed.

The study was able to reach the broad conclusions that:

- Thorium-based fuels are viable, indeed, they can perform well in modern water reactors. Thorium-plutonium fuels will be MOX fuel analogues. Existing MOX technology and licensing experience will greatly facilitate their entry-into-service.
- The full benefit of thorium as an energy source will be realised when closed fuel cycles are established.

Prior to this study the Norwegian government had commissioned its own one-year study into the many issues surrounding proposals to use thorium as a new energy resource — including in Norway [1].Thorium Fuel Development — Creating Value: following the afore-mentioned studies and in light of a large amount of technical and fuel market information, *Thor Energy* assessed whether there is

[1] Thor Energy AS, Oslo, Norway.
[2] Thor Energy AS, Oslo, Norway
[3] HEU is effectively unavailable on account of its proliferation sensitivity and it was not considered. U-233 was considered in a hypothetical pure form, though this material would in reality be blended into some mixed, proliferation-resistant form.

‘technology value’ to be captured by proceeding to develop licensable thorium fuel designs, and if so, how this should be done. *Thor Energy* subsequently made some key decisions and assessments, namely that:

- Thorium-plutonium fuels should be attractive to utilities when plutonium management and uranium / SWU savings become sufficiently strong imperatives.
- Licensing a new thorium-plutonium fuel will call for high quality technical data to support computer simulation of its safe operation in power reactor conditions.
- There is a paucity of data on the irradiation behaviour of thorium-plutonium oxide fuels — especially those with a composition and microstructure analogous to that of current MOX fuels.
- Due to the length of the fuel licensing process, testing activities should be commenced as soon as possible, with a view to lead-test rod/assembly (LTA) testing in a commercial power reactor.

There are very few fuel testing reactors, but one of these is at Halden, Norway. The competence and enthusiasm of the operator has encouraged *Thor Energy* to proceed.

2. The fuel irradiation experiment

Thor Energy’s largest single undertaking is the thorium-plutonium fuel irradiation experiment that will be performed in the Halden test reactor. The decision to proceed with this large (and expensive) project set in place a process for designing the experiment, entailing:

[i] Setting the main objective
[ii] Defining fuel behaviours to be characterized
[iii] Establishing experimental measurables
[iv] Defining test pellet properties
[v] Creating an experiment execution plan

Objective Setting: It is important for Thor Energy that the results of the test irradiation serve the ultimate goal of licensing a class of thorium-plutonium fuels4 — thus, the overall objective recognises that the Halden irradiation experiment is the first of a series of technical validation exercises. Its purpose is therefore: “ … to yield data that can be used to demonstrate the safe, long term performance of Thorium-Plutonium ceramic fuels, and that this information can directly support the planning and approval of an LTA irradiation for such fuel. ”

3. Fuel behaviours to characterize

3.1 Temperature and thermal property changes

The temperature profile in a fuel rod depends on its thermal conduction pathways. These changes through the irradiation period — most notably, the thermal conductivity of the pellet will decrease. Fuel temperature affects safety-related processes including fission gas release, and is important in its own right (assuring distance-from-melting and in estimating stored energy in the fuel). Thorium dioxide has a particularly good thermal conductivity for an oxide — better than that for uranium dioxide. But it drops with an increasing amount of dopant (such as plutonium), and also with increasing temperature [3]. Reliable thermal property data is sparse for thorium-plutonium mixed oxides [5]. Thorium oxide fuels are likely to manifest a different pellet-clad gap evolution compared to urania-based fuels due to a different thermal expansion coefficient, differing creep rates and a specific swelling tendency for the ThO2 matrix. Characterizing fuel pellet temperature evolution is therefore

[4] Nuclear fuel is an interesting ceramic system and it would be possible to design an irradiation experiment to study phenomena with purely scientific objectives. This is not *Thor Energy*’s intention, although it is expected that useful fundamental data will result from the undertaking.

important — but so is decoupling the effects of thermal conductivity and pellet-clad gap changes. Understanding the physical basis for these changes will serve parallel efforts to model the performance of thorium-plutonium fuels.

3.2 Fission gas release (FGR)

Fission gas release (FGR) threatens fuel cladding integrity through associated physical and corrosive stresses5. The robust ceramic fuel matrix accommodates these well, but as fuel ages these components diffuse to grain boundaries and eventually escape into the fuel rod void. The extent of FGR from oxide fuel is very dependent on temperature and therefore on power history. Thorium oxide fuels are expected to be better at retaining fission gases than are uranium fuels — despite having a greater relative yield of some volatile and gaseous elements [2]. FGR data from previous thorium fuel irradiations is rather inconclusive although a recent report shows promising behaviour for thorium-plutonium material [4]. FGR is one of the most important behaviours to characterize for the thorium-plutonium fuel. It needs to be quantified by; (i) its onset in terms of fuel burn-up, (ii) the amount released, expressed as a percentage of the total gas generated, and (iii) the composition of the released fission gas.

3.3 Mechanical interactions and changes

Densification and shrinkage may be important early in the fuel irradiation period. If this is excessive, heat removal will be compromised. If the fresh fuel pellet is of high density the effect will be small. Prior work [3] indicates that thorium fuel does not densify a great deal, nevertheless, the effect needs to be quantified for thorium-plutonium pellets of ‘typical’ density and porosity distribution. Pellet-Cladding Mechanical Interaction (PCMI) refers to stresses on the cladding (with axial and radial components) caused by fuel pellet contact. These in turn derive from pellet swelling, from creep and from cracked and relocated pellet fragments. Thorium fuel ceramics are reported to swell and creep differently as they burn, and this needs to be measured in terms of collective PCMI impact. Significant restructuring takes place within a fuel ceramic at high burn-up due to the large amount of retained fission products and the long-term neutron fluence. Restructured fuel is more porous, more fragmented, has smaller grains and can release more fission gas. The onset and extent of these changes in thoria-based fuel ceramics needs to be quantified and compared with urania-based fuels.

3.4 Chemical interactions

Over long irradiation periods, chemical interactions will occur between a ceramic fuel and the inner face of the zirconium cladding. Chemical changes also take place in the fuel matrix itself. Stress Corrosion Cracking (SCC) is a damaging process in which cladding is corrosively attacked where small cracks have been generated through some mechanical stress. Iodine is known to be particularly effective at causing SCC. There is a need to observe for SCC in thorium fuels since the collective yield of iodine isotopes is quite high for U-233 fissions. Oxygen is ‘liberated’ and moves extensively within an operating fuel ceramic. Its behaviour affects a number of processes including FGR and grain growth [2]. Thorium dioxide has a lower oxygen retention capacity than UO2 due to its single (+4) oxidized state. Indeed, this is one of the most significant differences between the two fuel matrices. The experiment seeks to quantify / identify fuel behaviour differences6 (compared to MOX) resulting from a different oxygen migration potential in ThO2.

---

[5] Xenon and krypton are the fission gases produced in largest quantities. Helium is also produced from various nuclear reactions. Iodine and cesium are volatile at fuel operating temperatures.

[6] Differences may be evident in the behaviour of certain fission elements with high oxygen affinity (*eg*, Mo, Tc, Zr, Ru) − these elements may migrate differently in thorium fuel.

4. Experimental measurables

A number of measurements are required in order to characterize the most important behaviours for the thorium-plutonium fuel material — these are summarized in the following Tables. Knowledge of fuel-pin power histories is also needed for making behavioural assessments.

Thermal Behaviour to Characterize	Data Needed to Quantify Behaviour	
	On-line Experimental Measurables	*Data from Pre/PIE Measurements*
Thermal Conductivity Decay	Centerline temperature (global indication)	Thermal conductivity of fresh pellet, Thermal conductivity of spent fuel
Thermal Conduction Pathway Changes	Centerline temperature (global indication) Cladding elongation (gap closure)	Neutron radiography, Microscopy

FGR Behaviour to Characterize	Data Needed to Quantify Behaviour	
	On-line Experimental Measurables	*Data from Pre/PIE Measurements*
FGR Onset	Rod pressure, Centerline temperature	
FGR Amount	Rod pressure	Rod-puncture gas analysis
FGR Composition		Rod-puncture gas analysis

Mechanical Behaviour to Characterize	Data Needed to Quantify Behaviour	
	On-line Experimental Measurables	*Data from Pre/PIE Measurements*
Cracking		Neutron radiography, Gamma scanning
Densification	Fuel-column elongation, Temperature	
PCMI and Swelling	Fuel-column elongation, Cladding elongation, Centerline temperature	Microscopy, Fuel rod profilometry
High Burn-up Structure	Rod pressure, Fuel-column elongation, Cladding elongation, Temperature	Thermal conductivity, Microscopy

Chemical Behaviour to Characterize	Data Needed to Quantify Behaviour	
	On-line Experimental Measurables	*Data from Pre/PIE Measurements*
Stress Corrosion Cracking		Microscopy and EPMA, Rod puncture gas analysis, Neutron radiography
Oxygen Mobility and High-Oxygen-Affinity Fission Products		Microscopy and EPMA, Rod-puncture gas analysis

5. Test pellet properties

Thor Energy entered into dialog with a number of potential providers of a batch of thorium-plutonium oxide fuel pellets that would be 'representative of a commercial, mixed, thorium oxide ceramic fuel'. A pellet specification document was concurrently produced in order to put appropriate limits and guidelines on the properties that are central to conducting a productive irradiation experiment.

From this iterative process *Thor Energy* learned that:

[i] There is a trade-off to consider between specifying tight limits on a parameter, and the higher rejection rate that this will cause.

[ii] Specifying an exact value or range for a pellet parameter may be less important than accurately knowing / measuring that which exists in the finished product.

[iii] Direct QC measurements can be difficult or impossible on plutonium-containing material but in these cases, sufficient confidence can often be provided through the use of accredited Quality Assured processes. Furthermore there may be a possibility to specify assays on 'surrogate' material produced using the same techniques and equipment. In any case, the QA plan for the pellet production campaign is a very important document.

The suite of physical / chemical properties which define the batch of thorium-plutonium fuel pellets are broadly categorised as those relating to composition, microstructure and pellet shaping.

5.1 Composition

The fissile plutonium content is clearly of central importance in the pellet specification. The isotopic make-up (fissile quality) should be as representative of spent LWR fuel as possible (ie, quite high), but this factor turns out to be equally dependent on institutional availability and other 'political' limitations. The source plutonium raises the issue of americium content, which ideally should be fairly low, but which may be appreciable due to the long storage times for some research-size batches of plutonium. An assessment of the likely helium generation arising from the americium may warranted.Metallic impurities are generally easy to assay — even in plutonium-containing fuels. Limits for key metals can be specified according to existing MOX fuel standards [6] and also against other references describing MOX pellet manufacture (note however, that some very low reported levels for certain elements would not be appropriate as QA limits). Special consideration may need to be made for the non-metallic elements; hydrogen, nitrogen and carbon. It can be difficult or impossible to have these measured in a plutonium handling laboratory so it may be necessary to rely on QA assurances existing for the pellet fabrication process. Also, it may be worth examining the underlying reason for specified limits for these elements, since they may not be particularly relevant in a fuel testing context (eg, for C).

The stoichiometry of the ceramic must be addressed in any specification for a thorium-plutonium fuel with relatively high Pu content. This is due to a tendency (or real risk) for plutonium dioxide to become reduced (and lose oxygen) in the reductive sintering environment — resulting in a hypo-stoichiometric fuel. This would raise uncertainties about the test pellet platform and compromise the ability to draw conclusions about the performance of the thorium-plutonium fuel ceramic. Additional oxidative heat treatments may need to be considered. An 'effective boron concentration' can be a useful QA factor to apply since it puts special focus on limits for highly neutron-absorbing elements (the list of which needs to be agreed, eg, whether hafnium is included).

5.2 Microstructure

Average ceramic grain-size needs to be addressed since it is undesirable to have a fuel material that is either very fine-grained, or overly coarse-grained. Standards [6] define a rather broad acceptable range. The specification will depend on whether the use of grain growth promoters is acceptable, and

also on sintering time limitations. A minimum grain-size specification may be warranted. The distribution of grain-sizes within the fuel ceramic should also be addressed to ensure that it is not highly bimodal (small grains + big grains). The density of the thorium-plutonium fuel ceramic needs to be high in order to ensure that pellets are conductive and geometrically stable [2, 3]. A minimum density needs to be agreed by supplier and purchaser — this largely being a compromise based on achievable pellet density and low rejection rate. The extent and the nature of the residual porosity is important in terms of fuel behaviour, but it is not a controllable parameter. Effort should put into characterizing the pore shape and porosity distribution in pellets that have passed density and other QA criteria. It is also worthwhile to estimate the extent to which the fuel may densify by performing a re-sintering test. Excessive shrinkage indicates that there is too much fine porosity.

5.3 Shaping

Diameter is the most significant shape parameter for the experimental pellets — this is dictated by experimental goals (eg, whether high burn-up is required quickly), rig neutronics considerations and the choice of cladding diameter and initial pellet-clad gap. Pellet dishing is seen as preferable since it provides a means of separating the effect of centerline thermal expansion from other causes of stack length elongation such as pellet swelling.

6. Experimental execution

Thor Energy commissioned a ‘pre-project’ from the Institutt for Energteknikk (IFE) — the Halden reactor operators — in order to survey the issues associated with executing a thorium-plutonium fuel irradiation experiment in their facility. This yielded much useful information at the rod and rig level.

6.1 Rig layout

Experimental arrangement options were presented based on an appropriate reactor rig. The fuel pins can be tested in a ‘double cluster’ of 12 pins, each of ~25cm active length; or in a ‘single cluster’ of 6 pins, each of ~50cm active length. Approximate power / burn-up histories were calculated for rigs comprising likely arrangements of thorium-plutonium, MOX and reference UOX fuels. This proved very useful in planning the fissile content for the test pellets.

6.2 Instrumentation

IFE have a strong record in instrumenting fuel pins with an impressive number of precision on-line measuring devices. The main instruments to select from for this experiment are for measuring: (i) rod internal pressure, (ii) centerline pellet temperature, (iii) fuel stack elongation, (iv) cladding elongation. The combination of these instruments for specific fuel pins is still to be finalised but most rods will be fitted with thermocouples and pressure transducers.

6.3 Rod design

Two simple, but very important parameters need to be defined at the stage when the fuel pellets are assembled into test rods. The first is the fill gas (typically helium at a pressure of several bar) which can be modified to include argon or xenon, thereby lowering the thermal conductivity of the pellet-clad gap. This means that the fuel pin will run ‘hotter’. Fill gas variation is thus a useful control option and is being considered as a means to derive information that will address the temperature ↔ FGR / swelling relation. The second rod parameter is that of the size of the pellet-clad gap. This should be selected within a ‘normal’ range for commercial fuel, but the choice within this range depends largely on experimental goals, ie, when pellet-clad gap closure is appropriate for achieving those goals. Thorium oxide is reported to expand and creep less than uranium oxide and thus a slightly narrower gap is indicated.

6.4 Discharge schedule

Post-irradiation examination of intermediate burnup thorium-plutonium fuel is a requirement in this experiment. Thus, the discharge of a thorium test pin at around 24 MW•d/kgHM is forseen (along with a MOX comparator pin), with this repeated at burnup levels of 35–40 MW•d/kgHM and 50–55 MW•d/kgHM. Pins from the lower cluster will exhibit an axially graded burnup due to the tapering flux profile they experience where they sit in the reactor core.

7. Conclusion

The irradiation experiment being planned and supported by *Thor Energy* will yield unique and valuable information in the form of internal data from operating thorium-plutonium fuel rods.

This experimental data will serve parallel efforts to build reliable fuel performance codes that are tailored for thorium-plutonium fuel. This is particularly important. A predictive capability for in-core fuel behaviour is an essential element in a safety analysis package for a new fuel. *Thor Energy* has already started working on adapting fuel performance codes to apply to thorium-plutonium fuels.

REFERENCES

[1] Research Council of Norway and the Ministry of Petroleum and Energy, Thorium as an energy source — opportunities for Norway, Final report of the Thorium Report Committee, Oslo, (2008), www.regjeringen.no/upload/OED/Rapporter/ThoriumReport2008.pdf.

[2] BELLE, J., BERMAN, R.M. Thorium dioxide: properties and nuclear applications, U.S. Department of Energy, DOE/NE–0060, (1984).

[3] VERVERFT, M., et al., Oxide fuels: microstructure and composition variations (OMICO), Final Report of the "OMICO Project" performed as part of the European Atomic Energy Community's Fifth Framework Programme (FP5), Contract FIKS–CT–2001–00141, (2007).

[4] KARAM, M., DIMAYUGA, F.C., MONTIN, J., ission gas release of (Th,Pu)O_2 CANDU fuel, Proceedings of the 10th CNS International Conference on CANDU Fuel, Ottawa, 2008. AECL Paper: CW–124950–CONF–002.

[5] BAKKER, K., et al., Critical evaluation of the thermal properties of ThO_2 and $Th_{1-y}U_yO_2$ and a survey of the literature data on $Th_{1-y}Pu_yO_2$, J.Nucl.Materials **250**, (1997), p. 1–12.

[6] ASTM Standard C833–2001, Standard specification for sintered (Uranium-Plutonium) dioxide pellets, ASTM International, West Conshohocken PA, (2001).

Current Status of the Development Project on Erbia Credit Super High Burnup Fuel

M. Yamasaki [1], H. Unesaki [2], A. Yamamoto [3], T. Takeda [4], M. Mori [5]

Abstract. In order to reduce the number of spent fuel assemblies and to improve fuel cycle economics, the development project on 'Erbia credit Super High-Burnup' (=Er-SHB) fuel with above 5 wt% uranium enrichment is in progress. The program covers wide aspect of the development of LWR fuel, in which low content of Erbia is fully distributed. In this paper, (1)outline of the concept of Er-SHB fuel, (2) measurement and analyses results of critical assembly experiment with fully Erbia loaded core, (3) 'Erbia COntent for Sub-criticality judgment (=ECOS) diagram' defined by a series of criticality safety analyses for typical geometries, are presented.

1. Introduction

An extended longer cycle operation and higher discharge burnup are believed to be effective to realize better economy of generation cost. However, it is known that as the cycle length becomes longer, as the batch averaged discharge burnup becomes lower. This means cycle length and discharge burnup is conflicting each other then there should exist the optimal point of generation cost in some condition. Actually in some papers focusing on this complex proposition, it is mentioned that the optimal discharge burnup will be around 60 to 70 GW•d/t and its corresponding enrichment should be above 5 wt% in PWR [1–2].

However, the value of '5 wt%' is a current criticality safety restriction in front-end of fuel cycle stream, such as fabrication, transportation, storage and so on. Therefore, straightforward approach of higher enrichment fuel requires major modifications and re-licensing of these facilities, then that considerable cost may spoil the economic advantage of the higher enrichment fuels. In a past session of American Nuclear Society (ANS) in 1998, sponsored by Nuclear Criticality Safety Division (NCSD), this challenge were named as "the 5wt% Barrier: Nuclear Criticality Safety in the Production of Extended-Burnup Fuel" [3–4].

The components of "the 5 wt% enrichment Barrier" can be summarized as follows;

– Lack of critical experiments at the range of 5 to 10 wt% enrichment, which makes difficult to validate a criticality safety analysis code in licensing process.

– The impact on the plant safety of the fact that a criticality accident can occur above 5 wt%. In the light of this fact, the Japanese Authority's guideline requests that the venders should address the detection equipments and the termination measures against a criticality accident when they use above 5 wt% UO_2 powder [5].

– The impact of reduced subcritical limits, which induces a reduction of the amount of treated UO_2 fuel. This means the efficiency, such as transport, fabrication, storage and so on, should be decreased as well.

To solve these issues, the development program on Erbia credit Super High Burnup (=Er-SHB) Fuel has been launched by the authors since 2005[6– 9]. The detail of Er-SHB fuel is described in later

[1] Nuclear Fuel Industries, Ltd., 950–1 Asashiro-Nishi, Kumatori-cho, Sennan-gun, Osaka, Japan.
[2] Kyoto University, 2–1010 Asashiro-Nishi, Kumatori-cho, Sennan-gun, Osaka, Japan.
[3] Nagoya University Furo-cho, Chikusa-ku, Nagoya, Japan.
[4] Fukui University, 3– 9– 1 Bunkyo, Fukui-shi, Fukui, Japan.
[5] Nuclear Engineering, Ltd., 1–3–7 Tosabori, Nishi-ku, Osaka, Japan.

section, but its basic concept represents adding low content (>0.2 wt%) of Erbia in all UO_2 powder, so that a reactivity of high enrichment (>5 wt%) fuel should be suppressed under that of current fuel assemblies, i.e. below 5 wt% enrichment. Since Erbia is mixed into UO_2 powder at the time after a re-conversion process, the advantage of negative reactivity credit of Erbia can be taken in the most criticality safety issues appearing after the re-conversion process.

Although Erbia is one of the major burnable absorber used in LWRs and has rich experience, the concept of Er-SHB fuel is completely different from the conventional Erbia fuel. Currently, Erbia is used to control in-core power distribution and to suppress excess reactivity, and loaded in some portion of fuel rods in an assembly. Contrary to this on the Er-SHB fuels, Erbia is added in all the fuel rods to meet the criticality safety requirements.

The development program for the Er-SHB fuel covers wide aspect of the development of fully Erbia distributed fuel, as follows;

1) Critical experiments of Erbia core at the range of ^{235}U enrichment is 5 to 10 wt%

2) Development of an uncertainty reduction technique for neutronics parameters

3) Criticality safety analysis using Erbia credit

4) Fabrication test and physicochemical properties measurement of Erbia-bearing fuel pellet

5) Core design using the Er-SHB fuel assemblies

6) Applicability of burnup credit for the Er-SHB fuels

7) Effect on the back-end stream such as disposal of high-level radioactive waste (HLW), etc.

The five organizations who are involved in this development project are NFI, Osaka University, Nagoya University, Kyoto University and NEL. NFI is taking a role of project manager. This project is subsidized by the Innovative and Viable Nuclear Energy Technology (IVNET) development framework of Ministry of Economy, Trade and Industry (METI). Since FY2008, some part of this project is merged into Japanese National Project named ‘the Development Project on Next Generation Light Water Reactor’ that is also supported by METI. The original part of the project, which is described in this paper, is still conducted by above five organizations.

In this paper, (1) outline of the concept of Er-SHB fuel, (2) measurement and analyses results of critical experiment with fully Erbia loaded core, (3) ‘**E**rbia **CO**ntent for **S**ub-criticality judgment (=ECOS) diagram’ defined by a series of criticality safety analyses for typical geometries, are presented.

2. Concept of Er-SHB fuel

Criticality safety is one of the major concerns of an extended high burnup fuel whose ^{235}U enrichment is above 5 wt%. Currently, the limitation of 5 wt% enrichment is used throughout the front-end stream of LWR fuels. In the Er-SHB fuel, Erbia is mixed into UO_2 powder just after the re-conversion process. Since Erbia is a neutron absorber, reactivity of UO_2 can be suppressed. By properly adjusting the content of Erbia, reactivity of Erbia-mixture fuel can be lower than that of current fuels whose enrichment is 5 wt%. Such Erbia-mixed fuel can be handled in similar way with the current fuels. In other words, by adding Erbia as burnable absorber, higher enrichment fuel (>5 wt%) can be handled by conventional equipments in the front-end stream. Such simplification of fabrication process will contribute to reduce fuel costs. There are another neutron absorbers commonly used in LWR than Erbia, e.g., boron and gadolinia, those are more familiar because of rich experiences in LWR fuels. However, these materials are difficult to be used as the present concept because of following reasons;

– Absorption cross section of gadolinia is much larger than that of Erbia, as shown in Figure 1. Therefore, in the case where gadolinia is mixed into all the fuels as burnable absorber, reactivity hold-down by gadolinia at BOL becomes too large as shown in Figure 2. The cores loaded with such fuels would be difficult to control the core reactivity. (Remember that the poison is mixed into all UO_2 powder in the fuel)

– Furthermore, gadolinia burns out too rapidly due to its 'blackness' hence reactivity change during burnup becomes extremely quick and large. Such rapid variation of reactivity makes in-core power peaking to be too steep.

– On the contrary, since absorption cross section of Erbia is smaller than that of Gadolinia, initial reactivity of Erbia-bearing fuel becomes appropriate. The moderate burnup behavior gives appropriate design window for reload core analyses (Figure2).

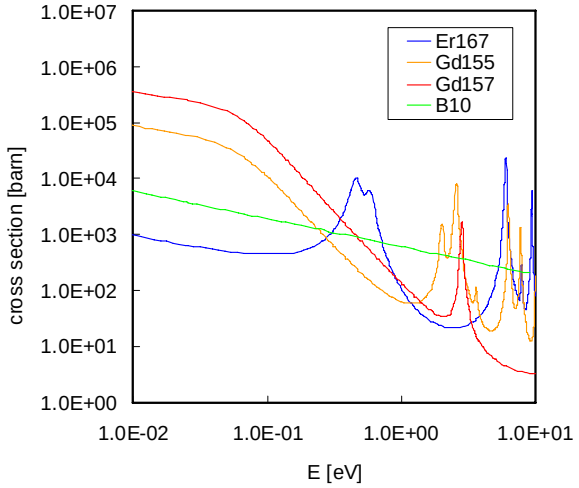

FIG. 1. Cross sections of various burnable absorbers.

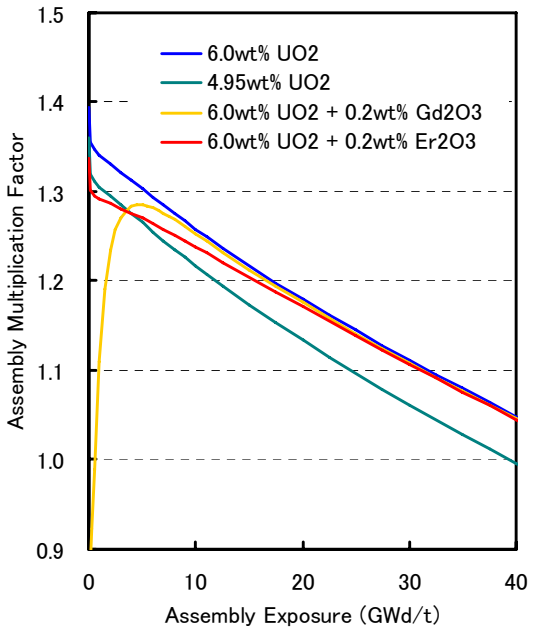

FIG. 2. Multiplication factor versus burnup for various PWR fuels.

3. Critical experiments in KUCA

Erbia has rich experience as burnable absorber in LWR. From this point of view, neutronics property can be adequately predicted in LWR core conFigurations. However, the major objective of adding Erbia into all UO_2 powder is countermeasure of criticality safety issues. In the criticality safety analysis, many conFigurations with various moderator conditions should be analyzed. Furthermore, Erbia will be used with higher enrichment (>5 wt%) fuels, which is not commonly used in LWRs. Therefore, new critical experiments that can provide appropriate verification data are highly desirable.

In the conventional critical facility with pin-types, Er bearing fuel pellets should be prepared in advance to critical experiments. Therefore, content of Erbia is fixed to specific values and difficult to change. Furthermore, in order to change neutron spectrum, i.e. moderation ratio ($H/^{235}U$), different lattice pitch, insertion of water displacement micro-rods and/or different moderator materials should be used. Since such experiments would require considerable efforts, systematic investigation on Erbia content and neutron spectrum variation would be restricted.

These experimental data are so valuable to validate neutronic analysis codes, those are used for criticality safety analysis of Er-SHB fuel.

3.1 General description on KUCA

Kyoto University Critical Assembly (KUCA) has a solid moderated plate type fuel cores. A schematic view of the core is shown in Figure 3.

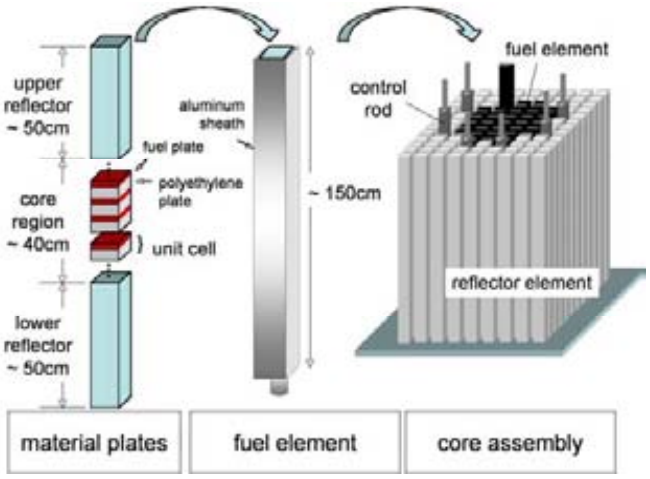

FIG. 3. A schematic view of solid moderated core.

As the fuel plate in KUCA, 1/16 inch (1.6 mm) thickness high enriched (93 wt%) U-Al alloy (EU) and 1mm thickness natural uranium metal (NU) are used. Both of them have 2 inches (50.8 mm) square shape in radial direction. For moderator material, polyethylene and graphite plate of various thicknesses are used. Adjusting a combination of fuel and moderator plates, various fuel enrichments and moderation ratio can be simulated. Adding those plates, in order to perform critical experiments with massive loading of Erbia, one thousand pieces of thin Erbia coated graphite plates are prepared. Figure 4 shows the Erbia-coated graphite plate which consists of graphite plate (50.8 mm×50.8 mm×1.5 mm) with 0.2 mm depth engraved surface where Erbia is coated with 30 micro meter thickness. The amount of Erbia per plate is approximately 0.3 g. In order to perform critical experiments with massive loading of Erbia, one thousand pieces of the Erbia coated graphite plates are prepared.

FIG. 4. Erbia-coated graphite plate.

The first fully Erbia-loaded core (refer as core-1 in this paper) has achieved critical in December 2006. Following the first experiment, another two criticality experiments have conducted from December 2007 to January 2008. Average enrichment of core-1 is 5.4 wt% and average content of Erbia is 0.3 wt%. Average enrichment of another two criticality experiments in KUCA (refer to them as core-2 and core-3) are 5.4 wt% and 9.6 wt%, and average content of Erbia are 0.3 wt% and 0.6 wt%, respectively. Following those experiments, the forth core (refer to this core as core-4), had achieved critical in December 2008. This core is aimed to contain rather high content of Erbia into whole core. The realized Erbia content is 1.12 wt% and an average enrichment of core-4 is 9.6 wt%, same as core-3. The core properties of above four cores are summarized in Table 1.

Cell structures of each core and core conFigurations of the fuel elements are shown in Figure 5 and Figure 6 respectively. Neutron spectrum of those cores, which is obtained by cell calculation using SRAC code [10] are shown in Figure 7.

As described in Table 1, the series of these experiments appropriately cover the features of Er-SHB fuel such as;

– At the range of uranium enrichment is above 5 wt% from 5 to 10 wt%

– Erbia is fully loaded into the whole core of which content is rather low compare to conventional Erbia fuel (0.3 to 1.12 wt%)

– A moderator ratio varies from 48 to 274, which represents various neutron spectra from hard to soft.

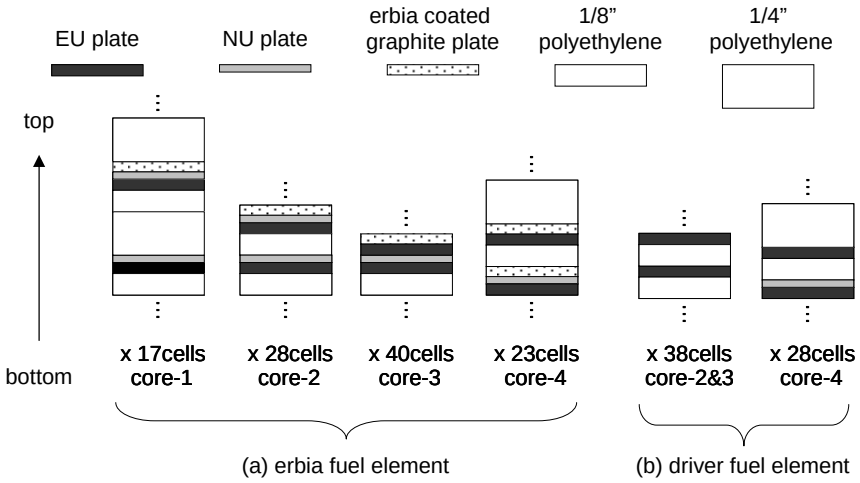

FIG. 5. Cell structure of fuel element.

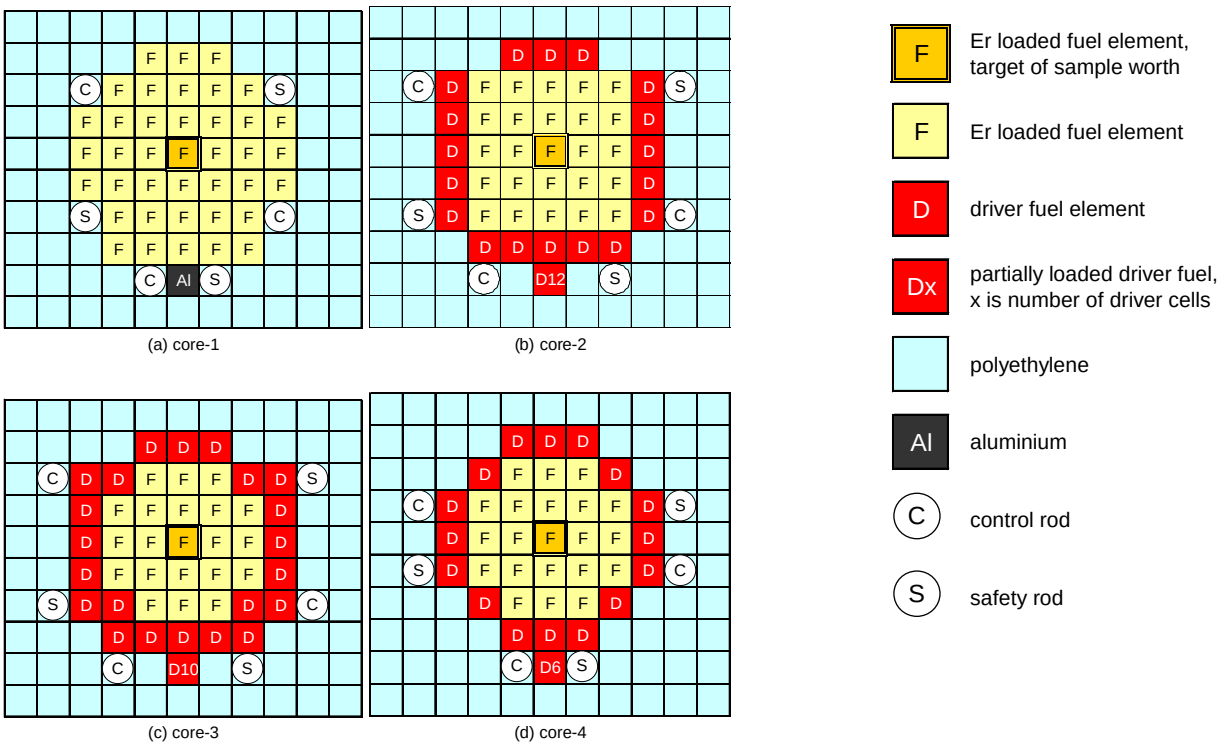

FIG. 6. Core configuration of fuel elements.

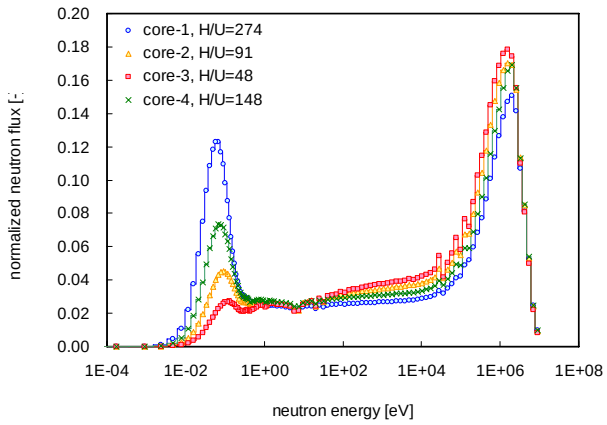

FIG. 7. Neutron spectrum of each core.

TABLE 1. COMPARISON OF CORE PARAMETERS

Case	Average enrichment	Er content*1	H/^{235}U	Outline
Core–1	5.4 wt%	0.3 wt%	274	Homogeneously Er loaded core Very soft spectrum
Core–2	5.4 wt%	0.3 wt%	91	Zone type core with driver Simulate PWR spectrum
Core–3	9.6 wt%	0.6 wt%	48	Zone type core with driver Harder spectrum
Core–4	9.6 wt%	1.12 wt%	148	Zone type core with driver Higher Er content

**1: Erbia / U-total.*

3.2 Experiment

3.2.1 Criticality

For each core, approach to criticality has been performed based on inverse multiplication method. The inverse multiplication curves versus the number of loaded fuel elements were calculated prior to the experiments using the continuous energy Monte Carlo code MVP [11]. The pre-calculated curves shows in excellent agreement with the actual measurements. The detailed reactivity is adjusted by control rod. After achieving criticality, all control rods are withdrawn then the excess reactivity of each core is measured by using the period method. In the period method, the effective delayed neutron fraction and prompt neutron life time have been evaluated by the deterministic code SRAC.

3.2.2 Erbia sample worth

Erbia sample worth is defined as reactivity induced by replacing a Erbia plate with a graphite plate. The measurement of Erbia sample worths has been carried out in this series of experiments. This measurement is aimed at providing the database for confirmation of erbium cross section and improvement of prediction uncertainties of Er-SHB PWR core characteristics using the generalized bias factor method. In the experiment, the Erbia-coated graphite plates loaded in the central fuel element (See Figure 6) are replaced by the graphite plates one by one. This replacement has been made axially from the middle height of the fuel element then expanding to top and bottom direction symmetrically; the number of Erbia-coated graphite plates is increased in several steps until all the plates in the central fuel element were replaced. The Erbia sample worth was measured as reactivity difference caused by the replacement. The reproductivity of the Erbia sample worth measurement, defined as the relative standard deviation for several measurements, is estimated to be less than 3% for most cases.

3.3 Analysis

3.3.1 Criticality

Analyses of criticality have been performed by using the energy Monte Carlo code MVP. The core geometries and material compositions were treated rigorously as file as possible. The nuclear data libraries used in the MVP analyses are JENDL-3.3, ENDF/B-VI.8, JEFF-3.0, ENDF/B-VII.0 and JEFF-3.1. Neutron multiplication factor, k_{eff}, for each core is evaluated from statistical results of total 50 000 000 (= 50 millions) histories, i.e., 50 000 histories/ batch × (1 050 total batches − 50 skipped batches).

Figure 8 shows the comparison of C/E values of k_{eff} for different nuclear data libraries. Here, the error bars represent the 3σ statistical errors of Monte Carlo calculations. For all cases, the C/E values of k_{eff} are predicted within 0.998− 1.004 and the maximum differences among libraries are approximately 0.003, thus the prediction accuracy of criticality for Erbia loaded core is validated. As shown in Figure 8, there are some notable trends among the libraries, e.g., JEFF-3.1 and especially ENDF/B-VII.0 tend to overestimate k_{eff}, and contrary ENDF/B-VI.8 tends to underestimate compared with another libraries. It is supposed that the significant differences between ENDF/B-VI.8 and ENDF/B-VII.0 results are mainly caused from difference in ^{238}U capture cross section.

3.3.2 Erbia sample worth

In order for analyses of Erbia sample worth, firstly the Monte Carlo code MVP was intended to use. Shown in Figure 7 as an example, the results of MVP agree with experiment within statistical errors of Monte Carlo calculations. However, because the absolute value of the Erbia sample worth is too small, the statistical errors are comparable large to quantitatively investigate the differences among nuclear data libraries.

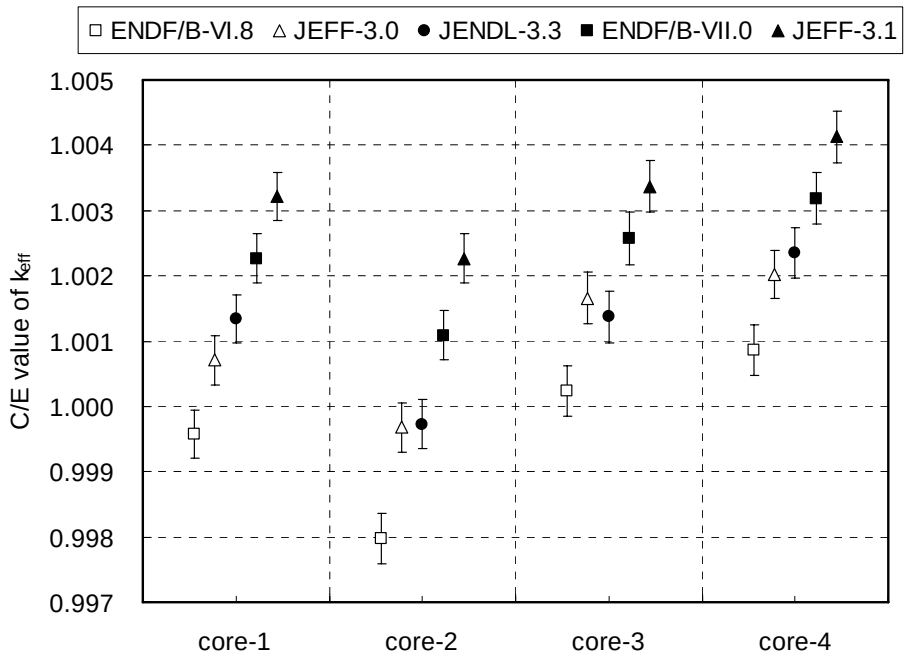

FIG. 8. Numerical results of k_{eff} by Monte Carlo code MVP.

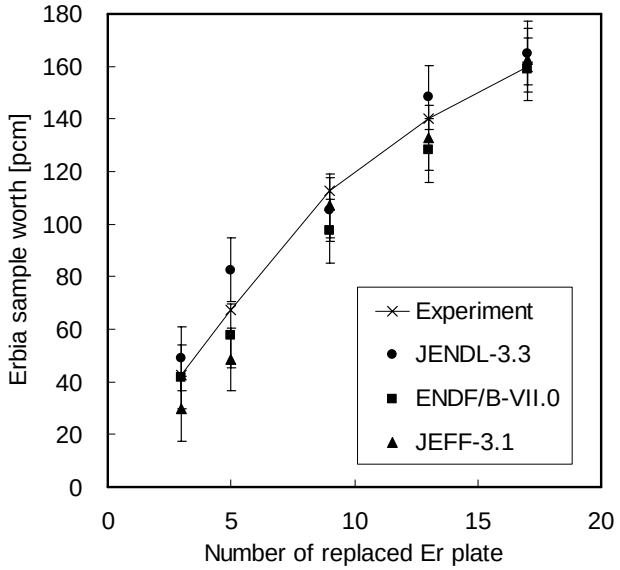

FIG. 9. Numerical results of Erbia sample worth by Monte Carlo code MVP (core-1).

Therefore, analyses of Erbia sample worth have been performed by using the deterministic code SRAC. The numerical results are evaluated by perturbation theory using 3-D XYZ diffusion calculation with 30 energy groups. Same as the criticality analyses, several nuclear data libraries were used for analyses. Numerical results of Erbia sample worth by 3-D XYZ diffusion calculation are summarized in Figure 10. Taking into account that the experimental accuracy for Erbia sample worth, which is approximately 3%, it could be concluded that the agreement between calculation and measurement of Erbia sample worths are reasonable. However, it is noted that there are downward trends of the C/E values for all core conFiguration as the number of replaced Er plate are increased. There seems to be some considerations for the treatment of heterogeneous effects in the fuel elements should needed, then further study will be performed to re-evaluate the C/E values.

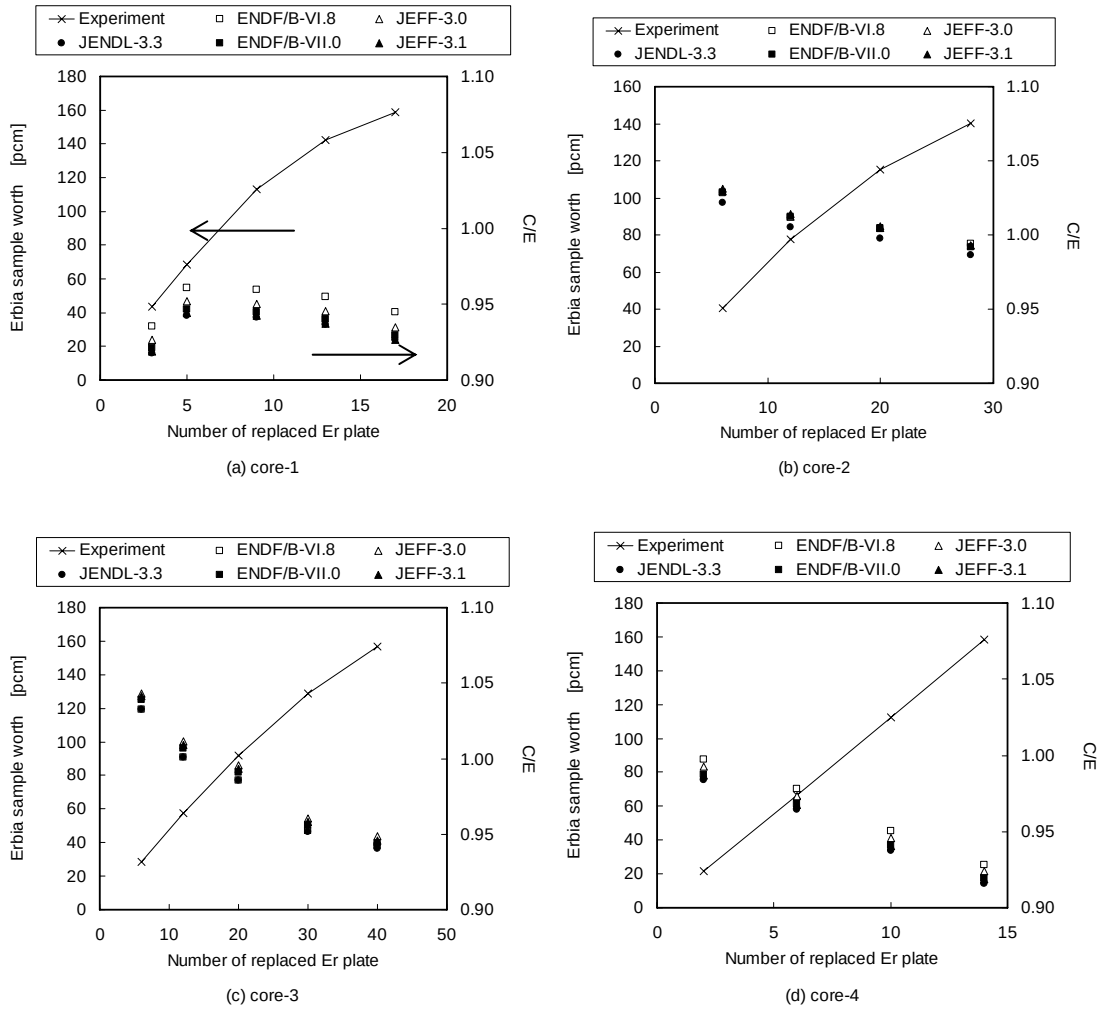

FIG. 10. Numerical results of Erbia sample worth by 3-D XYZ diffusion calculation.

4. Criticality safety analysis

In this section, from the viewpoint of criticality safety for fabrication facilities, the sufficient of Erbia content for Er-SHB fuel is evaluated. The contents of Erbia is determined in order to secure the same criticality safety level as the conventional fuels whose enrichment is 5 wt% or lower.

Three kinds of condition are evaluated. The first one is simple geometric shapes, the second one is a large sphere with moisture control and the third one is fuel assemblies in storage rack.

4.1 Calculation method and validation data

In criticality safety analysis for fabrication plant, KENO V.a and 44-group library equipped in SCALE5 [12] code system are used for calculate neutron multiplication factor (k_{eff}) and criticality safety data, because SCALE5 has a lot of experiences for such analyses purpose.

As a first step, the validity of our analysis scheme is checked by comparison with well-known results, whose enrichment is 5 wt% or lower and whose geometry is simple shapes such as sphere, cylinder and slab without neutron absorber. As a typical case, the result of the sphere UO_2 volume on corresponding to the lower limit of k_{eff} is shown in Figure 11. The calculated results for simple shapes agree with the reference [13] as shown in Figure 11. From these results, it is confirmed the validity of our analysis code and scheme.

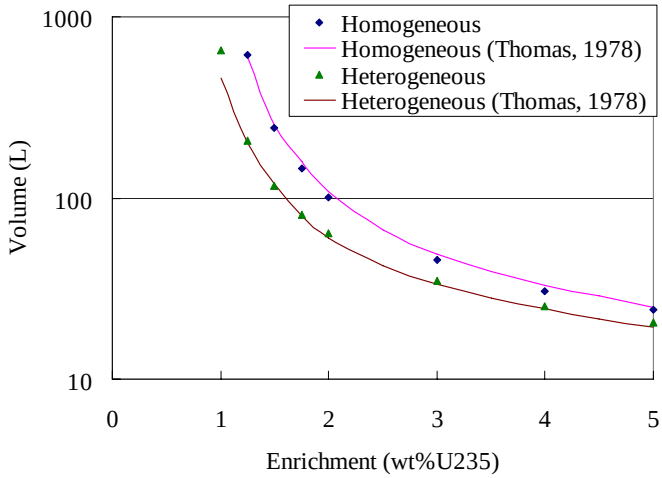

FIG. 11. Volume of UO_2 sphere of the lower limit.

Because of a shortage of benchmark data of criticality experiment with Erbia, criticality experiments are conducted in KUCA, as described in section 3. The criticality analyses for KUCA are performed by using a continuous energy Monte Carlo code MVP because in SCALE library, only two isotopes of Erbia (^{166}Er and ^{167}Er), which have large absorption cross section, are considered. However, considering the consistency and experience with current criticality safety analysis for fuel facilities, the SCALE system is used in this section.

In comparison with the measured data and the calculation results by MVP, k_{eff} bias with Erbia for each library is consistent with that of without Erbia. Because the negative reactivity caused by Erbia is mainly by ^{166}Er and ^{167}Er, the impact of neglecting the other isotopes such as ^{168}Er or ^{170}Er are also negligible for k_{eff} evaluation. Therefore, it is expected the criticality analysis on Erbia by SCALE will comparable to that by MVP. In order to assure this, series of criticality analyses for KUCA experiments by SCALE are undergoing, now.

In the calculations of k_{eff} for enrichment of 5 wt% or lower without Erbia, criticality parameters are optimized so that the reactivity becomes maximal under criticality safety control of each geometry. As a same manner, in evaluation of Erbia content for enrichment higher than 5 wt%, criticality parameters are similarly optimized under the same criticality safety control, and the Erbia content is determined so that the k_{eff} is equivalent to the ones for enrichment of 5 wt% without Erbia. Therefore, by adding the obtained Erbia content, criticality safety is secured in the equivalent criticality safety control.

4.2 Calculated geometories

4.2.1 Simple shapes

Simple shapes such as sphere, cylinder and slab, for sub-criticality condition are very important data, that are often used for the purpose of the criticality safety control. In this section, it is considered the simple geometric shapes that are surrounded by water reflector. Each homogeneous mixture of UO_2 and water, and heterogeneous UO_2 and water are respectively considered as fuel material. In this paper, the result of sphere is representatively described, because others show a almost similar behaviour.

The dimension of geometry (radius, thickness, and so on) is a criticality safety control factor, and determined so that the k_{eff} equal to the lower limit of subcriticality (= 0.98). Other parameters concerning neutron moderation are optimized. In these manners, 1) the ratio of UO_2 to water in the homogeneous case, and 2) the radius and the pitch of pellet in the heterogeneous case, are changed in a

physically possible range. As a result of homogeneous sphere, the radius of 5 wt% enrichment is 18 cm.

4.2.2 Large sphere with moisture control

By restricting the moisture condition as a criticality safety control factor, the amount of fuel in a facility has increased in comparison with simple shapes. Here, we consider a homogeneous sphere made of UO_2 and water surrounded with water reflector. The range of parameters is determined to cover the practical condition as follows.

- Moisture: H/U (number density ratio) ≤ 1
- Powder density: $UO_2 \leq 3.5$ g/cm^3
- Volume of sphere: 800 L (Radius: ~ 58 cm)

The k_{eff} of this large sphere of 5 wt% enrichment is calculated to be 0.874. Therefore, the Erbia content for the large sphere whose enrichment is above 5 wt% is determined so that the k_{eff} becomes 0.874, while changing the parameters of H/U and powder density in the above mentioned ranges. The results will be shown in the section 4.3.

4.2.3 Fuel assemblies in storage rack

In order to reduce the neutron interaction between each assemblies, structural material with neutron absorber (here, borated SUS) is constructed around the fuel assembly. A practical fuel assembly storage rack could be variously designed in order to satisfy the limitation of k_{eff} which depends on the structural material, dimensions (ex.: rack pitch, thickness, distance between assembly and absorber), placement, type of fuel assembly, number of array, and so on.

Here, the calculated geometry of the fuel assembly storage rack is modelled to be simplified as shown in Figure 12. The fuel assembly is conventional 17×17 type PWR fuel assembly, but its enrichment is set to 5 wt% (the current upper limit) and pellet density is set to 100%TD. The structure of fuel assembly except the fuel rod (grid, nozzle, and so on) is not considered. The fuel assembly storage rack is an infinite array in horizontal direction, and water reflector is assumed at the top and bottom in vertical direction. In order to consider the optimal neutron moderation in the calculations, the storage rack is assumed fully flooded with water and the water density is changed uniformly from 0% to 100%.

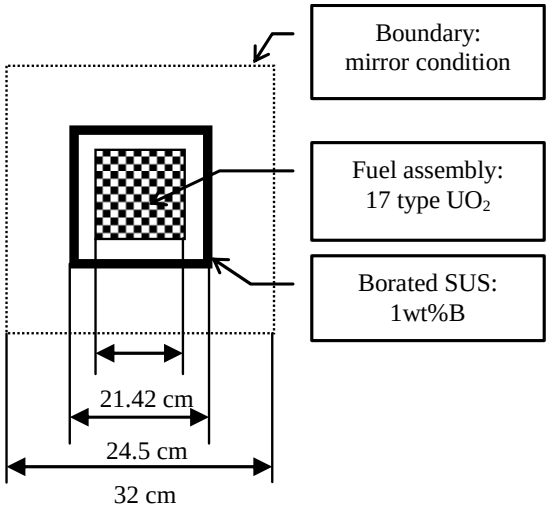

FIG. 12. Horizontal geometry of fuel assembly storage rack.

The k_{eff} of this fuel assembly storage rack of 5 wt% enrichment is calculated to be 0.937. Therefore, the Erbia content for the fuel assembly storage rack whose enrichment is above 5 wt% is determined so that the k_{eff} becomes 0.937, while changing water density. Other parameters except enrichment and Erbia content (geometry, structural materials, and so on) are fixed.

4.3 Results of Erbia content

4.3.1 Simple shapes

The result of Erbia content for homogeneous sphere is representatively shown in Table 2. As shown in Table 2, the Erbia content of simple shapes increases linearly with increase of enrichment.

Homogeneous and heterogeneous simple shapes (sphere, cylinder and slab) are summarized as follows.

- Erbia contents of the homogenous cases are greater than that of heterogeneous cases, where the neutron spectra of the homogeneous cases are consistently slightly harder than that of the heterogeneous cases.

- Erbia contents are almost the same among the homogeneous simple shapes.

- The ratio of $H/^{235}U$ for the optimal moderation condition increase linearly with increase of enrichment of ^{235}U.

Therefore, the simplification to use the result of the homogeneous sphere for all simple shapes is conservative in the viewpoint of criticality safety.

Table 2. Calculated result for homogeneous sphere

Enrichment (wt%)	Erbia content (wt%)	Powder density (g/cm^3)	$H/^{235}U$
5	0.00	2.22	118
6	0.28	1.69	150
7	0.58	1.64	175
8	0.89	1.47	204
9	1.19	1.32	233
10	1.15	1.16	263

4.3.2 Large sphere with moisture control

As the result of Erbia content for large sphere with moisture control, calculated result of k_{eff} for enrichment of 5 wt% and powder density in the practical parameter ranges is shown in Figure 13, at first. As shown in Figure 13, k_{eff} of this geometry increases monotonously with increase of H/U.

In cases with enrichment of above 5 wt%, k_{eff} increases with change of the parameters similarly. The calculated result of k_{eff} for enrichment of above 5 wt% in case of powder density of 3.5 g/cm^3 without Erbia is shown in Figure 14. The Erbia content to secure the equivalent criticality for enrichment of 5 wt% is shown in Figure 15. The Erbia content shows similar behaviour of k_{eff} and it becomes maximal at the maximal points in the parameter ranges.

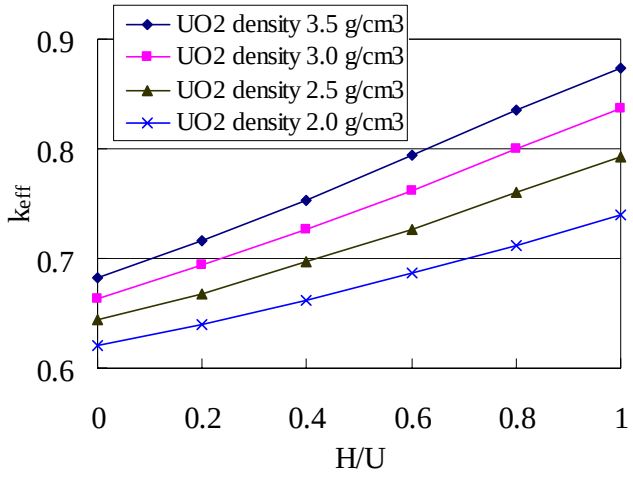

FIG. 13. Calculated results of k_{eff} for the large sphere with moisture control (enrichment 5 wt%).

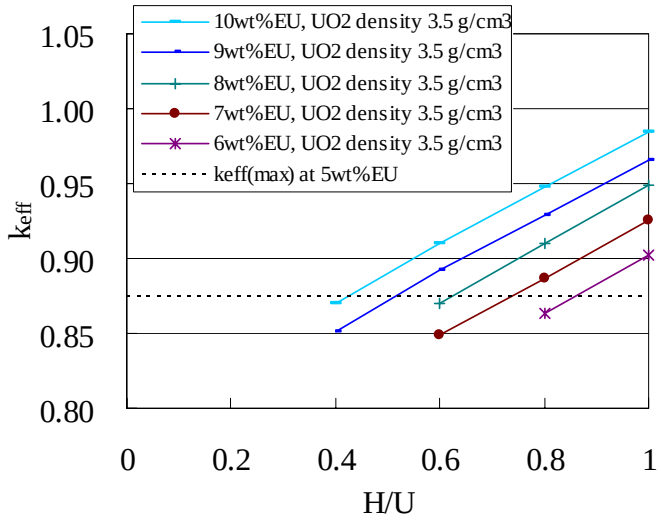

FIG. 14. Calculated results of k_{eff} for the large sphere with moisture control (enrichment higher than 5 wt%).

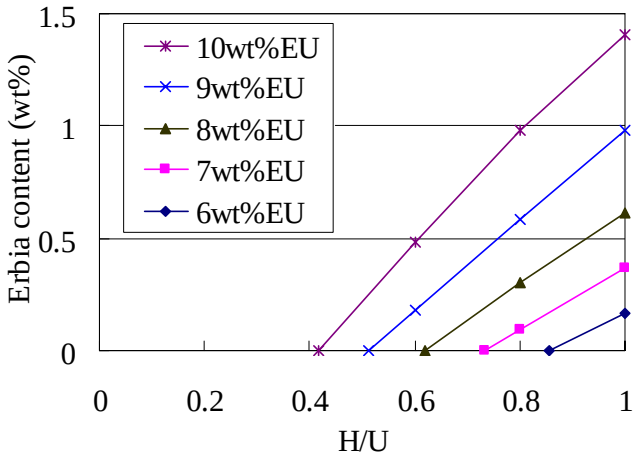

FIG. 15. Calculated results of Erbia content for the large sphere with moisture control.

4.3.3 Fuel assemblies in storage rack

The results of fuel assemblies in storage rack, whose enrichment is from 5 wt% to 10 wt% and without Erbia, is shown in Figure 16. Seeing in Figure 16, there is a hump of k_{eff} in the condition of low water density. In Table 3, the maximum value of k_{eff} and its water density, and k_{eff} at the fully flooded condition are shown. As shown in Figure 16 and Table 3, the point of water density that gives the maximum of k_{eff} jumps from 100% to 12% with the increase of enrichment from 5 wt% to 6 wt%, and it decreases slightly with increase of enrichment from 6 wt% to 10 wt%. Namely, the increasing change of k_{eff} at the lower water density is greater than that at the fully flooded condition.

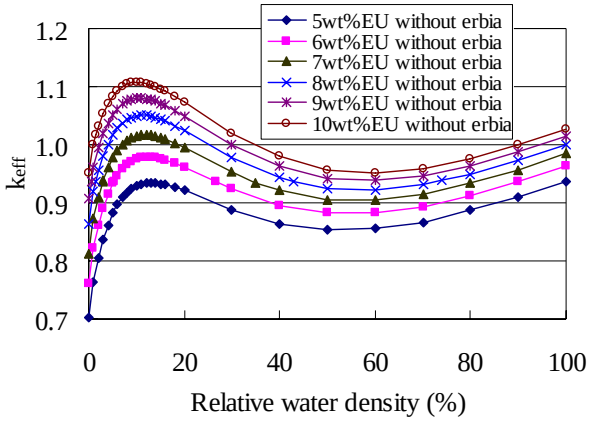

FIG. 16. Calculated results of k_{eff} for the fuel assembly storage rack without Erbia.

TABLE 3. CALCULATED RESULTS FOR THE FUEL ASSEMBLY STORAGE RACK WITHOUT ERBIA

Enrichment (wt%)	5	6	7	8	9	10
Maximal k_{eff}	0.937	0.979	1.017	1.051	1.080	1.108
Water (%)	100	12	12	11	11	10
k_{eff} at 100%	0.937	0.964	0.985	1.001	1.015	1.026

The hump of k_{eff} at low water density is observed in some case of repeated geometry where the neutron interaction between the units becomes large in the hard spectral condition. Figure 16 indicates that the maximal k_{eff} for above 5 wt% enrichment might appear at low water density, even in the case that a fuel assembly storage rack is designed so that the maximal k_{eff} for 5 wt% enrichment appears at the fully flooded condition.

The Erbia content of the fuel assembly storage rack to secure the equivalent criticality for enrichment of 5 wt% is shown in Figure 17.

As shown in Figure 17, the Erbia content of the fuel assemblies in storage rack also has a hump at a low water density. However, the point of water density that gives the maximum value of Erbia content is less than that of k_{eff} and the peak of the Erbia content is very steep. It is important to note that the reactivity worth of Er at low water density becomes small. It is found that the small reactivity of Er in the hard spectral condition makes its content very high in order to retain the large k_{eff} of above 5 wt% enrichment fuel at low water density.

Beware of the large amount of Erbia content at the low water density that induces the more neutron interaction, when the Erbia credit is introduced into a facility with repeated geometry.

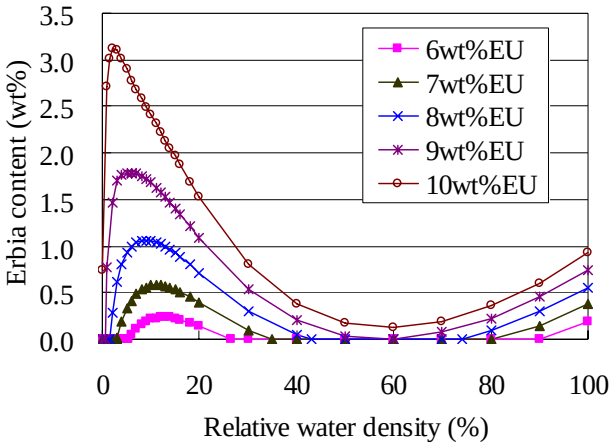

FIG. 17. Calculated results of Erbia content of the fuel assembly storage rack.

4.4 ECOS diagram

Based on the above mentioned results, the Erbia content versus uranium enrichment is shown in Figure 18. This Figure has been named ECOS (**E**rbia **CO**ntent for **S**ub-criticality judgment) diagram. The area above the curves shown in the ECOS diagram is judged to be sub-critical.

As shown in Figure 18, the rapid increase of required Erbia content for fuel assembly storage rack is caused by the repeated geometry in the hard spectral condition as mentioned in the previous section.

Refer to the feasibility study by the authors on the Er-SHB fuel loaded PWR core, the Er-SHB fuel is designed as around 6 wt% enrichment and Erbia content is 0.4 wt% [10]. It can be seen that the required Erbia content is around 0.3 wt% for uranium enrichment is 6 wt%. Therefore, the fuel design mentioned above (6 wt% enrichment with 0.4 wt% Erbia) can be judged as secure sub-critical.

Although the evaluated facilities are selected and modelled in sufficient consideration, it is desirable that all the facilities concerning Erbia credit should be evaluated in detail when it is introduced into a practical fuel cycle process.

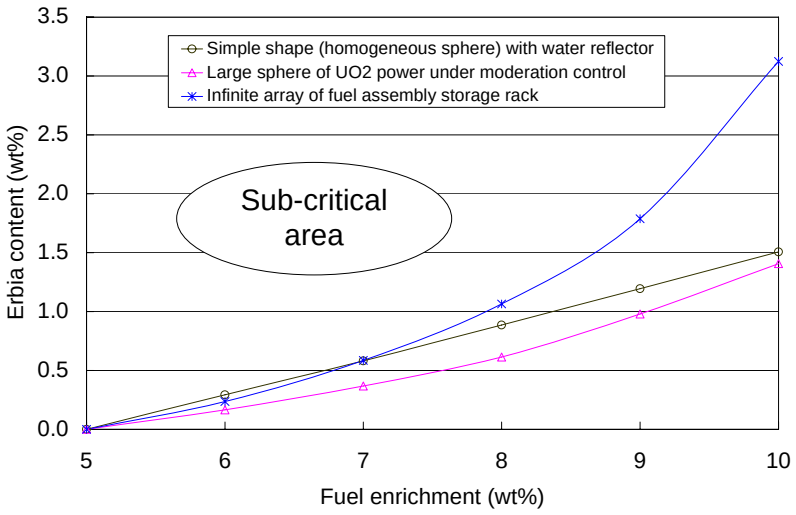

FIG. 18. Erbia content for sub-criticality judgment (ECOS) diagram.

5. Conclusions

In order to reduce the number of spent fuel assemblies and then to improve fuel cycle economics, the development project on Er-SHB fuel with high uranium enrichment is in progress. The program covers wide aspect of the development of LWR fuel such as critical experiments, criticality safety analysis using Erbia credit, physicochemical properties measurement of Erbia-bearing fuel pellet, and so on.

As the first topics of this paper, the outline and main concept of Er-SHB fuel was described. This concept represents adding low content (>0.2 wt%) of Erbia in all UO_2 powder, so that a reactivity of high enrichment (>5 wt%) fuel should be suppressed under that of current fuel assemblies, i.e. below 5 wt% enrichment. Since Erbia is mixed into UO_2 powder at the time after a re-conversion process, the advantage of negative reactivity credit of Erbia can be taken in the most criticality safety issues appearing after the re-conversion process.

Secondly, the measurement and analysis results of a series of fully Er-loaded core experiments are presented. A series of these experiments are appropriately cover the features of Er-SHB fuel, such as the range of uranium enrichment of 5 to 10 wt%, fully Erbia loaded into the core of which content is rather low (below 1.12 wt%), a moderator ratio varies from 48 to 274, which can represent various neutron spectra from hard to soft. These experimental data will be so efficient to validate neutronic analysis codes, which are used for criticality safety analysis of Er-SHB fuel.

Thirdly, criticality safety analyses are performed with introducing the concept of the Erbia credit. Based on the comprehensive criticality safety analyses for typical geometries, the Erbia content versus uranium enrichment is determined as the ECOS (**E**rbia **CO**ntent for **S**ub-criticality judgment) diagram. Er-SHB fuel is judged to secure sub-critical based on the ECOS diagram.

Consequently, the feasibility of Er-SHB fuel concept is confirmed from the nuclear physics point of view. Another development items, such as;

- Fabrication test and physicochemical properties measurement of Erbia-bearing fuel pellet
- Core design using the Er-SHB fuel assemblies
- Applicability of burnup credit for the Er-SHB fuels
- Effect on the back-end stream such as disposal of high-level radioactive waste (HLW)

are also investigated in the development program.

REFERENCES

[1] GREGG, R., WORRALL, A., Effect of highly enriched / highly burnt UO_2 fuels on nuclear design parameters and economics, Advances in Nuclear Fuel Management III (ANFM 2003), Hilyon Head Island, (2003), CD-ROM.

[2] SECKER, J.R., OZER, O., et al., Optimum discharge burnup and cycle length for PWRs, Advances in Nuclear Fuel Management III (ANFM 2003), Hilton Head Island, (2003), CD-ROM.

[3] DAMON, D.R., MOREY, D.C., Criticality safety limits at 5 to 20% enrichment, American Nuclear Society Annual Meeting, Nashville, (1998).

[4] PAULSON, L.E., PETERS, W.C., GE validation to support fuel fabrication up to 10% enrichment", American Nuclear Society Annual Meeting, Nashville, TN USA, (1998).

[5] NUCLEAR SAFETY COMMISSION, Regulatory guide on the specific uranium fuel fabrication facilities, (2000), in Japanese.

[6] TAKEDA, T., SANO, T., KITADA, T., KUROISHI, T., YAMASAKI, M., UNESAKI, H., A new uncertainty reduction method for PWR cores with Erbia bearing fuel, Proc. Int. Conf. on the Physics of Reactors, Nuclear Power: A Sustainable Resource, Interlaken, (2008), CD-ROM.

[7] UNESAKI, H., TOSHIKAZU, T., YAMAMOTO, A., MORI M., YAMASAKI, M., Integral experiment on Erbia-loaded thermal spectrum cores using Kyoto University Critical Assembly, Proc. Int. Conf. on the Physics of Reactors, Nuclear Power: A Sustainable Resource, Interlaken, (2008), CD-ROM.
[8] KUROISHI, T., YAMASAKI, M., Evaluation of Erbia content in Er-SHB fuel for criticality safety of fabrication facilities, Proc. Int. Conf. on the Physics of Reactors, Nuclear Power: A Sustainable Resource, Interlaken, Switzerland, (2008), CD-ROM.
[9] SUGIMURA, N., IMAMURA, M., MORI, M., YAMASAKI, M., Burnup credit of Erbia super-high-burnup fuel," Proc. Int. Conf. on the Physics of Reactors, Nuclear Power: A Sustainable Resource, Interlaken, (2008), CD-ROM.
[10] OKUMURA, K., KUGO, T., KANEKO, K., et al., SRAC2006 : a comprehensive neutronics calculation code system, JAEA-Data/Code 2007–004, (2007).
[11] NAGAYA, Y., OKUMURA, K., MORI, T., et al., MVP/GMVP Version 2: general purpose Monte Carlo codes for neutron and photon transport calculations based on continuous energy and multigroup methods, JEARI **1348**, (2005).
[12] BOWMAN, S. M., 2005. SCALE: A modular code system for performing standardized computer analyses for licensing evaluations, ORNL/TM-2005/39, Version 5, Vols. **I–III**, (2005). Available from Radiation Safety Information Computational Center at Oak Ridge National Laboratory as CCC-725.
[13] THOMAS J. T., Ed., 1978, Nuclear Safety Guide, TID-7016, Revision2, NUREG/CR-0095, ORNL/NUREG/CSD-6, Prepared for the U.S. Nuclear Regulatory Research Under Interagency Agreement DOC 40-550-75.

Minimization of Inner Diametric Tolerance of Annular Pellet for Dual Cooled Fuel[1]

Y.W. Rhee[2], D.J. Kim[3], J.H. Kim[4], J.H. Yang[5], K.S. Kim[6], K.W. Kang[7], K.W. Song[8]

Abstract. Fabrication methods of an annular pellet with highly precise diametric tolerances have been investigated. Three new approaches were applied in order to achieve a better diametric tolerance. First, we have tried to introduce a new compaction process which combined a usual double-act pressing and a cold isostatic pressing. Secondly, annular compacting mold with inclined inner and outer surfaces was designed by considering a difference in the diametric changes depending on the pellet height during sintering. Finally, a rigid rod inserted sintering process was applied in order to minimize a diametric tolerance. A green annular pellet was firstly compacted with a double-acting press and then sintered after a precisely-machined rigid rod was inserted. Sintered annular pellets which were fabricated by the above processes show better inner diametric tolerances without an inner surface grinding.

1. Introduction

A dual cooled annular fuel consists of internal and external cladding tubes in which annular pellets are stacked and cooling water flows in both internal and external coolant passages. In order to increase the power density of a Pressurized Water Reactor fuel assembly, a dual cooled annular fuel has been seriously considered as a favorable option. A conFigurationally inherent merit of an annular fuel such as an increased heat transfer area and a thin pellet thickness results in a lot of advantages from the point of a fuel safety and its economy [1].

There must be a lot of considerations in the various fields to introduce an internally and externally dual cooled annular fuel to commercial PWR reactors. One of the most important issues is a heat flux split toward an internal cladding and an external cladding due to the gap conductance asymmetry which results from a preferential expansion of a fuel pellet toward the outside during an irradiation [2, 3]. Gap conductance is directly related to the inner and outer gap thicknesses. Initial gap thicknesses can vary with a pellet's dimensions which are affected by a reactor operation condition. Recently, it is suggested that a fuel rod with a smaller inner gap and a larger outer gap can reduce this gap conductance asymmetry [3]. This approach can be effective only after a fabrication technology with precise tolerance is achieved.

Annular pellet with precisely controlled diametric tolerance is an essential element to actualize the dual cooled fuel. From the viewpoint of the fuel pellet fabrication, however, the unique shape of annular fuel pellet causes challenging difficulties to satisfy a diametric tolerance specification. Because of an inhomogeneous green density distribution along the compact height, an hour-glassing usually occurred in a sintered cylindrical PWR fuel pellet fabricated by a conventional double-acting press [4]. Thus, a sintered pellet usually undergoes a centerless grinding process in order to secure a pellet's specifications. In the case of an annular pellet fabrication using a conventional double-acting press, the same hour-glass shape would probably occur. The outer diameter tolerance of an annular pellet can be controlled easily similar to that of a conventional cylindrical PWR pellet through a

[1] This has been carried out under the Nuclear R&D Program supported by the Ministry of Education, Science and Technology, Republic of Korea.
[2] Korea Atomic Energy Research Institute, Daejeon, Republic of Korea.
[3] Korea Atomic Energy Research Institute, Daejeon, Republic of Korea.
[4] Korea Atomic Energy Research Institute, Daejeon, Republic of Korea.
[5] Korea Atomic Energy Research Institute, Daejeon, Republic of Korea.
[6] Korea Atomic Energy Research Institute, Daejeon, Republic of Korea.
[7] Korea Atomic Energy Research Institute, Daejeon, Republic of Korea.
[8] Korea Atomic Energy Research Institute, Daejeon, Republic of Korea.

centerless grinding. However, it appears not to be simple in the case of an inner surface grinding. It would be the best way to satisfy the specifications for the inner diameter in an as-fabricated pellet.

This paper reviews three approaches that we are trying to find a way to minimize the diametric tolerance of the sintered annular pellet. We focused on the tolerance of the inner diameter in as-sintered annular pellet without surface grinding.

2. Experimental procedure

2.1 Uni-axial double act pressing and cold isostatic pressing

Annular fuel pellets were prepared by the Integrated Dry Route (IDR) UO_2 powder. The powder was pre-compacted under 10 MPa by using a cold isostatic press. A pre-compacted lump of UO_2 powder was crushed and granulated with 20 mesh sieves. The granules were mixed with a 0.3 wt% of zinc stearate in a tumbling mixer for 30 min.

The compaction was conducted in a double acting press by using an annular shaped mold with 12.31 mm in the inner diameter and 17.85 mm in the outer diameter, respectively. Some of those compacts were pressed again in a cold isostatic press (CIP) under 300 MPa with a stainless steel rod inserted. The green densities were varied from about 54%TD to about 56%TD after CIP. Dimensional changes of the annular compacts after a cold isostatic pressing were measured by using a 3-dimensional measuring system (VERTEX 230, MicroVu). The compact is about 11 mm in height and about 18 mm and 12.4 mm in outer and inner diameter, respectively.

The compacts were sintered at the 1730 °C for 4 h in H_2 atmosphere. The heating and cooling was at a rate of 5 K/min.

2.2 Uni-axial single act pressing with the inclined mold

ADU route UO_2 powder was used for a sample preparation. The powder was pre-compacted under 70 MPa by using a cold isostatic press. Pre-compacted lump of UO_2 powder was crushed and granulated with 20 mesh sieve. The granules were mixed with a 0.3 wt% of zinc stearate in a tumbling mixer for 30 min. The compaction was conducted in a single acting press by using two types of annular molds. One is an ordinary annular mold with straight inner and outer surfaces and the other is a newly designed annular mold with inclined inner and outer surfaces.

The dimensions of the annular compacts were measured by using a 3-dimensional measuring system. The compact is about 12 mm in height and about 18 mm and 12 mm in outer and inner diameter, respectively.

The compacts were sintered at 1730 °C for 4h in H_2 atmosphere. The heating and cooling is at a rate of 5 K/min.

2.3 Rod-inserted sintering

Samples were prepared from the IDR route UO_2 powder. The powder was pre-compacted under 10 MPa by using a cold isostatic press. Pre-compacted lump of UO_2 powder was crushed and granulated with 20 mesh sieves. The granules were mixed with a 0.3 wt% of zinc stearate in a tumbling mixer for 30 min.

The compaction was conducted in a double acting press under about 400 MPa by using an annular shape mold. Dimensions of the annular compacts were measured by using a 3-dimensional measuring system.

The compacts were sintered at 1600 °C for 12 h in H_2 atmosphere with a precisely machined rigid rod inserted. The heating and cooling is at a rate of 5 K/min.

2.4 Sintered density and diametric tolerances

In the above three cases, the sintered density was measured by the water immersion method. The inner and outer diameters of the sintered pellets were measured carefully as a function of the pellet height by using a 3-dimensional measuring system. Centerless grinding was conducted to control the outer diameter.

3. Results and discussion

Figure 1 shows a typical sintered annular pellet of about 14 mm in outer diameter and a typical sintered cylindrical solid pellet of about 8 mm in diameter after sintering at 1730 °C for 4 h in H_2 atmosphere. Sintered densities of both pellets were around 96.5% of the theoretical density.

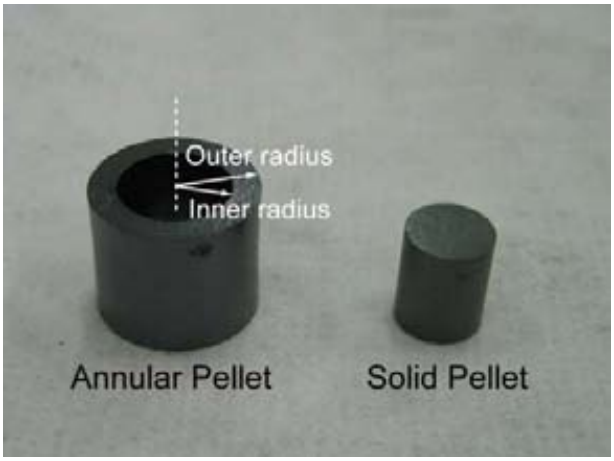

FIG. 1. Sintered annular pellet and solid pellet.

Figure 2 shows the green density distribution according to die-pressing conditions for a cylindrical pellet during uni-axial pressing. Due to an inhomogeneous green density distribution along the compact height, an inhomogeneous sintering deformation usually occurred in a sintered cylindrical PWR fuel pellet fabricated by a conventional uni-axial pressing. An inhomogeneous green density distribution in a powder compact is attributed to granule to granule frictions and granule to pressing mold wall frictions. Frictions result in an irregular pressing load distribution in a powder compact. Thus, a centerless grinding is necessary for a conventional sintered PWR pellet in order to secure the diametric tolerance specifications.

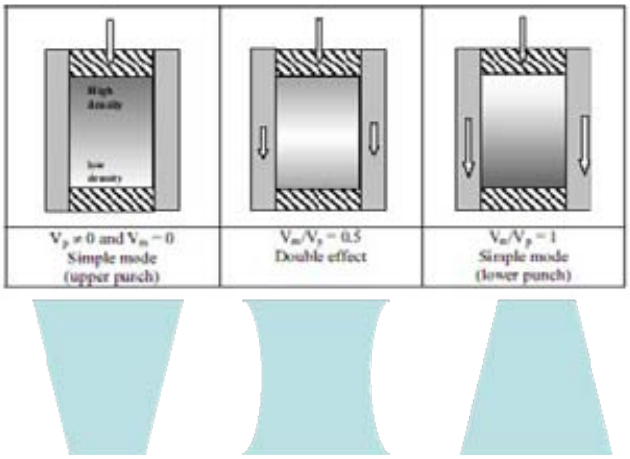

FIG. 2. Green density distribution according to die-pressing conditions for a cylindrical pellet during uni-axial pressing.

The same inhomogeneous sintering deformation was shown in an annular pellet fabricated by a conventional uni-axial pressing. Figure 3(a) and (b) show the measured inner and outer diameters of the sintered annular pellet as a function of the pellet height for a single act pressing and a double act pressing, respectively. An inhomogeneous sintering deformation occurred after sintering at 1730 °C and the sintered pellet had different inner and outer diameters according to the pellet height, even though an annular green compact has constant inner and outer diameters along the pellet height direction.

Diametric tolerances in Figure 3 are about several tens micrometers for inner and outer diameter. Tolerance in outer diameter can be reduced by a centerless grinding, but an inner surface grinding is not as easy as a centerless grinding. The above inner diametric tolerance is not acceptable for the provisional specification of an annular fuel pellet.

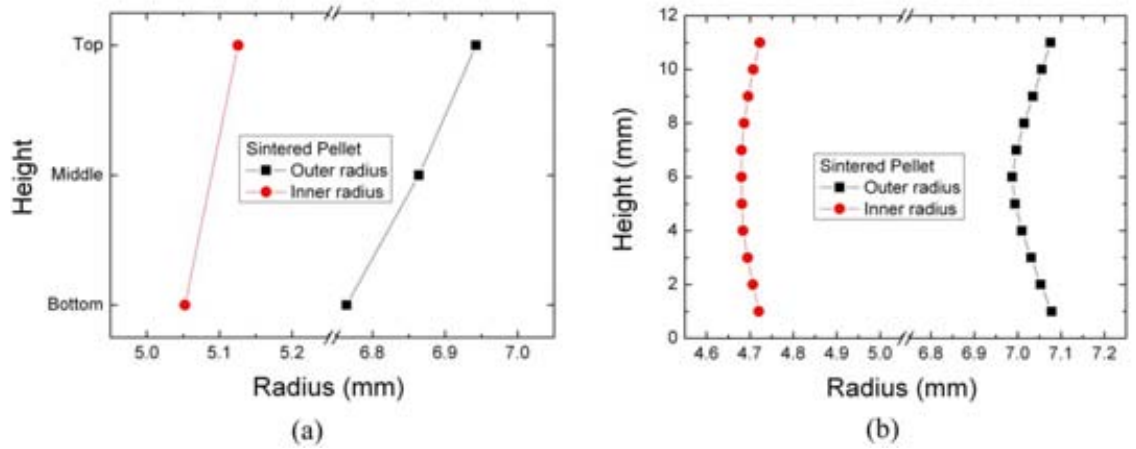

FIG. 3. Measured inner and outer radius distributions of the sintered annular pellet; (a) single-acting press and (b) double-acting press.

3.1 Uni-axial double act pressing and cold isostatic pressing [5]

In order to mitigate the green density difference in annular compact and to obtain a homogeneous green density distribution, a new compaction process which combines the usual double-acting pressing and cold isostatic pressing was tried. An additional compaction was conducted by using a cold isostatic press after making the annular compact by a conventional double-acting press.

Figure 4 shows a schematic diagram of this process. A green annular pellet was made in a double-acting press. The green density distribution of an annular compact was indicated by the darkness in the green pellet. As shown in Figure 4, the middle portion has a lower green density than those of the top and the bottom portions of the green pellet fabricated by a double-acting press [4]. Annular compact pressed again in a cold isostatic press with a precisely-machined stainless steel rod inserted. The inserted metal rod acts as a support for maintaining a flat inner surface during a cold isostatic pressing. Thus, the deformation will only occur at the whole outer surface of the green annular pellet. The amount of the deformation will be inversely proportional to the initial green density.

A diametric deformation of an annular compact during a cold isostatic pressing was shown in Figure 5(a). Red circles represent the inner and outer diameters of an annular compact fabricated by a double-acting press. Black squares indicate the inner and outer diameters of an annular compact after a cold isostatic pressing. Inner diameters maintain a constant value which is independent of the compact height. However, the outer surface was deformed similarly to that of the sintered annular pellet and the outer diameters have different values according to the compact height. Considering the difference in the diametric changes depending on the pellet height, it is thought that the green annular pellet might have a homogeneous green density distribution after a cold isostatic pressing.

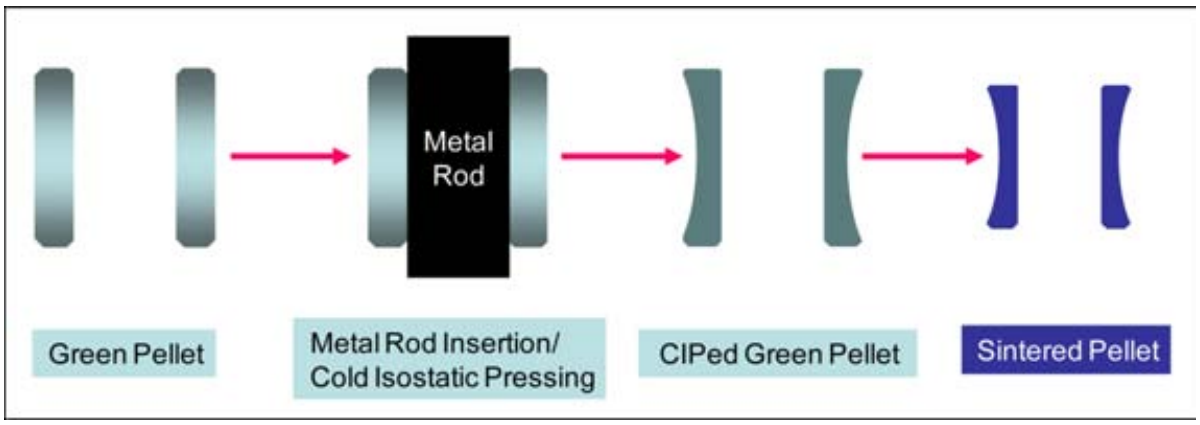

FIG. 4. Schematic diagram of uni-axial double act pressing and cold isostatic pressing process.

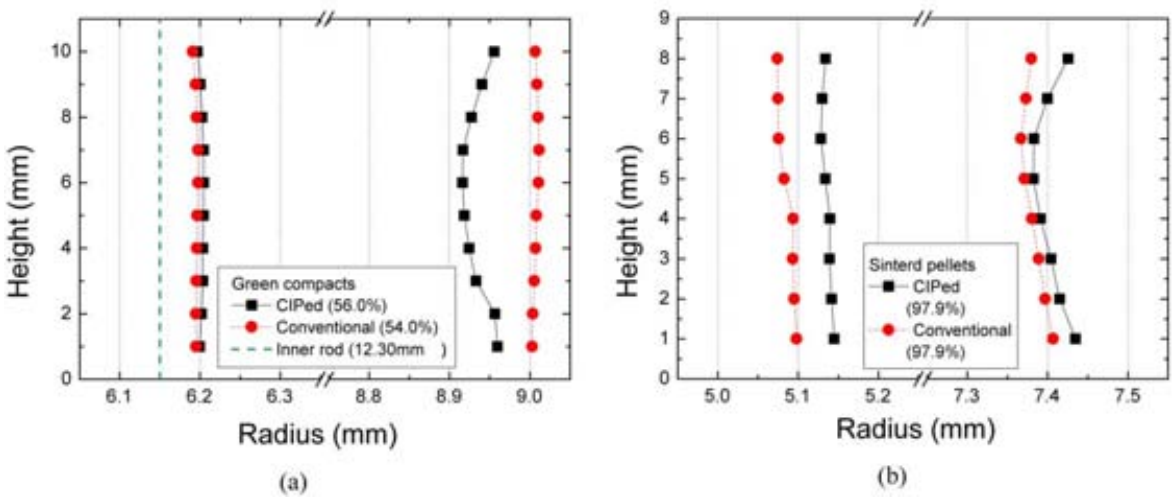

FIG. 5. Measured inner and outer radius of (a) green annular pellet made by a metal rod-inserted cold isostatic pressing and (b) sintered annular pellet as a function of pellet height. Red circles indicate the inner and outer radius made by a conventional double-acting pressing.

Figure 5(b) shows the measured inner and outer diameters of the sintered annular pellet as a function of the pellet height. Black squares indicate the outer and the inner diameters after sintering a cold isostatic pressed green annular compact in Figure 5(a). A cold isostatic pressed green compact appears to undergo isotropic shrinkages during sintering as shown in Figure 5(a) and Figure 5(b). It suggests that the sintering stress might act hydrostatically and the green density inhomogeneity of a cold isostatic pressed green compact might be very small. The measured diameters of the sintered annular pellets in Figure 5(b) are 14.809 ± 0.039 mm and 10.273 ± 0.012 mm in outer and inner diameter, respectively.

3.2 Uni-axial single act pressing with the inclined mold [6]

As shown in Figure 2, the green density gradient in a powder compact depends on the pressing direction and the amount of the sintering deformation is inversely proportional to the initial green density. In a single-act pressing, the top or the bottom portion which is far from the acting punch surface has the lowest green density. Based on this correlation, annular compacting mold with inclined inner and outer surfaces was designed by considering a difference in the diametric changes depending on the pellet height during sintering.

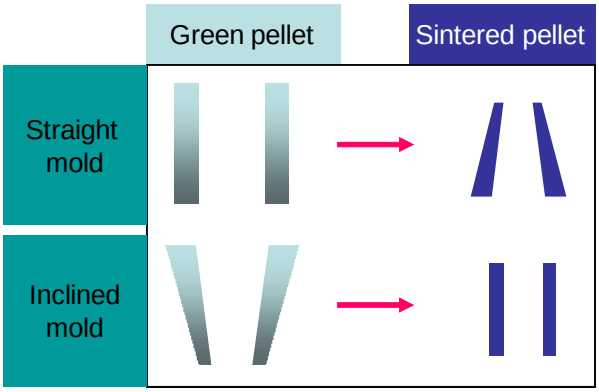

FIG. 6. Schematic diagram of the sintering deformation of annular compact with flat and inclined surfaces.

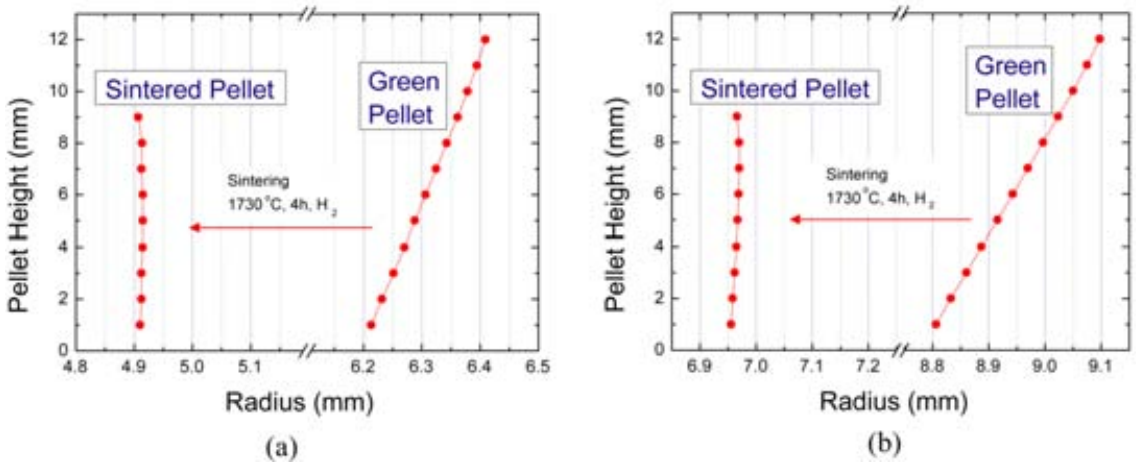

FIG. 7. Measured inner and outer diameter distributions of the inclined annular compact and the sintered annular pellet, (a) inner diameter and (b) outer diameter.

Figure 6 shows a schematic diagram of the sintering deformation of annular compact with inclined inner and outer surfaces. The darkness in the green pellet indicates the green density distribution of an annular compact. Inner and outer diameters of an inclined annular green compact increased with decreasing the green density. An inclined annular green compact becomes a sintered annular pellet with flat inner and outer surfaces after sintering because the amount of the sintering deformation is inversely proportional to the initial green density.

We designed a compacting mold with inclination angles of 1.11° and 1.52° for inner and outer surfaces, respectively. By using a compacting mold with inclined surfaces and a single-acting press, an annular pellet can be fabricated successfully with a tolerance of less than ± 13 μm which is the diametric tolerance specification of a conventional PWR fuel pellet.

The measured inner and outer diameters of the green annular compact and the sintered annular pellet are presented in Figure 7 as a function of the pellet height. Inner and outer diameters of an inclined annular green compact increased along with the pellet. However, the sintered pellet appears to have constant inner and outer diameters along the pellet height direction after sintering at 1730 °C. Thus, the sintered annular pellet fabricated by an inclined mold has excellent inner and outer diametric tolerances of less than ± 5 μm and ± 10 μm for the inner and outer diameters, respectively.

3.3 Rod-inserted sintering

Finally, we are trying to reduce the inner diametric tolerance during sintering process by using a precisely machined rigid rod as an inner surface deformation stopper of an annular pellet. The inserted rigid rod acts as a support for maintaining a flat inner surface during sintering.

the cooling stage because of the small linear thermal expansion coefficient of tungsten, about 4.5×10^{-6} K^{-1}. That of UO_2 is about 9.8×10^{-6} K^{-1} for $273\ K \leq T \leq 923\ K$ and about 11.8×10^{-6} K^{-1} for $923\ K \leq T \leq 3120\ K$ [7]. Smaller linear thermal expansion coefficient of tungsten than that of UO_2 might induce the tensile stress on the sintered annular pellet. Thus, the linear thermal expansion coefficient of a deformation stopper must be similar or larger than that of UO_2 in order to prevent the fracture of the sintered annular pellet during the cooling stage.

Tungsten rod was selected firstly because of its rigidness at high temperature and its inertness in H_2 atmosphere. No deformation occurs in the tungsten rod after sintering with an annular compact. Figure 8 shows the fractured sintered annular pellet. Fracture ought to occur during

The fully densified UO_2 rod was chosen as a deformation stopper. Figure 9 shows the status of the UO_2 rod and the annular pellet during a UO_2 rod inserted sintering process. The diameter of a UO_2 rod measured by using a 3-dimensional measuring system is 10.18 ± 0.005 mm, and it does not changed after sintering and dividing from annular pellet.

Figure 10(a) and (b) show the measured inner and outer diameters of the sintered annular pellet as a function of the pellet height with and without inserting the UO_2 rod, respectively. It shows a diametric deformation of a green annular pellet during sintering. Inner diameters maintain a constant value which is independent of the pellet height in Fig 10(a); however, the outer surface was deformed similar to that of the sintered annular pellet in Figure 3 and Figure 5. The outer diameters have different values according to the pellet height.

The measured diameters of the sintered annular pellet are 14.786 ± 0.015 mm and 10.185 ± 0.006 mm in outer and inner diameter, respectively. The inserted UO_2 rod successfully acts as a stopper for maintaining a flat inner surface during sintering. It appears that the inhomogeneous deformation only occurs at the outer surface of the annular pellet.

Figure 10(b) shows the measured diameters of the sintered annular pellet without inserting the UO_2 rod. The measured outer and inner diameters are 14.735 ± 0.030 mm and 10.146 ± 0.023 mm, respectively. Diametric tolerances are much larger than those of the UO_2 rod inserted sintered annular pellet.

FIG. 8. Fractured annular pellet after tungsten rod inserted sintering.

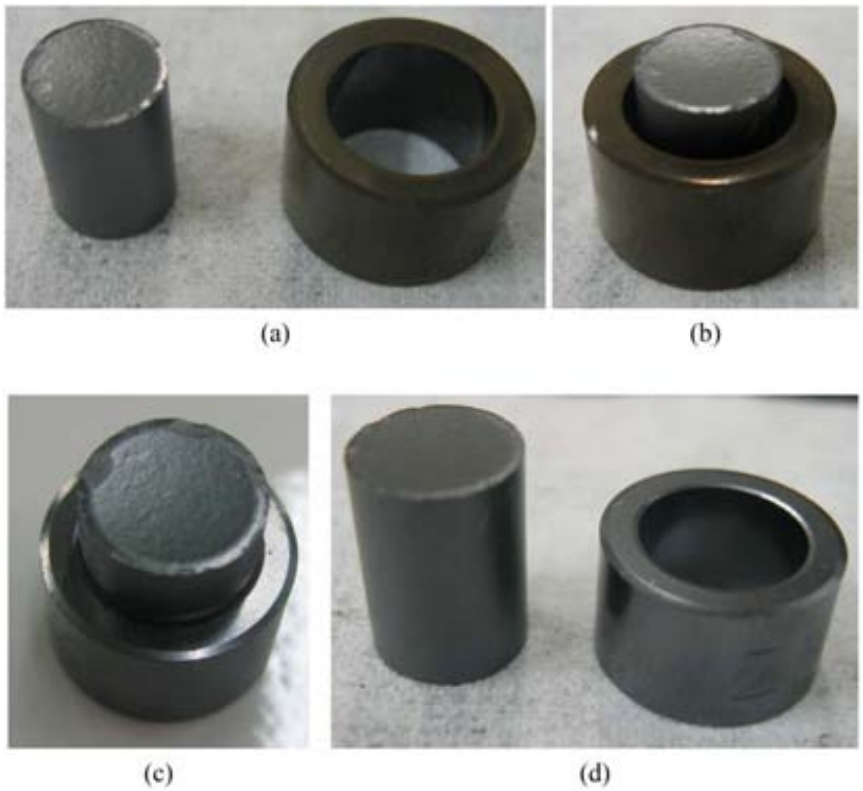

FIG. 9. (a) UO2 rod and green annular compact. (b) Green annular compact inserted with a UO2 rod. (c) As-sintered annular pellet inserted with a UO2 rod. (d) Sintered annular pellet after removing a UO2 rod.

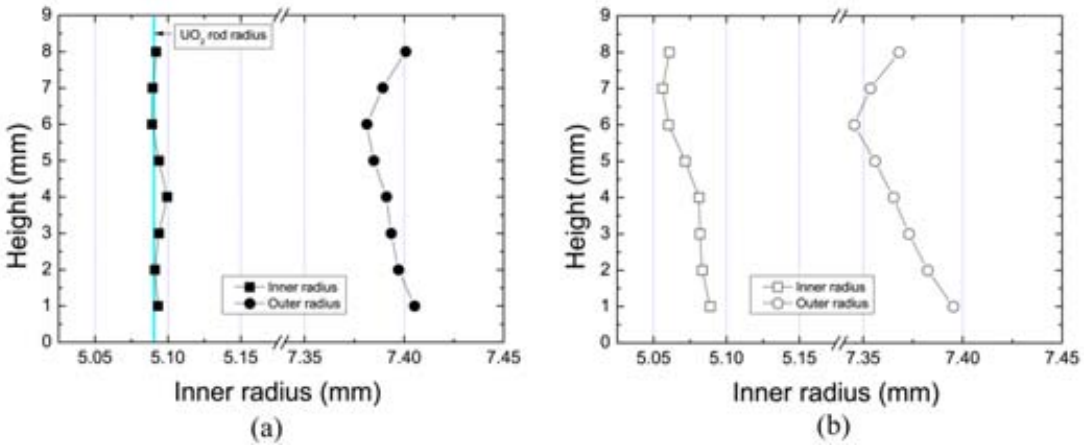

FIG. 10. Measured inner and outer radius distributions of the annular pellet after sintering (a) with a UO_2 rod inserted and (b) without a UO_2 rod inserted.

By using the UO_2 rod inserted sintering method, the inner diametric tolerance, about ± 6 μm, was significantly improved compared with that of the sample in Figure 10(b). This value is comparable to the tolerance of the centerless-ground outer surface, less than ± 5 μm, and it is acceptable for the commercial specification of PWR fuel pellet without an inner surface grinding. The tolerance in the outer diameter can be reduced by a centerless grinding. Thus, both the inner and outer diametric tolerances can satisfy the provisional specification of an annular fuel pellet which is less rigorous than that of commercial PWR fuel pellet.

4. Conclusions

In order to improve the inner diametric tolerance of an as-sintered annular pellet for a dual cooled fuel, three new fabrication methods have been introduced. Inner diametric tolerances of sintered annular pellets were measured without an inner surface grinding.

A new compaction process which combined a usual double-act pressing and a cold isostatic pressing enables us to obtain the annular compact with more homogenized green density distribution. A sintered annular fuel pellet with good inner diametric tolerance has been fabricated by using a new compaction process.

An annular compacting mold with inclined inner and outer surfaces was designed by considering a difference in the diametric changes depending on the pellet height during sintering. Highly precise inner diametric tolerance can be achieved by using a newly designed compaction mold with inclined mold surfaces and a single acting press.

When we applied a UO_2 rod inserted sintering process in order to minimize a diametric tolerance, annular compact was firstly compacted with a double-acting press and then sintered with a precisely-machined UO_2 rod inserted. A UO_2 rod could prevent an inhomogeneous deformation of the inner surface during sintering, and thus, it reduced the inner diametric tolerance of a sintered annular pellet.

REFERENCES

[1] HEJZLAR, P., KAZIMI, M. S., Annular fuel for high-power-density pressurized water reactors: motivation and overview, Nuclear Technology **160**, (2007), p.2–15.

[2] FENG, D., et al., Thermal-hydraulic design of high-power-density annular fuel in PWRs, Nuclear Technology **160**,(2007), p.16–44.

[3] YUAN, Y., et al., Thermomechanical performance of high-power-density annular fuel, Nuclear Technology **160**, (2007), p.135–149.

[4] DELETTE, G., et al., Finite element modelling of the pressing of nuclear oxide powders to predict the shape of LWR fuel pellets after die compaction and sintering, in Advanced Fuel Pellet Materials and Design for Water Cooled Reactors, IAEA–TECDOC–**1416**, Vienna, (2004), p.21–30.

[5] RHEE, Y. W., et al., Fabrication of sintered annular fuel pellet for HANARO irradiation test, J. Nucl. Sci. Technol., submitted

[6] RHEE, Y. W., et al., Annular fuel pellet fabrication without surface grinding, in Korean Nuclear Society Spring Meeting, Jeju, (2009).

[7] MARTIN, D. G., The thermal expansion of solid UO_2 and (U, Pu) mixed oxides - a review and recommendations, J. Nucl. Mater.**152**, (1988), p.94–101.

A New Uncertainty Reduction Method for Fuel Fabrication Process and PWR Cores with Erbia-Bearing Fuel

T. Sano[1]

Abstract. The concept of a fuel fabrication system with Erbia bearing high burnup fuel has been proposed. The Erbia is added to all fuel with over 5% ^{235}U enrichment to retain the neutronics characteristics to that within 5% ^{235}U enrichment. There is a problem of the prediction accuracy of the neutronics characteristics with Erbia bearing fuel because of the short of experimental data of Erbia bearing fuel. The purpose of the present work is to reduce the uncertainty. A new method has been proposed by combining bias factor method and the cross section adjustment method. The cross section adjustment method is applied only to erbium (Er). And the neutronics characteristic except Er is improved by the bias factor method. The main contribution of Er is neutron capture. To evaluate the accuracy of k_{eff}, the Erbia worth is the suitable experimental data. Therefore, the prediction accuracy of neutronics characteristics of Er is improved through the cross section adjustment using the sample worth. In the case of the blending machine (H/U=0) for the fuel fabrication process, the uncertainty reduction, which shows the rate of reduction of uncertainty, of the k_{eff} is 0.604 by the present method and 0.555 by the conventional bias factor method. In the case of H/U=1.0, the uncertainty reduction by the present method was 0.760. Using the bias factor method, the uncertainty reduction was 0.593. The prediction uncertainty was significantly reduced by the present method. For the PWR core, the uncertainty reduction, which shows the rate of reduction of uncertainty, of the k_{eff} is 0.865 by the present method and 0.801 by the conventional bias factor method. Thus the prediction uncertainties are reduced by the present method compared to the bias factor method.

1. Introduction

The introduction of high burnup fuel has efficient use of uranium resources. To achieve higher burnup, it is necessary to increase the ^{235}U enrichment. However, for the existing commercial nuclear power reactors and nuclear fuel fabrication processes, the ^{235}U enrichment must be less than 5 wt% from the viewpoint of criticality safety.

The addition of Erbia (erbium oxide; Er_2O_3) to the fuel that is over 5 wt% ^{235}U enrichment does not change the neutronics characteristics of the core or the fuel fabrication process relative to fuel that is under 5 wt% ^{235}U [1].Thus, no additional change is required in the conventional core management and fuel fabrication system. However, we have no experience for a fuel fabrication process that involves Erbia bearing fuel and the PWR core with full-core loaded Erbia. Therefore, there is a question of the prediction accuracy of the neutronics characteristics with the Erbia loaded super-high burnup fuel because the use of Erbia may produce additional uncertainty of the neutronics characteristics. To reduce the uncertainty of neutronics characteristics, there are two methods: the bias factor method [2] and the cross section adjustment method [3].

In the bias factor method, the bias factor, which is defined as the ratio of measured data and the calculated data, is obtained using the data from a critical experiment. This factor is a multiplier that is applied to the calculated neutronics characteristics of a target system to improve the accuracy. This method is simple and easy to apply to design calculations. However, this method has a drawback in that only one measured neutronics characteristics is used for a relevant target system. To minimize this drawback, we have introduced the generalized bias factor method, which effectively utilizes a few experiment data [5].

Compared to the bias factor method, the cross section adjustment method can utilize a wide range of neutronics characteristics. The adjusted cross sections proved recommended values for a cross section evaluation and also reliably predict neutronics characteristics of the target core. However, the cross section adjustment method requires a lot of experimental data in order to obtain a reasonable adjustment of cross sections.

[1] Research Reactor Institute, Kyoto, Japan.

In this paper, we have combined the generalized bias factor method and the cross section adjustment method. The cross section adjustment method is applied only to erbium (Er). Therefore, few experimental data is required for the adjustment. The neutronics characteristics, except for Er, are improved by the generalized bias factor method. In the calculation of the bias factor, only a few data is required. So as a whole, only a few experimental data is required. This is the advantage of the present method compared to the combined method.

In the present method, the Er cross section is adjusted by taking into account that the main reaction of Er is neutron capture. To evaluate the accuracy of the neutron capture rate of Er, the Erbia worths serve as good experimental data. Therefore, the cross section uncertainty of Er is improved through the cross section adjustment using these worths.

The theory is shown in Section 2, and the results are shown in Section 3. From these results some conclusions are drawn and shown in Section 4.

2. Theory

The effective neutron multiplication factor of the Erbia bearing fuel system can be written as

$$\frac{1}{k_{eff}} = \rho + \frac{1}{k_{eff,0}} \ , \tag{1}$$

where ρ is the Erbia worth, and $k_{eff,0}$ is the neutron multiplication factor for the system without the Erbia. Here we do not consider the calculational error because this error can be reduced by using the Monte Carlo method. The ρ and $k_{eff,0}$, calculated by using a cross section set, have errors due to the cross section errors $\Delta\sigma$. Therefore, the uncertainty of k_{eff} , $d\left(k_{eff}\right)$, is expressed by

$$\frac{1}{(k_{eff})^2} d\left(k_{eff}\right) = -\rho G_\rho \Delta\sigma + \frac{1}{k_{eff,0}} G_k \Delta\sigma \ , \tag{2}$$

where

G_k is the sensitivity coefficient of $k_{eff,0}$ relative to cross section change,

G_ρ is the sensitivity coefficient of ρ relative to cross section change,

$\Delta\sigma$ is relative cross section error.

The relative cross section error $\Delta\sigma$ and the sensitivity coefficient G_R $\left(R = k, \rho\right)$ are defined as follows:

$$\Delta\sigma = \frac{d\sigma}{\sigma} \ , \tag{3}$$

$$G_R = \frac{dR}{R} \Big/ \frac{d\sigma}{\sigma} \ , \tag{4}$$

where R denotes the $k_{eff,0}$, ρ .

We assume that there is no correlation between the Er cross section and other cross sections. Under this assumption, the relative variance of k_{eff} is expressed by

$$V\left(k_{eff}\right) = k_{eff}^{\,2}\left(G_1 V_{Er} G_1^t + G_2 V_\sigma G_2^t\right), \tag{5}$$

where

$$G_1 = G_\rho \rho \ , \tag{6}$$

$$G_2 = \frac{1}{k_{eff,0}} G_k \ , \tag{7}$$

and V_{Er} is the cross section covariance matrix only for Er , V_σ is the cross section covariance matrix except for Er and the superscript t denotes the transposition.

Equation (5) denotes that uncertainty of the Erbia bearing fuel system is composed of two terms. One is the uncertainty of the Erbia worth and the other is that of $k_{eff,0}$.

One can use the bias factor for the $k_{r,eff,0}$ prediction of a target core. The subscript *r* stands for a target core. In this case, $\tilde{k}_{r,eff,0}$ of the target core is expressed by

$$\tilde{k}_{r,eff,0} = k_{r,eff,0} \times f \ , \tag{8}$$

where f is the bias factor for a critical mock-up core and is defined by

$$f = \frac{k_{e,eff,0}^e}{k_{e,eff,0}^c}, \tag{9}$$

where $k_{e,eff,0}^e$ and $k_{e,eff,0}^c$ are the measured neutron multiplication factor and the calculated neutron multiplication factor for the critical mock-up core, respectively.

Equation (8) can be written as

$$\tilde{k}_{r,eff,0} = k_{r,eff,0}^0 \left(1 + G_{r,k}\Delta\sigma\right) \times \frac{1+\Delta E_k}{1+G_{e,k}\Delta\sigma}, \tag{10}$$

where $k_{r,eff,0}^0$ is the true value of the target core, $G_{r,k}$ is the sensitivity coefficient of the target core, $G_{e,k}$ is the sensitivity coefficient of the critical mock-up core, and ΔE_k is the experimental error of k_{eff} of the critical mock-up core. In this paper, the method error is neglected. Therefore, the variance of Eq.(10) is expressed by

$$V\left(\tilde{k}_{r,eff,0}\right) = \Delta G_k V_\sigma \Delta G_k^t + V\left(E_k\right), \tag{11}$$

where ΔG_k is the sensitivity coefficient difference between the critical mock-up core and the target core, and $V\left(E_k\right)$ is the variance of the measured k_{eff} of the critical mock-up core, $k_{e,eff,0}^e$.

Next, let us consider the reduction of the first term of Eq.(5). When the Er cross section uncertainty is large, the first term becomes large, and the uncertainty of k_{eff} increases. The uncertainty of the first term of Eq.(5) is reduced by using the cross section adjustment method. To reduce the uncertainty, one can utilize the Erbia worth measured by critical experiments. Using the adjustment method, the adjusted cross section of Er is given by [3].

$$\sigma = \sigma_0 \left(1 + V_{Er} G_{e,\rho}{}^t \left[G_{e,\rho} V_{Er} G_{e,\rho}{}^t + V(E_\rho) \right]^{-1} \frac{\left[\rho_e^e - \rho_e^c(\sigma_0) \right]}{\rho_e^c(\sigma_0)} \right), \tag{12}$$

where σ_0 is the cross section before adjustment, $G_{e,\rho}$ is the sensitivity coefficient for the Erbia worth of the critical assembly, $V(E_\rho)$ is the variance of the measured Erbia worth, ρ_e^e is the measured Erbia worth and $\rho_e^c(\sigma_0)$ is the Erbia worth of the critical assembly calculated by using σ_0.

The variance of $\rho_r^c(\sigma)$ is expressed by [3]

$$V\left[\rho_r^c(\sigma)\right] = G_{r,\rho} V_{Er}' G_{r,\rho}{}^t , \tag{13}$$

where V_{Er}' is the covariance of the adjusted cross section, and is given by [3]

$$V_{Er}' = V_{Er} - V_{Er} G_{e,\rho}{}^t \left[G_{e,\rho} V_{Er} G_{e,\rho}{}^t + V(E_\rho) \right]^{-1} G_{e,\rho} V_{Er} . \tag{14}$$

The variance of the effective neutron multiplication factor for the target core is given by

$$V(\tilde{k}_{eff}) = k_{eff}{}^2 \left\{ G_{r,\rho} V_{Er}' G_{r,\rho}{}^t \rho^2 + \frac{1}{k_{eff,0}{}^2} \left[\Delta G_k V_\sigma \Delta G_k{}^t + V(E_k) \right] \right\} . \tag{15}$$

Finally, the uncertainty reduction (UR) [6] of the neutronics characteristics is defined by

$$UR = 1 - \frac{V(\tilde{k}_{eff})}{V(k_{eff})} . \tag{16}$$

where $V(k_{eff})$ is defined by Eq. (5).

3. Numerical result

3.1 Calculational model

Here, the blending machine of the fuel powder in the fuel fabrication process and the PWR core are selected as the target systems.

The blending machine has $800l$ capacity and is approximated by an R-Z homogenous model in the neutronics calculations. In this paper, the blending machine has a water reflector from the viewpoint of criticality safety. Figure 1 shows the calculational geometry of the blending machine. The temperature is 300K. The UO_2 powder in the blending machine has a bulk density of 3.5 g/cm^3 and the ^{235}U enrichment is 5.4 wt%. The enrichment of Er relative to U is 0.3 wt%. Two cases of the prediction accuracy for the neutron multiplication factor (k_{eff}) are considered. One case is without moderation (H/U=0) in the blending machine. Although the blending machine has watertight construction, the UO_2 powder has a slight water content when considering the moisture in the air. Therefore, assuming a

possible maximum water content, the number density ratio of H to U was set to 1.0 for the second case.

The PWR core is approximated by an R-Z geometry as shown in Figure 2. The 5.4wt% ^{235}U enriched UOB2B fuels are loaded. The enrichment of Er to U is 0.3wt%. The temperature is 300K.

The experiments of Erbia worth were performed at the Kyoto University Critical Assembly (KUCA). The Erbia plates loaded in the central fuel element were gradually replaced with graphite plates. The measured Erbia worths for five different cases were used.[1)] The calculational geometry is approximated by an R-Z geometry as shown in Figure 3. The calculated worth and the C/E value are shown in Table 1.

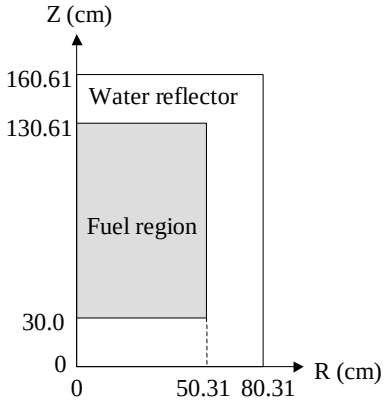

FIG. 1. Calculational geometry of a blending machine

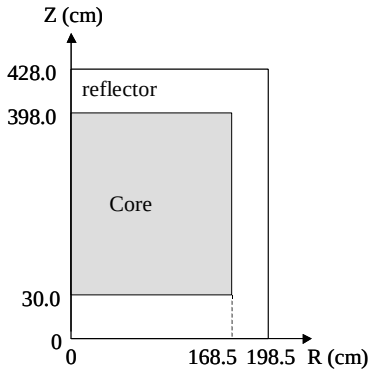

FIG. 2. Calculational geometry of a PWR core

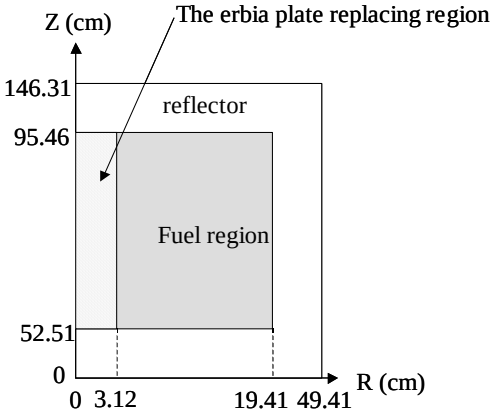

FIG. 3. Calculational geometry of KUCA core

TABLE 1. CALCULATED ERBIA WORTH AND C/E VALUE OF KUCA EXPERIMENT

Number of replacements	Calculated sample worth $(\Delta k/k)$	C/E
3	4.11×10^{-4}	1.09
5	7.07×10^{-4}	1.13
9	1.27×10^{-3}	1.11
13	1.44×10^{-3}	1.12
17	1.67×10^{-3}	1.10

To analyze the critical assembly and the target system, the 107-group cross section set processed by using the cell calculation code SRAC [7] with JENDL–3.3 [8] was utilized. The multiplication factor and the Erbia worth are calculated by diffusion theory. The sensitivity coefficients were calculated using the generalized perturbation theory code SAGEP [9]. In the cross section adjustment, the 18–group ^{167}Er capture cross section processed from JENDL–3.3 was adjusted by using all the measured worths. The cross section covariance matrix was taken from JENDL–3.3. However, the covariance matrix for Er is not present in JENDL–3.3, ENDF/B–IV [10], ENDF/B–VI R8 [11] or JEFF–3.0 [12]. So, we compared the ^{167}Er capture cross sections of JENDL–3.3, ENDF/B–IV, ENDF/B–VI R8 and JEFF–3.0 in Figure 4. In this Figure, the differences between the JENDL–3.3 and the other libraries are about 10%. Thus, we assumed that the Er cross section errors are 10% in all energy regions. The experimental errors of Erbia worths are reported to be 3% [3].

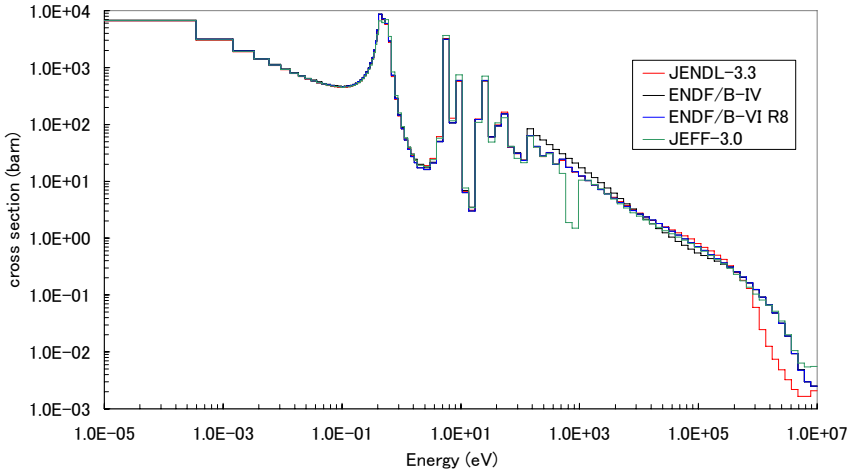

FIG. 4. Comparison of ^{167}Er capture cross sections in each nuclear data library

3.2 Cross section adjustment

In this section, the cross section adjustment by using the measured Erbia worths from KUCA is described. The sensitivity coefficients for the Erbia worth of the 9 Erbia plates replacement with respect to the Er capture cross sections are shown in Figure 5. We can see that the sensitivity coefficients of the Er nuclides other than ^{167}Er can be neglected. Figure 6 shows the comparison of the sensitivity coefficients for the Erbia worth with respect to ^{167}Er capture cross section, ^{238}U capture cross section and ^{235}U fission cross section. In this Figure, the sensitivity coefficients for the Erbia worth with respect to the ^{238}U capture cross section and the ^{235}U fission cross section have a relatively small effect on the prediction uncertainty of the Erbia worth. We note that the Er cross section uncertainties are assumed to be 10%. In this paper, the ^{167}Er capture cross section is only adjusted using all the measured worths. Figure **7** shows the ^{167}Er capture cross section before and after adjustment and the alteration rate is shown in Figure 8. The maximum alteration rate is -1.6% in the 12th energy group.

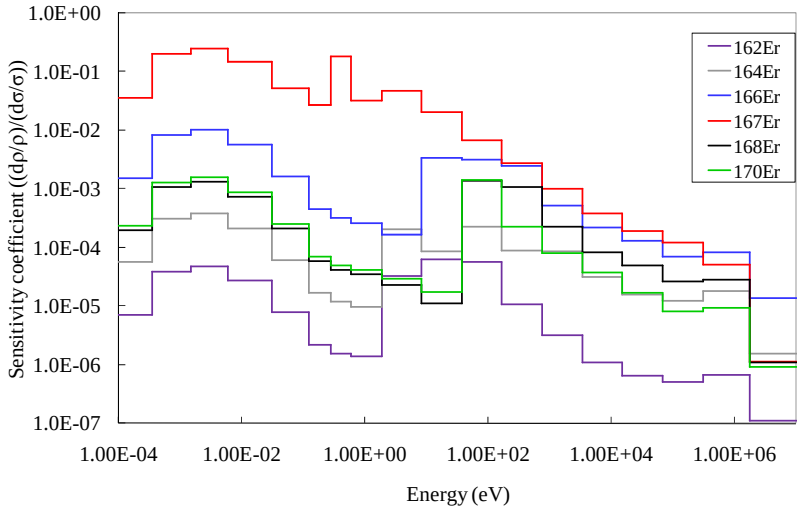

FIG. 5. Sensitivity coefficients for Erbia worth of the 9-Erbia plates replacement with respect to Er capture cross section.

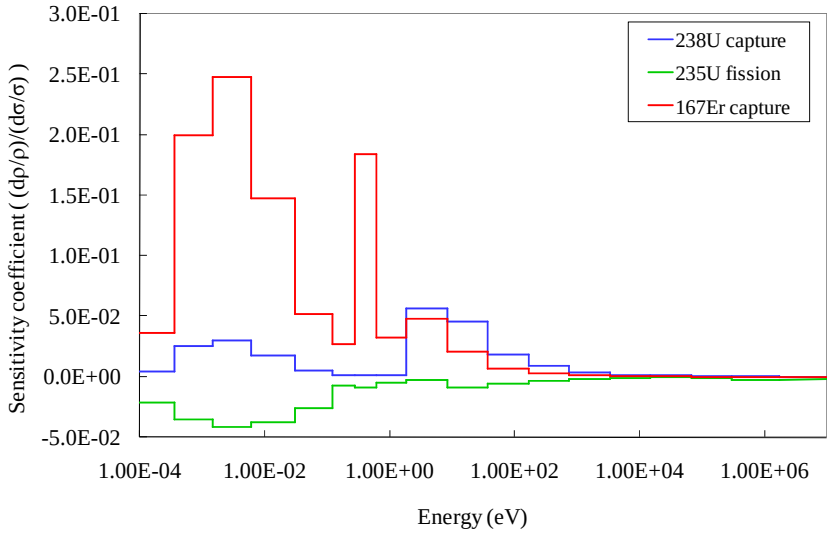

FIG. 6. Sensitivity coefficients for Erbia worth of the 9-Erbia plates replacement with respect to ^{167}Er capture cross section, ^{238}U capture cross section and ^{235}U fission cross section.

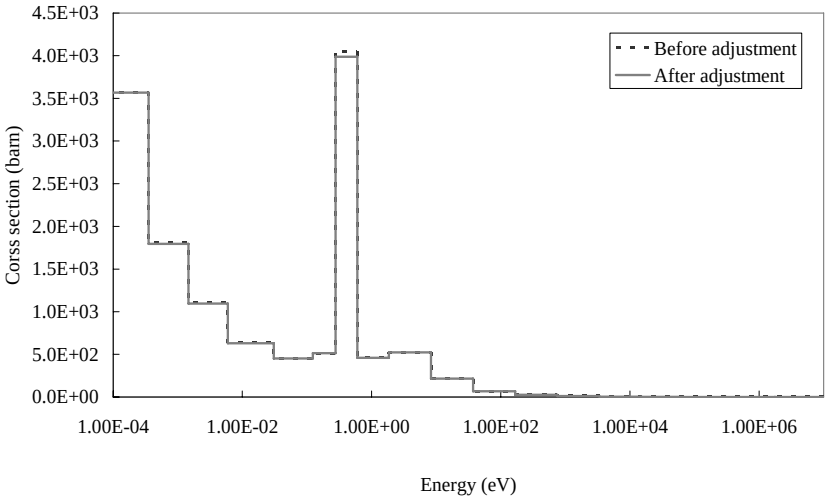

FIG. 7. ^{167}Er capture cross section before and after adjustment

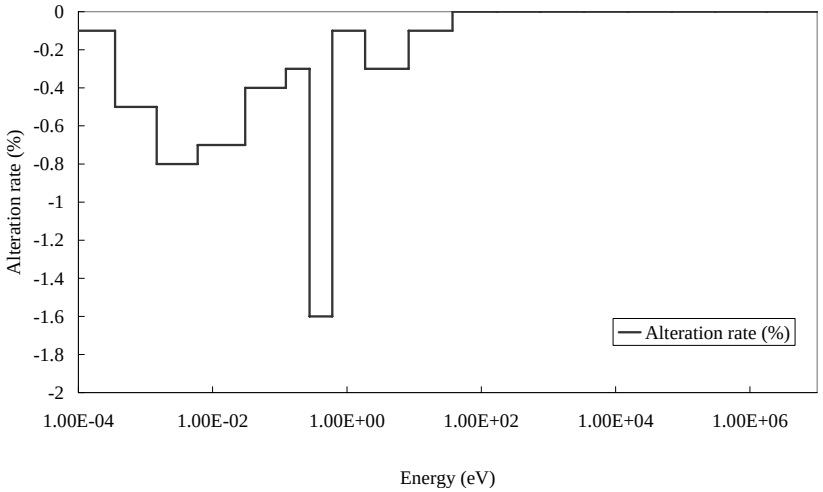

FIG. 8. Alteration rate of ^{167}Er capture cross section due to adjustment.

3.3 Calculation results for the blending machine

In this section, we evaluate the uncertainty reductions of the neutron multiplication factor (k_{eff}) in the blending machine.

First, the case without hydrogen in the blending machine is evaluated. The k_{eff} value with the Erbia is 0.6210 and that without the Erbia is 0.6361. The calculated Erbia worth is $3.823\times10^{-2}\,\Delta k/k$. Table 2 shows the comparison of the prediction uncertainty and the uncertainty reduction (UR) by the present method and the bias factor method. In the bias factor method, the data of k_{eff} from a KUCA critical experiment with a full core of Erbia bearing fuel [1] was used to obtain the bias factor for k_{eff}. The experimental error of k_{eff} is reported to be 0.03% [13]. The calculated k_{eff} is 1.002. This bias factor method is independent of the ΔE_ρ (refer to Eq.(15)), because the bias factor is directly applied only to the k_{eff} using Eq.(11). In the bias factor method, the Er cross section uncertainties are set to 10%. Using the bias factor method, the uncertainty reduction is 0.555. When one uses the present method, the uncertainty reduction is 0.604. In the present method, the k_{eff} from two KUCA critical experiments without Erbia [14] are used for the generalized bias factor method. The experimental data of k_{eff} were measured in a 93% high enrichment uranium core (A3/8”P36EU) and in a 93% high enrichment uranium core with thorium (B6/8”P17EU-Th-EUEU).

TABLE 2. COMPARISON OF PREDICTION UNCERTAINTIES AND UNCERTAINTY REDUCTIONS FOR k_{eff} IN A BLENDING MACHINE (H/U=0.0)

	Uncertainty (%)	UR
Present method	0.495	0.604
Bias factor method	0.525	0.555
Case without experimental data	0.787	0.000

Figure 9 shows the components of the prediction uncertainty. We can see that for the present method, the uncertainty of erbium is remarkably reduced compared to the bias factor method. Here, the uncertainty of uranium is different between the present method and the bias factor method. This is because the sensitivity coefficients of uranium for the critical assembly are different. In the present method, the sensitivity coefficients of uranium are calculated using the data for the experiment without Erbia. However, in the bias factor method, the sensitivity coefficients of k_{eff} are calculated using the data from the KUCA critical experiment with fuel containing Erbia, and the core is different from that without Erbia. The sensitivity coefficients of ^{238}U capture and ^{235}U fission cross sections are shown in Figure 10 and Figure 11, respectively. The sensitivity coefficients used for the generalized bias factor method are not similar to the sensitivity coefficients for the blending machine. Therefore, the uncertainty of uranium by the bias factor method is more reduced than the present method and the total prediction uncertainty of the k_{eff} by the present method is reduced only a little compared to the bias factor method.

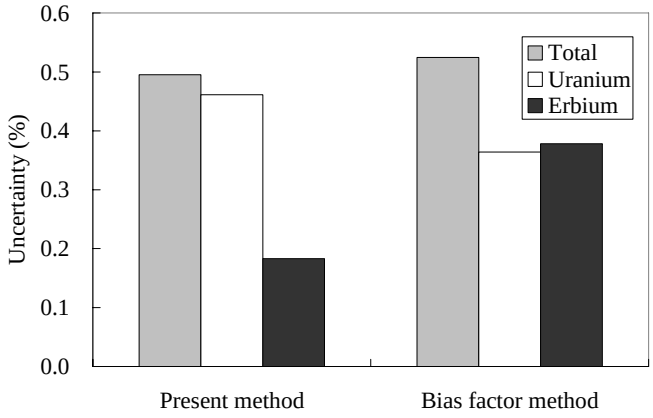

FIG. 9. Components of prediction uncertainty of k_{eff} in a blending machine (H/U=0.0).

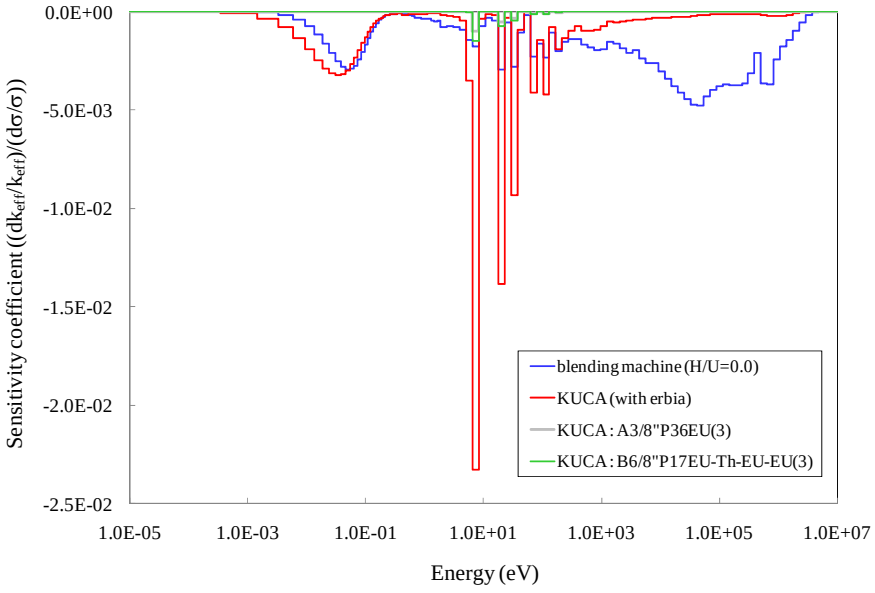

FIG. 10. Sensitivity coefficients of k_{eff} with respect to ^{238}U capture cross section.

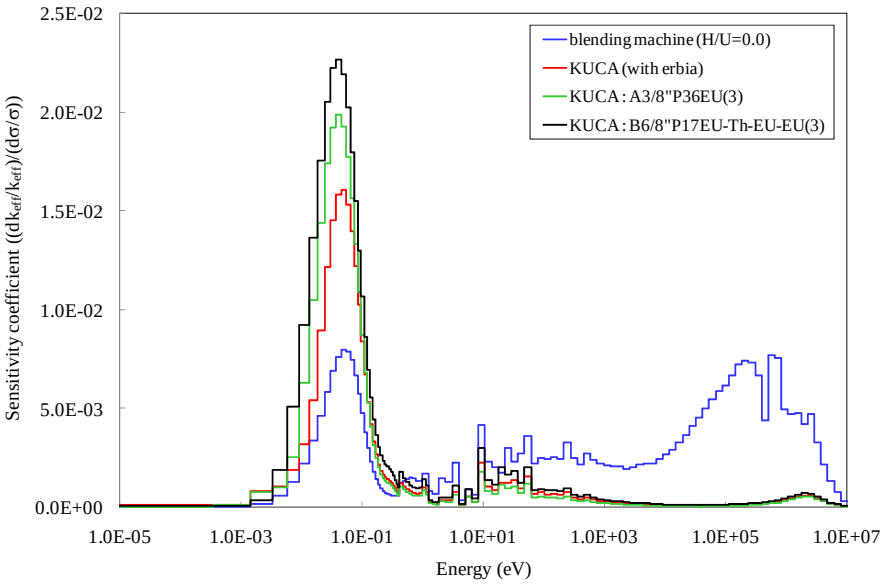

FIG. 11.: Sensitivity coefficients of k_{eff} with respect to ^{235}U fission cross section.

Next we evaluate the prediction uncertainty in the case of H/U=1.0. The k_{eff} with Erbia is 0.8026 and that without Erbia is 0.8287. The Erbia worth is $3.924\times10^{-2}\,\Delta k/k$. Table 3 shows the prediction uncertainties and the uncertainty reductions of the k_{eff} when we use the present method and the bias factor method. The prediction uncertainty by the bias factor method is 0.539% and the uncertainty reduction is 0.593. However, in the present method, the prediction uncertainty is reduced and the uncertainty reduction is improved compared to the bias factor method.

TABLE 3. COMPARISON OF PREDICTION UNCERTAINTIES AND UNCERTAINTY REDUCTIONS FOR k_{eff} IN A BLENDING MACHINE (H/U=1.0)

	Uncertainty (%)	UR
Present method	0.414	0.760
Bias factor method	0.539	0.593
Case without experimental data	0.845	0.000

Figure 12 shows the components of the prediction uncertainty. The uncertainties of uranium are almost same between the present and the bias factor method because the neutron spectrum of the blending machine (H/U=1.0) is soft compared to the case of H/U=0.0 as shown in Figure 13. Therefore, the uncertainty of the uranium is reduced because the sensitivity coefficients with respect to uranium cross sections for the blending machine are close to KUCA. We can see that the component of the Erbia uncertainty by the present method is reduced compared to the bias factor method, which is the same as the case of H/U=0.0.

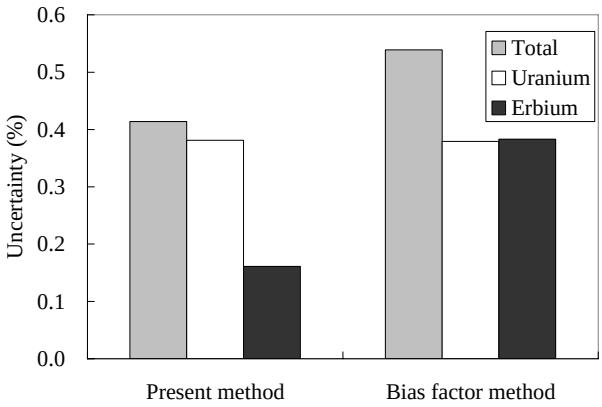

FIG. 12.: Components of prediction uncertainty of k_{eff} in a blending machine (H/U=1.0).

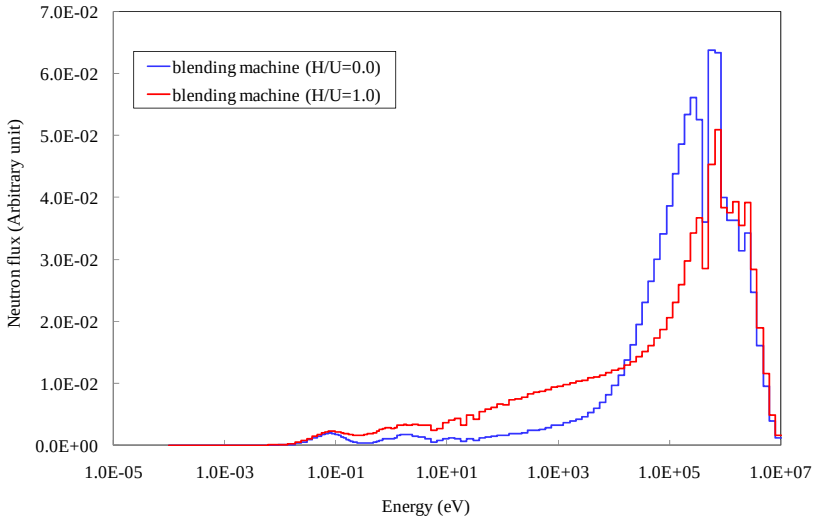

FIG. 13. Comparison of neutron spectrum between the case of H/U=0.0 and H/U=1.0.

3.4 Calculation results for the PWR core

In this section, we evaluate the uncertainty reductions of the neutron multiplication factor (k_{eff}) in the PWR core. The k_{eff} value with the Erbia is 1.0072 and that without the Erbia is 1.0479. The calculated Erbia worth is $3.856\times10^{-2}\ \Delta k/k$. Table 4 shows the comparison of the prediction uncertainty and the uncertainty reduction by the present method, the bias factor method and the conventional method without experimental data.

TABLE 4. COMPARISON OF PREDICTION UNCERTAINTIES AND UNCERTAINTY REDUCTIONS FOR k_{eff} IN A PWR CORE

	Uncertainty (%)	UR
Present method	0.322	0.865
Bias factor method	0.392	0.801
Case without experimental data	0.879	0.000

When one uses the present method, the uncertainty of k_{eff} is reduced to 0.322% $(\Delta k / k)$, and the uncertainty reduction is 0.865. Compared to the UR of 0.801 for the bias factor method, the uncertainty reduction for the present method is improved. Figure 14 shows the components of the prediction uncertainty for the present method and the bias factor method. We can see that for the present method, the Erbia worth uncertainty is reduced compared to the bias factor method. Therefore, the total prediction uncertainty of the k_{eff} by the present method is reduced compared to the bias factor method.

In addition, compared to the case of the blending machine, the contribution becomes small. This is because the variance of k_{eff} is obtained by $\Delta G V \Delta G$, when ΔG is the sensitivity coefficient difference. And the sensitivity coefficients for the PWR core are similar to those for KUCA (see Figure 15). The neutron spectrum is shown in Figure 16.

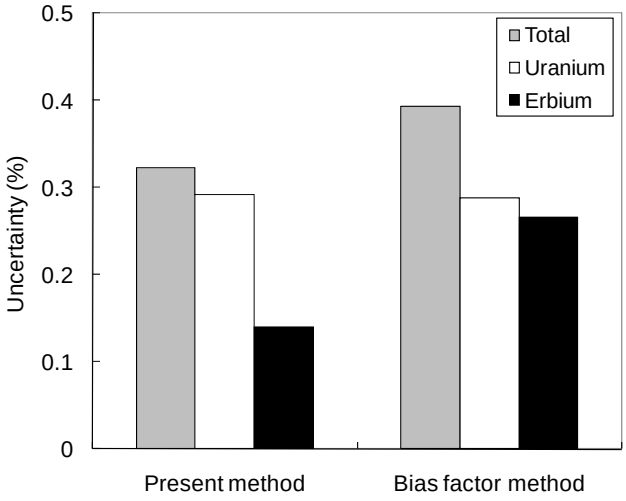

FIG. 14. Comparison of prediction uncertainty of keff in the PWR core.

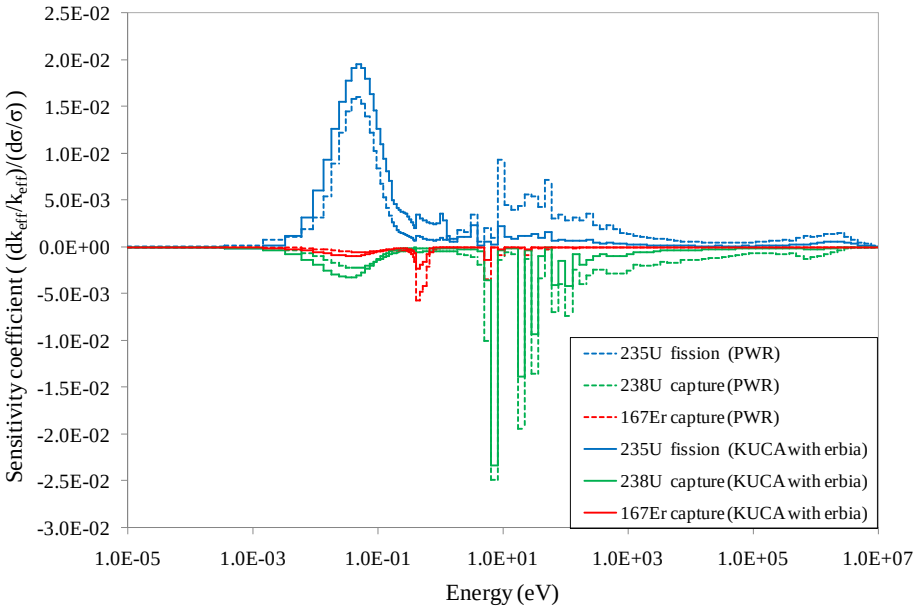

FIG. 15. Sensitivity coefficients of keff for a PWR core and KUCA.

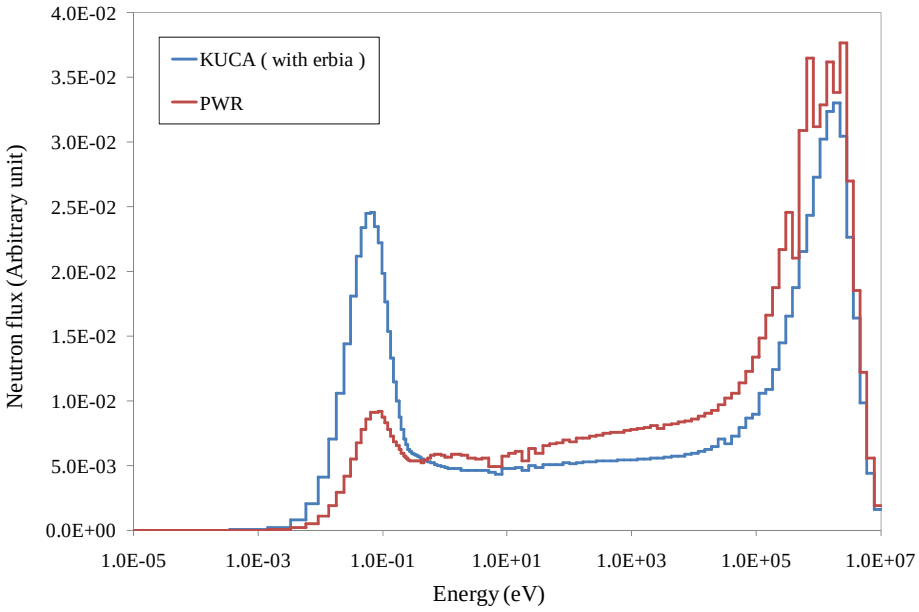

FIG. 16. Comparison of neutron spectrum.

4. Conclusion

A new method was proposed by combining the generalized bias factor method and the cross section adjustment method. The present method was applied to evaluate the prediction uncertainty of neutronics characteristics of the blending machine and the PWR core with Erbia bearing fuel. The uncertainty of the erbium for the target blending machine and the PWR core were reduced by means of the cross section adjustment using Erbia worths from a critical mock-up core.

The prediction uncertainties of the k_{eff} were evaluated using the experiment data of the Erbia worths obtained from KUCA experimental data.

In the blending machine (H/U=0.0), the uncertainty reduction of the k_{eff} by the present method was 0.604. On the other hand, when using the bias factor method, the uncertainty reduction was 0.555. The uncertainty reduction by the present method is slightly larger than that by the bias factor method though the uncertainty of erbium is significantly reduced by the present method. This is because the uncertainty of uranium has a large contribution and the sensitivity coefficients of k_{eff} with respect to uranium cross sections for the generalized bias factor method are much different from those for the blending machine.

In the case of H/U=1.0, the uncertainty reduction by the present method was 0.760. Using the bias factor method, the uncertainty reduction was 0.593. The prediction uncertainty was significantly reduced by the present method. The result indicated that the prediction uncertainties of the neutronics characteristics in fuel fabrication processes loaded with Erbia bearing fuel were improved by the present method.

The uncertainty reduction of the k_{eff} in the PWR core was 0.865 by the present method. On the other hand, when using the bias factor method, the uncertainty reduction was 0.801. The result indicated that the prediction uncertainty of the neutronics characteristics in the PWR core was improved by the present method.

This method can be applied to other cases such as loading a new burnable poison or TRU.

ACKNOWLEDGEMENT

This work is supported by the Innovative and Viable Nuclear Energy Technology (IVNET) development framework of the Ministry of Economy, Trade and Industry (METI), in Japan.

REFERENCES

[1] YAMASAKI, M., et al., Current status of development of Erbia-bearing super high burnup fuel, (Proc. ICAPP'07), Nice Acropolis, (2007), [CD-ROM].
[2] KAMEI, T., YOSHIDA, T., Error due to nuclear data uncertainties in the prediction of large liquid-metal fast breeder reactor core performance parameters, Nucl. Sci. Eng. **84**, (1983), p.83.
[3] TAKEDA, T., YOSHIMURA, A., Prediction uncertainty evaluation methods of core performance parameters in large liquid-metal fast breeder reactors, Nucl. Sci. Eng. **103**, (1989), p.157.
[4] SANO, T., TAKEDA, T., Generalized bias factor method for accurate prediction of neutronics characteristics, J. Nucl. Sci. Technol. **43**, (2006), p.1465.
[5] TAKEDA, T., et al., Analysis of uncertainty reduction of factor for determining critical mock-up of an innovative long-life fast reactor, Proc. of ICAPP'05, Seoul, (2005) p.5444.
[6] OKUMURA, K., et al., SRAC95 : General purpose neutronics code system, JAERI-Data/Code 96–015, Japan Atomic Energy Research Institute, (1996), in Japanese.
[7] SHIBATA, K., et al., Japanese Evaluated Nuclear Data Library Version 3 Revision-3 : JENDL-3.3, J.Nucl.Sci.and Technol. **39**, (2002), p.1125.
[8] HARA, A., TAKEDA, T., et al., SAGEP : two-dimensional sensitivity analysis code based on generalized perturbation theory, JAERI-M 84–065, Japan Atomic Energy Research Institute, (1984), in Japanese.
[9] GARBER., D., ENDF/B Summary Documentation, BNL-17541, 2nd Edition, (1975).
[10] ROSE, P., et al., ENDF-201, ENDF/B-VI Summary Documentation, MOD1 New Evaluation (ENDF/B-VI) 4th ed., BNL-NSC-17541, Brookhaven National Laboratory, (1991).
[11] The JEFF-3.0 Nuclear Data Library, JEFF Report **19**, (2005).
[12] UNESAKI, H., Private communication.
[13] UNESAKI, H., et al., Development of Erbia-bearing super high burnup fuel (2) preliminary experiment using KUCA, 2006 Fall Meeting of the Atomic Energy Society of Japan, K08 (2006), in Japanese.

Investigation of Liquid Metal Bonded Hydride Fuels for LWRs — A Review

K.A. Terrani[63], M. Balooch[64], D.R. Olander[65], E. Greenspan[66]

Abstract. Hydride fuels have been proposed for power production applications in LWRs. The fuel consists of uranium-zirconium hydride pellets clad with Zircaloy tubing. The fuel-cladding gap is filled with a liquid lead-tin-bismuth alloy. Incentives for hydride fuel incorporation into LWRs are briefly reviewed followed by a detailed discussion of material properties, steady-state and transient behaviour, and irradiation effects on hydride fuels. The discussion is based on historical data from the SNAP program and General Atomics' TRIGA reactors and recent research conducted at Universities of Tokyo and California, Berkeley.

1. Introduction

Hydride fuels generally consist of fissile/fertile materials that are mixed into a metal hydride matrix. Historically the most common type of hydride fuel is that of metallic uranium particles dispersed in a zirconium hydride matrix, $(U,Zr)H_x$. This fuel was originally developed for the Systems for Nuclear Auxiliary Power (SNAP) program by National Aeronautics and Space Administration (NASA) starting in the late 1950s [1]. A nuclear-reactor-powered satellite (SNAP-10) was launched into the space in 1965. During the same period General Atomics developed and commissioned its TRIGA type research reactors with a similar hydride fuel.

Both of the above reactor designs took advantage of the benefits gained from comingling of the moderator and the fuel; most notably the high power density and the strong negative fuel temperature reactivity feedback. Hydride fuels however, have never been used for high-power applications such as the oxide fuels utilized in commercial nuclear power plants. The fuel designs and performance parameters of oxide and hydride fuels are compared in Table I. The SNAP-8 [2] and the Romanian TRIGA [3] were (are) high-power versions of the SNAP and TRIGA-type reactors. Due to the advantages of hydride fuel over uranium oxide, a new type of hydride fuel explicitly designed for commercial Light Water Reactors (LWR) is proposed [4].

Recent research activities on potential improvements accrued by incorporation of hydride instead of oxide fuels in LWRs were supported through U.S. Department of Energy's (DOE) NERI [4]. This work was performed in a partnership between the University of California, Berkeley, the Massachusetts Institute of Technology, and the Westinghouse Electric Company. The research covered various disciplines including neutronics, thermal hydraulics, fuel-rod vibration and mechanical integrity, and economics. The proposed fuel rod design and properties have been previously discussed in detail [5]. The fuel element consists of $U_{0.32}ZrH_{1.6}$ fuel clad in Zircaloy with a liquid lead-tin-bismuth (Pb-33wt%Sn-33wt%Bi) alloy filling the fuel-cladding gap.

A brief review of improvement possibilities in the performance of PWRs and BWRs by fuelling them with hydride rather than oxide fuel based on this recent body of work is given in Section 2. In the following section, fundamental materials properties of hydride fuel needed for utilization in LWRs will be examined. This review is based on historic data as well as the recent work performed at the nuclear materials laboratory at University of California, Berkeley. This paper aims to provide a comprehensive picture regarding the feasibility of incorporating hydride fuels into existing and new LWRs.

[63] University of California, Berkeley, United States of America.
[64] University of California, Berkeley, United States of America.
[65] University of California, Berkeley, United States of America.
[66] University of California, Berkeley, United States of America.

TABLE 1. PROPERTIES AND OPERATING PARAMETERS FOR VARIOUS HYDRIDE AND OXIDE FUELLED REACTORS

Reactor Type	SNAP-8	Romanian TRIGA	LWR Hydride	LWR Oxide
Fuel Type	U-$ZrH_{1.6}$	U-$ZrH_{1.6}$	U-$ZrH_{1.6}$	UO_2
U-235 enrichment%	93	19.7	12.5	< 5
Weight fraction U	0.10	0.45	0.45	-
U/Zr atomic ratio	0.04	0.32	0.32	-
Fuel density (g/cm^3)	6.1	7.3	7.3	10.5
Uranium Density 10^{21} (cm^{-3})	1.4	5.7	5.7	24.4
Clad diameter (cm)	1.4	1.3	1.2	1.2
Clad material	Hastelloy	Incoloy 800	Zircaloy	Zircaloy
Coolant	NaK	Water	Water	Water
Inlet coolant temperature (ºC)	520	60	290	290
Max fuel temperature (ºC)	620	820	550	1450
Power (MW(t))	0.6	14	4000	3800
Average LHR (W/cm)	77	350	175	175
Max LHR (W/cm)	140	800	375	375

2. Incentives for using hydride fuel in LWRs

From 2002 to 2008 the University of California at Berkeley Nuclear Engineering Department in collaboration with MIT, Westinghouse and Argonne National Laboratory with funding from a couple of NERI projects, investigated improvement possibilities in the design and performance of commercial PWRs and BWRs that are fuelled with hydride instead of oxide fuel. An extensive description of the pros and cons of hydride fuel versus oxide fuel for LWR identified in these studies is given in the special issue of Nuclear Engineering and Design that summarizes these projects [4]. Briefly, it was found that hydride fuel can safely operate in PWRs and BWRs having comparable or higher power density relative to typical oxide-fuelled LWRs. The most promising applications of hydride fuel identified are the following.

2.1 PWRs

Use of hydride fuel enables recycling plutonium in PWRs more effectively than is possible with oxide fuel by virtue of a number of unique features of hydride fuel; reduced inventory of ^{238}U and increased inventory of hydrogen. As a result, the hydride-fuelled cores can fission approximately 64% of the loaded plutonium at the first recycle; this is nearly double the fractional transmutation of plutonium attainable with MOX fuel [6,7]. The subject fuel has the geometry of the optimized PWR hydride fuel and plutonium is incorporated into the fuel as a separate PuH_2 phase making a PuH_2-$ZrH_{1.6}$ fuel. Plutonium, as opposed to uranium, forms a stable hydride with similar crystal structure to that of zirconium hydride.

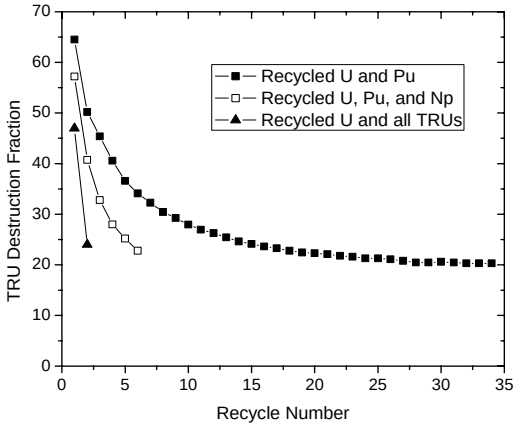

FIG. 1. TRU destruction fraction as a function of recycle number [6].

Moreover, the hydride fuel PuH_2-$ZrH_{1.6}$ allows multi-recycling of plutonium in PWRs an unlimited number of times when uniformly loaded in all fuel assemblies in the core. The number of recycles feasible with MOX fuel is highly limited because the coolant void coefficient becomes positive after the first or second recycle. This unique feature of hydride fuels is due to the incorporation of a significant fraction of the hydrogen moderator in the fuel thereby reducing the effect of spectrum hardening due to coolant voiding accidents; the large void reactivity coefficient remains negative. It was additionally found that hydride fuels allow multi-recycling of Pu+Np at least 6 times, before getting a positive void reactivity feedback. The number of recycles for the entire TRU stream is limited by positive large void reactivity feedback to 2 or 3 times. Figure 1 shows the TRU destruction capability for such cores with different constituents loading taking into account the reactivity coefficient constraints.

2.2 BWRs

Oxide fuelled BWRs typically require approximately 1.5 times higher coolant-to-fuel volume ratio than their PWR counterparts. This is due to the relatively large coolant void fraction at the upper part of the core. Incorporating part of the moderator within the fuel, as in the case for hydride fuels, enables elimination of the dedicated moderator volumes within the fuel bundle, including water rods, partial length fuel rods, and water gaps not required for control blades insertion. This enables loading more fuel rods per unit core volume while reducing the heterogeneity of BWR fuel bundles, thus achieving flatter pin-by-pin power distribution. Meanwhile the cooled fuel rod surface area as well as the coolant flow cross-section area per given core volume has significantly increased. Figure 2 is one of the examples of such simplified BWR bundle design utilizing hydride fuels although non-uniform enrichment levels are still desirable due to the presence of water gaps when control blades are removed.

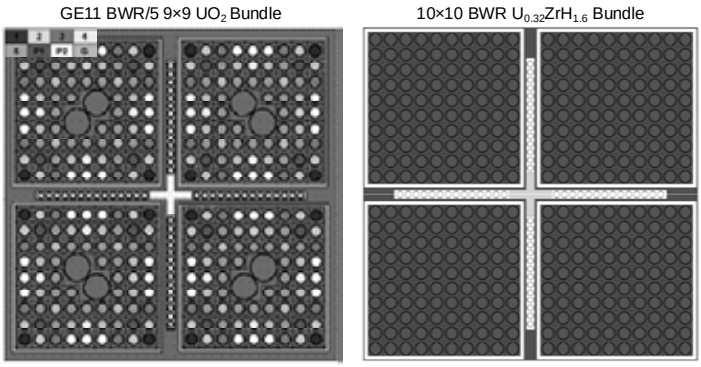

FIG. 2. GE11 BWR/5 oxide fuel bundle; 1-5, P1/P2, and G denote various enrichment, partial fuel length and gadolinia containing rods respectively (left). Uniform enrichment BWR hydride fuel bundle (right) [8].

The net result is up to 40% increase in the core power density and a reduction of the cost-of-electricity. Selected design and performance characteristics of several hydride fuelled bundles were compared with those of oxide fuelled bundles when the power is not constrained by the coolant pressure drop. For identical minimum critical heat flux ratio (MCHFR) and coolant exit quality (χ_{out}), the best performing hydride bundle design can safely operate at ~40% higher power than the reference 10x10 oxide fuel bundle; both bundles occupying the same volume. The corresponding peak hydride fuel rod temperature is only 563°C; significantly lower than the steady-state limit of 750°C. In the meantime the coolant pressure drop at this power level needs to be approximately twice of the nominal value (0.147 MPa) that could challenge the structural integrity of the core components [4].

3. As-fabricated hydride fuel properties

3.1 Fuel processing and structure

Hydride fuel fabrication involves alloying the metallic components of the fuel followed by a hydriding procedure. The uranium-zirconium alloys with the desired compositions are generally made by arc melting the metals together. The metal alloy then undergoes bulk hydriding at high temperatures (~ 700-900ºC) where the zirconium hydride phase is formed. The final fuel consists of metallic α-uranium phase (orthorhombic — *Cmcm* space group) and the δ-zirconium hydride (cubic — $Fm\overline{3}m$ space group) phase with H/Zr = 1.6. A typical microstructure of the fuel is shown in Figure 3; the metallic uranium particles appear as the dark regions surrounded by the bright zirconium hydride matrix. Historically HEU (high enriched uranium) was used in hydride fuel fabrication and the weight fraction of the metallic component was ~10wt%. Following termination of the SNAP program, low-enriched-uranium TRIGA fuel was introduced. The proposed LWR fuel contains the same weight fraction of uranium (45wt%) as current TRIGA fuel.

Uranium hydride (UH_3) is unstable at fuel processing temperatures and the hydrogen selectively leaches out zirconium atoms in the metallic solid solution. The hydrogen-to-zirconium ratio of the hydride matrix is selectively processed by close control of temperature and hydrogen gas pressure. Temperature, pressure, composition equilibria have been extensively studied for zirconium hydride and thermodynamic relationships relating these properties have been developed [10] (Figure 4, equation (1)). In equation (1) *C* is the H/Zr ratio.

$$p_{H_2-eq}\ [\text{atm}] = \left(\frac{C}{2-C}\right)^2 \exp\left(8.01 + 5.21C - \frac{172[\text{kJ}]}{RT[\text{K}]}\right) \qquad (1)$$

Other types of hydride fuels that have received considerable attention during the past decade are uranium-thorium-zirconium hydrides [12,13]. The fuel fabrication involves similar steps as described earlier. The microstructure however is quite different since a third ternary thorium-zirconium hydride ($ThZr_2H_x$ — cubic — $Fd\overline{3}m$ space group) phase is present (Figure 3). Similarly, the hydrogen stoichiometry is fixed by controlling the temperature and hydrogen gas pressure. However the hydrogen-to-metal ratios in the zirconium hydride and the thorium-zirconium hydride are not independent of one another, since the hydrogen activity in the two phases must be equal. Temperature, pressure, composition equilibria have also been experimentally studied for thorium-zirconium hydrides [14].

3.2 Hydrogen diffusion in the hydride matrices

The diffusion coefficient of hydrogen is an important parameter for timing the hydriding step during the fuel-fabrication process. In addition, fuel-performance modelling for steady-state and transient conditions requires this property. The diffusion coefficient of hydrogen in zirconium hydride has been thoroughly studied by pulsed-field-gradient NMR (nuclear magnetic resonance) [15]. Recently the hydrogen diffusivity in thorium-zirconium hydrides has been measured by means of quasielastic neutron scattering at the Spallation Neutron Source [16]. The Arrhenius dependence of the diffusion coefficient for the two hydride matrices is shown in Figure 5.

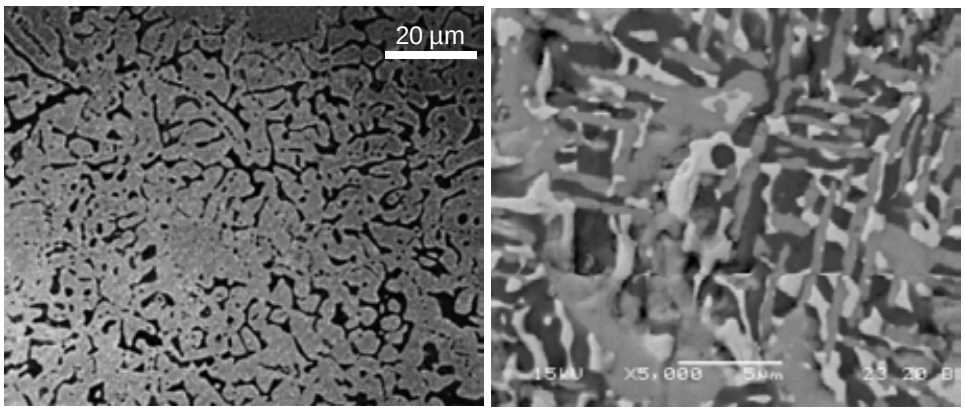

FIG. 3. Optical micrograph of the microstructure of U(45wt%)-$ZrH_{1.6}$ fuel. Uranium appears as the dark phase [9] (left). Backscattering electron image of $(U_4Th_2Zr_9)H_{1.5}$ fuel microstructure. α-U, $ThZr_2H_7$ and δ-$ZrH_{1.6}$ phases appear as the brightest to the darkest regions respectively [13] (right).

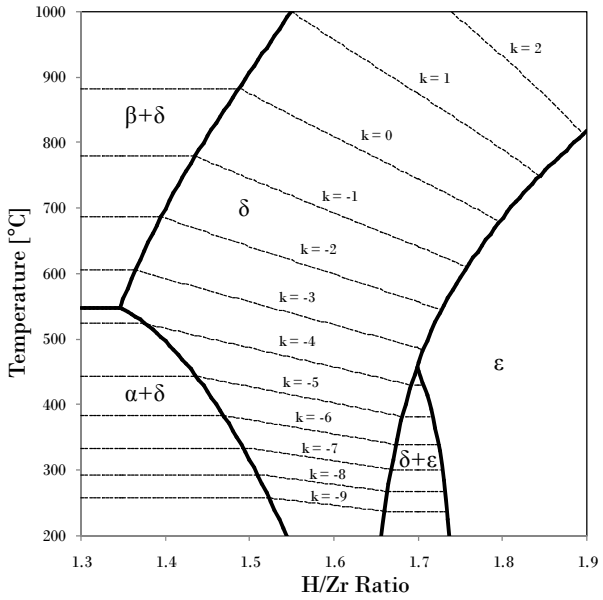

FIG. 4. Zirconium-hydrogen phase diagram [11] equilibrium H_2 isobars labelled as $P_{H2}=10^k$ atm [10].

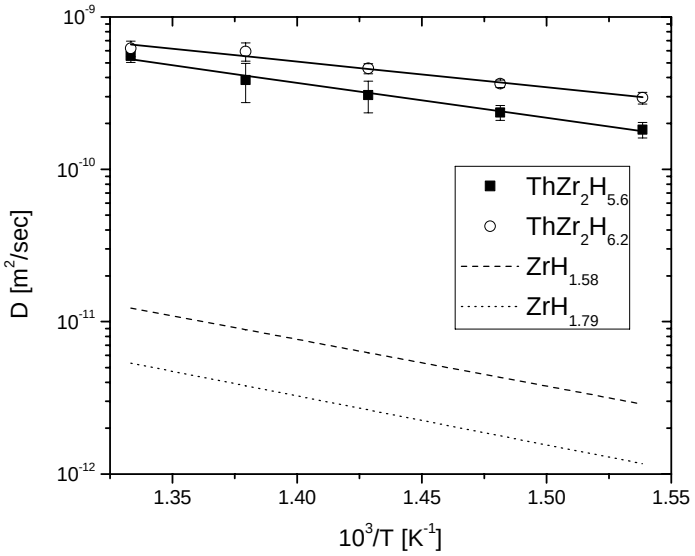

FIG. 5. Hydrogen diffusion coefficient in zirconium hydrides and thorium-zirconium hydrides [15,16].

3.3 Thermal properties

$(U,Zr)H_x$ fuels enjoy ~5 times higher thermal conductivity than that of oxide type. This greatly reduces the temperature gradient across the fuel. Thermal conductivity and heat capacity of the uranium-zirconium hydride fuel as a function of temperature and H/Zr ratio have been measured across a broad range of those parameters and presented in Figure 6 [17]. Similar properties have been extensively studied for U-Th-Zr hydrides and reported in Ref. [18]. Figure 7 shows the thermal conductivity as a function of temperature of various unirradiated hydride fuels as well as oxide fuel at different burnups.

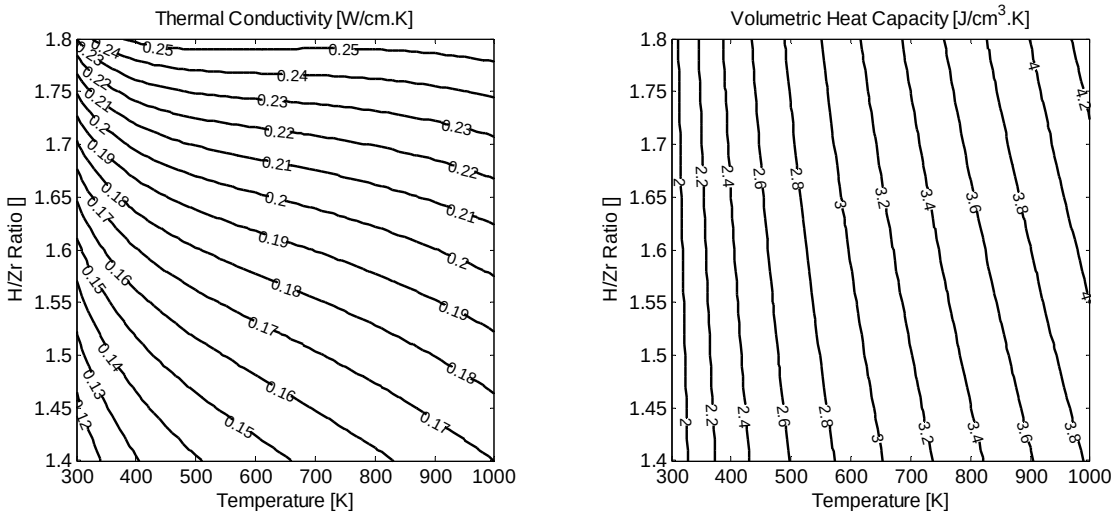

FIG. 6. Thermal conductivity and volumetric heat capacity of as-fabricated U(45wt%)-$ZrH_{1.6}$ as a function of temperature and hydrogen stoichiometry [17].

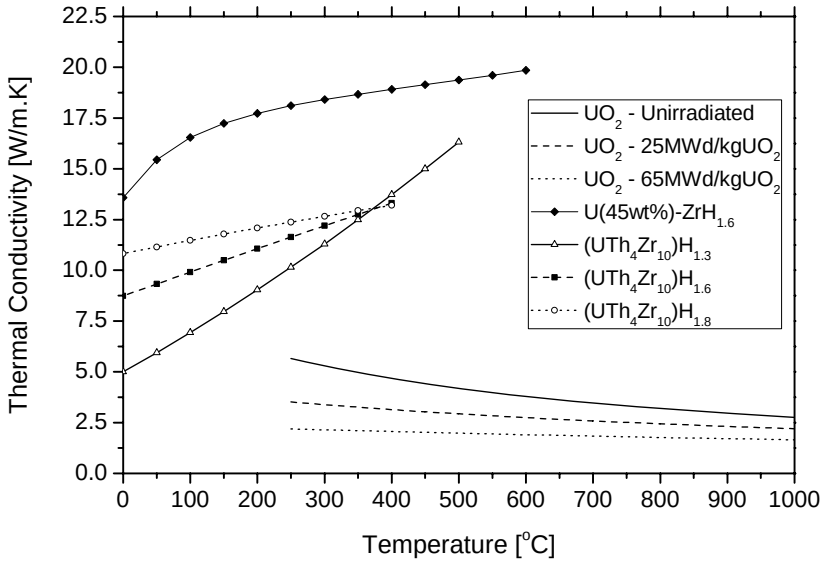

FIG. 7. Thermal conductivity of various fuels as a function of temperature [17–19].

3.4 Mechanical properties

Elastic properties of hydride fuel constituents have been measured separately in as-fabricated fuel by nanoscale indentation at UC Berkeley as shown in Figure 8 [13]. Elastic modulus of zirconium hydride is a relatively weak function of hydrogen stoichiometry and is studied in detail in Ref. [20]. The elastic modulus of thorium-zirconium hydride is a strong function of hydrogen-to-metal ratio (Figure 9). Hydride fuels are classified as metal-ceramic matrix composites and are very brittle.

3.5 Liquid-metal gap filler

A lead-tin-bismuth alloy (Pb-33wt%Sn-33wt%Bi) that is liquid during reactor operation (120ºC melting point) is proposed as a substitute for the conventional helium-filled fuel-cladding gap. Thermal conductivity of the liquid-metal (LM) is approximately two orders of magnitude larger than that of helium gas, effectively eliminating the temperature drop across the gap during operation. This permits designing fuel rods with larger fuel-cladding gaps that can eliminate pellet-cladding mechanical interaction (PCMI). Utilization of liquid metal also prevents formation of local hot spots on the cladding and the fuel (i.e. when the fuel is chipped or cladding is dented or ballooned). The fuel temperature is also reduced by eliminating the gap temperature drop. The liquid metal does not react with either oxide or hydride fuels or the coolant water and adequately wets the surface of both fuel and the Zircaloy cladding. Fabrication of full-length liquid-metal-bonded oxide fuels has been successfully demonstrated [21].

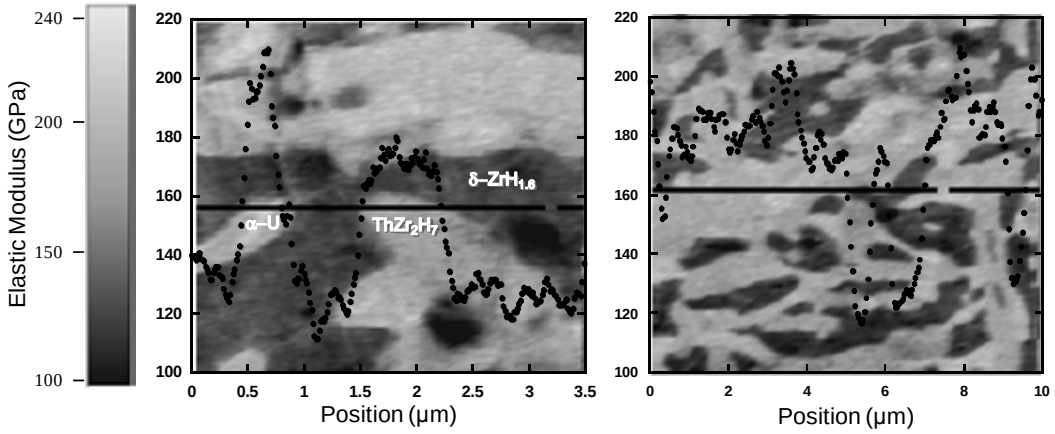

FIG. 8. Elastic modulus of $(U_4Th_2Zr_9)H_{1.5}$ constituents determined by nanoscale dynamic stiffness mapping [13].

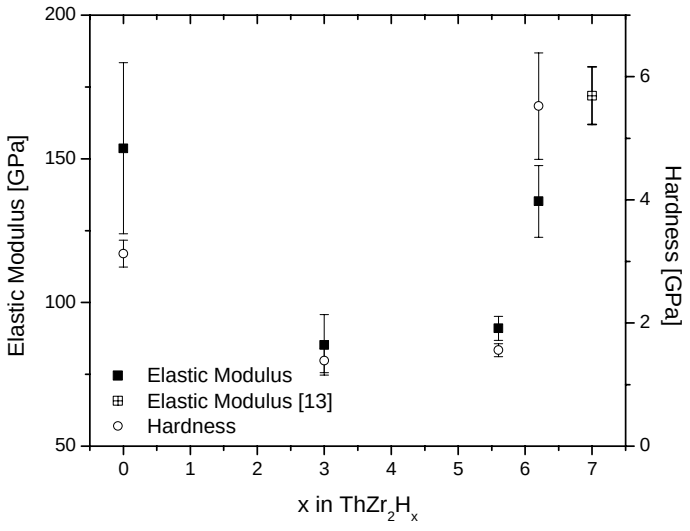

FIG. 9. Elastic modulus and hardness of $ThZr_2H_x$ determined by nanoscale indentation.

3.6 Steady-state fuel behaviour

Although the temperature gradient in the fuel is small, hydrogen redistribution takes place due to the large heat of transport (5.3 kJ/mole) associated with thermal diffusion of hydrogen in zirconium hydride. Hydrogen tends to accumulate in the cold regions (fuel surface) [22]. The combined gradients in temperature and hydrogen concentration induce stresses across the fuel-pellet radius that are very different from what is calculated for oxide fuel. In the hydride fuel both the azimuthal and axial stresses are strongly compressive at the surface and tensile at the fuel center. Figure 10 shows temperature and hydrogen concentration profiles and the axial stress (largest stress component) across the fuel radius at different operating powers. The fuel-cladding gap is filled with liquid metal and the coolant temperature is at 300ºC.

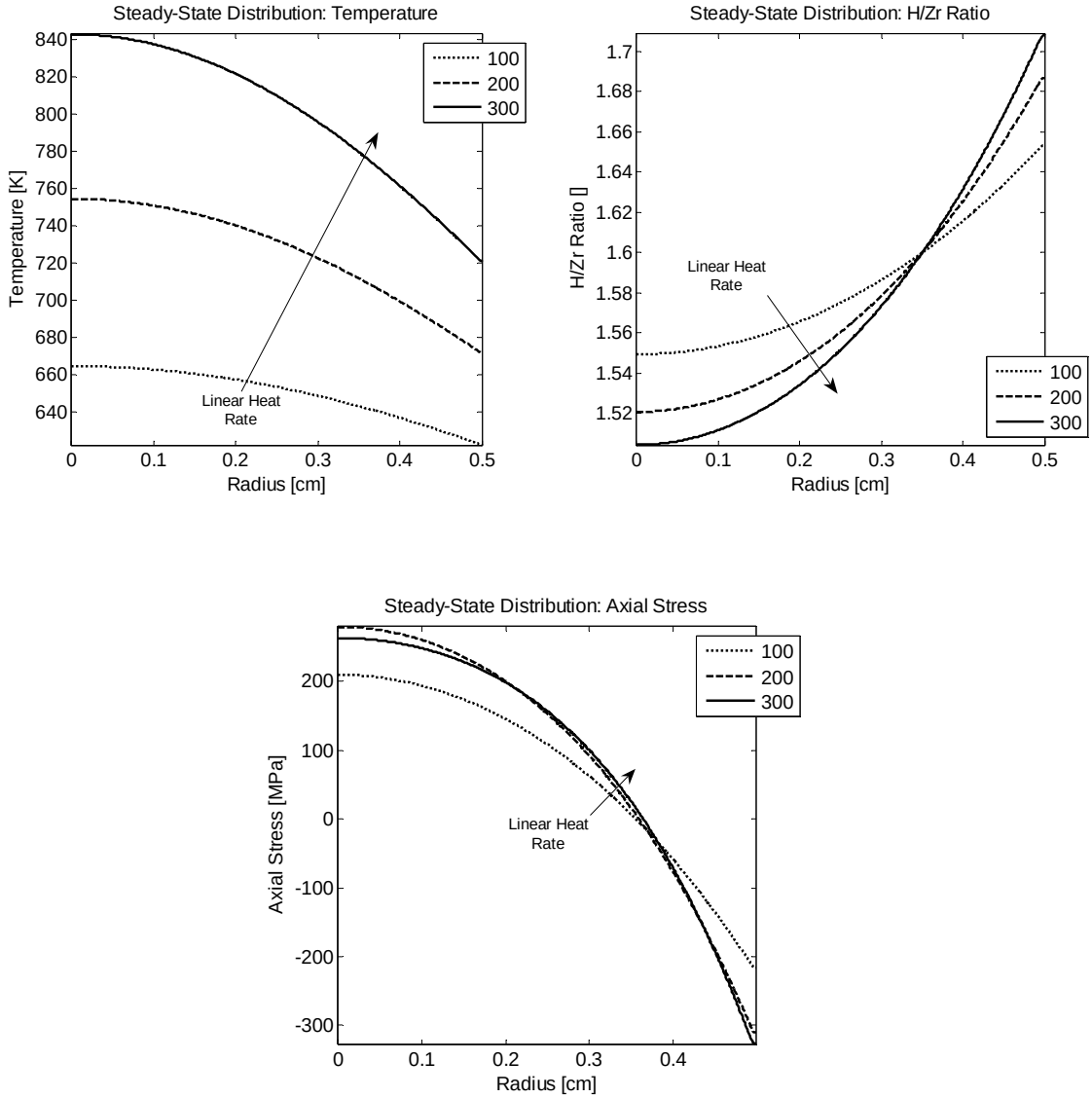

FIG. 10. Steady state temperature, hydrogen concentration and axial stress distribution across U(45wt%)-ZrH1.6 fuel pellet at different operating powers [17].

3.7 Transient fuel behaviour

The behaviour of the fuel in a simple transient is simulated by coupling the time-dependent heat conduction and hydrogen diffusion equations [17]. Starting from steady-state operation at a linear heat rating of 300 W/cm, the transient consisted of a square power pulse twice the nominal LHR for the duration of 2.5 seconds. The surge in power was then followed by a SCRAM (power dropped to 5%) while the coolant temperature remained constant during the process. The evolution in the temperature and stress across the fuel are shown in Figure 11 (negligible hydrogen redistribution took place). The fuel temperature increases quickly in response to the power pulse while the magnitude of the temperature remains within the safe operational window. The stress response is remarkable in the sense that the stress across the fuel (radial, azimuthal, and axial components) is reduced during the transient due to larger thermal stresses that counteract expansion in regions of high hydrogen concentrations.

3.8 Compatibility with Zircaloy cladding

Due to its superior neutronic and corrosion properties, Zircaloy is the cladding of choice for LWR fuel rods. Zirconium, however, is a strong getter of hydrogen and significantly embrittles upon reaction with hydrogen. It is therefore essential to limit hydrogen transport from the fuel to the cladding. Liquid-metal could be potentially utilized for this purpose and was preliminarily investigated [23]. Hydrogen has low solubility in liquid-metal (few hundred ppm at 450ºC) and its diffusion coefficient is fast, comparable to what is reported for hydrogen diffusion liquid tin [24]. Samples of Zircaloy were pressed against hydride fuel immersed in a pool of liquid metal at 375ºC at different contact pressures for a period of one month. For one of the samples, a gap of 25μm was maintained between the hydride fuel and the cladding. When contact was made between the fuel and the cladding, regardless of the contact pressure, cladding underwent hydriding and cracking was readily observed. The Zircaloy sample that was separated from the fuel by the thin liquid-metal-filled gap appeared to remain intact and damage-free (Figure 12). Diffusion in the liquid metal is fast and the rate- limiting step responsible for hydrogen transport from the fuel to the cladding is unknown (in the case that a liquid metal filled gap is maintained between the fuel and the cladding). Currently experiments are underway to examine compatibility of hydride fuel with the cladding when in addition to liquid metal, a thin layer (~2 μm) of zirconium oxide (tetragonal) is present on the Zircaloy surface.

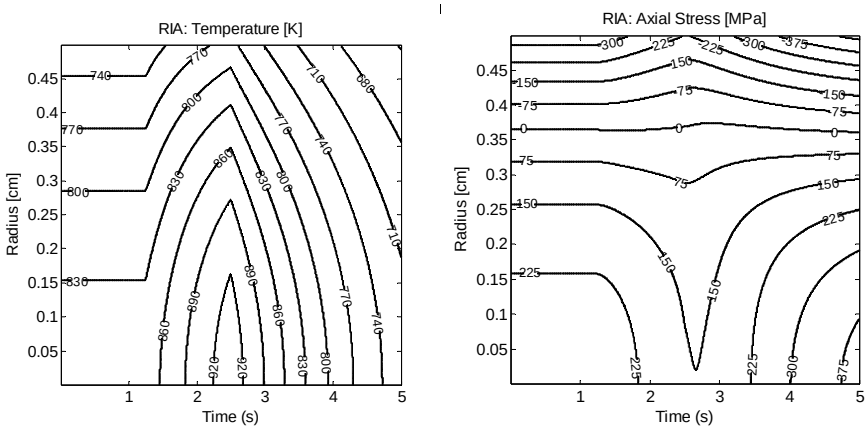

FIG. 11. Fuel temperature and axial stress response during the transient [17].

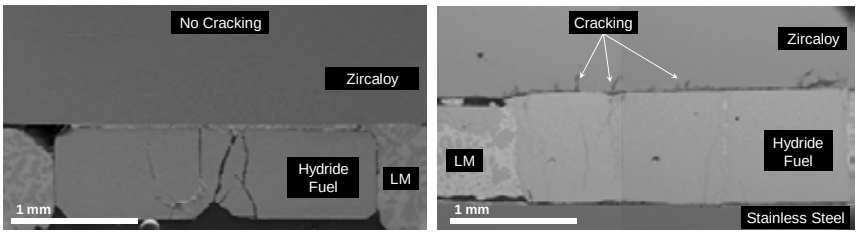

FIG. 12. Hydride fuel-Zircaloy cladding interface: undamaged cladding adjacent to 25μm LM filled gap (left). Damaged Zircaloy at 120MPa contact pressure with hydride fuel (right) [23].

3.9 Kinetics of Hydrogen desorption and adsorption

Kinetics of hydride fuel dehydriding when immersed in liquid metal is unknown. However hydrogen desorption and adsorption kinetics from and on zirconium hydride when exposed to a gaseous phase have been investigated [25]. This information is essential for determining optimum fuel processing methods and also for predicting fuel behaviour during reactor operation. Two different methods have been utilized to study the kinetics of hydrogen desorption and adsorption on zirconium hydride; one involves thermogravimetric techniques while the other is a measurement of hydrogen pressure buildup due to dehydriding in a closed system. The kinetics of hydrogen desorption and adsorption are both surface limited and are zeroth-order with respect to hydrogen concentration. As expected the adsorption kinetics show a first-order dependence on the hydrogen gas pressure. The Arrhenius dependence of the zeroth-order desorption and adsorption rates constants are determined by the experimental techniques described above and are shown in Figure 13.

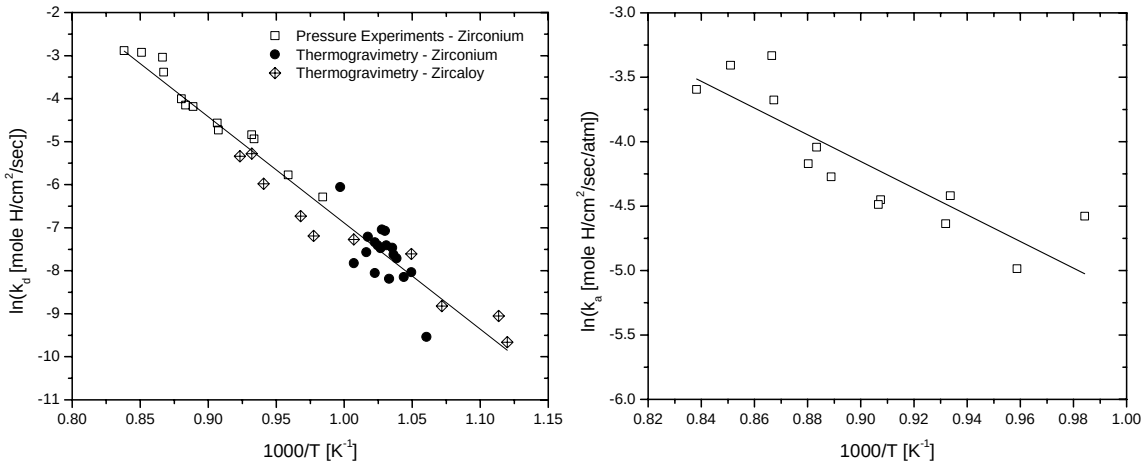

FIG. 13. Arrhenius rates of hydrogen desorption (left) from and adsorption (right) on δ-$ZrH_{1.6}$ [25].

4. Irradiation effects and behaviour

4.1 Neutron flux and power distributions

Since the moderator is bound to the fuel, the neutron spectrum within the hydride fuel differs significantly from oxide fuels. In the latter, thermal neutrons, generated by moderation that takes place in the adjacent coolant, are present at high concentration at the periphery of the fuel; however their population quickly decreases in the central regions. This causes deviations from a uniform power profile distribution and leads to phenomena such as the rim effect. The presence of hydrogen within the fuel mitigates this issue; almost uniform power is maintained across the fuel radius. The difference in power from the fuel surface to center in hydride fuels is less than 6% as opposed to ~15% in oxide fuels. As shown in Figure 14, the neutron spectra at different radial locations are also almost equivalent across the radius of a hydride fuel. The power profile and radial neutron spectra were calculated using a simple pin cell model in MCNP (Monte Carlo N-Particle Transport Code).

4.2 Swelling under irradiation

Most of the data describing swelling behaviour of hydride fuels dates back to the SNAP program [26]. An early-stage ‘offset’ swelling observed prior to a burnup of 0.1% FIMA (fissions per initial metal atom) is very large in magnitude and strongly temperature- and flux-dependent. Following this stage, a temperature- and flux-independent swelling linear with respect to burnup is present due to fission product formation (~3% per%FIMA) [5]. SNAP tests utilized sophisticated experimental apparatus where the effects of flux and temperature on swelling rate were separated. The evolution of swelling as a function of burnup at various flux and temperature points is shown in Fig 15. The influence of flux (burnup rate) on the offset swelling rate is opposite of what is observed in swelling of metals

where swelling rate (due to void growth) is directly proportional to square root of flux [27]. Offset swelling also disappears at temperatures below 650ºC. Zirconium hydride (δ and ε phases) irradiated up to very large fluences showed none or very negligible swelling [28]. In the SNAP studies offset swelling is attributed to voids that form near the uranium particles in the hydride matrix.

Swelling in hydride fuels is heterogeneous, while that in oxide fuel is homogeneous. Fission in hydride fuels is limited to the uranium particles that are distributed in the hydride matrix. The dominant portion of atomic displacements in the hydride matrix can be attributed to the high-energy fission fragments that escape from the uranium particles and cause significant damage at particle's periphery. Understanding the underlying mechanism of this phenomenon is necessary in order to assess the applicability of SNAP swelling data to predicting swelling behaviour of the proposed LWR-type hydride fuel. The uranium particles in the SNAP fuel were ~ 5μm in diameter, ~40μm apart and 93% enriched in U-235. As shown in Figure 1, the U(45wt%)-$ZrH_{1.6}$ fuel consists of larger uranium particles placed much closer to one another. The U-235 enrichment in the proposed fuel is 12.5% which implies significantly less fission events within each uranium particle. These differences could greatly alter the extent and distribution of those local phenomena that collectively produce the macroscopically observed offset swelling.

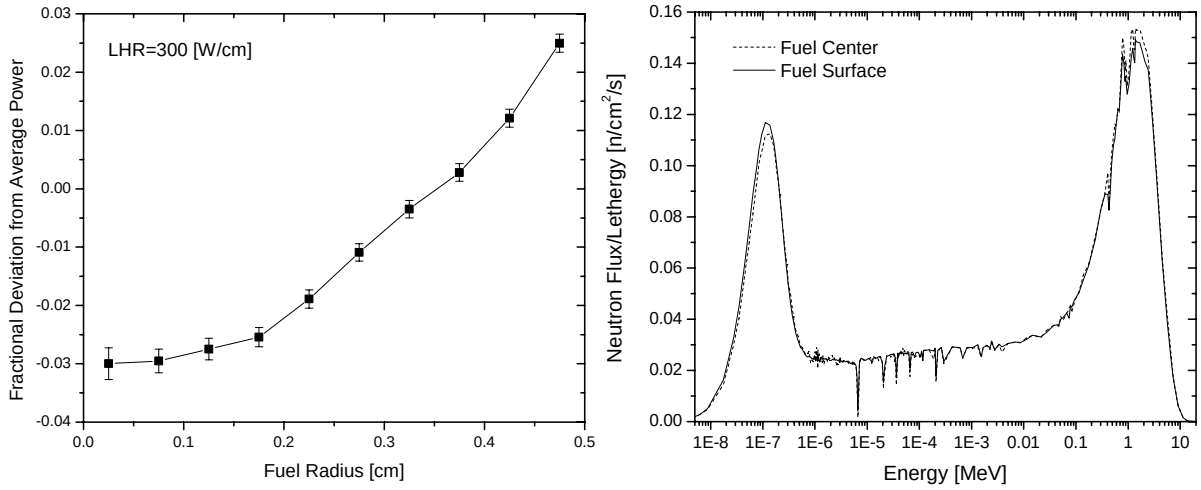

FIG. 14. MCNP calculation of: Power distribution across the fuel radius at LHR = 300 W/cm (left). Neutron flux spectra at the fuel surface and center (right).

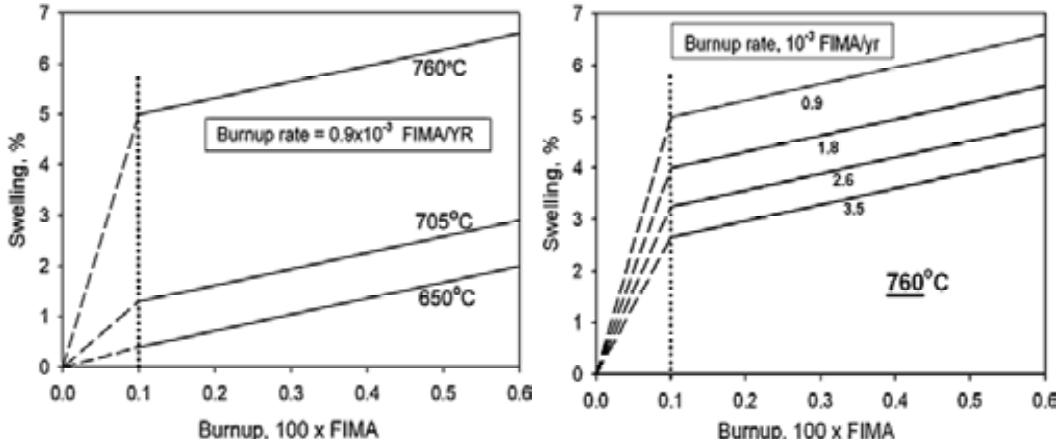

FIG. 15. Swelling behaviour of SNAP Fuel (U(10wt%)$ZrH_{1.6}$) as a function of burnup at various temperatures and burnup rates [5].

4.3 Fission gas release (FGR)

Fission gas release in uranium-zirconium hydride fuels has been investigated by two different experimental means. The first method involves in-pile irradiation experiments in which the sample temperature is controlled by electrical heating. Air or helium gases are used to sweep any released gaseous species to a trap where gamma ray measurements are conducted. The results of these experiments represent the equilibrium ratio between the release rate and birth rate of the gaseous fission products. The second set of experiments involves post-irradiation annealing conducted at different time durations and temperatures on samples that were initially irradiated up to ~2×10^{13} fissions/cm^3 at room temperatures. The results of the annealing experiments are the ratio of the total amount of fission gas released during the annealing (corrected for decay) to the total extent produced during the irradiation. Figure 16 shows the summary of all the data generated through both of the described procedures. All the data is from experiments conducted at General Atomics, with exception of 10 wt%U samples in the post-irradiation annealing experiments that is from the SNAP program [29]. Based on the available in-pile irradiation data, excellent fission gas retention is observed up to temperatures around 800ºC. The observed release-to-birth-rate ratio is smaller than would be calculated due to recoil according to Eq. (2) [27]:

$$\frac{R}{B} = \bar{P}\left(\frac{S}{V}\right)\mu \qquad (2)$$

where $\bar{P}$, S, V, and μ are the escape probability (~0.25), fuel surface area, fuel volume, and the effective fission product range within the fuel, respectively. The GA specimens had an average surface- to-volume ratio of 0.39. The fission-product range within the fuel is that of 100MeV fission products in uranium and zirconium hydride weighted by their respective volume fractions in the fuel and is ~9μm. The calculated release-to-birth rate ratio could then be calculated as 8×10^{-4}, which is larger than that observed experimentally. At high temperatures it is possible to discern much lower release-to-birth rate ratios for high uranium content fuels. This observation refers back to the discussion regarding the microstructure of LEU fuel as opposed to the HEU fuel, where larger uranium particles effectively contain the fission products at high temperatures.

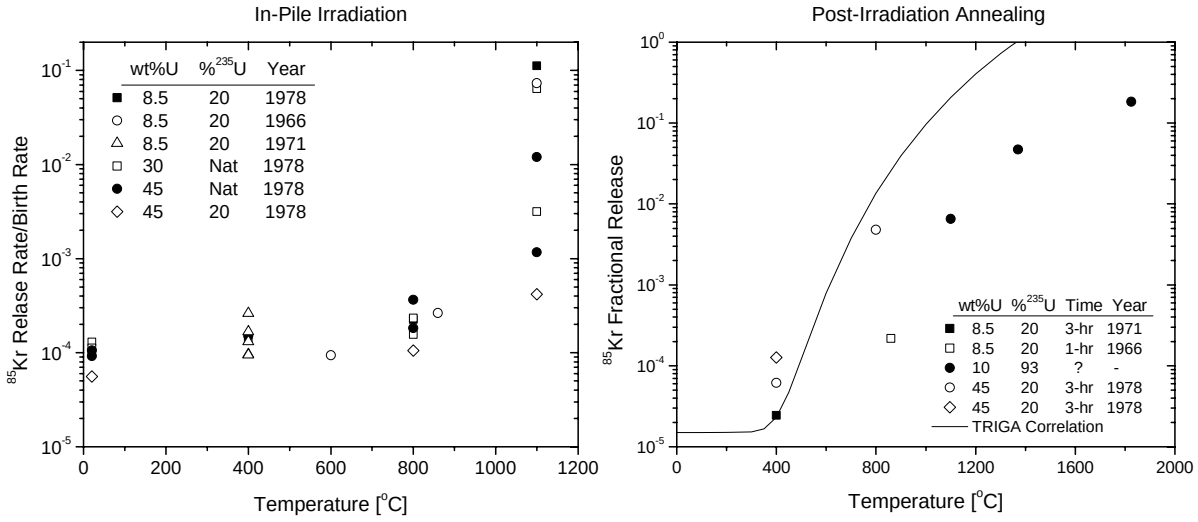

FIG. 16. Fission gas release to birth rate ratio as a function of temperature (left). Fractional fission gas release as a function of post-irradiation annealing temperature (right) [29].

Interpretation of the post-irradiation annealing data is more challenging since different annealing times are compared to one another and detailed description of the SNAP (10wt%-U, 93% enriched U-235) experiments are unknown. The line in the Figure is a conservative empirical correlation developed by General Atomics during the certification process of the TRIGA reactors [29]. Overall very good fission gas retention properties is observed up to temperatures significantly higher than what is expected to be experienced by the fuel during steady state and transient conditions.

4.4 Irradiation effects on U-Th-Zr Hydrides

Two uranium-thorium-zirconium hydrides, $(UThZr_4)H_{1.7}$ and $(UTh_2Zr_6)H_{1.3}$, were irradiated at the Japan Materials Testing Reactor (Japan) [30]. The irradiation temperature and uranium enrichment in the samples are unknown. The samples were investigated by electron microscopy and Vickers micro hardness testing at fluneces of 7.4×10^{22}, 2.2×10^{23}, and 7.4×10^{23} n/m^2 of thermal neutrons corresponding to approximately 0.3, 0.9 and 3.1% of U-235 atom burnup. A maximum of ~15% decrease in hardness was observed at highest dose. No change in dimensions, mass, and microstructure of the samples were observed. The good irradiation performance of the fuels were attributed to their fine microstructure where all the phase boundaries provide strong sink for the produced defects.

5. Conclusions

Hydride fuels potentially offer significant benefits over currently-deployed oxide fuels for LWR operation with minimal change in core design and components. Uranium-zirconium hydrides have successfully operated at higher temperatures and linear heat generation rates than required for operation in LWRs. Use of hydride fuels in today's research reactors continues due to a long track record of successful operation and positive experience. Use of liquid metal gap filler in conjunction with hydride fuels effectively compensates for the relatively large volumetric swelling of hydride fuel and eliminates many of the pellet cladding interaction issues. The result is a high power density fuel that operates at much lower temperature than that of oxide type. Many of the positive features and specific aspects of hydride fuels that have been discussed here portray them as a strong candidates for an advanced fuel in future power-generation applications.

Although a large amount of knowledge is available based on the current and historical data on properties and behaviour of hydride fuels, due to complexity and nature of the nuclear fuel applications, much further work is required. In addition to small-scale laboratory experiments, irradiation of liquid-metal-bonded hydride fuel under conditions reproducing LWR environments is essential in drawing a more comprehensive picture with regards to feasibility of hydride fuel incorporation into LWRs and also building confidence among vendors and utilities in adopting this concept.

REFERENCES

[1] GYLFE, J.D., et al., Evaluation of Zirconium hydride as moderator in integral boiling water super heat reactors, NAA–SR–5943, (1960).

[2] PARKER, T.G., Process development and fabrication of Zirconium hydride hastelloy X clad fuel elements, AI–AEC–13082, (1973).

[3] BRETSCHER, M.M., etal., Transition from HEU to LEU fuel in Romania's 14–MW TRIGA re actor, ANL/CP—74817, (1991).

[4] Full issue, Hydride fueled LWRs, Nucl. Eng. Des. **239**, (2009), p.1373–1570.

[5] OLANDER, D., etal., Uranium–Zirconium hydride fuel properties, Nucl. Eng. Des., **239,** (2009) , p.1406–1424.

[6] GANDA, F., etal., Plutonium and minor actinides multi-recycling in PWR using hydride fuels, I nternational Conference on Reactor Physics, PHYSOR'08, Interlaken, (2008).

[7] GANDA, F., et al., Plutonium recycling in hydride fueled PWR cores, Nucl. Eng. Des. **239**, (2009), p.1489–1504.

[8] FRATONI, M., etal., Neutronic design of hydride fueled BWRs, Nucl. Eng. Des. **239,** (2009), p.1531–1543.
[9] CHESWORTH, R., etal., Final results of qualification testing of TRIGA fuel, Intern. Meeting O n Reduced Enrichment for Research and Test Reactors, Petten, (1985).
[10] W. WANG, etal., Thermodynamics of the Zr-H system, J. Am. Ceram. Soc., **78**, (1995), p.3323–28.
[11] MOORE, K., etal., Phase studies of Zr-H system at high hydrogen concentrations, J. Nucl. Mate r., **27**, (1968), p.316.
[12] YAMAMOTO, T., etal., Development of new reactor fuel materials: hydrogenation properties o f U–Th–Zr alloys and neutron irradiation effects on their hydrides, J. Nucl. Mater., **247**, (1997), p.339–344.
[13] TERRANI, K., et al., Fabrication and characterization of Uranium–Thorium–Zirconium hydride s, J. Nucl. Mater., **392**, (2009), p.151–157.
[14] BARTSCHER, W., Equilibria and thermodynamic properties of the $ThZr_2$-H system, J. Less Co mm. Metal., **136**, (1988), p.385.
[15] MAJER, G., etal., The mechanism of hydrogen diffusion in Zirconium dihydrides, J. Phys.: Con dens. Matter, **6**, (1994), p.2935.
[16] TERRANI, K., et al., Incoherent quasielastic neutron scattering study of hydrogen diffusion in Thorium-Zirconium hydrides, J. Nucl. Mater., submitted for publishing.
[17] TERRANI, K., et al., Transient hydride fuel behavior in LWRs, J. Nucl. Mater., **392**, (2009), p. 192.
[18] TSUCHIYA, B., Thermal diffusivity measurement of Uranium–Thorium–Zirconium hydride, J. Alloy. Compd. **312** (2000), p.104–110.
[19] WIESENACK, W., etal., Assessment of UO_2 conductivity degradation based on in-pile tempera ture data, OECD Halden Reactor Project, HWR-469, (1996).
[20] YAMANAKA, S., Thermal and mechanical properties of Zirconium hydride, J. Alloy. Compd. **293–295**, (1999), p.23.
[21] WONGSAWAENG, D., et al., A liquid-metal bond for improved LWR fuel performance, Nucl. Technol., **159**, (2007), p.279.
[22] SOMMER, A., etal., Thermal diffusion of hydrogen in nonstoichiometric Zirconium- dihydride, NAA-SR-5066, (1960).
[23] TERRANI, K., et al., Liquid metal as a gap filler to protect Zircaloy cladding from hydride fuel, Proceedings of Top Fuel 2009, Paris, (2009), Paper 2071.
[24] SACRIS, E., etal., The diffusion of hydrogen in liquid Ni, Cu, Ag, and Sn, Metal. Trans., Vol **1/ 12**, (1970), p.3377.
[25] TERRANI, K., et al., The kinetics of hydrogen desorption from and adsorption on Zirconium hy dride, J. Nucl. Mater., submitted for publishing.
[26] LILLIE, A., etal., Zirconium hydride fuel element performance characteristics, Atomics Internat ional/ USAEC Rept.AI-AEC-13084, (1973).
[27] OLANDER, D.R., Fundamental aspects of nuclear reactor fuel elements, Nat'l. Tech. Info. Serv ices. Document No. 26711, (1976).
[28] SIMNAD, M.T., The U–ZrH_x alloy: its properties and use in TRIGA fuel, Nucl. Eng. Design **64** , (1981), p.403.
[29] BALDWIN, N.L., etal., Fission product release from TRIGA-LEU reactor fuels, General Atomi cs Report GA-16287, (1980).
[30] YAMAMOTO, T., et al., Preparation, analysis and irradiation of hydride U–Th–Zr alloy sample s for a new fuel, J. Alloy. Compd. **271–273**, (1998), p.702–706.

LIST OF PARTICIPANTS

S. Abolhassani-Dadras	Paul Scherrer Institute (PSI), Villigen, Switzerland
K. Backman	Westinghouse Electric Sweden AB, Västerås, Sweden
H. Bairiot	FEX, Mol, Belgium
P. Blanpain	AREVA NP, Lyon, France
B. Briyatmoko	National Nuclear Energy Agency (BATAN), Serpong-Tangerang, Indonesia
S. Caruso	Nordostschweizerische Kraftwerke (NOK), Döttingen, Switzerland
S. Castañiza	National Atomic Energy Commission of Argentina CNEA, Buenos Aires, Argentina
C. Degueldre	Paul Scherrer Institute (PSI), Villigen, Switzerland
C. Delafoy	AREVA NP, Lyon, France
J. Dus	Swiss Federal Nuclear Safety Inspectorate (ENSI), Villigen, Switzerland
M. Durazzo	Nuclear and Energy Research Institute IPEN, São Paulo, Brazil
D. Gavillet	Paul Scherrer Institute (PSI), Villigen, Switzerland
A. Gorzel	Swiss Federal Nuclear Safety Inspectorate (ENSI), Villigen, Switzerland
I. Günther-Leopold	Paul Scherrer Institute (PSI), Villigen, Switzerland
W. Grant	Canadian Nuclear Safety Commission, Ontario, Canada
H. Hamilton	Atomic Energy of Canada Limited (AECL), Chalk River, Canada
Y. Heo	Korea Nuclear Fuel Co. Ltd., Daejeon, Republic of Korea
V. Inozemtsev	International Atomic Energy Agency
J.R. Jones	St. James House, Cheltenham, United Kingdom
J.F. Kelly	Thor Energy AS, Oslo, Norway
G. Kuri	Paul Scherrer Institute (PSI), Villigen, Switzerland
J. Laine	STUK - Radiation and Nuclear Safety Authority, Helsinki, Finland
A.V. Lysikov	JSC ‘VNIINM’, Moscow, Russian Federation

K. Macku	Swiss Federal Nuclear Safety Inspectorate (ENSI), Villigen, Switzerland
M. Martin	Paul Scherrer Institute (PSI), Villigen, Switzerland
E.N. Mikheev	JSC 'VNIINM', Moscow, Russian Federation
V.V. Novikov	JSC 'VNIINM', Moscow, Russian Federation
Y.V. Pimenov	JSC 'TVEL', Moscow, Russian Federation
R. Pomirleanu	Westinghouse Electric Company, Monroeville, United States of America
M.A. Pouchon	Paul Scherrer Institute (PSI), Villigen, Switzerland
D. Pramanik	Department of Atomic Energy India, Hyderabad, India
P.N. Prasad	Nuclear Power Corporation of India Limited (NPCIL), Mumbai, India
Y.W. Rhee	Korea Atomic Energy Research Institute, Daejeon, Republic of Korea
T. Sano	Research Reactor Institute Kyoto University, Kyoto, Japan
L. Taivalaho	STUK - Radiation and Nuclear Safety Authority, Helsinki, Finland
K.A. Terrani	University of California, Berkeley, United States of America
A.D. Tomov	Nuclear Power Plant Kozloduy, Kozloduy, Bulgaria
E. Wang	China North Nuclear Fuel Co. Ltd., Baotou, China
A. Wensauer	AREVA NP, Erlangen, Germany
B. Wernli	Paul Scherrer Institute (PSI), Villigen, Switzerland
M. Yamasaki	Nuclear Fuel Industries Ltd., Osaka, Japan

No. 21, July 2006

IAEA
International Atomic Energy Agency

Where to order IAEA publications

In the following countries IAEA publications may be purchased from the sources listed below, or from major local booksellers. Payment may be made in local currency or with UNESCO coupons.

Australia
DA Information Services, 648 Whitehorse Road, Mitcham Victoria 3132
Telephone: +61 3 9210 7777 • Fax: +61 3 9210 7788
Email: service@dadirect.com.au • Web site: http://www.dadirect.com.au

Belgium
Jean de Lannoy, avenue du Roi 202, B-1190 Brussels
Telephone: +32 2 538 43 08 • Fax: +32 2 538 08 41
Email: jean.de.lannoy@infoboard.be • Web site: http://www.jean-de-lannoy.be

Canada
Bernan Associates, 4611-F Assembly Drive, Lanham, MD 20706-4391, USA
Telephone: 1-800-865-3457 • Fax: 1-800-865-3450
Email: order@bernan.com • Web site: http://www.bernan.com

Renouf Publishing Company Ltd., 1-5369 Canotek Rd., Ottawa, Ontario, K1J 9J3
Telephone: +613 745 2665 • Fax: +613 745 7660
Email: order.dept@renoufbooks.com • Web site: http://www.renoufbooks.com

China
IAEA Publications in Chinese: China Nuclear Energy Industry Corporation, Translation Section, P.O. Box 2103, Beijing

Czech Republic
Suweco CZ, S.R.O. Klecakova 347, 180 21 Praha 9
Telephone: +420 26603 5364 • Fax: +420 28482 1646
Email: nakup@suweco.cz • Web site: http://www.suweco.cz

Finland
Akateeminen Kirjakauppa, PL 128 (Keskuskatu 1), FIN-00101 Helsinki
Telephone: +358 9 121 41 • Fax: +358 9 121 4450
Email: akatilaus@akateeminen.com • Web site: http://www.akateeminen.com

France
Form-Edit, 5, rue Janssen, P.O. Box 25, F-75921 Paris Cedex 19
Telephone: +33 1 42 01 49 49 • Fax: +33 1 42 01 90 90 • Email: formedit@formedit.fr

Lavoisier SAS, 14 rue de Provigny, 94236 Cachan Cedex
Telephone: + 33 1 47 40 67 00 • Fax +33 1 47 40 67 02
Email: livres@lavoisier.fr • Web site: http://www.lavoisier.fr

Germany
UNO-Verlag, Vertriebs- und Verlags GmbH, August-Bebel-Allee 6, D-53175 Bonn
Telephone: +49 02 28 949 02-0 • Fax: +49 02 28 949 02-22
Email: info@uno-verlag.de • Web site: http://www.uno-verlag.de

Hungary
Librotrade Ltd., Book Import, P.O. Box 126, H-1656 Budapest
Telephone: +36 1 257 7777 • Fax: +36 1 257 7472 • Email: books@librotrade.hu

India
Allied Publishers Group, 1st Floor, Dubash House, 15, J. N. Heredia Marg, Ballard Estate, Mumbai 400 001,
Telephone: +91 22 22617926/27 • Fax: +91 22 22617928
Email: alliedpl@vsnl.com • Web site: http://www.alliedpublishers.com

Bookwell, 24/4800, Ansari Road, Darya Ganj, New Delhi 110002
Telephone: +91 11 23268786, +91 11 23257264 • Fax: +91 11 23281315
Email: bookwell@vsnl.net • Web site: http://www.bookwellindia.com

Italy
Libreria Scientifica Dott. Lucio di Biasio “AEIOU”, Via Coronelli 6, I-20146 Milan
Telephone: +39 02 48 95 45 52 or 48 95 45 62 • Fax: +39 02 48 95 45 48

Japan
Maruzen Company, Ltd., 13-6 Nihonbashi, 3 chome, Chuo-ku, Tokyo 103-0027
Telephone: +81 3 3275 8582 • Fax: +81 3 3275 9072
Email: journal@maruzen.co.jp • Web site: http://www.maruzen.co.jp

Korea, Republic of
KINS Inc., Information Business Dept. Samho Bldg. 2nd Floor, 275-1 Yang Jae-dong SeoCho-G, Seoul 137-130
Telephone: +02 589 1740 • Fax: +02 589 1746
Email: sj8142@kins.co.kr • Web site: http://www.kins.co.kr

Netherlands
Martinus Nijhoff International, Koraalrood 50, P.O. Box 1853, 2700 CZ Zoetermeer
Telephone: +31 793 684 400 • Fax: +31 793 615 698 • Email: info@nijhoff.nl • Web site: http://www.nijhoff.nl

Swets and Zeitlinger b.v., P.O. Box 830, 2160 SZ Lisse
Telephone: +31 252 435 111 • Fax: +31 252 415 888 • Email: infoho@swets.nl • Web site: http://www.swets.nl

New Zealand
DA Information Services, 648 Whitehorse Road, MITCHAM 3132, Australia
Telephone: +61 3 9210 7777 • Fax: +61 3 9210 7788
Email: service@dadirect.com.au • Web site: http://www.dadirect.com.au

Slovenia
Cankarjeva Zalozba d.d., Kopitarjeva 2, SI-1512 Ljubljana
Telephone: +386 1 432 31 44 • Fax: +386 1 230 14 35
Email: import.books@cankarjeva-z.si • Web site: http://www.cankarjeva-z.si/uvoz

Spain
Díaz de Santos, S.A., c/ Juan Bravo, 3A, E-28006 Madrid
Telephone: +34 91 781 94 80 • Fax: +34 91 575 55 63 • Email: compras@diazdesantos.es
carmela@diazdesantos.es • barcelona@diazdesantos.es • julio@diazdesantos.es
Web site: http://www.diazdesantos.es

United Kingdom
The Stationery Office Ltd, International Sales Agency, PO Box 29, Norwich, NR3 1 GN
Telephone (orders): +44 870 600 5552 • (enquiries): +44 207 873 8372 • Fax: +44 207 873 8203
Email (orders): book.orders@tso.co.uk • (enquiries): book.enquiries@tso.co.uk • Web site: http://www.tso.co.uk

On-line orders:
DELTA Int. Book Wholesalers Ltd., 39 Alexandra Road, Addlestone, Surrey, KT15 2PQ
Email: info@profbooks.com • Web site: http://www.profbooks.com

Books on the Environment:
Earthprint Ltd., P.O. Box 119, Stevenage SG1 4TP
Telephone: +44 1438748111 • Fax: +44 1438748844
Email: orders@earthprint.com • Web site: http://www.earthprint.com

United Nations (UN)
Dept. I004, Room DC2-0853, First Avenue at 46th Street, New York, N.Y. 10017, USA
Telephone: +800 253-9646 or +212 963-8302 • Fax: +212 963-3489
Email: publications@un.org • Web site: http://www.un.org

United States of America
Bernan Associates, 4611-F Assembly Drive, Lanham, MD 20706-4391
Telephone: 1-800-865-3457 • Fax: 1-800-865-3450
Email: order@bernan.com • Web site: http://www.bernan.com

Renouf Publishing Company Ltd., 812 Proctor Ave., Ogdensburg, NY, 13669
Telephone: +888 551 7470 (toll-free) • Fax: +888 568 8546 (toll-free)
Email: order.dept@renoufbooks.com • Web site: http://www.renoufbooks.com

Orders and requests for information may also be addressed directly to:

Sales and Promotion Unit, International Atomic Energy Agency
Vienna International Centre, PO Box 100, 1400 Vienna, Austria
Telephone: +43 1 2600 22529 (or 22530) • Fax: +43 1 2600 29302
Email: sales.publications@iaea.org • Web site: http://www.iaea.org/books

10-38331